Earth-Science Reviews 178 (2018) 438–514

Contents lists available at ScienceDirect

Earth-Science Reviews

journal homepage: www.elsevier.com/locate/earscirev

Invited review

Global review of human-induced earthquakes

Gillian R. Foulger[a,*], Miles P. Wilson[a], Jon G. Gluyas[a], Bruce R. Julian[a], Richard J. Davies[b]

[a] Department of Earth Sciences, Durham University, Durham DH1 3LE, UK
[b] School of Civil Engineering and Geosciences, Newcastle University, Newcastle upon Tyne NE1 7RU, UK

ABSTRACT

The Human-induced Earthquake Database, *HiQuake*, is a comprehensive record of earthquake sequences postulated to be induced by anthropogenic activity. It contains over 700 cases spanning the period 1868–2016. Activities that have been proposed to induce earthquakes include the impoundment of water reservoirs, erecting tall buildings, coastal engineering, quarrying, extraction of groundwater, coal, minerals, gas, oil and geothermal fluids, excavation of tunnels, and adding material to the subsurface by allowing abandoned mines to flood and injecting fluid for waste disposal, enhanced oil recovery, hydrofracturing, gas storage and carbon sequestration. Nuclear explosions induce earthquakes but evidence for chemical explosions doing so is weak. Because it is currently impossible to determine with 100% certainty which earthquakes are induced and which not, *HiQuake* includes all earthquake sequences proposed on scientific grounds to have been human-induced regardless of credibility. Challenges to constructing *HiQuake* include under-reporting which is ~30% of M ~4 events, ~60% of M ~3 events and ~90% of M ~2 events. The amount of stress released in an induced earthquake is not necessarily the same as the anthropogenic stress added because pre-existing tectonic stress may also be released. Thus earthquakes disproportionately large compared with the associated industrial activity may be induced. Knowledge of the magnitude of the largest earthquake that might be induced by a project, M_{MAX}, is important for hazard reduction. Observed M_{MAX} correlates positively with the scale of associated industrial projects, fluid injection pressure and rate, and the yield of nuclear devices. It correlates negatively with calculated inducing stress change, likely because the latter correlates inversely with project scale. The largest earthquake reported to date to be induced by fluid injection is the 2016 M 5.8 Pawnee, Oklahoma earthquake, by water-reservoir impoundment the 2008 M ~8 Wenchuan, People's Republic of China, earthquake, and by mass removal the 1976 M 7.3 Gazli, Uzbekistan earthquake. The minimum amount of anthropogenic stress needed to induce an earthquake is an unsound concept since earthquakes occur in the absence of industrial activity. The minimum amount of stress *observed* to modulate earthquake activity is a few hundredths of a megapascal and possibly as little as a few thousandths, equivalent to a few tens of centimeters of water-table depth. Faults near to failure are pervasive in the continental crust and induced earthquakes may thus occur essentially anywhere. In intraplate regions neither infrastructure nor populations may be prepared for earthquakes. Human-induced earthquakes that cause nuisance are rare, but in some cases may be a significant problem, e.g., in the hydrocarbon-producing areas of Oklahoma, USA. As the size of projects and density of populations increase, the potential nuisance of induced earthquakes is also increasing and effective management strategies are needed.

1. Introduction

Natural processes that modulate the spatial and temporal occurrence of earthquakes include tectonic stress changes, migration of fluids in the crust, Earth tides, surface ice and snow loading, heavy precipitation, atmospheric pressure changes, sediment unloading and groundwater loss (e.g., Kundu et al., 2015). Such processes perturb stress on faults by only small amounts but, since rock failure in earthquakes is a critical process, nucleation of each event is ultimately brought about by a final, incremental change in stress. It is thus unsurprising that anthropogenic activity that perturbs stress in the crust, even slightly, can modulate seismicity. In most cases such effects probably go unnoticed (Section 7.1) but as industrial projects proliferate and grow in scale the number of cases where a link is obvious is increasing.

Mining- and dam-induced earthquakes have been recognized for several decades. Now concern is growing about earthquakes induced by hydraulic fracturing for shale-gas extraction and waste-water disposal

* Corresponding author.
E-mail address: g.r.foulger@durham.ac.uk (G.R. Foulger).

http://dx.doi.org/10.1016/j.earscirev.2017.07.008
Received 5 January 2017; Received in revised form 19 July 2017; Accepted 23 July 2017
Available online 26 July 2017

by injection into boreholes. Seismicity may also increase in hydrocarbon reservoirs as they enter their late phases of production. The full extent of human activities that may induce earthquakes is, however, wider than generally appreciated. We conducted an extensive search to build as complete a catalog as possible of cases of induced seismicity reported to date. Our work expands previous reviews that include a general overview by McGarr et al. (2002), lists by Nicol et al. (2011) and Suckale (2009), and a review of 198 M ≥ 1 events by Davies et al. (2013). Our new database of human-induced earthquakes, *HiQuake*, contains over 700 cases of anthropogenic projects postulated to induce earthquake activity. It is publically available at www.inducedearthquakes.org (Wilson et al., 2017).

We constructed *HiQuake* by searching for case histories in published papers, conference abstracts, books, reports and the world-wide web, and through personal communications. The credibility of individual cases varies from extremely low to overwhelming, with most cases in between. There is no rigorous way of quantifying the likelihood that a particular claim for human induction is correct, and many arguments for anthropogenesis are presented as tentative by authors and challenged by other researchers, e.g., the 1983 M_W 6.2 Coalinga, California, event (Section 3.3.2). There is thus no rigorous way of defining a "credibility cut-off" below which a case history should be excluded from the database. For this reason we adopted the only reliable policy which was to include all cases without regard to plausibility. *HiQuake* thus lists all projects proposed on scientific grounds (not religious or moral) to have induced earthquakes and judgment regarding the credibility of any individual case is the responsibility of the user. *HiQuake* therefore comes with a caveat emptor. It is up to the database user to judge the strength of arguments for anthropogenic induction of any particular case included. For convenience, details of our information sources are included in the database.

In this paper we present the basics of relevant, fundamental, but sometimes-misunderstood background issues. Following this we give examples of seismicity postulated to be related to:

a) Surface operations,
b) Extraction of mass from the subsurface,
c) Introduction of mass into the subsurface, and
d) Explosions.

We sub-divide each category. In some cases, categorization is tentative because more than one anthropogenic process preceded or was ongoing at the time of the earthquakes, e.g., fluid extraction and injection are often conducted simultaneously in hydrocarbon reservoirs. Finally, we summarize features of the database and comment on related issues with which scientists are currently grappling.

1.1. Intraplate earthquakes

Plate tectonic theory in its simplest form considers plates to be rigid and expects most large earthquakes to occur in plate boundary zones. The fact that intraplate earthquakes occur, and may be large, is prima facie evidence that the plates are not rigid but also deform in their interiors. Intraplate stress changes cyclically as stress diffuses through them following the great[1] earthquakes and volcanic events that sum to bring about what geologists model as smooth plate movements (Foulger et al., 1992; Heki et al., 1993). The configuration of plate boundaries is geometrically unstable and evolving. For example, in Europe the formation of extensional features such as the Rhine Graben (Germany) is likely a consequence of southerly migration of the collision zone between Africa and Europe ("slab roll-back"). Intraplate European seismicity is probably related to the same process (Fig. 1) (Nielsen et al., 2007).

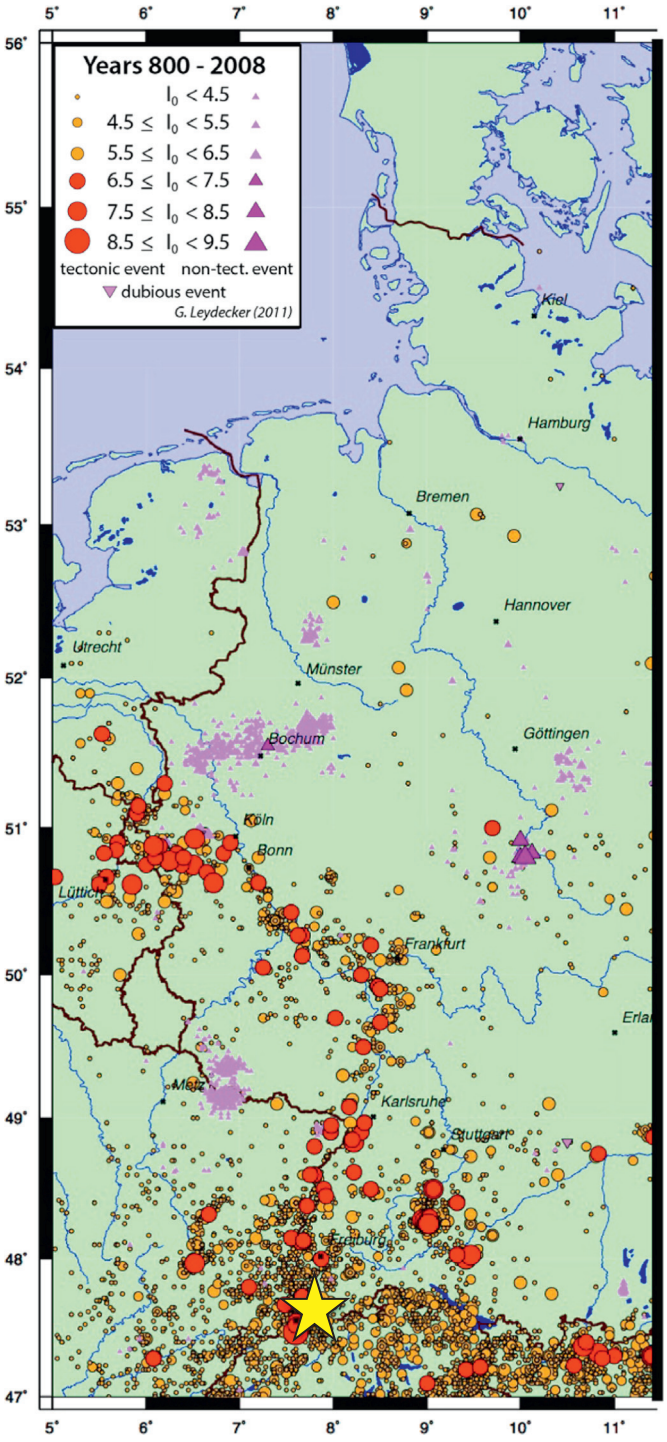

Fig. 1. Map of central Europe showing historical earthquakes with different epicentral intensities from 800 CE (from Stein et al., 2015). Yellow star: city of Basel, Switzerland.

Intraplate seismicity is commonly assumed to be spatially stable so future earthquakes occur where events have occurred in the past. This assumption has recently been re-visited as a result of geodetic work done in the New Madrid Seismic Zone, USA (e.g., Newman et al., 1999; Stein et al., 2009). There, it is generally expected that future large earthquakes will follow the damaging 1811–1812 sequence of four M ≥ 7 earthquakes (e.g., Johnston and Schweig, 1996). As a result, significant resources have been invested in earthquake hazard mitigation. Recent GPS surveying has, however, failed to detect any ongoing

[1] Earthquakes are classified as Great (8 or more), Major (7–7.9), Strong (6–6.9), Moderate (5–5.9), Light (4–4.9) and Minor (3–3.9).

strain build-up (Stein et al., 2009). This led to the proposal that the spatial distribution of intraplate earthquakes in general is not stationary and that the locations of past large earthquakes are not a good predictors of future earthquakes (Liu and Stein, 2016). Wrong forecasts of the location of future large earthquakes may lead to inefficient deployment of hazard-reduction resources and thus have significant implications for public safety.

A non-stationary spatial pattern of seismicity accords with evidence that the crust is critically stressed in most intraplate regions. Stress measurements made in boreholes commonly show that stress is close to the depth-dependent strength of the crust as estimated by laboratory experiments (e.g., Brudy et al., 1997; Zoback and Healy, 1984). The ambient pore pressure is generally close to hydrostatic, the crust is pervasively faulted, and faults that are well oriented for slip in the ambient stress field are commonly close to failure. This is consistent with observations that human-induced seismicity may occur, and even be large, in regions that have been historically aseismic.

1.2. Induced, triggered, stimulated, and nuisance earthquakes

Many if not all earthquakes induced by human activity release more stress than artificially added to the crust. McGarr et al. (2002) suggested the terms "induced" for earthquakes where the stress change caused by human activity is comparable to the shear stress causing a fault to slip, "triggered" where the anthropogenic stress change is much smaller, and "stimulated" where there are insufficient data to make the distinction.

It is beyond dispute that in many cases seismic strain energy released in earthquakes is many orders of magnitude larger than that introduced into the crust by the industrial activity. In this paper, however, we use the term "induced" for all earthquakes related to human activity because:

a) All earthquakes probably release some pre-existing strain energy and are thus likely to be "triggered". Only where rock is entirely unstressed initially could this not be so and that is not possible in a heterogeneous, gravitating half-space. Even nuclear tests, which are purely explosive sources, trigger the release of some regional tectonic stress as shown by shear components in their focal mechanisms (e.g., Toksöz and Kehrer, 1972).
b) The amount of tectonic strain energy loaded into the crust that is relieved seismically, on what time-scale, and the amount released aseismically are poorly understood. In rapidly deforming regions aseismic deformation can be measured geodetically (e.g., Heki et al., 1997) and surface subsidence is commonly observed above producing reservoirs (e.g., the Wilmington Oilfield, California; Kovach, 1974; Nagel, 2001). Only a fraction of the total strain energy is relieved seismically but it is difficult to determine what this fraction is. Surface geodetic data have low sensitivity to fault motion at depth. Estimates of the percentage of strain energy dissipated aseismically vary from ~20% to 1000% of that released seismically (Villegas-Lanza et al., 2016). The recent under-prediction of the magnitude of the 2011 M_W 9 Tohoku-oki, Japan, earthquake which killed >18,000 people and did incalculable economic damage, showed that our assumptions regarding the length of the "seismic cycle" may be incorrect. Even large earthquakes may not relieve all the stress on a fault so our ability to estimate long-term stress buildup in the crust is limited. The same considerations hold true for industrial projects. If the timescale of energy release is underestimated, and with it the size of the largest expected earthquake (which dominates the energy budget because of the fractal nature of earthquake magnitudes), the maximum expected earthquake magnitude (M_{MAX}) may be underestimated.
c) It is at best impractical and at worst fundamentally impossible to determine how much of the strain energy released in a seismic event pre-existed. Even in cases where the energy released is comparable to that industrially added (e.g., McGarr, 1991), much of the latter may have been relieved by aseismic deformation such as ground subsidence or inflow of water at depth. These processes may themselves trigger earthquakes or load adjacent regions to seismic failure (e.g., Guglielmi et al., 2015).

We use the term "induced" neutrally, and without implications for the origin of the total seismic stress change, in accord with the usage of the Committee on Induced Seismicity Potential (Hitzman, 2013). That committee uses the term "induced" to mean "earthquakes related to human activities".[2]

We use the term "nuisance" earthquakes for those that cause societal inconvenience. This inconvenience may be physical or psychological. It includes objectionable damage to infrastructure or the environment, public concern, annoyance or distress about ground shaking, noise or environmental effects such as hydrological changes. Clearly no seismological parameter, e.g., magnitude or intensity of ground shaking, can quantify nuisance because it is dependent on the culture of those affected. Nuisance earthquakes are those that need health-and-safety management. That requires an evidence base to which it is hoped the present review will contribute.

1.3. Factors involved in the nucleation of earthquakes

Shear slip on fault planes, with or without crack-opening or closing components, is the most common earthquake source process. Factors involved in nucleation, i.e. the onset of motion, include:

- the coefficient of friction on the fault plane;
- compressive normal stress on the fault plane;
- pore pressure in the fault zone; and
- shear stress on the fault.

According to the widely used Coulomb Theory, the shear stress required for failure τ is

$$\tau = \tau_0 + \mu(\sigma_n - p) \quad (1)$$

where τ_0 is the cohesion, μ is the coefficient of friction, σ_n is the normal stress across the fault, and p is the pore pressure in the fault zone (e.g., McGarr et al., 2002). The onset of an earthquake may thus result from reduction of the cohesion or normal stress on the fault plane or increase in the shear stress or pore pressure.

The loss or gain of overlying mass, introduction of fluid into a fault zone, or the imposition of vertical and/or horizontal stress by other means, e.g., stress transfer from nearby earthquakes, can bring a fault closer to failure. Where there are rapid temperature changes, e.g., where cold water is injected into geothermal areas, thermal effects may also be a significant.

Both the addition and removal of material industrially is associated with earthquakes. Removal of water from aquifers (Section 3.1) and rock from mines (Section 3.2) may reduce the confining stress on fault planes. Introduction of water via reservoir impoundment (Section 2.1.1) or injection (Section 4.1) may alter the fluid pressure in fault zones. Cessation of groundwater pumping, e.g., out of mines, may result in influx of groundwater and increase in pore pressure (Section 4.1.7). Addition of solid mass at the surface may also alter hydrological

[2] *"Some researchers (e.g., McGarr et al., 2002) draw a distinction between "induced" seismicity and "triggered" seismicity. Under this distinction, induced seismicity results from human-caused stress changes in the Earth's crust that are on the same order as the ambient stress on a fault that causes slip. Triggered seismicity results from stress changes that are a small fraction of the ambient stress on a fault that causes slip. Anthropogenic processes cannot "induce" large and potentially damaging earthquakes, but anthropogenic processes could potentially "trigger" such events. In this report we do not distinguish between the two and use the term "induced seismicity" to cover both categories."* Quoted from Hitzman, M. W. (Ed.) (2013), Induced Seismicity Potential in Energy Technologies x + 248 pp., National Academies Press, Washington, D.C.

conditions (Section 2.1.2).

Theories for the mechanism of induced earthquakes include the asperity model of Pennington et al. (1986) which suggests that fluid extraction results in differential compaction or aseismic fault motion, increasing stress on locked faults. This stress is eventually relieved when asperities break. The poroelastic model of Segall (1985, 1992) suggests that declining pore pressures resulting from fluid extraction cause contraction of the reservoir rocks and stress build-up. *Ad hoc* theories for individual earthquakes may provide candidate explanations *a posteriori*. However, developing a method that can reliably predict *a priori* which industrial projects will induce earthquakes and which not remains a work in progress.

1.4. Earthquake locations

Earthquakes in the *HiQuake* database span the period 1868 to 2017. Seismological technology has improved vastly during this period, but even today the standard of monitoring is non-uniform. Many projects may not be monitored at all until nuisance seismicity begins. In contrast, others may be monitored by dense seismic networks installed well in advance to obtain a pre-operational baseline (e.g., Cladouhos et al., 2013). As a result, data in *HiQuake* such as locations, magnitudes and focal mechanisms are non-uniform in quality.

Inaccurate hypocentral locations hamper efforts to associate earthquakes with operations, especially if the errors are larger than the separation between boreholes or producing horizons. An example is the case of the Crooked Lake, Alberta, earthquake sequences, thought to have been induced by shale-gas hydrofracturing (Section 4.1.6) (Schultz et al., 2015). A pre-operational seismic baseline was not available for medium-magnitude earthquakes, there was little information on local crustal structure, and most of the seismic data were from stations > 100 km away. As a result, it is unclear whether the lack of spatial correlation of some events with operations is real or a consequence of inaccurate locations.

The largest source of hypocentral uncertainty is imperfect knowledge of crustal structure. This factor is not included in the error estimates computed by many commonly used hypocenter-location programs which typically base uncertainty estimates on root-mean-square arrival-time residuals, assuming no errors in the crustal model used. Such residuals may be unrealistically small for systematically mislocated hypocenters. Advanced earthquake location methods using relative locating ("double-differencing"; Waldhauser and Ellsworth, 2000) or waveform cross-correlation (Got et al., 1994) can improve the accuracy of locations *relative to one another* but do not reduce systematic errors in the absolute locations. Accurate depths may be out of reach if geometrically strong data are unavailable. Errors in hypocentral depth are typically 2–3 times the error in horizontal (epicentral) location. Insufficient stations and sparse networks are also hindrances (Section 4.2.1).

Obtaining accurate local crustal velocity models in the neighborhood of small-scale industrial projects may be challenging. Information may be limited to well-logs, global or national crustal models, or models from analogous geological areas (e.g., Schultz et al., 2015). Such models are not adequate for reducing location uncertainties to sub-hectometer (100 m) levels. Ideally, high-quality crustal models based on active-source seismic surveying and/or one- and three-dimensional inversions of local earthquake data will be available. Projects will be monitored by dense networks of seismic stations with stations every 1–2 km^2. Experimental designs of this kind can return locations accurate to about a hectometer. Reducing errors still further requires calibration shots (Foulger and Julian, 2014).

In order to inform discussions regarding whether earthquakes are induced or natural, a pre-operation baseline is required. For this purpose, seismic networks must be deployed prior to commencement of operations. An effort to establish such a baseline for the entire UK prior to possible expansion of shale-gas hydrofracturing was recently made by Wilson et al. (2015).

1.5. Earthquake magnitudes

Magnitudes given for earthquakes often differ by up to a whole magnitude unit because:

- Traditional scales such as local magnitude (M_L) use measurements of the amplitudes of certain seismic phases recorded on seismic stations. Amplitudes are a poor measure of the size of an earthquake because they are influenced by factors such as the orientation of the fault that slipped and source-to-station crustal structure. Because of these and other factors, measurements at different stations may yield different magnitudes for the same earthquake.
- Different magnitude scales such as M_L and surface-wave magnitude (M_s) use different types of seismic waves, resulting in both systematic and random differences in the magnitudes calculated. For example, shallow earthquakes excite stronger surface waves than deep earthquakes, so M_S underestimates the sizes of deeper earthquakes compared with M_L.
- Seismological practice is notoriously non-standard in respect of magnitudes, and local magnitude scales and practices often depart considerably from those originally defined. Many local seismic stations and networks use their own customized magnitude scales, often constructed by calibrating them using a few earthquakes measured in common with the nearest permanent or calibrated station. That station may in turn have been calibrated in the same way. M_L technically refers to recordings made on Wood-Anderson seismographs, but such instruments are now rare. As a result, magnitudes reported from one seismic network may not be comparable to those reported from another, even if the same magnitude scale has, in theory, been used.

It is beyond the scope of this paper to render all magnitudes to a single scale and in this paper we therefore do not discriminate between magnitude types reported. We record the information currently available in the *HiQuake* database, e.g., M_L (local magnitude), m_b (body-wave magnitude), M_S (surface-wave magnitude), M_d (duration magnitude) and M_W (moment magnitude). Where magnitude type is not specified we use the notation M. Where several different estimates are published, we preferentially cite M_W. If M_W is not available, and more than one other magnitude has been published, we cite the largest. Rendering all the magnitudes to M_W is a task for future work.

1.6. Earthquake counts

The total number of earthquakes detected for a sequence depends on the density of seismic monitoring. This may change with time, e.g., if additional seismic stations are installed after nuisance seismicity has begun. Earthquakes are a fractal phenomenon, and their numbers increase by about an order of magnitude for each reduction in magnitude unit. If earthquake counts are to be meaningfully compared, they must thus be related to a common low-magnitude cut-off threshold.

The numbers of earthquakes induced may be of interest where monitoring networks are stable since this parameter may serve as a sensitive strainmeter. As a result, earthquake counts have been particularly useful for monitoring active volcanoes. The availability of many earthquakes is an advantage for purposes such as tracking injected fluids. From the point of view of potential damage the earthquakes of most relevance are the relatively few large-magnitude events and possibly only the largest (M_{MAX}).

1.7. The database

The approach we used to construct the database is described in detail by Wilson et al. (2017). Challenges intrinsic to the task included:

Table 1
Data recorded in the database.

Column contents
Country
Project name
Project type (subclass)
Longitude
Latitude
Project end date
Project start date
End date of seismicity or monitoring
Start date of seismicity or monitoring
Magnitude type
Delay time
Date of largest earthquake
Depth of largest earthquake
Distance of largest earthquake from induction activity
Year of largest earthquake
Lithology/resource
Distance of furthest earthquake from induction activity
Depth of induction activity
Typical depth of earthquakes
Previous seismicity
Tectonic setting
Injection/extraction rate
Dam height
Total volume or mass injected/extracted
Units of injection/extraction rate
Maximum wellhead pressure during injection
Units of total volume or mass injected/extracted
Stress change postulated to have induced earthquake
Change in reservoir pressure
Bottom-hole temperature
Area of project
References
Notes
References used by Davies et al. (2013)
Project type

- Incomplete reporting (Section 7.1);
- Ambiguous reporting, e.g., “Seismicity is not reported”;
- Lack of reported data, e.g., operational parameters not given;
- Uncertainty regarding whether or not the earthquakes were induced, e.g., some postulated associations are based simply on short-term temporal correlations or weak spatial correlations unsupported statistically and possibly coincidences. We dealt with this by including all cases (Section 1);
- Multiple possible induction processes ongoing simultaneously, e.g., hydrocarbon extraction and wastewater injection;
- Non-uniformity of magnitude reporting (Section 1.5). We report M_W if available, and if not the largest other magnitude;
- Lack of suitable networks to detect earthquakes. For some studies, instruments were installed only after the onset of seismicity (Section 1.4);
- Poor location accuracies (Section 1.4).

A list of database column headings is given in Table 1. The full *HiQuake* database is available as an Excel spreadsheet and references as an EndNote library at http://www.inducedearthquakes.org.

1.8. Earthquakes and belief systems

Public attitudes to induced earthquakes may have major implications for industrial projects, but human reactions to earthquakes may not be based on science. Because of their apparently chaotic and spontaneous nature, and lack of obvious direct causes, earthquakes have for millennia been explained in terms of folklore, religion, and other belief systems (e.g., Harris, 2012). This includes Chinese, Russian and Japanese folklore and the religions of the ancient Greeks and Polynesians. All three mainstream Abrahamic religions–Christianity, Islam and Judaism–are based on ancient texts that attribute earthquakes to shortfalls in human moral behavior.

Recent cases where belief-system-based explanations for earthquakes have had significant societal impacts include:

- In 2015, the Malaysian government attributed a M_W 6.0 earthquake that killed 18 people to tourists posing nude on Mt. Kinabalu, one of the country's sacred mountains.
- In 2014 local people in the Altai Mountains, Siberia, attributed earthquakes to the removal of the mummified remains of a 5th-century BC noblewoman for archaeological research.
- In 2010, the American evangelist Pat Robertson attributed the devastating M_W 7.0 Haiti earthquake to an alleged “pact to the Devil” made by escaped slaves to ensure success of the successful 1791–1804 anti-slavery insurrection on the island.

These examples illustrate the importance of public information and outreach when planning industrial projects that might induce earthquakes.

2. Surface operations

2.1. Adding mass

Earthquakes have been postulated to have been induced by three kinds of surface-mass addition. These are water impoundment behind dams (168 cases), erecting heavy buildings (1 case), and engineering coastal sediments (1 case).

The earliest report of earthquakes induced by water reservoir impoundment is from Reservoir Mead, Nevada and Arizona, USA (Carder, 1945). Several probable water-reservoir-induced earthquakes have resulted in fatalities and extensive property damage. The largest earthquake claimed to have been induced in this way is the 2008 M ~8 Wenchuan, China, earthquake, which has been associated with impoundment of the reservoir behind the Zipingpu dam. Reports of earthquakes induced by erecting heavy buildings and engineering coastal sediments are, in comparison, rare.

2.1.1. Water impoundment behind dams

A well-studied example is that of the Koyna Dam, India (Fig. 2). A detailed overview of this case, along with a review of reservoir-induced earthquakes, is given by Gupta (2002). The 103-m-high Koyna Dam was raised in 1962 and contains a reservoir up to 75 m deep and 52 km long. Five years after it was completed, a sequence of earthquakes with magnitudes up to M_S 6.3 occurred causing ~200 deaths and slightly damaging the dam. The largest earthquake nucleated at shallow depth, probably < 5 km, and its epicenter was ~10 km downstream from the dam. Earthquake activity has continued subsequently, correlating to some extent with water level in the reservoir (Fig. 3) (Talwani, 1995). A M > 5 event occurs there about every four years.

A second notable example is the Nurek dam, Tadjikistan (Keith et al., 1982; Leith et al., 1981; Simpson and Soboleva, 1977; Simpson and Negmatullaev, 1981). Building of this dam began in 1961 and, at 317 m, it is currently the highest in the world. It contains a reservoir ~10 km^3 in volume (Fig. 4). The largest earthquake to have occurred there to date is the 1972 M_S 4.6 event (Simpson and Negmatullaev, 1981). Seismicity is ongoing and there is evidence for correlation with periods of increase in water depth (Fig. 5).

The largest-volume reservoir in the world is 1.64×10^{11} m^3 and is contained by the 111-m-high Aswan dam, Egypt. Earthquakes induced there are thought to occur in two depth intervals i.e. ~0–10 km and ~15–25 km (Figs. 6 and 7). This vertical separation is postulated to indicate two different processes/environments of induction (Awad and Mizoue, 1995). The largest earthquake observed there to date is the 1981 M 5.7 earthquake, thought to have nucleated in the deeper zone.

A rare case where induced seismicity damaged the dam itself is that

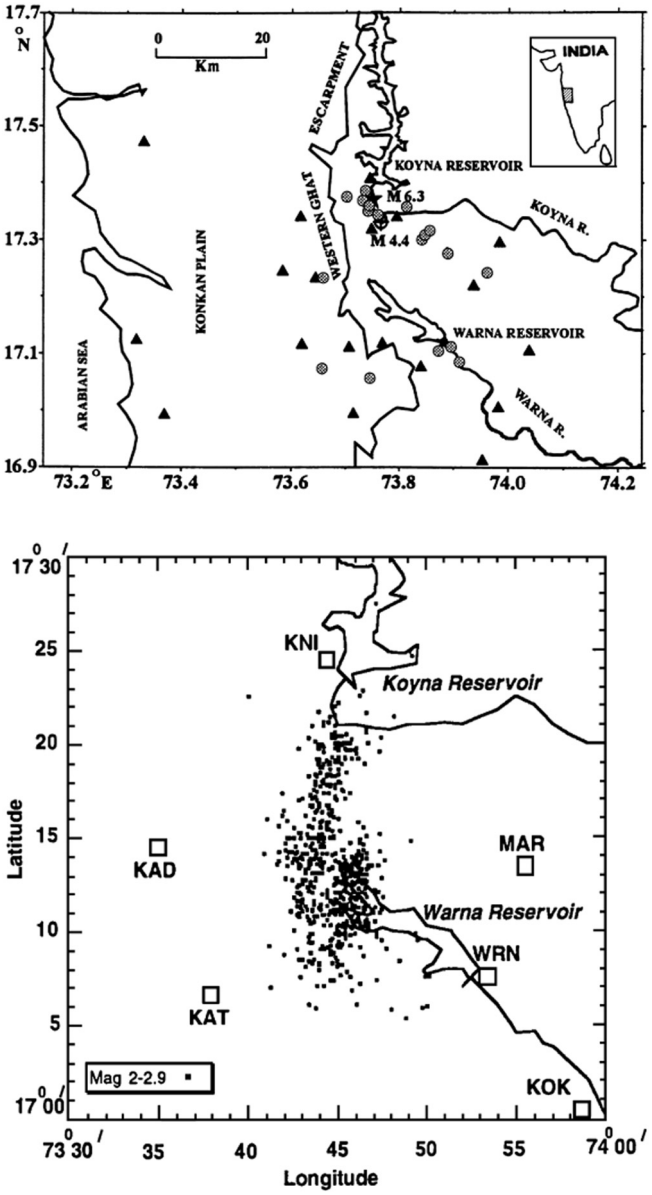

Fig. 2. Top: Map of Koyna area, India, showing the dam, reservoir, seismic stations (triangles) and boreholes (dots). Bottom: Same area showing earthquakes with M 2–2.9 for the period October 1993 to December 1994.
(From Gupta (2002).)

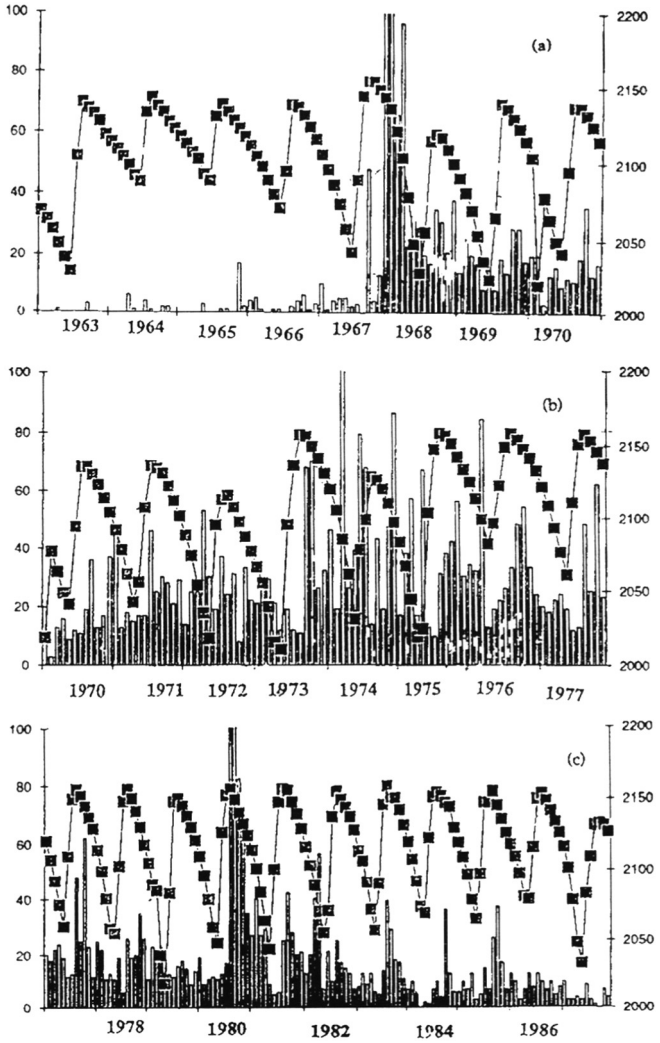

Fig. 3. Number of earthquakes in the region of the Koyna dam, India, for the period 1963–1986 (left axes), along with reservoir water level (right axes, in m).
(From Talwani (1995).)

of the 105-m-high Xinfengjian Reservoir, China. Impoundment of the 1.39×10^{10} m^3 volume reservoir began in 1959 and seismic activity started a month later. A M_S 6.1 earthquake occurred in 1962 which caused minor cracking of the dam.

A case of particular interest is that of the May 2008 M_W ~8 Wenchuan, China, earthquake (Fig. 8). This earthquake was so large relative to the height of the nearby Zipingpu dam (156 m) and the volume of the reservoir (~10^9 m^3) that it is controversial whether it was induced or not. It occurred ~20 km from the dam within months of full reservoir impoundment. The earthquake caused ~90,000 deaths, collapsed roads and bridges, and serious damaged >100 towns.

The activated zone lies at the transition between the low-strain-rate (<10^{-10}/year), stable Sichuan Basin and the tectonically active Tibet plateau where strain rates are >10^{-8}/year. The transition is marked by the multi-stranded Longmenshan fault zone which accommodates thrust and strike-slip motion. Paleoseismic work suggests an earthquake recurrence time of ~7000 years for M 7–8 earthquakes (Klose, 2012).

Prior to impoundment of the reservoir there had been ~40 recorded earthquakes per month in the vicinity of the dam. In October 2005, seismicity increased as impoundment started and the water level rose rapidly by ~80 m. The water level peaked in October 2006 at ~120 m above pre-impoundment levels. Earthquake activity surged to ~90 events per month but reduced thereafter (Fig. 9).

The 2008 M_W ~8 mainshock nucleated at ~16 km depth and thrust motion propagated up toward the surface beneath the reservoir. Rupture transitioned to strike-slip motion and propagated laterally along the fault in both directions, rupturing >300 km of the Longmenshan thrust belt with an average slip of 2.4 m, peaking at 7.3 m. The source time function, which lasted 90 s, indicated that failure occurred in five sub-events that sequentially released 9%, 60%, 8%, 17% and 6% of the total moment (Fig. 9) (Zhang et al., 2008, Yong Zhang, personal communication). The average stress drop during the earthquake was 18 MPa, peaking at 53 MPa. Like other great earthquakes, this event owed its large size to progressive activation of adjacent fault segments in a chain of sub-events.

The increase in shear and normal stresses, caused by the reservoir, that were orientated to encourage slip on the fault were no more than a few kPa (Klose, 2012). This is small, even compared with the stress changes associated with Earth tides (Section 7.3). Klose (2012) suggests that the additional stress modulated the timescale on which the earthquake occurred, advancing it in time by ~60 years. It has been much disputed whether such a small stress perturbation was sufficient

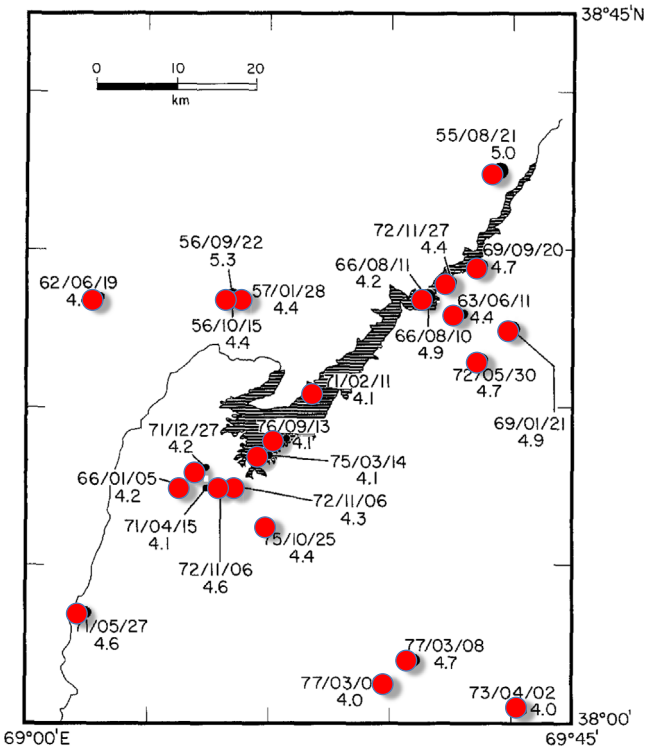

Fig. 4. Map of Nurek dam and reservoir, Tadjikistan, showing earthquakes with M ≥ 4.0 for 1955–1979.
(From Simpson and Negmatullaev (1981).)

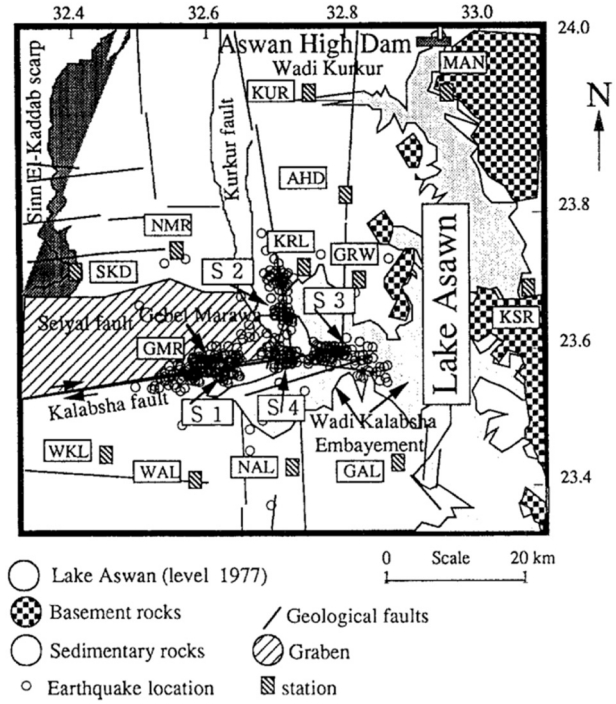

Fig. 6. Map showing Lake Aswan, Egypt, and epicenters of induced earthquakes. (From Awad and Mizoue (1995).)

to trigger such a large earthquake. A more relevant question is whether the reservoir could have induced the initial M_W ~7.5 sub-event, since it is that sub-event which started the cascade of segment failures that grew the earthquake to M_W ~8.

An unusual dam-related seismic sequence occurred in association with the Beni Haroun hydraulic complex in the Mila region, 30 km west of the city of Constantine, Algeria (Semmane et al., 2012). This complex comprises a main dam 120 m high and a reservoir with a capacity of ~10^9 m^3. It is connected by pipelines to the secondary Oued Athmania reservoir, ~15 km south of the main dam (Fig. 10). A 6-km section of pipeline passes through a mountain as a lined tunnel 1.4–3.6 m in diameter. To reach this part of the pipeline water is pumped up ~600 m higher than the Beni Haroun reservoir. The pipeline has a capacity of 600,000 m^3/day.

In 2007, a sequence of earthquakes up to M_d 3.9 occurred. It is thought to have been induced by leakage into the ground of ~400,000 m^3 of water as it was being pumped between the reservoirs. More than 7200 earthquakes were recorded over a ~2-month period. The water leaked from the tunnel via defective joints and penetrated deep into the ground via fractures, faults and karst cavities. Earthquakes started within days of the leakage (Fig. 10). The area had no prior record of such swarm activity and installation of the complex

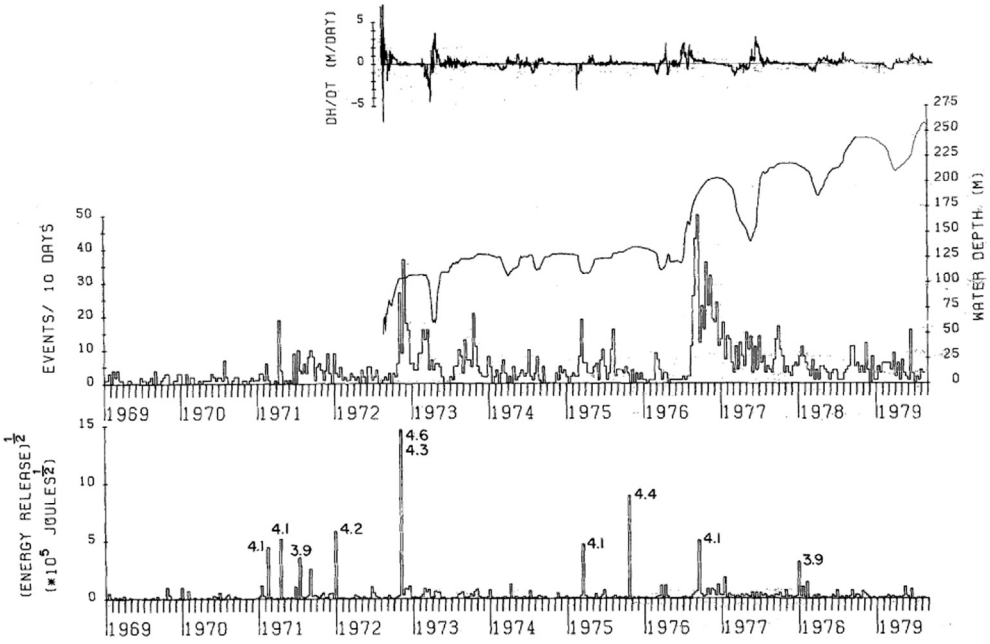

Fig. 5. Water depth and seismicity for 1969–1979 in the vicinity of Nurek dam, Tadjikistan.
(From Simpson and Negmatullaev (1981).)

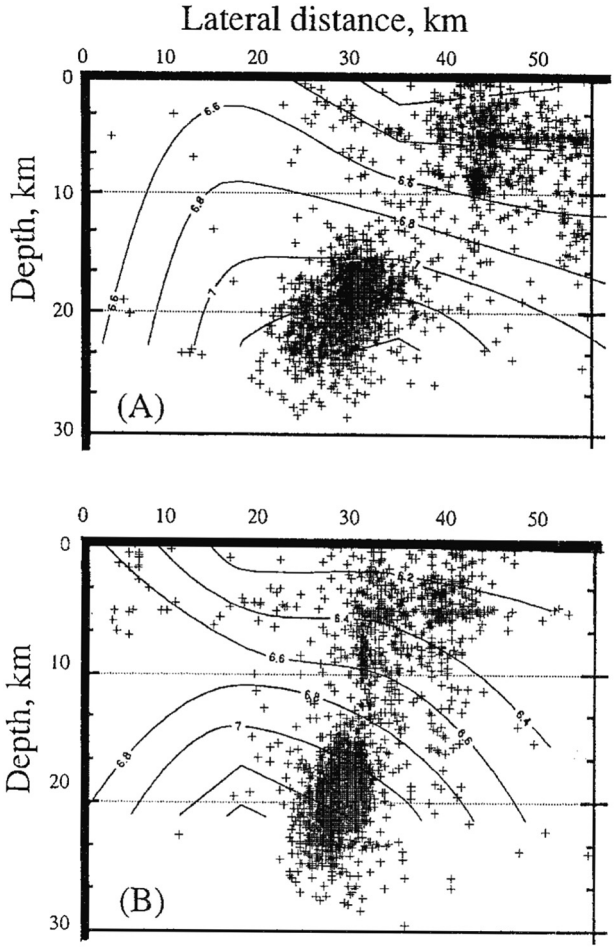

Fig. 7. Cross sections showing hypocentral distribution of earthquakes postulated to have been induced by impoundment of Lake Aswan.
(From Awad and Mizoue (1995).)

in 2000 had not been associated with an increase in seismicity. The events did no damage but were heard loudly and alarmed local people unaccustomed to earthquakes (Semmane et al., 2012).

The Colorado River, USA, contains numerous dams. The two largest are the 220-m-high Glen Canyon dam, a concrete arch that impounds Reservoir Powell, Arizona, and the Hoover dam, ~600 km further downstream, that impounds Reservoir Mead, mostly in Nevada. Glen Canyon dam is built in Mesozoic sedimentary rocks whereas the Hoover dam is built in Tertiary volcanics, part of the tectonically active basin-range province. In keeping with expectations, the latter is seismogenic but the former is not (Fig. 11).

Currently, attention is focused on the 181-m-high Three Gorges dam, China. Its 4×10^{10} m^3 water reservoir was fully impounded in 2010 and power generated came online in 2012. Total generation capacity is 22,500 MW. The area lies in a seismogenic region that includes two major fault lines. The reservoir is not the largest in the world, but earthquakes are already being reported with a M_L 4.6 event occurring in 2014.[3]

2.1.2. Erecting tall buildings

Lin (2005) suggested that erection of the ~500-m high Taipei 101 building, Taiwan, influenced the pattern of seismicity in the immediate neighborhood of the building. This 7×10^8 kg building increased stress on the ground at its base by ~0.47 MPa. In the eight-year period prior to building, nine earthquakes with $M_L \leq 2.0$ occurred whereas during the eight-year period that spanned construction and followed it, 20 earthquakes up to M 3.8 occurred. Earthquakes were unusually frequent during the construction period (Fig. 12).

This is the only published case to date proposing earthquakes were induced by erecting a heavy building. Taiwan lies in a convergent plate boundary zone where the Philippine Sea plate subducts beneath the Eurasian plate at the Manila trench. As a consequence it is seismically active.

This case raises the question of whether other such examples exist, e.g., in Japan. The building that is currently the tallest in the world, the 825-m-high Burj Khalifa, Dubai, weighs less than the Taipei 101 building, at only 4.5×10^8 kg. There are no known reports of changes in earthquake activity from the New York or Tokyo regions where large buildings are common, though to our knowledge the issue has not been studied in detail.

2.1.3. Coastal land gain

Klose (2007b) suggested that the 2007 M_L 4.2 Folkestone, Kent, UK, earthquake was triggered by geo-engineering of shingle accumulation in the harbor since 1806. There is substantial coastal land loss as a result of erosion to the southwest and northeast of Folkestone, but land gain by artificial shingle accumulation in Folkestone harbor has been ongoing for ~200 years. An estimated total of $\sim 2.8 \times 10^9$ kg had accumulated by 2007, four times the mass of the Taipei 101 building. This altered the stress by an estimated 0.001–0.03 MPa at 2 km depth. The earthquake epicenter lay ~1 km (epicentral error ~ 5 km) from the shingle, and nucleated at shallow depth.

2.2. Surface operations: removing mass

Operations that remove mass from the surface and are reported to induce earthquakes are limited to quarrying. *HiQuake* contains 16 such cases. The largest earthquake that has been associated with quarrying is the 2013 M 6.1 Kuzbass, Siberia, event (Emanov et al., 2014; Yakovlev et al., 2013). It occurred in the Bachatsky open-cast coal mine which is 10 km long, 2.2 km wide, excavated up to 320 m deep, and produces $> 9 \times 10^6$ t of coal per year. The earthquake collapsed buildings in local communities and was felt in neighboring provinces.

Moderate earthquake activity had been detected in the mine in early 2012 when a M_L 4.3 event and associated aftershocks occurred. A dense local seismic network was installed, and recorded a low level of small earthquakes with magnitudes up to ~M_L 2. Event magnitudes increased with time, and 15 months later a M_L 3.9 event occurred followed a month later by the M 6.1 mainshock.

2.3. Surface operations: summary

The impoundment of water in reservoirs behind dams induces earthquakes in abundance and accounts for 168 (24%) of all cases in *HiQuake*. Ignoring natural lakes where dams have made minor changes to the water level, reservoirs are up to 8502 km^2 in area (Lake Volta, behind the Akosombo Dam, Ghana). Earthquakes may thus be induced throughout relatively large regions.

Eight cases of induced earthquakes with M > 6 have been proposed, associated with the dams at Zipingpu (China), Lake Hebgen (USA) (Klose, 2013), Polyphyto (Greece), Koyna (India), Kariba (Zambia/Zimbabwe), Kremasta (Greece), Hsingfengkiang (China) and Killari (India). In China there are 348 reservoirs with volumes exceeding 0.1 km^3. Of these, 22 (6.3%) are reported to be seismogenic.

Gupta (2002) reviews theories for the mechanism of triggering. Stresses induced by reservoirs at the depths where earthquakes occur are small, perhaps of the order of 0.1 MPa. This is much smaller than the 1–10 MPa stress drops that are typical in earthquakes. They are, nevertheless, larger than seismogenic Earth tidal stresses (Section 7.3). The mechanism of induction may be that the surface load alters

[3] https://journal.probeinternational.org/2014/04/07/three-gorges-dam-triggers-frequent-seismic-activities/.

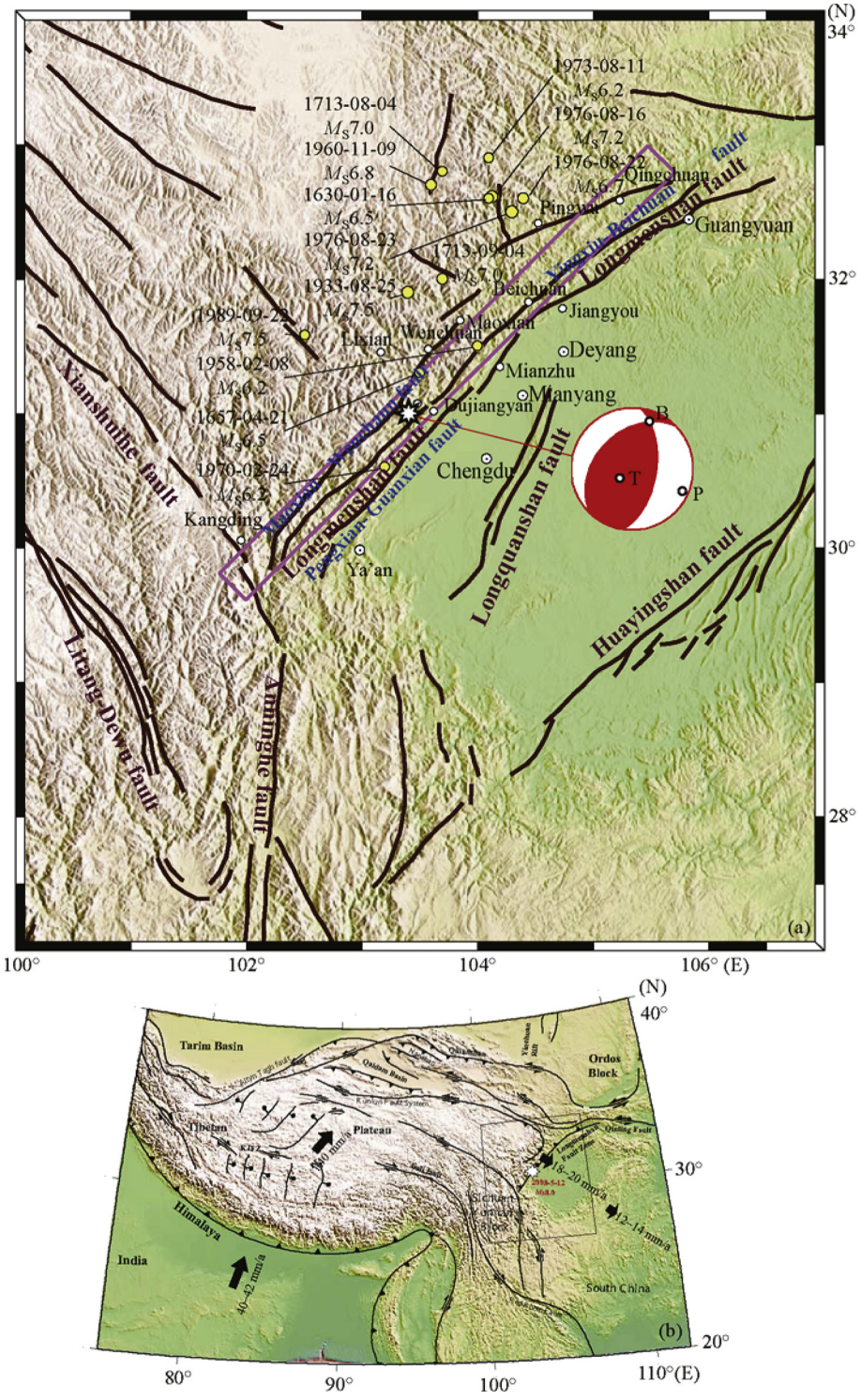

Fig. 8. Top: Area of the 2008 M_W ~8 Wenchuan, China, earthquake. Star: location of nucleation point of the mainshock; lines: main faults of the Longmenshan fault zone; yellow circles: historical earthquakes; white circles: main cities; lilac rectangle: projection of the fault plane that slipped; beach ball: lower hemisphere projection of the focal mechanism of the mainshock. Bottom: regional tectonic setting.
(From Zhang et al. (2008).)

hydraulic conditions at depth, causing fluid to migrate into fault zones and increase pore pressure. This may also explain the seismicity postulated to have been induced by the Taipei 101 building, Taiwan (Section 2.1.2) and shingle accumulation at Folkstone, UK (Section 2.1.3).

3. Extraction from the subsurface

3.1. Groundwater extraction

Five cases of earthquakes associated with artificial lowering of the water table have been postulated. The 2011 M_W 5.1 Lorca, Spain, event, suggested to have been induced by groundwater extraction (Fig. 13) (González et al., 2012), caused extensive damage to the town of Lorca, seriously damaging both modern and historic buildings, killing nine people and injuring several hundred (Fig. 14).

The region lies in a transpressive shear zone containing thrust- and strike-slip faults, in the Nubia-Eurasia plate boundary. The M_W 5.1 mainshock nucleated on the Alhama de Murcia fault at unusually shallow depth (~3 km). This fault has generated several large earthquakes over the past few centuries. Geodetic data from radar interferometry and GPS surveying constrained co-seismic deformation that

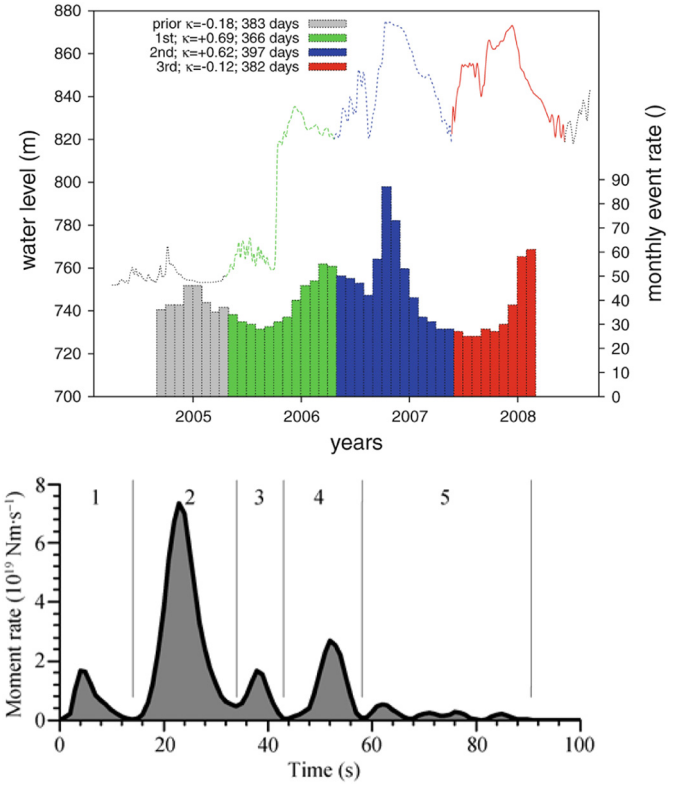

Fig. 9. Top: Water level change in the Zipingpu, China, water reservoir and earthquake event rate in the vicinity prior to the May 2008 M_W ~8 Wenchuan earthquake (from Klose, 2012). Bottom: Source time function of the 2008 great Wenchuan, China earthquake (from Zhang et al., 2008).

was consistent with slip of up to ~15 cm on a ~10 × 10 km section of the fault in the depth interval ~ 1–4 km (Fig. 15).

To the southeast, groundwater pumping 1960–2010 had lowered the water table by > 250 m. The surface had concurrently subsided by > 10 cm/year, totaling > 2 m. Significant environmental effects had occurred as a result (Fig. 16).

A slip deficit of up to ~12 cm had probably accumulated in the Alhama de Murcia fault since the previous large earthquake on the fault segment ~200 years earlier. Calculated Coulomb stress changes induced by water removal were consistent with a crustal unloading process that enabled tectonically accumulated stress to be released in the 2011 event. González et al. (2012) concluded that cumulative long-term hydraulic unloading, coupled with the location and type of the fault with respect to the depleting aquifer, contributed to the stress conditions that precipitated the earthquake.

Other cases of induced seismicity of this kind include the 2015 M_W 7.8 Gorkha, Nepal, earthquake which has been linked to groundwater depletion beneath the Indo-Gangetic Plain to the south (Kundu et al., 2015). This thrust earthquake caused ~8000 deaths and ~$10 billion of economic loss, ~50% of the Gross Domestic Product of Nepal.

The Indo-Gangetic Plain is the most intensely irrigated region in southeast Asia and has the highest population density. It covers ~2.5×10^6 km^2 and is home to ~0.5 billion people. Groundwater is extracted at a rate of ~23×10^{12} m^3/year, the largest rate of groundwater loss on Earth (Fig. 17). This load is being removed from the footwall of the Main Himalayan Thrust and encourages slip in the fault zone in a similar way to the Lorca case (Fig. 18) (Kundu et al., 2012).

The Coulomb failure stress change has been ~0.003–0.008 MPa since 1960 (Kundu et al., 2012). This is at the lower limit of that induced by Earth tides (Section 7.3) but is comparable to the natural rate of stress accumulation on the Main Himalayan Thrust of ~0.001–0.002 MPa/year. Dewatering of the Indo-Gangetic Plain is thus accelerating stress accumulation on the Main Himalayan Thrust by 4.5–20%.

Groundwater beneath the San Joaquin Valley, California, has been depleted by ~1.6×10^{11} m^3 over the past ~150 years (Amos et al., 2014; McGarr, 1991). The most rapid depletion occurs during the summer agricultural growing months and the most rapid natural recharge during the winter and spring. Annual fault-normal seasonal stress variations on the San Andreas fault zone from this source are ~0.001 MPa, encouraging earthquakes in summer and autumn. The stress rate is similar to that calculated for the Main Himalayan Thrust from dewatering the Indo-Gangetic Plain and the predicted seasonality in seismicity is seen in earthquakes with M > 1.25.

A similar process was suggested to modulate seismicity in the Gran Sasso chain in the central Apennines, Italy (Bella et al., 1998). There, tunneling for construction of a highway 1970–1986 significantly changed the hydrology of natural springs. Changes in the spatial pattern of local seismicity, an increase in seismic rate, and the occurrence of three M > 3 events were postulated to be linked to the hydraulic changes. Klose (2007a) attributes the 1989 M_L 5.6 Newcastle, New South Wales, Australia, event to the dewatering of deep coal mines.

3.2. Mining

Mine excavations perturb stresses in surrounding rocks and may reduce some components from values initially of the order of 100 MPa to atmospheric (0.1 MPa). The resulting stress differences can exceed the strength of competent rocks and cause earthquakes. These are traditionally known as “rock bursts” or “coal bumps”.

Lately, excellent seismic data have been recorded on dense, multi-component arrays installed for hazard mitigation purposes. Propagation paths are often short, pass through homogeneous rock, and data are free from the effects of the weathered surface layer that degrade surface observations. Significant advances in understanding the source physics of earthquakes have been achieved using these data. It has been shown that many mining-induced earthquakes have net implosive source mechanisms, consistent with partial closure of the artificial voids created by the removal of mass (e.g., Feignier and Young, 1992; Kusznir et al., 1982; Rudajev and Sileny, 1985; Wong and McGarr, 1990; Wong et al., 1989). Miller et al. (1998a, Section 3.4) give a detailed review of this.

3.2.1. Traditional mining

Mining seismicity may be disproportionately serious because of the large loss of life and resources caused. This includes environmental damage such as surface subsidence which may render buildings beyond repair. Mitigating mining-induced seismicity is a major technical challenge, and might become a limiting factor to the industry (e.g., Tang et al., 2010).

During the ~50-year period 1949–1997, over 2000 coal bursts occurred in 33 mines in China, killing several hundred people and costing > 1300 days in lost production (Tang et al., 2010). In 2007 some 102 coal mines and 20 other mines reported seismicity (Fig. 19). Seven of these were associated with events of M > 4.0 and 27 with events of M ≥ 3.0 (Li et al., 2007). Earthquakes are shallow, occurring at 0–7 km depth. The largest coal mining event that has occurred in China is the 1977 M_L 4.3 event at Taiji mine, Beipiao, Liaoning (Li et al., 2007).

Coal mining in China is increasing in depth of extraction and volume removed, and the problem of mining-induced seismicity is increasing also (Figs. 20 and 21). The demand for coal and other minerals requires, in the absence of other solutions, that this trend continues. The problem of mining-induced earthquakes may thus grow unless management solutions are found.

Perhaps the most spectacular case of mining-induced seismicity occurred in 1989 in the Volkershausen Ernst Thaelmann/Merkers potash mine, Germany. An event with M_L 5.6 (Bennett et al., 1994; Knoll,

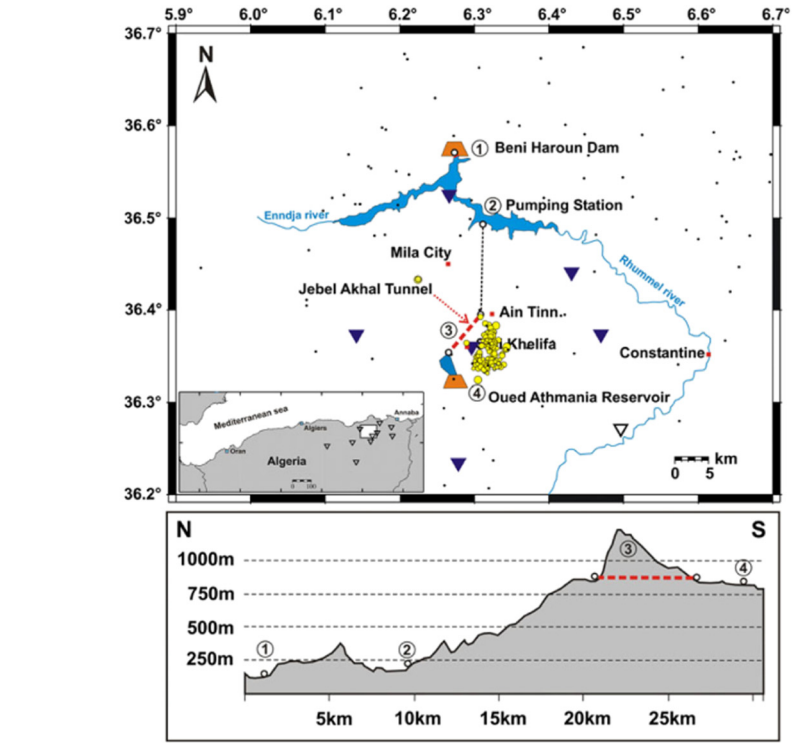

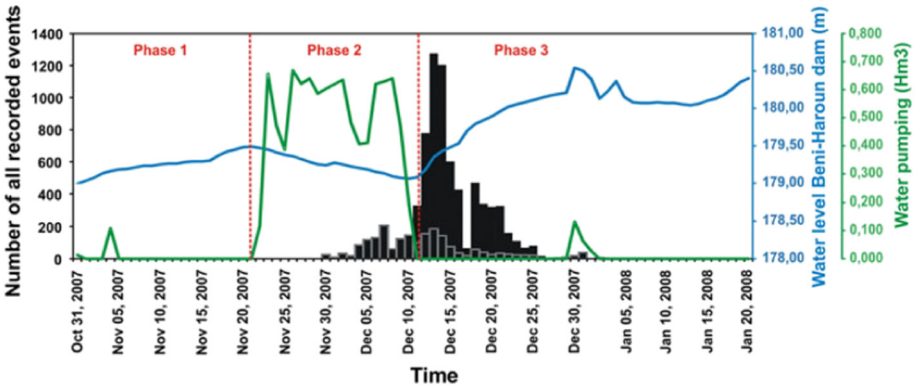

Fig. 10. Map of hydraulic system in Mila region, Algeria. Top: Water transport system (dashed lines) from Beni Haroun dam to Oued Athmania reservoir. Red dashed line: tunnel through Mt. Jebel Akhal; black dots: seismicity for 2006–2007; triangles: seismic stations; yellow dots: epicenters of earthquakes postulated to have been induced. Middle: topographic profile of hydraulic system. Bottom: Number of earthquakes recorded, water level in Beni Haroun dam, and volumes of water pumped vs. time around the seismogenic period. Black histogram: events recorded; gray histogram: events recorded by the network, discarding a temporary station deployed in the epicentral area for 17 days during the swarm. This exemplifies the effect of varying the number of seismic stations. (From Semmane et al. (2012).)

1990) was associated with the collapse of ~3200 pillars throughout an area of ~6 km^2 in the depth range 850–900 m. A large part of the local town of Düren was devastated, damaging several hundred buildings and totally destroying 19. Three people were killed and several injured. The event was probably multiple, with three main sub-events of M_L 4.4, 5.1 and 5.5. The M_L 5.5 sub-event was attributed partly to fluid waste injection which increased pore pressure by ~0.3–1.1 MPa, and this may have initiated an earthquake which led to collapse of the pillars (Knoll, 1990).

A case that involved litigation over the cause of a fatal mine-related earthquake is the 2007 M_W 4.1 Crandall Coal Mine, Utah, event. Nine miners and rescuers were killed by a gallery collapse. The cause of the collapse was variously attributed to triggering by a natural earthquake or unsafe back-stripping mining practices. The seismic moment tensor of the event was not consistent with shear slip on a fault, as expected for a natural earthquake, but with a rapidly closing crack, as expected for a gallery collapse (Fig. 22) (Dreger et al., 2008). The following year, the US Mine Safety and Health Administration levied fines totaling $1.85

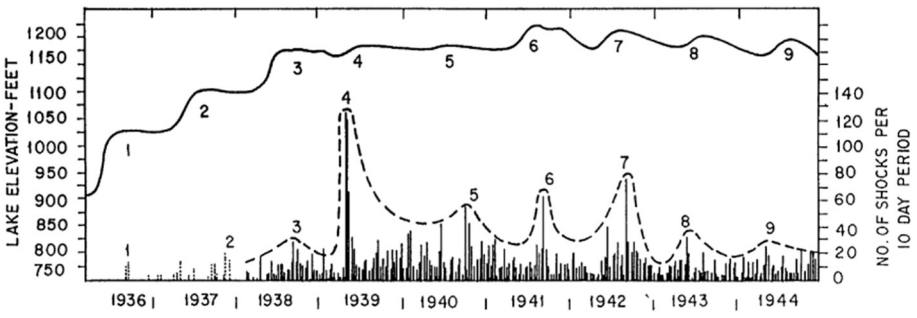

Fig. 11. Earthquakes and water level at Reservoir Mead, Arizona, which is impounded behind Hoover dam. (from Gupta (2002).)

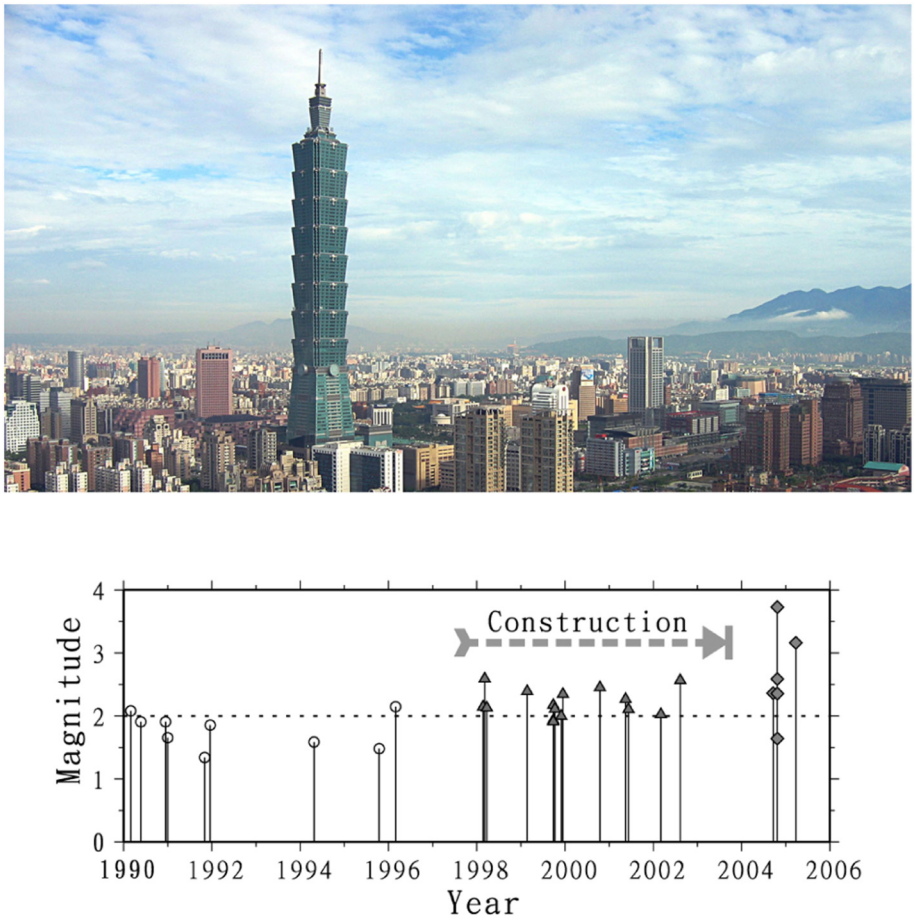

Fig. 12. Top: The Taipei 101 building, Taiwan (http://inhabitat.com/taipei-101-worlds-tallest-green-building/green-taipei-101-1). Bottom: Earthquake history for a 16-year period spanning the construction of the building. (From Lin (2005).)

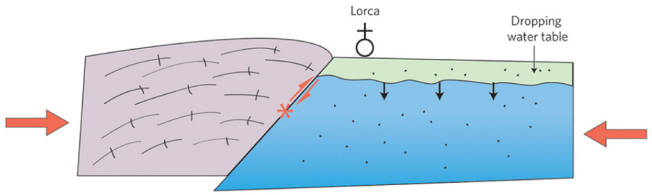

Fig. 13. Schematic figure showing the mechanism proposed by González et al. (2012) for inducing the 2011 M_W 5.1 Lorca, Spain, earthquake. (From Avouac (2012).)

million for unsafe mining practices at Crandall Coal Mine.

The UK has a long history of mining dating from the Neolithic period that includes flint, lead, copper, coal, tin and gold (Fig. 23). During the 19th and 20th centuries coal mining reached its peak and in 1913, ~ 3 x 10^8 t were extracted from 3024 mines. Some of these were excavated to depths of ~1200 m and extended several kilometers offshore beneath the North Sea.[4,5] *HiQuake* includes the largest earthquake recorded in each major UK coalfield.

Wilson et al. (2015) reviewed UK earthquakes to determine a national baseline for seismicity in advance of possible future shale-gas hydrofracturing. They used the earthquake database of the British Geological Survey. Of the ~8000 onshore British earthquakes in that catalog for 1970–2012 they estimated ~21% to have been anthropogenic, the majority caused by coal mining (Fig. 24). Coal production and earthquakes correlate (Fig. 25) (Wilson et al., 2015). A large reduction in seismicity accompanied a fall in production during the 1984–85 miners' strike. The economic cost of that strike is estimated to have been several billion pounds, from which it can be calculated that mitigation of each earthquake with $M_L \geq 1.5$ cost ~£10 million. The earthquake rate recovered in line with coal production when the strike ended in 1985.

The region most renowned for large mining-induced earthquakes is South Africa. There, two of the world's richest ore bodies are mined–the gold-bearing conglomerates of the Witwatersrand Basin and the platinum-bearing pyroxenites of the Bushveld Complex. Both bodies extend to depths of several kilometers, and mining depths exceed 3.5 km (Durrheim, 2010). The current regional stress field is extensional but tectonically inactive. Mining-induced earthquakes are accompanied by collapses of up to ~1 m in the vertical that contract galleries in the form of horizontal tabular voids for up to several kilometers of their lengths. Earthquakes up to m_b 5.6 have occurred (President Brand mine, Welkom, in 1994).

The problem of induced seismicity in South Africa became apparent early in the 20th century when mining penetrated to several hundred meters depth. It is now a major issue and great efforts are made to mitigate the risk. These include development of the safest possible mining techniques, optimal design of equipment, and seismological monitoring. Fatality rates have been reduced but still number several tens of deaths per year (e.g., Amidzic et al., 1999; Boettcher et al., 2015; deBruyn and Bell, 1997; Durrheim, 2010; Durrheim et al., 2013; Durrheim et al., 2006; Heesakkers et al., 2005; Jaku et al., 2001; Julià et al., 2009; Kozlowska et al., 2015; Lippmann-Pipke et al., 2011; Milev and Spottiswoode, 2002; Richardson and Jordan, 2002; Wright et al., 2003; Yabe et al., 2015; Ziegler et al., 2015).

An example is a M_L 4.0 event that occurred in Western Deep Levels East gold mine in 1996. It nucleated in complex geology ahead of

[4] https://www.gov.uk/government/statistical-data-sets/historical-coal-data-coal-production-availability-and-consumption-1853-to-2011.

[5] http://www.dmm.org.uk/mindex.htm.

Fig. 14. Destruction in the church of Santiago resulting from the 2011 M_W 5.1 Lorca, Spain, earthquake (https://en.wikipedia.org/wiki/2011_Lorca_earthquake).

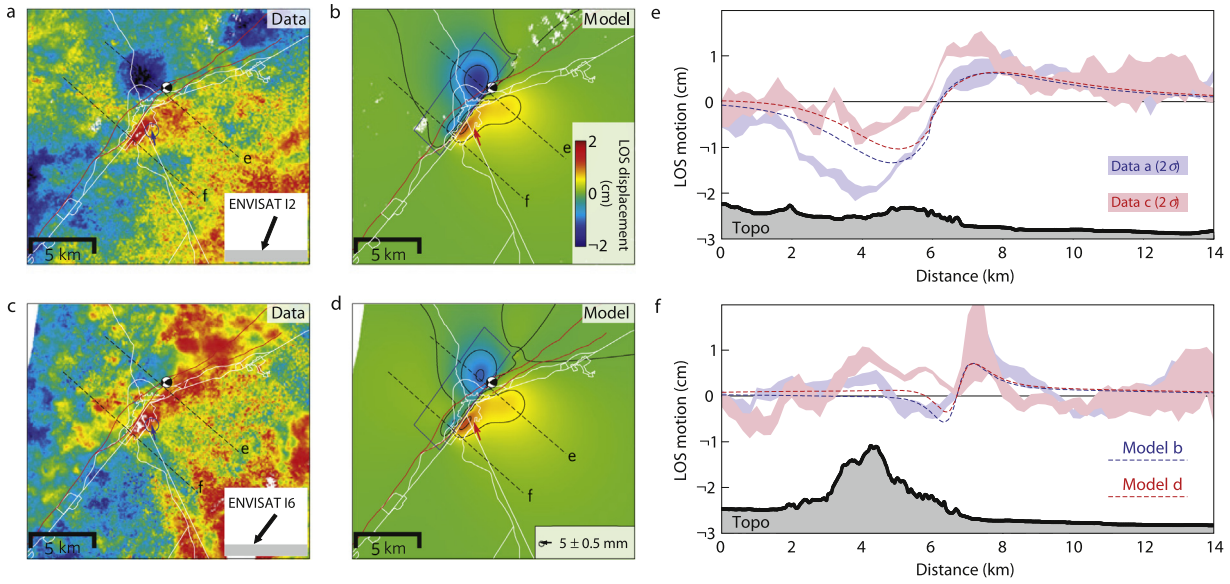

Fig. 15. (a–d): Ground deformation data and model for the 2011 M_W 5.1 Lorca, Spain, earthquake. (a and c): Descending line-of-sight (LOS) displacement map and horizontal GPS vector; (b and d): distributed slip model predictions. Insets in a and c indicate LOS angle, positive values away from the satellite. Blue rectangle: fault surface projection; dashed lines: profile locations; (e and f): observed and simulated data along two profiles, and local topography.
(From González et al. (2012).)

mining and extensively damaged the area. Work had involved removing a large pillar left by earlier, smaller-scale mining. This damaging earthquake had a significant impact and resulted in improved seismicity management strategies (Amidzic et al., 1999).

An even larger event, with M_L 5.3, occurred in the Klerksdorp district, South Africa, in 2005. It seriously damaged the nearby town of Stilfontein, injuring 58 people. Two mineworkers in a nearby gold mine were killed and thousands of others were evacuated. This earthquake was attributed to stress loading by past mining (Durrheim et al., 2006). It highlighted the problem of poor documentation of historic mining activities, a difficulty faced by all nations with long traditions of mining. It also showed that earthquakes induced by one industrial project can endanger others nearby. Its delayed occurrence illustrates that seismic hazard may remain a problem after mine closure.

McGarr (1992a) used the exceptionally high-quality data collected on the state-of-the-art monitoring networks installed in deep South African gold mines to derive full moment tensors for 10 Witwatersrand mining-induced earthquakes with M 1.9–3.3. The earthquakes were of two types. Seven involved substantial coseismic volumetric reduction combined with normal faulting and three had no significant volumetric component. Those with volumetric components probably involved interaction between a mine stope and a shear fault (McGarr, 1992a).

These conclusions were confirmed by later workers. Julià et al. (2009) obtained focal mechanisms for 76 mine tremors with M 0.5–2.6 at the deep AngloGold Ashanti Savuka gold mine. These events were recorded on 20 high-frequency geophones in the mine. The largest

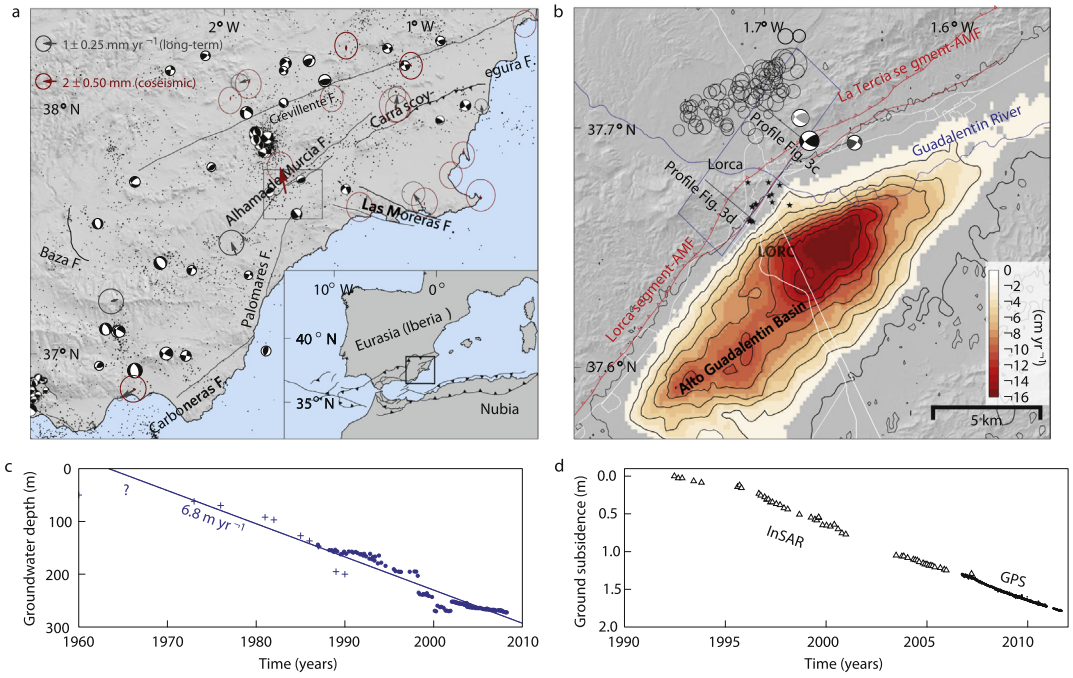

Fig. 16. Location and kinematics of the Lorca earthquake. a: southwest Spain seismicity (2000–2010), focal mechanisms (1970–2010), long-term GPS velocity (2006–2011, gray) and coseismic vectors (red). Major mapped faults are labeled. b: Lorca city and Alto Guadalentin Basin. Mainshock focal mechanisms (black), pre-shock (light gray), largest aftershock (dark gray), and relocated seismic sequence. Black stars are damage locations, red lines are faults. Contour lines indicate 2 cm/a InSAR subsidence due to groundwater pumping. Blue rectangle: fault surface projection. AMF, Alhama de Murcia Fault. c, Groundwater depth. d, InSAR (triangles) and line-of-sight (LOS)-projected GPS ground-surface subsidence at station LORC. (From González et al. (2012).)

principal stress was vertical and was relieved by a combination of volumetric closure and normal faulting, consistent with the vertical closure of galleries. Richardson and Jordan (2002) studied seismicity associated with five deep mines in the Far West Rand district using data recorded 1994–2000 on in-mine arrays. Seismic rates exceeded 1000 events/day. Some earthquakes occurred within 100 m of active mining faces. Those events were attributed to blasting, stress perturbations from the excavation, and closure of stopes. Other events were distributed throughout the mining region, had M > 3, and were similar to regional tectonic earthquakes.

3.2.2. Solution mining

Solution mining recovers minerals via boreholes drilled into the deposit. A lixiviant–a liquid used to dissolve the target mineral–is pumped into the resource via an injection borehole, circulates through the rock dissolving the mineral, and is extracted via a production well. The lixiviant may be water (e.g., to extract salt), or acid or sodium bicarbonate to extract metals (e.g., uranium, copper, gold or lithium).

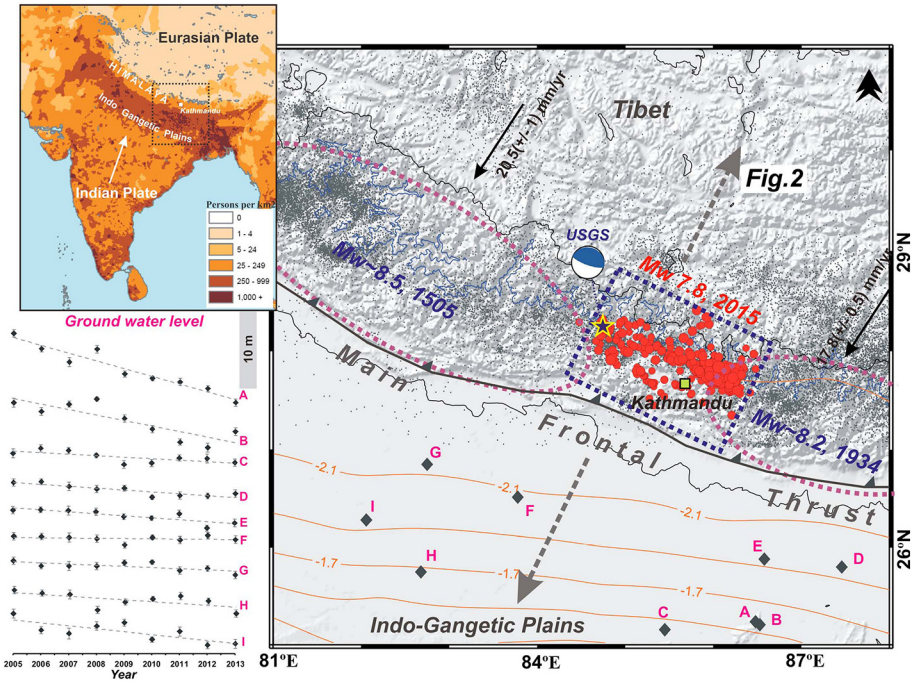

Fig. 17. Seismotectonic context of the 2015 M_W 7.8 Gorkha, Nepal earthquake. Black star: epicenter of the mainshock; red circles: aftershocks; black arrows: convergence rate; gray dots: mid-crustal seismicity 1995–2008; blue contour: 3500-m elevation; ellipses: approximate rupture locations of historic events since 1505; orange contours: anthropogenic groundwater loss in cm/a water thickness for the period 2002–2008 (multiply by 5 to get drop in water table); black diamonds: sampling sites; inset at left: site depletion trends; inset top left: population density (people/km^2).
(From Kundu et al. (2015).)

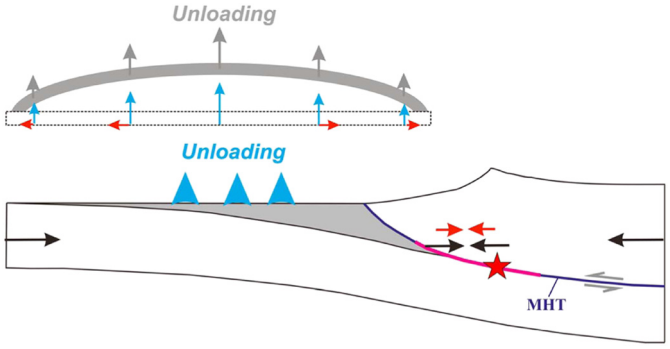

Fig. 18. Schematic diagram showing the effect of unloading by anthropogenic groundwater loss on the Main Himalayan Thrust. Dewatering induces a component of horizontal compression (red arrows) that adds to the secular interseismic contraction (black arrows) at seismogenic depths. Red star: the 2015 Gorkha, Nepal earthquake; pink line: the associated rupture.
(From Kundu et al. (2015)).

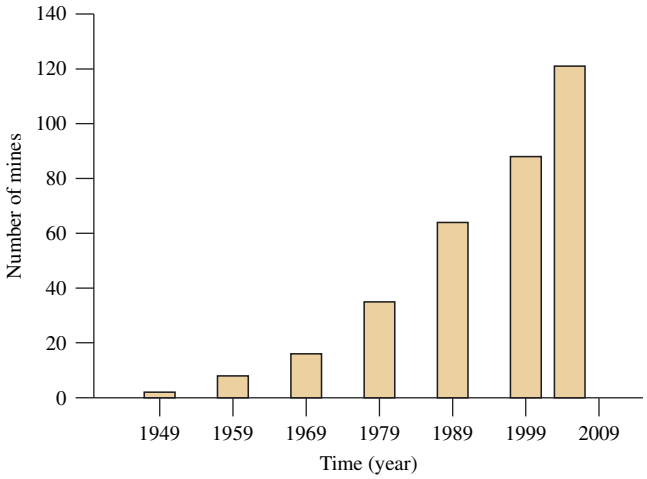

Fig. 20. Number of mines in China with rockburst hazard vs. time.
(From Li et al. (2007)).

Roughly half the world's uranium is produced by solution mining.

HiQuake contains eight cases of seismicity postulated to be associated with solution mining. At the Vauvert Field, France, brine is produced from a layer at 1900–3000 m depth comprising ~50% salt. Water is circulated through fractured zones via a well doublet. Some cavities created dissipate by salt creep but earthquakes occur where this process cannot keep up with mass removal. Seismicity also results from hydraulic fracturing used to create porosity. Over 125,000 earthquakes with M −3 to −0.5 occurred 1992–2007 have been located (Godano et al., 2010).

In the USA three cases are documented, from Attica and Dale (New York) and Cleveland (Ohio). Of three M_L ~5 events that occurred near Attica, in 1929, 1966 and 1967, two had hypocentral depths as shallow as 2–3 km (Herrmann, 1978). They are postulated to have been induced by salt solution mining (Nicholson and Wesson, 1992).

In China, a M_L 4.6 earthquake occurred in 1985 in association with solution mining of salt from depths of 800–1800 m at the Zigong salt mine, Sichuan Province (Li et al., 2007). This earthquake induced the highest intensity of ground shaking measured for any mining-induced earthquake in China. It is the largest mining-related event of any kind known from China.

At Mishraq, Iraq, earthquakes occurred in association with mining of sulfur by injecting hot (~150 °C) water at pressures of 0.6–0.8 MPa into layers up to 190 m deep (Terashima, 1981). Surface subsidence of up to several mm/day resulted in surface cracking. Felt earthquakes occurred 1973–1975 and were most numerous at times of high injection rate.

3.2.3. *Tunnel excavation*

Earthquakes accompanying excavation of tunnels and cavities have been reported in 20 cases. These include excavations for power-station housing (e.g., the underground powerhouse of the Pubugou, China hydroelectric station), water transport at hydro-electric and nuclear power stations (e.g., the Yuzixi hydro-electric station, China, and the Forsmark nuclear plant, Sweden), and road and railway transport (e.g., the Ritsem tunnel, Sweden, and the Qinling railway tunnel, China) (Tang et al., 2010).

The 57-km-long Gotthard Base Tunnel, Switzerland, part of the New Alpine Traverse through the Swiss Alps (Husen et al., 2012), was excavated for freight and passenger rail transport 2002–2006 using drilling and blasting. Three “Multi-Function Stations” (MFSs) divide the tunnel into five sections.

A series of 112 earthquakes with M_L −1.0 to 2.4 occurred

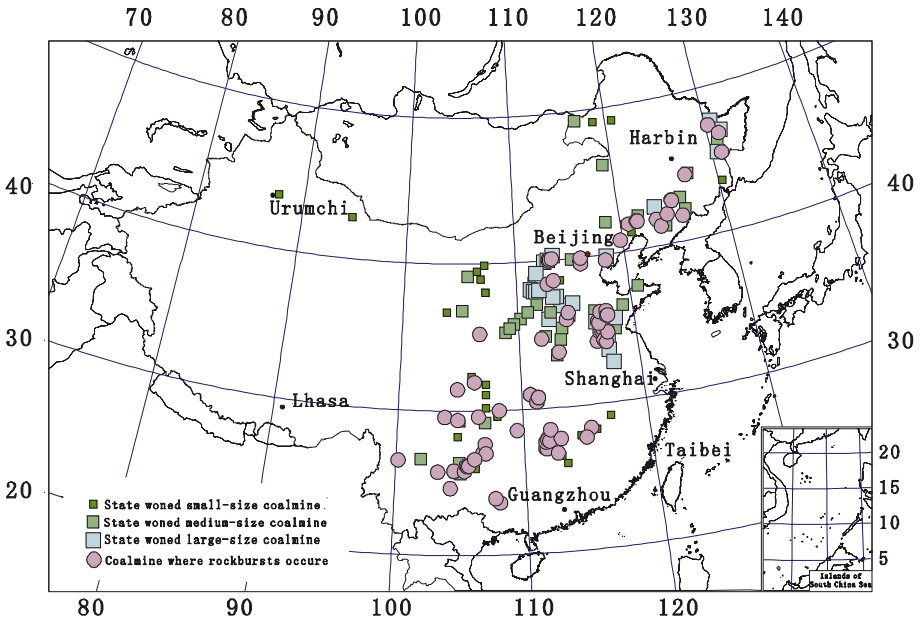

Fig. 19. Map of China. Green squares: Small, medium and large state-owned coal mines. Pink dots: Coal mines where mining-induced seismicity occurs.
(From Li et al. (2007)).

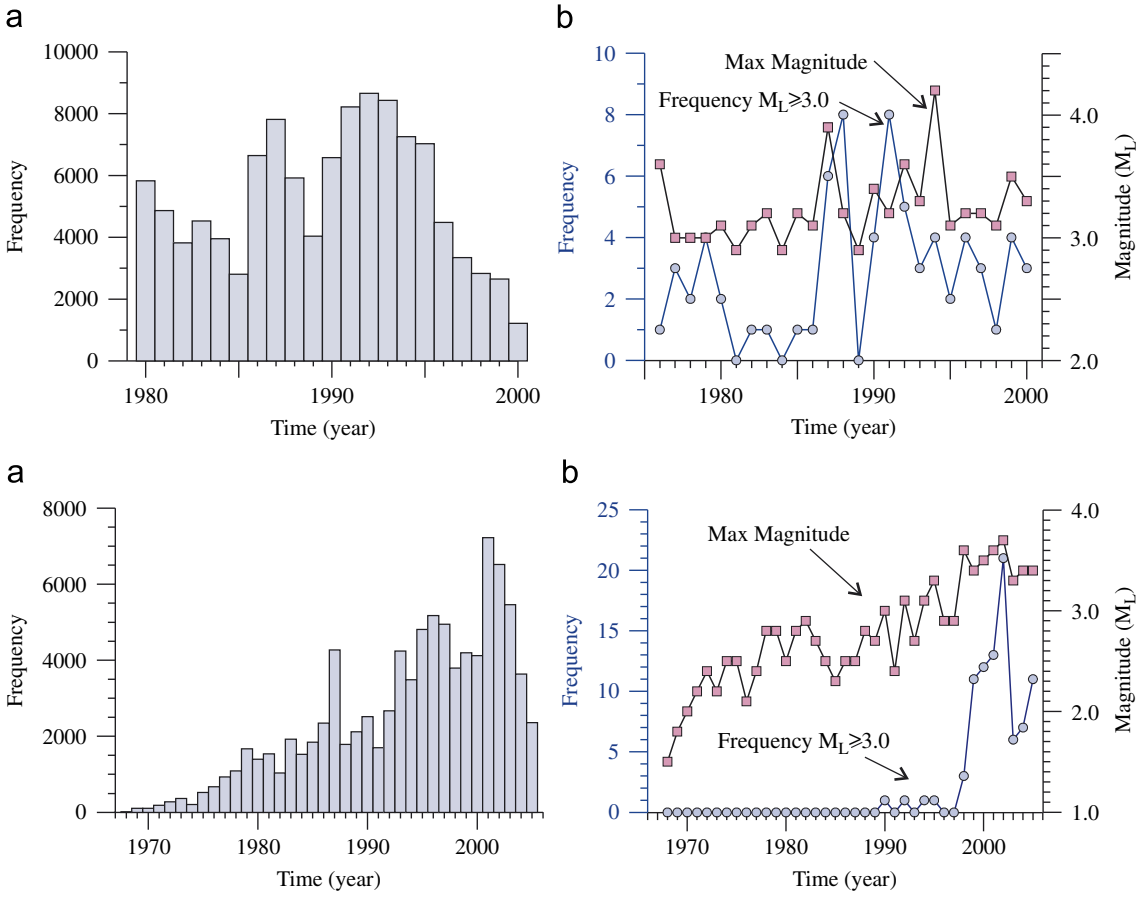

Fig. 21. Top panels: Mining-induced earthquakes at Mentougou coal mine, Beijing, (a) events M > 1.0, (b) events M > 3.0 and the maximum event magnitudes. Bottom panels: same as top panels except for the Fushun coal mine field in Liaoning Province.
(From Li et al. (2007)).

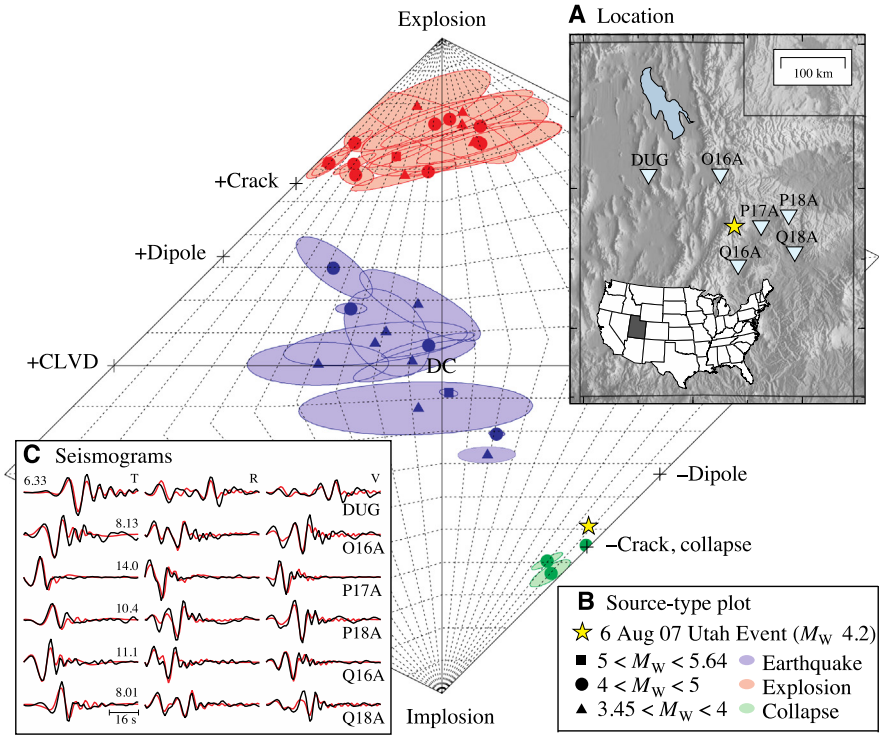

Fig. 22. (A) Locations of the 6 August 2007 Crandall mine, Utah, earthquake and six of the closest USArray and Advanced National Seismic System (ANSS) seismic stations. (B) Source-type plot showing separation of populations of earthquakes, explosions, and collapses. Yellow star shows the focal mechanism solution. (C) Observed seismograms (black) compared to synthetics (red) for the solution, which is similar to a horizontal closing crack (B). The maximum displacement (10–7 m) of each set of tangential (T), radial (R), and vertical (V) observations is given.
(From Dreger et al. (2008).)

Fig. 23. Surface imprints of Neolithic flint mining at Grimes Graves, Suffolk, England (www.english-heritage.org.uk).

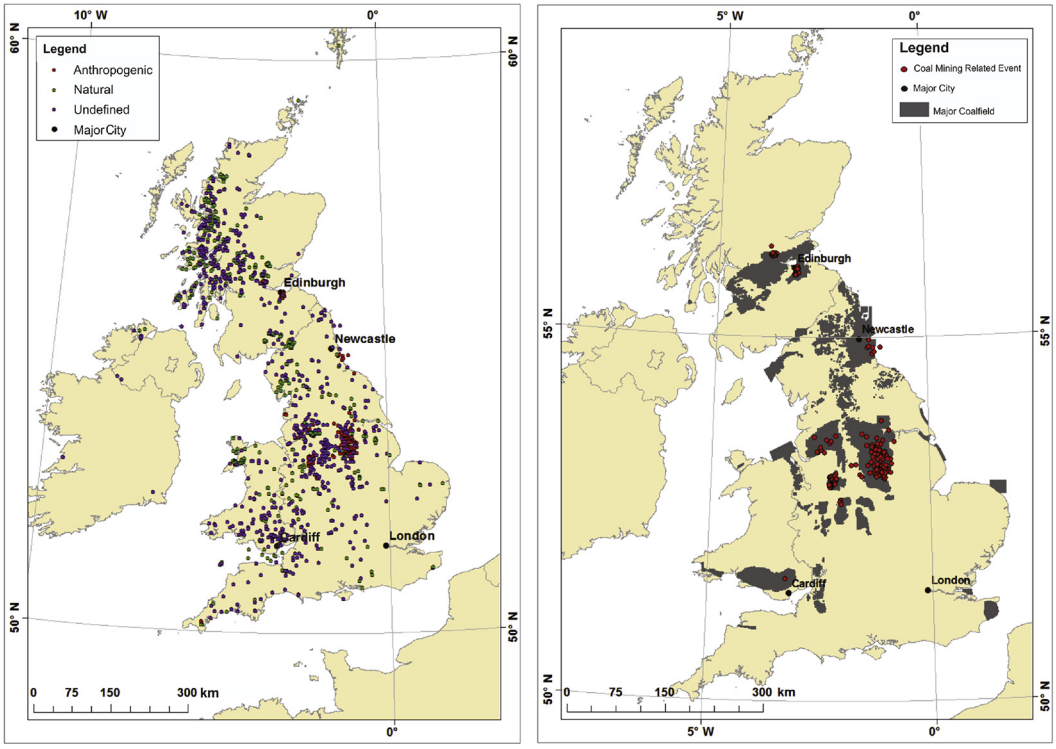

Fig. 24. For earthquakes with $M_L \geq 1.5$ for the period 1970–2012, left: map of the UK showing 1769 onshore seismic events categorized as anthropogenic (red), natural (green) and undefined (purple). Right: 369 events postulated to be induced by coal mining. These correlate spatially with major coalfields (dark gray).
(From Wilson et al. (2015).)

2005–2007 in association with excavation of the southernmost station, MFS Faido. The largest event was just 0.5–1.0 km deep and felt strongly at the surface. The station cavity was damaged including flaking of the reinforced walls and upwarping of the floor by ~0.5 m. The seismicity correlated spatially and temporally with excavation of the station (Figs. 26 and 27). Accurate locations obtained using a dense, temporary seismic network showed that the earthquakes occurred at a similar depth to the tunnel. Some correlated with rockbursts in the tunnel shortly after blasting.

The focal mechanism of the largest earthquake indicated normal faulting on a steep plane 50–170 m long belonging to the local fault system. The tunnel traverses igneous and metamorphic rocks and a complex of structures with different rheological properties, including faulted and heavily fractured sections. Modeling suggested the earthquakes resulted from an unfavorable juxtaposition of rocks with different rheologies in a fault zone. The horizontal stresses added by the excavations were relieved by shrinking of the tunnel which reactivated the fault zone.

3.3. Hydrocarbons

Suckale (2009, 2010) reviewed seismicity induced by hydrocarbon production. There are ~67,000 hydrocarbon fields worldwide (Li, 2011) including ~1500 giant and major fields, and ~1,000,000 producing oil and gas wells. Seismic response to production varies and no seismicity is reported for most fields. Reporting is, however, incomplete, and many fields are not instrumented (Section 7.1). Earthquakes account for only a small percentage of the deformation associated with reservoir compaction with the majority being taken up by ground subsidence or counteracted by fluid recharge from the sides.

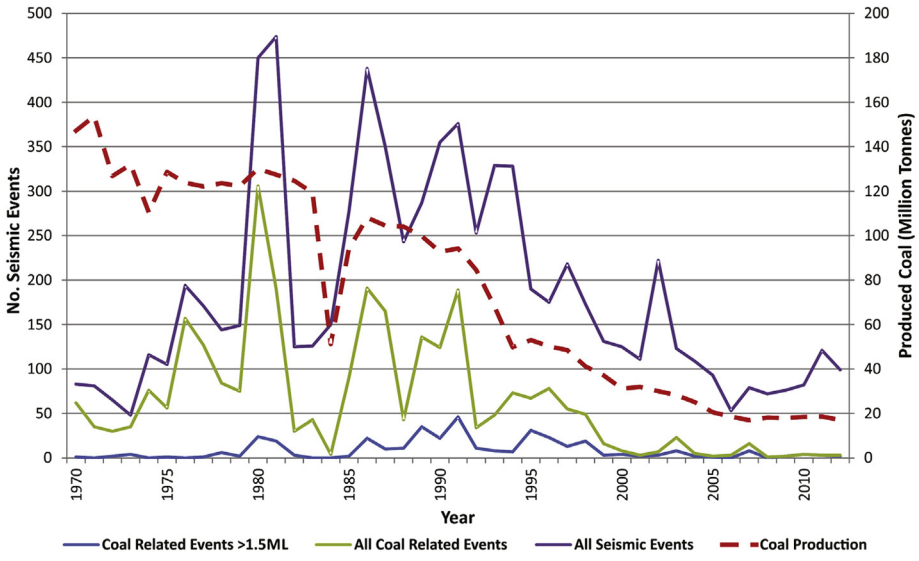

Fig. 25. UK coal production (dotted red line) vs. numbers of earthquakes postulated to be induced (blue line: $M_L \geq 1.5$, green line: all postulated coal-related events, purple line: all located earthquakes in the British Geological Survey database) for the period 1970–2012. The effect of the miners' strike of 1984 can be seen clearly in the drop in production and seismicity.
(From Wilson et al. (2015).)

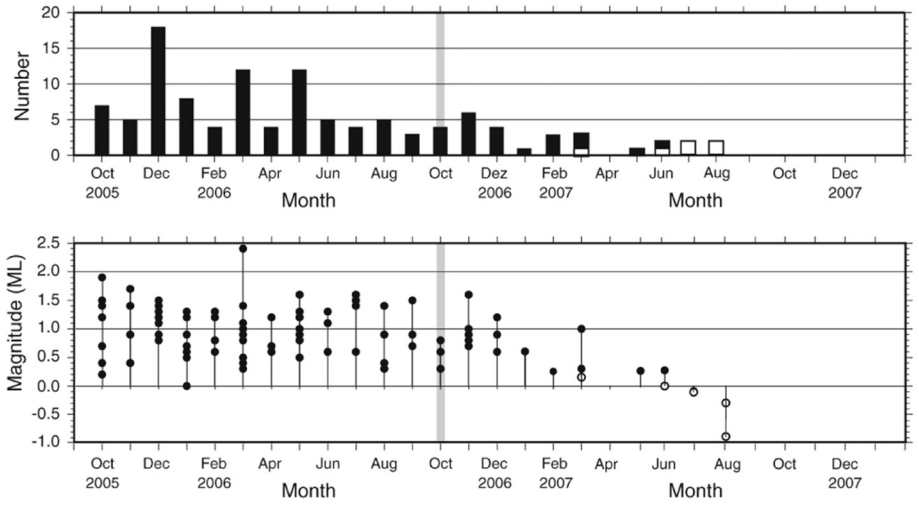

Fig. 26. Temporal evolution of the seismicity observed in the vicinity of the multi-function station Faido, Switzerland, October 2005–December 2007. Top: number of events per month. Bottom: local magnitudes. Open circles: earthquakes for which magnitude could only be computed using data from one station. Gray band marks the end of the excavation work.
(From Husen et al. (2012).)

The earthquakes reported often occur on faults that were either previously unknown or considered to be inactive.

3.3.1. Gas

There are 36 cases of seismicity postulated to have been induced by extraction of natural gas. These are from Canada (1 case), China (1 case), France (2 cases), Germany (7 cases), Italy (1 case), the Netherlands (18 cases), Oman (1 case), the USA (4 cases) and Uzbekistan (1 case).

The most extreme case is that of the Gazli reservoir, Uzbekistan. In 1976 and 1984, three M_S ~7 earthquakes occurred, seriously damaging the local town of Gazli and causing one death and ~100 injuries (Simpson and Leith, 1985). An additional M_S 5.7 event occurred in 1978. Events occurred as follows:

1956 the Gazli field was discovered;
1963 pipelines to the Urals industrial region were completed;
1966 production of ~20 × 10^9 m^3/year of gas began. Reservoir pressure was ~7 MPa;
1968–71 production peaked;
1976 pressure had declined to 3–3.5 MPa; two M_S ~7 earthquakes occurred;
1978 a M_S 5.7 earthquake occurred;
1984 a M_S ~7 earthquake occurred;
1985 pressure had declined to 1.5 MPa.

Gas was produced from a reservoir at ~2 km depth, hosted in an open anticline of tight Paleogene sandstones. This structure is cut by several blind faults and the M_S ~7 earthquakes are thought to have occurred on one of these (Fig. 28). Fault-plane solutions suggest that they occurred on a north-dipping, easterly striking thrust fault, consistent with regional tectonics. Extrapolation of this fault to shallow depth suggests that it intersects with the gas reservoir. In addition to this geometric correspondence, Simpson and Leith (1985) cite as additional evidence that these events were induced:

- previous seismic quiescence;
- an anomalous magnitude distribution which involved three M_S ~7 events rather than a mainshock-aftershock sequence;
- the large decrease in pressure in the reservoir; and
- unusual downwards rupture propagation.

That these earthquakes were induced has been challenged, e.g., by Bossu et al. (1996), on the grounds that the stress perturbation on the fault was too small to have triggered such large earthquakes. Possible analyses of this case are limited because data on operations are sparse. However, the Gazli case is important because of its implications for the maximum possible magnitude of earthquakes that could be induced by gas extraction.

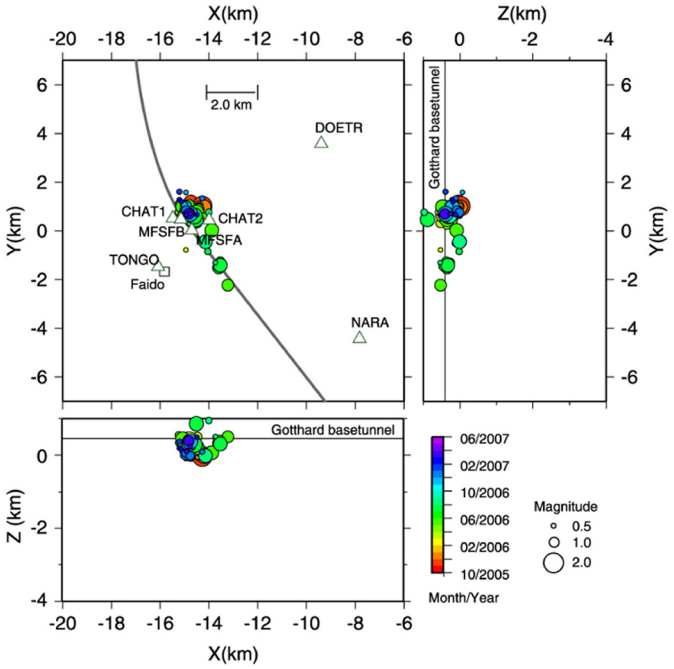

Fig. 27. Hypocenter locations of earthquakes in the vicinity of the multi-function station Faido, Switzerland, October 2005–June 2007.
(From Husen et al. (2012).)

The largest such postulated earthquake in Europe is the 1951 M 5.5 event that occurred in the previously aseismic Caviaga Gasfield, Po Valley, Italy (Caloi et al., 1956). There, large-scale extraction of methane at pressures > 10 MPa had been underway. The earthquake cannot be well studied because limited instrumentation was in place at the time. Simple analysis of paper recordings suggested that the largest, M_L 5.5 event, nucleated at ~5 km depth and had a thrust mechanism.

The case of Caviaga is the only M ≥ 5 gas-extraction-induced earthquake reported for Europe. Several other European gas-extraction projects are associated with M ≥ 4 seismicity. The Lacq Gasfield, France, has generated earthquakes up to M_L 4.2 and > 2000 were located there from 1974 to 1997 (Bardainne et al., 2008).

Production at Lacq started in 1957 with extraction of gas from a depth of 3.2–5 km, beneath a 600-m-deep oilfield. The reservoir occupies a 20-km-long fractured anticline in Mesozoic limestones sealed by Cretaceous marl. Reservoir pressure decreased from 66 MPa to 2.3 MPa 1957–2008 and the surface subsided ~6 cm.

The first earthquake noticed, the 1969 M 3–4 event, occurred after the gas pressure had declined to 36 MPa. This, and the subsequent seismicity, are unlikely to have been natural because of their location in the gas field and because Lacq is 30 km north of the nearest seismically active structure, the Pyrenean Frontal Thrust. About 70% of the earthquakes located above the gas reservoir, many on faults optimally-oriented with respect to the stress perturbation caused by gas removal. Poorly oriented faults tended to be aseismic. There is poor correlation between the surface subsidence and the seismicity. Seismicity migrated from the center to the periphery of the reservoir (Fig. 29). Comparison of the distribution of hypocenters with deformation models favored the model of Odonne et al. (1999) rather than that of Segall (1989) (Fig. 30).

In The Netherlands, ~300 gas fields are produced. Of these, just a few percent are seismically active but globally this is a high rate of reported seismogenesis. The induction mechanism is thought to be differential compaction (Gee et al., 2016).

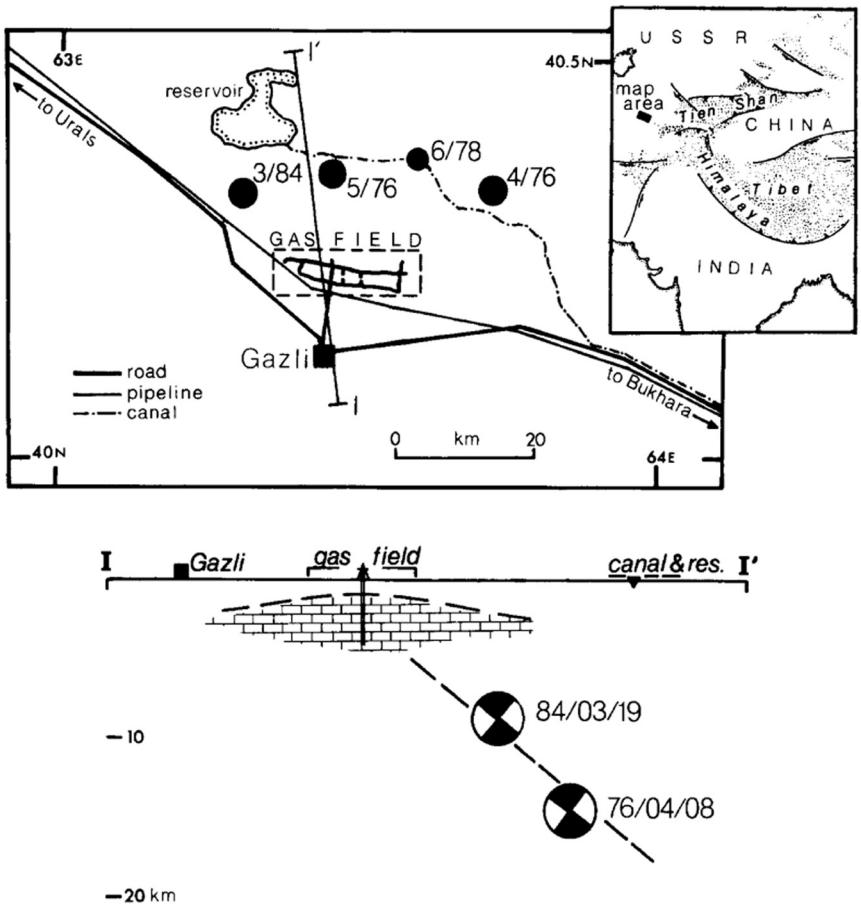

Fig. 28. Top: Map of the Gazli, Uzbekistan, area showing epicenters of the three M ~7 earthquakes in 1976 and 1984, and the M 5.7 earthquake in 1978. Bottom: Cross-section with hypocenters projected at their distance from the town of Gazli, with focal mechanisms of the M_S 7.0 events of 8 April 1976 and 19 March 1984. The fault plane (dashed line) is deduced from geodetic data. (From Simpson and Leith (1985).)

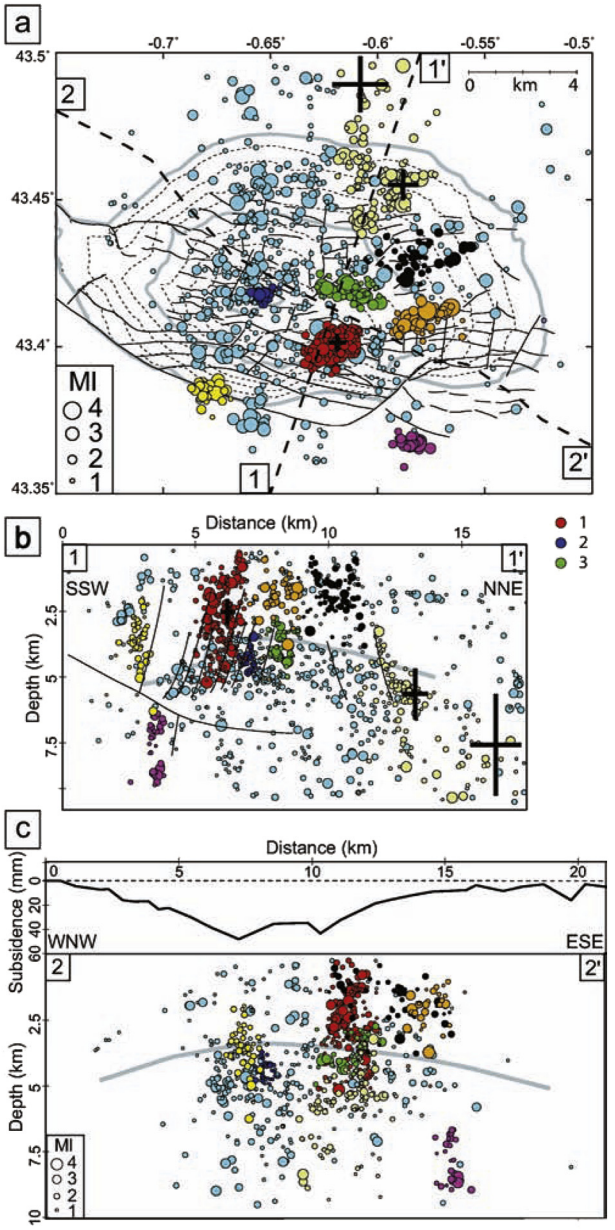

Fig. 29. Seismicity in the Lacq Gasfield, France. (a) Map view and location of cross-sections. Inset shows location in the region. (b) SSW-NNE cross-section and (c) WNW-ESE cross section. Colors: different earthquake clusters; dashed and solid gray lines: isobaths of the gas field; black lines: faults; crosses: location uncertainties for three swarms. (From Bardainne et al. (2008).)

One of the largest earthquakes attributed to induction in The Netherlands is the 2012 Groningen M_L 3.6 event. In addition to this a further 8 events with M > 3.0 have occurred in that field (Fig. 31). Seismicity was first recorded in December 1991 when the reservoir reached ~28% depletion, some 28 years after the start of gas extraction in 1962 (Fig. 32).

The Netherlands has a low rate of historic seismicity compared with neighboring countries where much higher rates are associated with the Upper Rhine Graben (Figs. 33 and 34) (van Eck et al., 2006). Currently, the majority of earthquakes in the northern Netherlands is associated with gas extraction. Several hundred have been recorded in the Groningen Field. This reservoir, the largest natural gas field in Europe and the tenth-largest in the world, originally contained ~3×10^9 m^3 of gas in a porous sandstone formation up to 300 m thick and 45 × 25 km in area. Both the seismic rate and the magnitudes of the largest

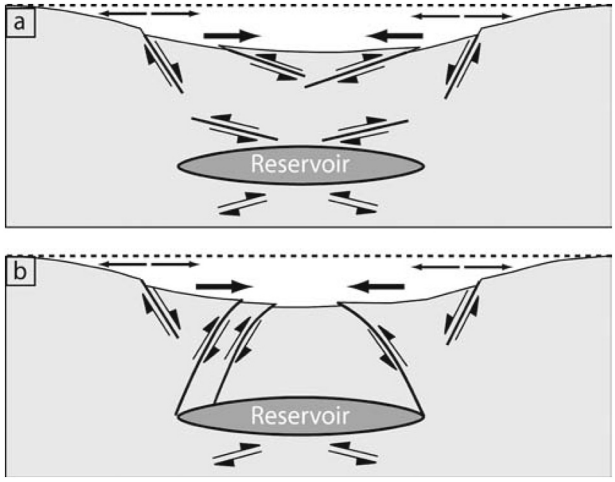

Fig. 30. Deformation models of (a) Segall (1989), and (b) Odonne et al. (1999) for a depleting subsurface reservoir. Both models predict extensional deformation on the flanks and compressional deformation centrally in the field. (From Bardainne et al. (2008).)

earthquakes have increased with time (Fig. 32). An apparent increase in the slope of the Gutenberg-Richter distribution (the "*b*-value") with time is consistent, however, with a progressive reduction in the proportion of large to small earthquakes (van Eck et al., 2006; Van Wees et al., 2014). Reservoir compaction is greatest in two northwesterly trending zones of the reservoir and the earthquakes correlate with the southernmost of these (Fig. 35).

A renowned case in the USA is the Fashing Gasfield, Texas (Fig. 36) (Pennington et al., 1986). Production there started in 1958 from 3.2 km depth. By 1983 the pressure had decreased by ~7 MPa and a M 3.4 earthquake occurred (Fig. 37). The depleting reservoir was replenished by reinjecting produced water. In 1992 a M 4.3 earthquake occurred and in 2011 a M_W 4.8 event. This case is usually considered jointly with the nearby Imogene Oilfield (Section 3.3.2).

3.3.2. Oil

In many oilfields multiple processes are underway simultaneously including oil and gas extraction, waste-water disposal, water injection to aid oil recovery and hydrofracturing or thermal fracturing. It may thus be difficult to attribute unambiguously any seismicity to oil extraction alone (Section 1.7). Nevertheless, we have identified eight cases where earthquakes have been postulated to be associated with oil extraction. These are from the USA, Iran, Russia and Norway. This is very few compared with the ~1,000,000 producing oilfields worldwide (Section 3.3).

One of the earliest reports of earthquakes accompanying oil production is from Goose Creek, Texas, where small earthquakes occurred in the 1920s (Fig. 38). Following the extraction of several million barrels of oil an area ~10 km^2 in size subsided by up to 1 m over an ~8-year period (Nicholson and Wesson, 1992; Pratt and Johnson, 1926). Goose Creek is a coastal region and a substantial area sank below sea level requiring industrial infrastructure to be adapted to the flooded conditions.

The largest earthquake attributed to oil extraction in *HiQuake* is the M_W 6.2 1983 Coalinga, California, event. This event, along with the 1985 M_W 6.1 Kettleman North Dome earthquake and the 1987 M_L 5.9 Montebello Fields (Whittier Narrows) earthquake, both in California, were attributed to the removal of oil from fields in uplifting anticlines (McGarr, 1991). The Coalinga and Whittier Narrows events were widely felt and caused multiple deaths and injuries (Fig. 39).

All three events nucleated at ~10 km depth. McGarr (1991) suggested that net extraction of oil and water reduced the average density of the upper crust, and that the seismic deformation approximately

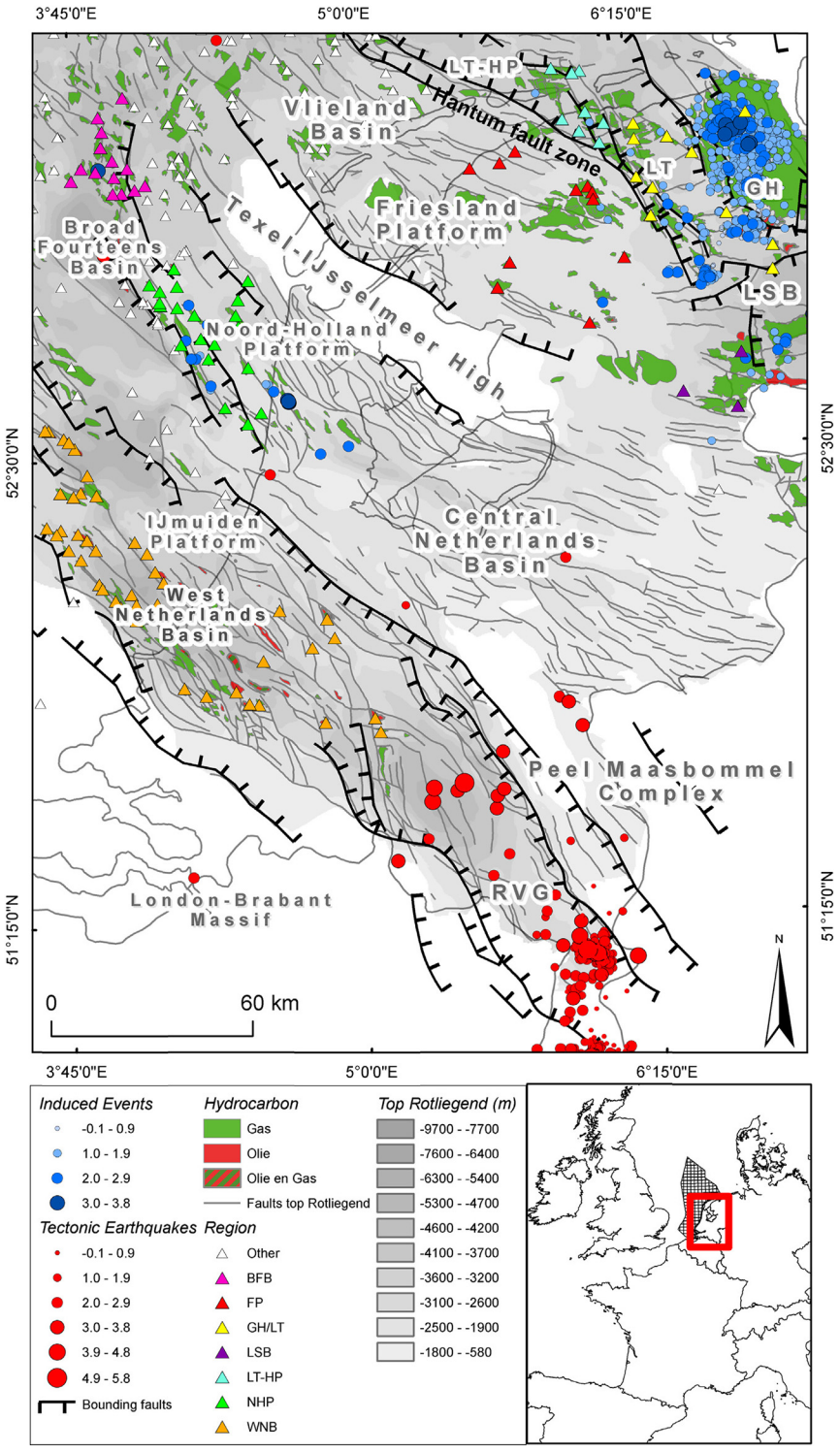

Fig. 31. Tectonic map, seismicity, and hydrocarbon reservoirs in the Netherlands. Regional location of the main map is shown in the lower right panel. Red circles: natural seismicity; blue circles: induced seismicity; green: gas reservoirs; red: oil reservoirs; solid lines: major fault zones; triangles: where leak-off tests have been performed. BFB = Broad Fourteen Basin, FP = Friesland Platform, GH/LT = Groningen High/Lauwerszee Trough, LSB = Lower Saxony Basin, LT-HP = Lauwerszee trough-Hantum Platform, NHP = Noord Holland Platform, WNB = West Netherlands Basin, RVG = Roer Valley Graben, PB = Peelrand Block, EL = Ems Low. (From Van Wees et al. (2014).)

restored isostatic equilibrium (Fig. 40). This was challenged by Segall (1989) who concluded that depletion of the reservoir would have only loaded the nucleation region by ~0.01–0.03 MPa. Nicholson and Wesson (1992) suggested that the earthquake might have occurred in response to larger stresses imposed by fluids migrating into the mid-to-lower crust. They suggested changes in pressure resulting from withdrawal of oil induced fluid migration and brought the fault closer to failure. The Coalinga earthquake has also been attributed to extraction of groundwater for irrigation from the nearby San Joaquin valley (Section 3.1) (Amos et al., 2014). The Coalinga earthquake contributed to stress released six years later in the 1989 M_W 6.9 Loma Prieta earthquake. This event ruptured a section of the San Andreas fault system 96 km south of San Francisco causing 63 deaths, 3757 injuries and $5.6–6 billion of damage (Reasenberg and Simpson, 1992). The 1933 M_L 6.3 Long Beach, California, earthquake which killed > 100 people and did $40 million of damage may have resulted from oil production in the nearby Wilmington and Huntington Beach Oilfields (Section 4.1.3) (Nicholson and Wesson, 1992).

There is little dispute that earthquakes were induced primarily by oil extraction from the Imogene Oilfield, Texas (Pennington et al.,

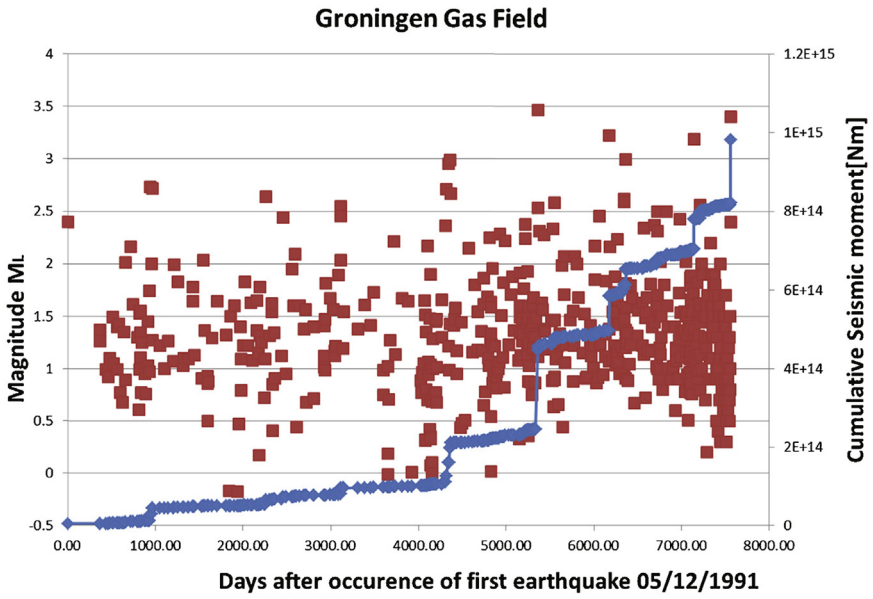

Fig. 32. Magnitude of induced events in the Groningen Gasfield, Netherlands, 5 December 1991–16 August 2012, and cumulative seismic moment in N m.
(From Van Wees et al. (2014).)

1986). This field lies ~25 km from the seismogenic Fashing Gasfield (Section 3.3.1; Fig. 36). In 1984 a M_L 3.9 earthquake occurred in the Imogene Oilfield, followed by aftershocks 2–3 km deep near the reservoir bounding fault.

The Imogene Oilfield occupies Cretaceous limestone bounded by high-angle faults that splay at shallow depth. Production began in 1944 from a 33-m-thick horizon at 2.4 km depth. By 1973 reservoir pressure had dropped from 25 MPa to ~10 MPa. It was flooded 1972–1978 with 55,000 m^3 of water via injection wells to mitigate this pressure reduction. This is, however, much less than the ~1 million m^3 of oil and gas produced, and flooding ceased several years before the 1984 earthquake. As a consequence, the seismicity has been attributed to depressurization of the field as a result of oil depletion.

The most spectacular example of subsidence and induced earthquakes associated with a producing oilfield is that of the Wilmington Field, California (Figs. 41 and 38). Oil production began in 1936 and over the following 30 years up to 9 m of subsidence and 3.6 m of horizontal contraction occurred. Strain rates were >1000 times greater than along locked sections of the San Andreas fault (Kovach, 1974; Segall, 1989).

Earthquakes began to occur above and below the reservoir when reduction in pressure reached ~10 MPa. Eight earthquakes with M_L 2.4–5.1 occurred on shallow, low-angle bedding planes. The largest, which occurred in 1949, sheared off hundreds of production wells causing >$9 million of damage. An area of ~5.7 km^2 was affected and up to 20 cm of ground deformation occurred (Nicholson and Wesson, 1992; Segall, 1989). Seven of the earthquakes occurred during the oil production period and one after significant water flooding began in 1958 to mitigate the subsidence. No further earthquakes occurred after 1961 and subsidence had been arrested by 1966. In this case seismicity may have been stopped, rather than induced, by the introduction of fluids.

Despite large quantities of oil being produced in the Middle East there are only two accounts of earthquakes postulated to have been induced by extraction there. One reports hundreds of earthquakes up to M_L 4.24 in the Uthmaniyah-Hawaiyah and Haradh divisions of the Ghawar oil/gas field, Saudi Arabia. These earthquakes occurred underneath producing horizons and are attributed to fluid extraction. Focal mechanisms suggest the active elements are crust-penetrative basement faults (Mogren and Mukhopadhyay, 2013).

The other example is from Kuwait, where 465 M 0.3–4.3 earthquakes occurred 1997–2007. A large percentage occurred in the oilfields, including the Sabiriyah, Raudhatain, Bahra, Minagish, Umm Gudair, Wafra, Abduliyah and Dharif Fields (Fig. 42). Some of this activity is likely associated with oil extraction (Al-Enezi et al., 2008). The largest proposed induced event related to Middle Eastern oilfields is the 1993 M 4.7 event in Kuwait. It may have been induced by the 1990 gushing and burning of oil wells by Iraqi armed forces leading to rapid pore pressure reduction and changes in subsurface stress (Bou-Rabee and Nur, 2002).

3.4. Geothermal production (heat/fluids)

Small, natural earthquakes are common in wet, high-temperature geothermal areas, and were known in Iceland as “hverakippur” (trans: “hot-spring bump”) before they were studied scientifically. They are likely caused by a combination of active tectonics in plate-boundary zones and volcanoes, and natural geothermal heat loss. The latter causes cooling and contraction of the geothermal heat source and stress is relieved by rock fracturing with a component of tensile failure. Both the opening and closing of voids have been identified seismically (Foulger, 1988a, 1988b; Foulger and Long, 1984; Foulger et al., 1989; Miller et al., 1998a; Miller et al., 1998b; Ross et al., 1999). Production from geothermal fields by extraction of hot fluids will enhance natural fluid- and heat-loss and may increase seismic rates.

As for hydrocarbon reservoirs, it may be difficult to attribute confidently earthquakes in exploited geothermal areas where multiple processes are underway. They may also be induced by natural recharge, either shallow, cold groundwater or deep hot water. *HiQuake* contains only six cases where earthquakes are postulated to have been induced by geothermal production. These cases are the Cerro Prieto Field, Mexico (Glowacka and Nava, 1996), the Reykjanes and Svartsengi Fields, Iceland (Keiding et al., 2010), Larderello, Italy (Batini et al., 1985), The Geysers, USA (Eberhart-Phillips and Oppenheimer, 1984) and Olkaria, Kenya (Simiyu and Keller, 2000).

The largest were strike-slip events in the Imperial Valley (1979, M_L 6.6), Victoria (~30 km southeast of the Cerro Prieto field; 1980, M 6.1), and at Cerro Prieto (1987, M 5.4) (Fig. 43). Glowacka and Nava (1996) base this proposal on qualitative correlations between increased fluid extraction and seismic moment release, with delays of ~1 year (Fig. 44).

Electrical power production at Cerro Prieto began in 1973. Steam and water at 250–350 °C is produced from 1500 to 3000 m depth. Over 1 km^3 of fluid was extracted 1973–1996. The region is part of the plate

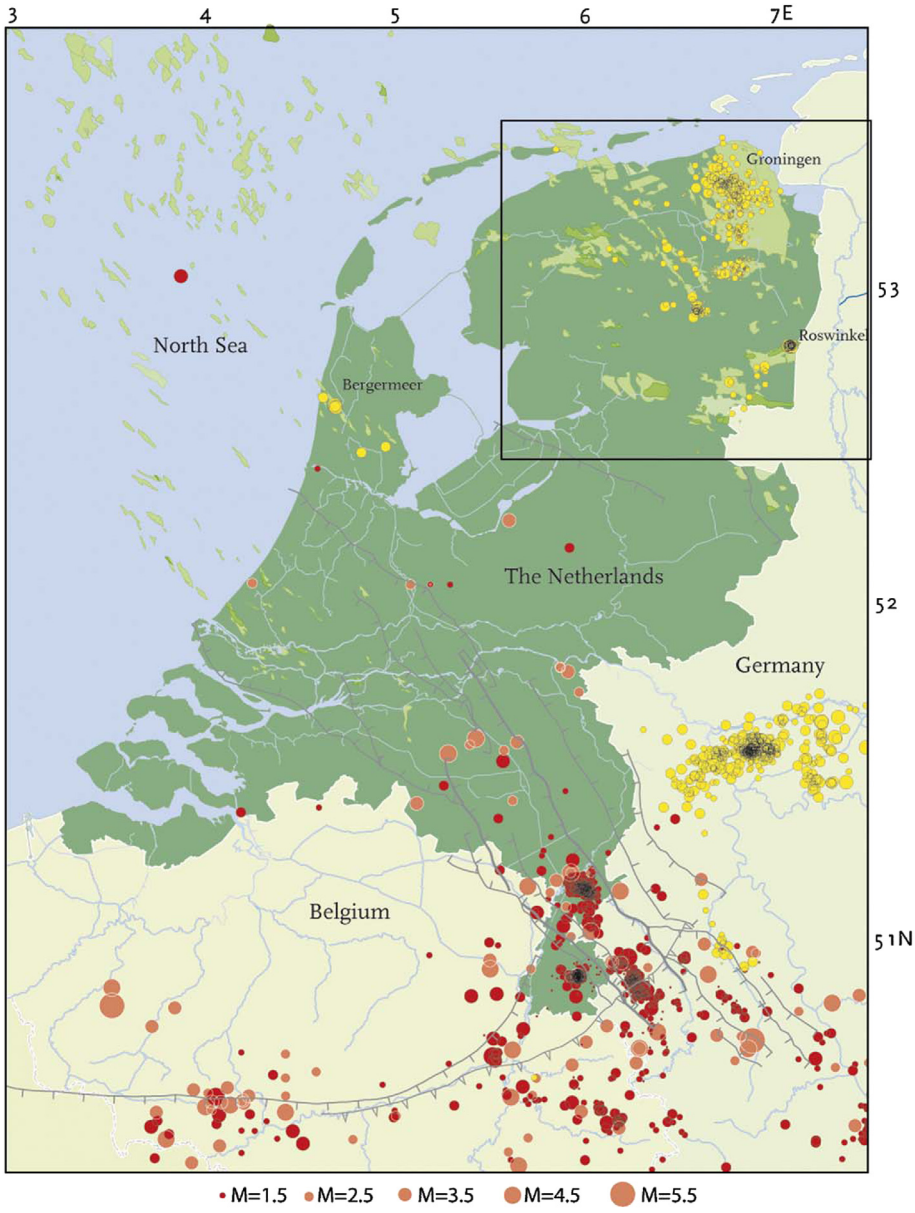

Fig. 33. Seismicity in the Netherlands and surrounding region since 1900. Red circles: natural tectonic earthquakes; yellow circles: suspected induced earthquakes (usually mining or gas exploitation); gray solid lines: mapped faults in the upper-North-Sea formation; light green: gas fields. Detail of boxed region shown in Fig. 34. (From van Eck et al. (2006).)

boundary between the Pacific and North America and tectonics are dominated by the strike-slip Imperial fault which has a history of M > 6 earthquakes. Glowacka and Nava (1996) found the numerical data insufficient to support statistically a correlation between production and large earthquakes but argue that pore pressure decreases of a few MPa in the geothermal field were sufficient to have triggered them. Majer and McEvilly (1981, 1982) suggested, on the basis of data from local, temporary seismic networks, that earlier increases in production correlated with increases in small earthquakes.

Correlation between geothermal production and earthquakes has been proposed at the Reykjanes and Svartsengi geothermal areas, Iceland (Keiding et al., 2010). In some areas, deformation associated with extension along the plate boundary and ~5 cm/a of subsidence resulting from geothermal fluid extraction were detected 1992–2009 using Interferometric Synthetic Aperture Radar (InSAR) and GPS data. Swarms of earthquakes up to M_L 4.1 occurred on the flanks of the rifts containing the geothermal areas. The events were postulated to have been induced by stress changes from geothermal fluid extraction (Fig. 45) but it is not possible to rule out a tectonic origin.

The Geysers geothermal field, California, is a vapor-dominated field that has been exploited for over 150 years, lately generating electricity. It is intensely seismically active (Fig. 46) and earthquakes occurred even before large-scale fluid injections began (Fig. 47). The pre-injection seismicity, and some current seismicity, is likely production-related (Eberhart-Phillips and Oppenheimer, 1984). It is difficult to distinguish production- from injection-related seismicity because both processes are underway simultaneously. Over the last 50 years or so, the seismic rate has, however, correlated grossly with injection (Section 4.1.5).

3.5. *Extraction from the subsurface: summary*

Mining is the commonest cause of extraction-related earthquakes and contributes 267 cases to *HiQuake*. Five cases relate to groundwater and six to geothermal resources. The largest earthquakes postulated to be induced by subsurface extraction are the M_W 7.8 Gorkha, Nepal, earthquake, the M_L 6.1 Bachatsky, Russia, earthquake, the M_S 7.3 Gazli, Uzbekistan earthquake and the M_L 6.6 Cerro Prieto, Imperial Valley, Mexico, earthquake.

In the case of groundwater-withdrawal cases, stress changes as small as 0.001 MPa have been postulated to induce events (e.g., for the 2015

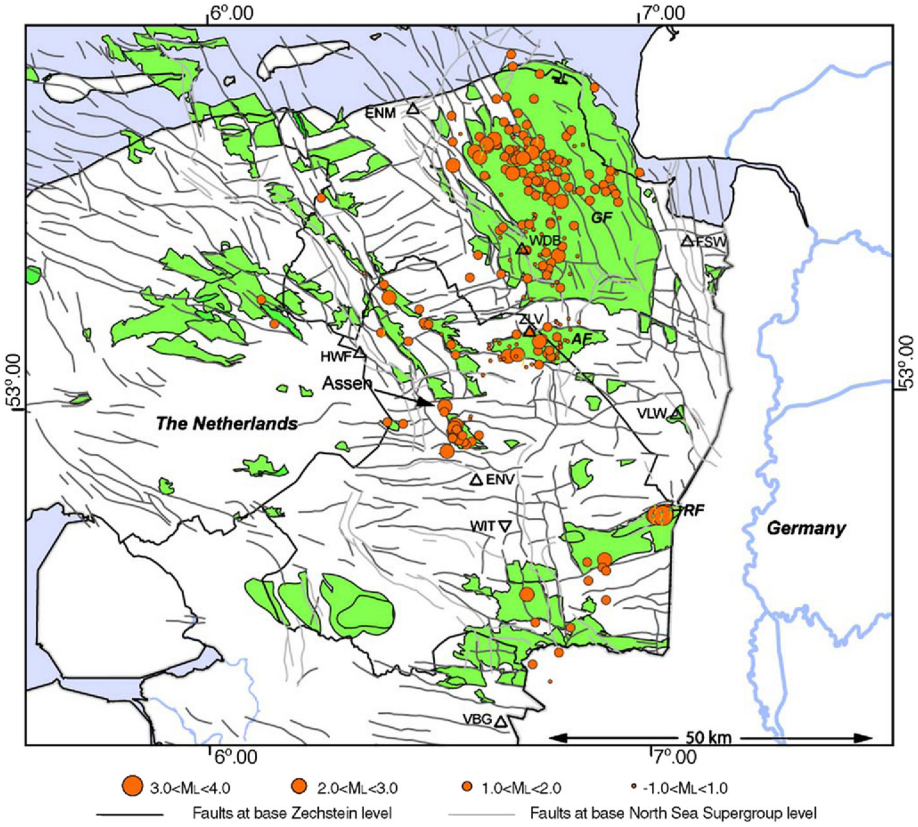

Fig. 34. Map showing produced gas fields (green), major fault structures and seismicity (orange dots) in the northeast Netherlands (boxed region of Fig. 33). RF: Roswinkel Field; GF: Groningen Field; EF: Eleveld Field; AF: Annerveen Field.
(From van Eck et al. (2006).)

M_W 7.8 Gorkha, Nepal, earthquake; Kundu et al., 2015). This is small even compared with Earth tides (Section 7.3). The ability of such small stresses to induce earthquakes is theoretically in keeping with the self-similar, critical earthquake nucleation process. However, such small effects may be comparable to many other natural and anthropogenic processes such as weather and the expansion of cities.

The sizes of postulated gas-extraction induced earthquakes are shown in Fig. 48 for the 35 cases where this parameter is reported. There is a continuous spectrum of sizes with the exception of the M_S 7.3 Gazli, Uzbekistan, event, which is 1.8 magnitude units larger than the second largest.

Although oil extraction removes large masses from the crust, few earthquakes have been attributed to this process. Possible reasons are:

- the process is only weakly seismogenic, perhaps because natural aquifer influx (peripheral or bottom water) partially replaces mass extracted;
- under-reporting; and
- ambiguity of induction process, since fluid injection often accompanies production.

4. Injection into the subsurface

The burgeoning issue of injection-related earthquakes was highlighted by Ellsworth (2013) who pointed out the recent dramatic increase in earthquake rate for M ≥ 3 events in the central and eastern USA. More than 100 such earthquakes occurred annually, on average, 2010–2012 compared with just 21 events/year on average 1967–2000. Despite incomplete reporting, *HiQuake* shows that increasing incidence of injection-related earthquakes is not confined to the USA.

Fluids are injected into the ground for diverse reasons including (Table 2):

- solution mining (Section 3.2.2);
- disposal of by-products;
- enhancing oil recovery;
- fracturing rock (i.e. the very process that causes earthquakes);
- research into the earthquake nucleation process;
- disposing of hot waste water;
- underground storage of natural gas, hydrogen and compressed air; and
- CO_2 geostorage to reduce emissions.

In addition, passive groundwater inflow may occur when reservoirs are produced, or pumping to suppress groundwater levels is terminated in abandoned mines.

HiQuake contains 180 cases where injections have been postulated to induce seismicity. Whereas in general, the removal of mass from the crust is expected to reduce the normal stress that prevents slip on faults, the introduction of fluids into faulted rock is expected to increase the pore pressure that encourages failure. Both these changes thus, capriciously, are expected to induce earthquakes. In the case of injections, in addition to the direct hazard from earthquakes, there is the added risk that if the target formation or its caprock are ruptured the injected fluid might escape. This could add to hazard, e.g., where the injectate is polluted water, natural gas or CO_2.

4.1. Liquid

4.1.1. Military waste

HiQuake contains only one case where seismicity was, to a high degree of confidence, induced by the injection of military waste. This is the legendary case of the so-called Denver earthquakes. It raised widespread awareness among seismologists and the general public that human activity can induce earthquakes.

The incident began in 1961 when the Army Corps of Engineers drilled a 3.7-km deep well into highly fractured crystalline Precambrian basement at the Rocky Mountain Arsenal, northeast of Denver,

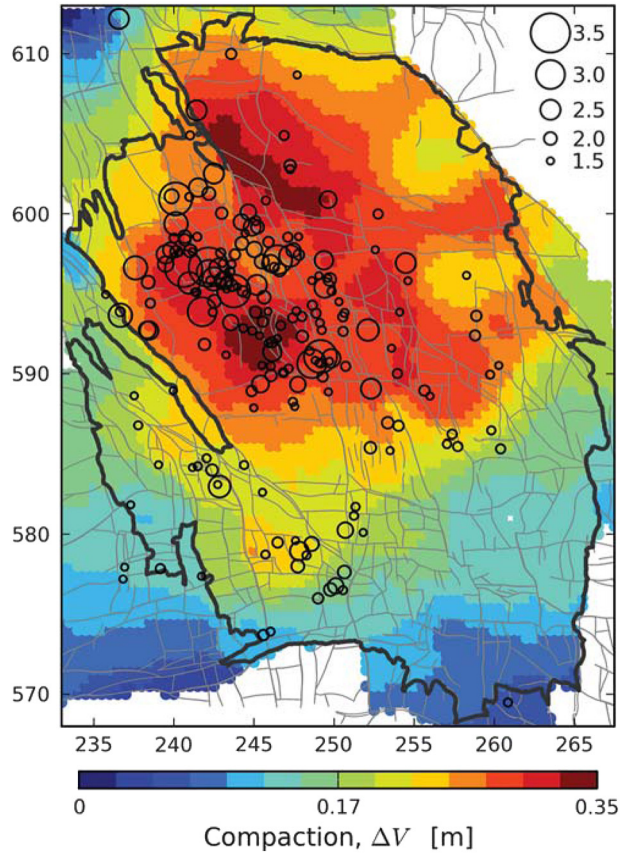

Fig. 35. The Groningen Gasfield. Earthquake epicenters for events with M ≥ 1.5 for the period 1995–2012, superimposed on a model of reservoir compaction for 1960–2012. Black line: perimeter of the Groningen Gasfield; thin gray lines: faults close to the reservoir level. Map coordinates are kilometers in the Dutch national triangulation coordinate system (Rijksdriehoek).
(From Bourne et al. (2015).)

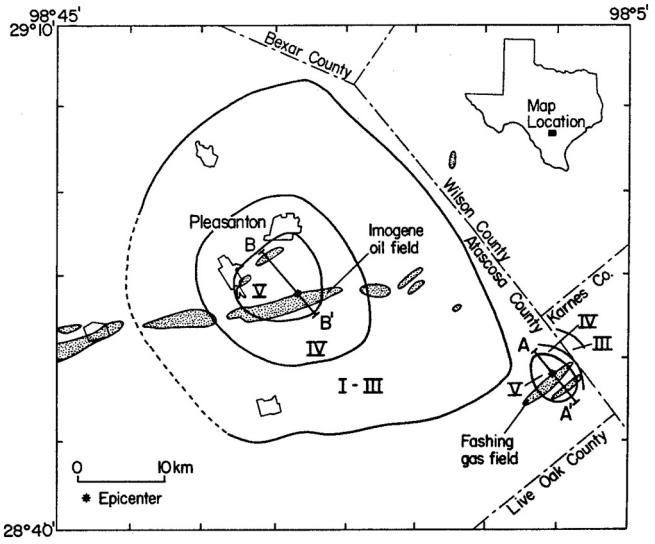

Fig. 36. Oilfields and gas fields in the Imogene/Fashing area, south Texas, where earthquakes are postulated to have been induced. Shaded regions are more prominent fields. Isoseismals for the largest events on the Modified Mercalli intensity scale are shown.
(From Pennington et al. (1986).)

Colorado (Evans, 1966; Hsieh and Bredehoeft, 1981). The purpose of the well has been reported to have been disposal of contaminated wastewater which was done by injection into the bottom, unlined,

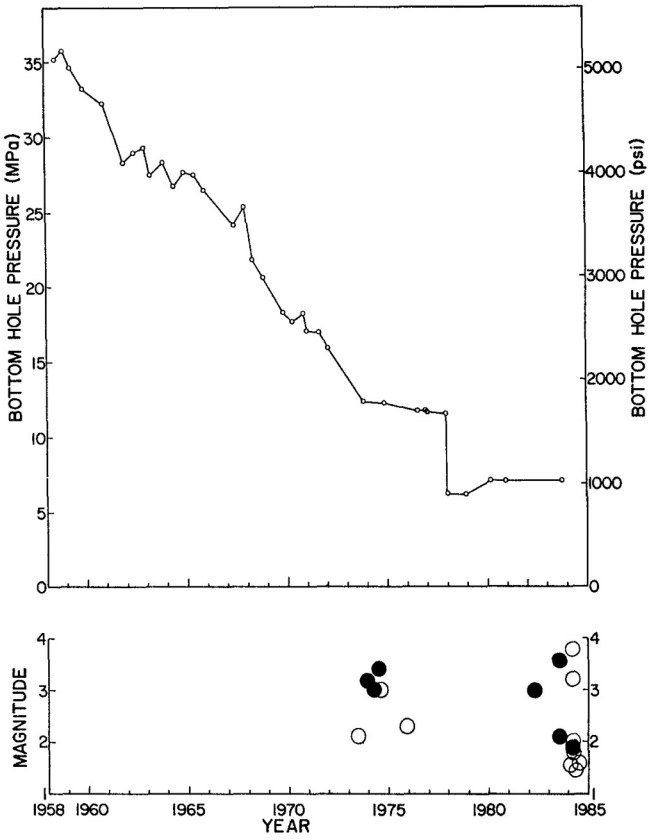

Fig. 37. Pressure history of a well near the fault in the Fashing Gasfield along with known earthquakes in the Fashing-Pleasanton area. Black dots: earthquakes from the Fashing area; open circles: earthquakes from the Pleasanton (Imogene) area.
(From Pennington et al. (1986).)

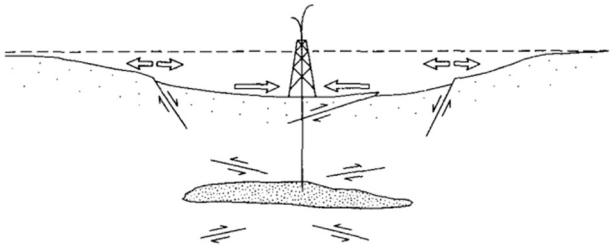

Fig. 38. Schematic cross section summarizing surface deformation and faulting associated with fluid withdrawal. Normal faults develop on the flanks of the field, as observed at the Goose Creek, Texas, Oilfield. Reverse faults develop above reservoirs as observed at Wilmington, Buena Vista Hills, the Pau Basin and beneath the Strachan Field.
(From Segall (1989).)

21 m. Disposal began in March 1962 at pressures ranging from atmospheric to ~7.2 MPa above formation pressure. In the four-year period up to 1966 625,000 m^3 of fluid were injected.

Minor earthquakes started to occur in the Denver area shortly after injection began and by 1967 over 1500 earthquakes, some of which were M 3–4, had been recorded (Fig. 49). The correlation between volume injected and frequency of earthquakes, along with epicenters located < 8 km from the well, led Evans (1966) to suggest they had been induced.

Although waste disposal ceased in 1966, earthquake activity continued and in 1967 three earthquakes with $M_L > 5$ occurred, damaging infrastructure in Denver. Seismicity then declined and by the early 1980s had essentially ceased. Ironically, the large earthquakes that occurred after the end of injection weakened the temporal correlation between earthquakes and injection and thus the case argued for

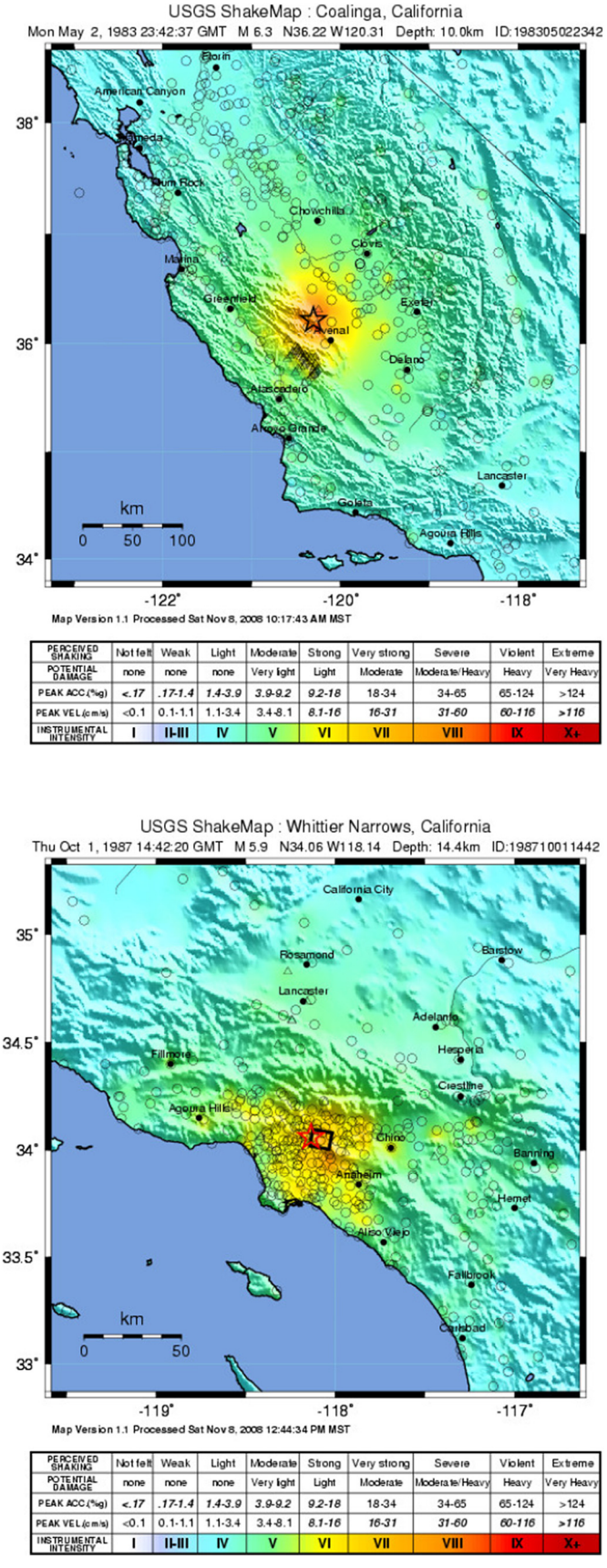

Fig. 39. U.S. Geological Survey shake maps (http://earthquake.usgs.gov/earthquakes/shakemap/). Top: 1983 M_W 6.2 Coalinga, California earthquake, which injured 94 people and was felt throughout half the state. Bottom: 1987 M_L 5.9 Whittier Narrows, California earthquake, which killed six people. Ground shaking was felt throughout the regions shown in the maps and ranged from Light (cool colours) to Severe (warm colours). See the U.S. Geological Survey webpage for more details.

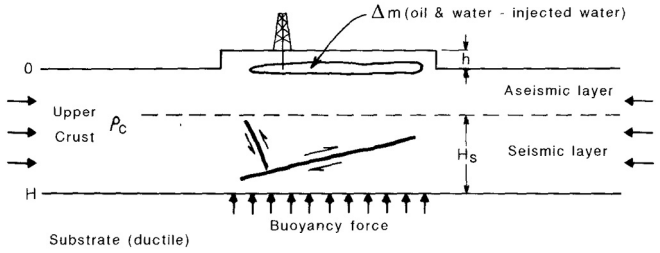

Fig. 40. Schematic cross section showing proposed crustal response mechanism to oil production. Mass removal results in a vertical force imbalance causing seismic deformation in the seismogenic layer. This deformation, together with aseismic deformation in the shallow crust, restores isostatic balance.
(From McGarr (1991).)

induction. Diffusion of the fluid would have continued after injection stopped, however, and could account for the ongoing seismicity (Healy et al., 1968).

4.1.2. Wastewater disposal

Large quantities of connate brine, sometimes mixed with water, are typically co-produced with oil, especially as fields age. Water-to-oil ratios may exceed 20 (Gluyas and Peters, 2010). It is commonly re-injected into depleted oilfields for disposal, to maintain reservoir pressure, and to promote sweep thus aiding oil recovery. Injected cold water commonly leads to thermal fracturing, especially in low-permeability reservoirs. Thermal fracturing is a desirable outcome as it facilitates lower injection pressures (and thus lower pump power requirements and costs) to be used. In California alone there are currently ~2300 wastewater injection wells.

HiQuake contains 33 cases of induced seismicity attributed to waste fluid injection. Of these, three are in Canada, two in China, one in Italy and 27 in the USA. An interesting case is that of Paradox Valley, Colorado, so-named because the Dolores River runs transversely across the valley. This case is noteworthy because of the apparently large distances from the injecting well of some of the postulated induced earthquakes (Ake et al., 2005; Block et al., 2015; King et al., 2014; Yeck et al., 2015).

At Paradox Valley, brine is injected into a sub-horizontal layer of Mississippian-age limestone at the bottom of a 4800-m-deep well. The objective is to reduce the salinity of Dolores River water and, as a consequence, the Colorado River into which it flows. Salt enters the Dolores River by inflow of groundwater ~8 times more saline than sea water. To manage this, shallow brine is extracted from the ground from nine production wells and re-injected at greater depth via a single disposal well at surface pressures up to 35 MPa (Yeck et al., 2015). Continuous injection has been underway since 1996. In the following two decades > 5700 earthquakes surmised to have been induced were located, including a M 4.3 event in 2000 (Fig. 50). Some epicenters lie > 10 km from the disposal well and a few are up to ~25 km distant.

The 1986 M_W 4.9 Painesville, Ohio, earthquake was possibly induced and occurred close to critical infrastructure (Ahmad and Smith, 1988; McGarr, 2014; Nicholson et al., 1988). This event, which was felt in 11 states and parts of Canada, occurred in Precambrian basement. It was within 17 km of the Perry Nuclear Power Plant on the edge of Lake Erie, and ground acceleration reached 0.23 g. The injection of 1.2×10^6 m^3 of liquid agricultural waste into three wells ~12 km away was implicated. These injections began in 1976. The mainshock and associated M < 2.5 aftershocks thus occurred a decade after injections began by which time pressure had increased by 11.8 MPa at the injection location.

Whether this earthquake sequence was induced is controversial. Prior to instrumentation, similar earthquakes occurred in 1906, 1928, 1943 and 1958 (i.e. about every ~20 years) in the area. The 1986 earthquakes thus may have been natural. The long delay of seismicity after the start of injection also erodes confidence that the two processes

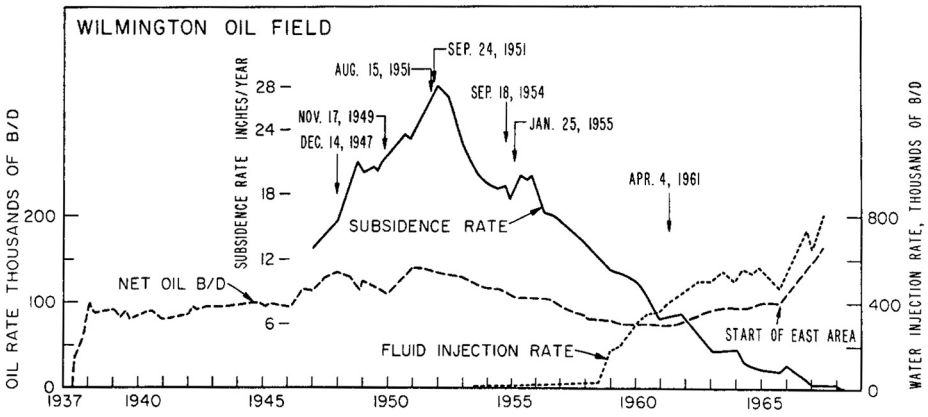

Fig. 41. For the Wilmington Oilfield, California, subsidence rate in the center of the field, oil production and water injection rates. Arrows show dates of major damaging earthquakes.
(From Kovach (1974).)

were linked (Hitzman, 2013). However, the many cases of postulated delayed earthquake induction that have occurred subsequently render it more plausible that the 1986 Painesville earthquakes were induced.

A European case is that of the 2012 M_L 5.9 Emilia-Romagna, Italy, earthquake sequence which resulted in 27 fatalities (Cartlidge, 2014). It was postulated that hydrocarbon exploitation at the Mirandola Field and geothermal exploitation at Casaglia contributed to stress changes that induced this sequence.

Because of serious impact to people and infrastructure a commission was established to investigate whether it was induced (Styles et al., 2014). The commission found statistical correlations with production parameters in the weeks before the earthquakes but concluded stress changes resulting from reservoir depletion had not contributed. It concluded that, while an anthropogenic effect could not be ruled out, it was "highly unlikely" that the sequence had been induced.

A link between injection pressure and induced earthquakes is reported for the Huangjiachang Gasfield, Sichuan Basin, China (Lei et al., 2013). Few earthquakes occurred there until injection wellhead pressure exceeded 2 MPa. After that, > 5000 M > 1.0 earthquakes occurred close to reservoir depth, the largest with M_L 4.4.

The Sichuan Basin is relatively tectonically stable with sparse historic seismicity. Gas occupies shallow, high-porosity Paleozoic and Mesozoic limestone/dolomite anticlines. Faults cross both reservoirs and basement. The Huangjiachang Gasfield is small and hosted in fractured, jointed, karstified Permian limestone at 2500 m depth. Wastewater injection began there in 2007. For the first two years, water was introduced under atmospheric pressure and seismic rates were low. In 2009 injection pressures were increased, ultimately reaching

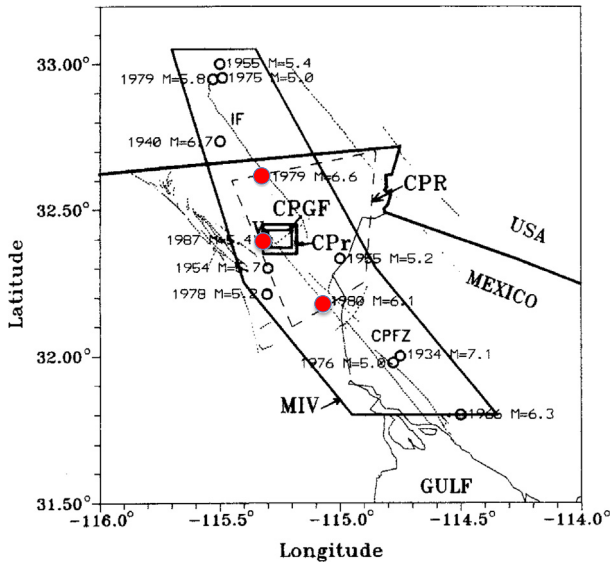

Fig. 43. The Cerro Prieto geothermal field. Circles: earthquakes with M ≥ 5; red dots: earthquakes proposed to have been induced (the 1979 M_L 6.6 Imperial Valley earthquake, the 1980 M_L 6.1 Victoria earthquake, and the 1987 M_L 5.4 Cerro Prieto earthquake); dotted lines: faults; IF: the Imperial fault; CPFZ: Cerro Prieto fault zone; V: the Cerro Prieto volcano.
(From Glowacka and Nava (1996).)

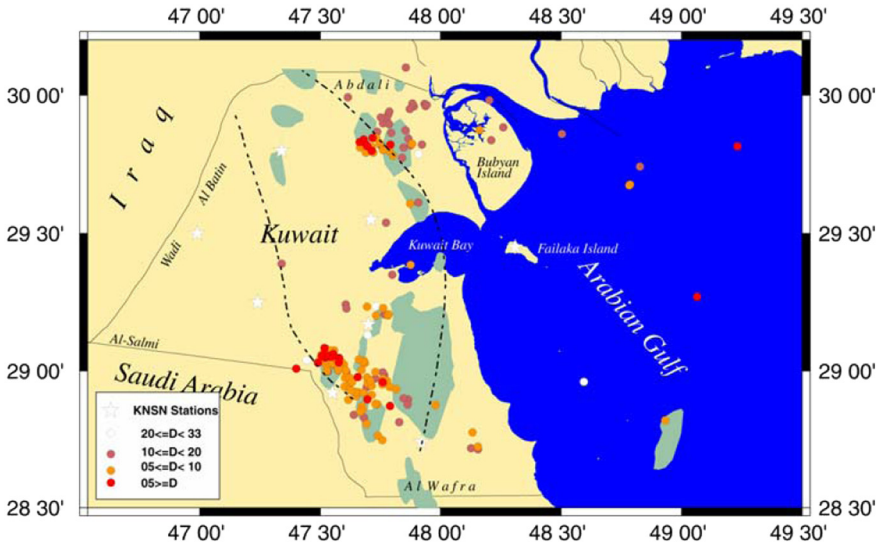

Fig. 42. Seismicity of Kuwait for the period March 1997–October 2007.
(From Al-Enezi et al. (2008).)

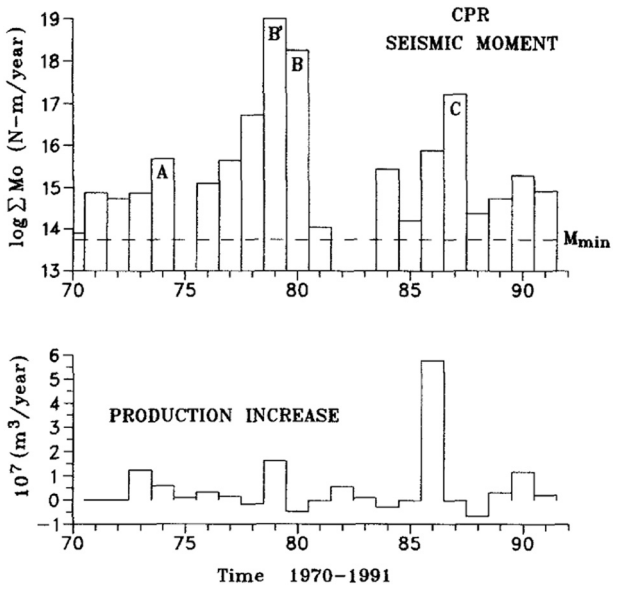

Fig. 44. For the Cerro Prieto geothermal field, Mexico, top: annual seismic moment release; bottom: production rate.
(From Glowacka and Nava (1996).)

2.1–2.9 MPa, and earthquakes began to occur.

Particularly vigorous seismicity was reportedly induced by wastewater disposal in the Rongchang Field, also in the Sichuan Basin (Lei et al., 2008). Starting in 1989, two months after water injection began > 32,000 earthquakes up to M_L 5.2 were recorded. The largest event reactivated a thrust fault in the basement and earthquake locations suggested that failure occurred in both reservoir and basement.

An unprecedented surge in seismic rate occurred in Oklahoma in 2009 (Fig. 51) (Ellsworth, 2013). During 2008–2013 Oklahoma was the most seismically active state in the USA for M > 3 earthquakes, exceeding even California, which hosts the San Andreas fault zone, and the New Madrid Seismic Zone, formerly considered to be the most hazardous intraplate seismic zone in the USA. The largest event since 1950 in the New Madrid Seismic Zone has been M 4.9. In Oklahoma the M_W 5.8 Pawnee earthquake occurred in 2016.

Faults in Oklahoma are widespread but only one is known to have been active historically. This is the Meers fault, which is thought to have generated M 6.5–7 earthquakes over the last 3500 years (McNamara et al., 2015). The injection of water for enhanced oil recovery has been practiced in Oklahoma since the 1930s and the 1952 M ~5.6 event (the El Reno earthquake) may have been related to oil and gas extraction (Nicholson and Wesson, 1992). Hough and Page (2015) investigated whether the population of Oklahoma has been sufficiently stable historically for comparable earthquake activity to have been noted. The population has been large and well-distributed since the early 20th century, suggesting that that knowledge of M ≥ 4 earthquakes is nearly complete (Fig. 52). The occurrence of industrially induced earthquakes in Oklahoma currently are essentially beyond doubt.

As elsewhere, multiple industrial processes are underway simultaneously in the hydrocarbon fields of Oklahoma so it is difficult to be certain which induced any particular earthquake. In addition to production there are ~7000 injection wells that are used for:

- disposal of produced brine (the dominant use);
- enhanced oil recovery;
- hydrofracturing to increase permeability in shale; and
- disposal of hydrofracture fluid.

Most of the fluid is injected into the Arbuckle Group, a sequence of carbonates and sandstones overlying Precambrian crystalline basement (Fig. 53).

The largest and most damaging earthquake to have occurred in Oklahoma is the 2016 M_W 5.8 Pawnee earthquake. This exceeded the well-studied 2011 M_W 5.7 Prague earthquake which is confidently associated with wastewater disposal into a depleted oilfield (e.g., Keranen et al., 2013). The Prague earthquake was felt in 17 states and in Chicago, 1000 km away. It caused considerable damage, destroying 14 houses and injuring two people. This and the Pawnee earthquake are the largest in the world associated with waste-water disposal and have led to re-assessment of the potential size of injection-induced earthquakes and the delay time following the onset of operations.

Earthquake activity in the Prague area began in February 2010 with a M_W 4.1 earthquake in the Wilzetta Oilfield. This lies within the ~200-km-long Pennsylvanian Wilzetta fault zone (Fig. 54). In 2011 the activity culminated in the Prague sequence that included three earthquakes with M_W 5.0, 5.7, and 5.0 in November, and prolific aftershocks. Hypocentral locations and focal mechanisms from 1183 aftershocks clarified the geometry of the hypocentral zone (Fig. 55) (Keranen et al., 2013). Strike-slip motion occurred on steeply dipping planes that intersect sedimentary layers and basement. The tip of the initial rupture plane lay within ~200 m of active injection wells at ~1 km depth.

In the Wilzetta zone, oil is contained in fault-bounded structural traps that are barriers to fluid migration through the porous limestone host formation. Where the Prague sequence occurred, production has been ongoing since the 1950s but has now declined. Three waste-disposal injection wells which came online in 1993 are nearby (Fig. 55). They inject water into sealed rock compartments at ~1.3–2.1 km depth.

Over the 17-year period 1993–2011 injection pressure increased from atmospheric, reaching 3.6 MPa by 2006. Seismicity may have started when the injected volume exceeded that extracted from the fault-bounded compartment. Once the compartment had been refilled ongoing injection may have reduced confining stress on the reservoir-

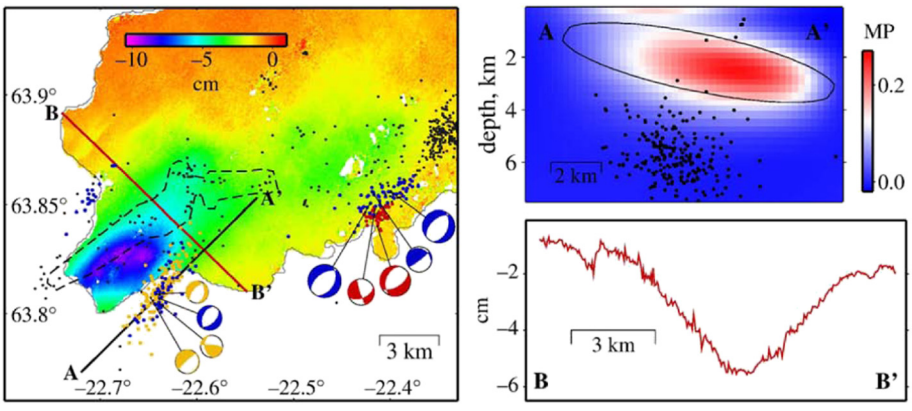

Fig. 45. For the Reykjanes and Svartsengi geothermal fields, southwest Iceland, left: the near-vertical radar displacement field June 2005–May 2008, earthquake locations and focal mechanisms. Black dots: background events. Distinct swarm events are shown for 2006 (orange), 2007 (red) and 2008 (blue). Stippled outline: location of the 1972 swarm activity from Klein et al. (1977). Top right: profile AA′ shows the predicted change in Coulomb failure stress for normal slip on NE-SW-trending fault planes, computed using an elastic half-space ellipsoidal source model for subsidence around the Reykjanes geothermal field. Bottom right: profile BB′ shows the observed near-vertical radar displacement across the Reykjanes subsidence bowl.
(From Keiding et al. (2010).)

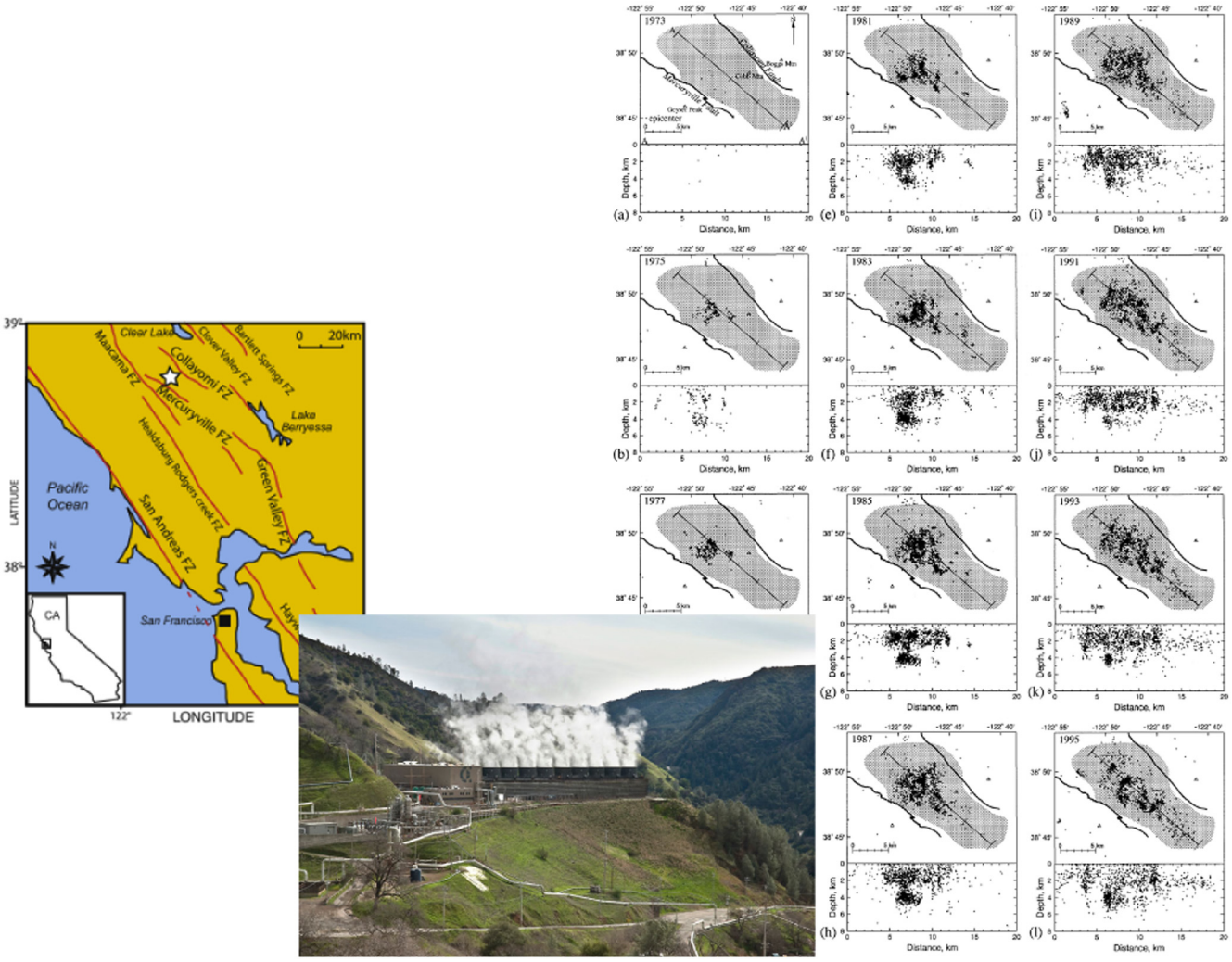

Fig. 46. The Geysers geothermal field, California. Left: regional map showing location of the field. Middle: McCabe Units 5 and 6 at The Geysers (http://www.energy.ca.gov/tour/geysers/). Right: maps of seismicity at The Geysers at biannual intervals from 1973 to 1995. Locations are from the Northern California Seismic Network catalog for earthquakes with M > 1.2. Gray area: steam field. Line shows line-of-section for depth sections below each map.
(From Ross et al. (1999).)

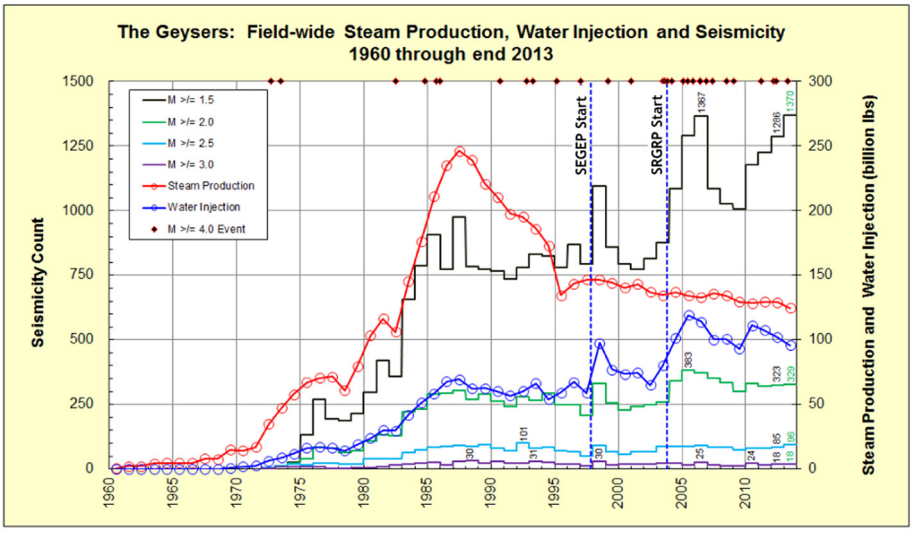

Fig. 47. Yearly field-wide steam production, water injection and seismicity 1960–2013. Earthquakes with M ≥ 4 are indicated as red diamonds along the top boundary of the graph.
(From Hartline (2014).)

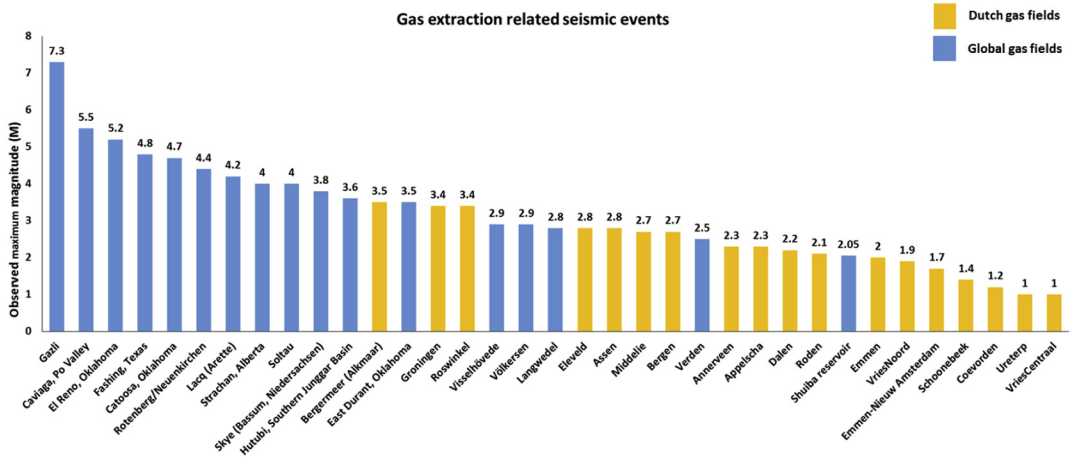

Fig. 48. M_{MAX} for seismic sequences postulated to be induced by the extraction of natural gas at the 35 fields where this parameter is reported. The Hutubi, northwest China case is associated with both extraction and storage (Tang et al., 2015).

Table 2
Classification categories of underground injection wells in The Code of Federal Regulations of the USA (40 CFR 144.6-Classification of wells).[a]

Class of well	Purpose
Class I	Industrial and municipal waste disposal wells
Class II	Oil and gas related injection wells
Class III	Injection wells for solution mining
Class IV	Shallow hazardous and radioactive injection wells
Class V	Wells for injection of non-hazardous fluids into or above underground sources of drinking water
Class VI	Wells used for geologic sequestration of CO_2

[a] https://www.epa.gov/uic/general-information-about-injection-wells#regulates.

bounding faults which failed as a consequence. More stress was released than corresponds to the total volume injected, so tectonic stress was probably also released. Both injection and M > 3 earthquakes continue in the Wilzetta Field.

Fig. 56 shows seismicity and oil production in Oklahoma over the last century. Between 2009 and 2014, 26 M ≥ 4 events occurred in the state with over 100 M ≥ 3.5 events in 2014 alone. Monthly statewide wastewater injectate volume has doubled since 1997 (Walsh and Zoback, 2015). Correlations between earthquakes and injection or production are rare, and Fig. 57 shows earthquakes and fluid injections for the entire state and for individual study areas. Earthquakes do not correlate with faults and most earthquakes occur in the least faulted part of Oklahoma.

Faults that fail in Oklahoma are probably those favorably oriented relative to the regional stress direction. Most events occur at 5–6 km depth in the basement on faults kilometers or tens of kilometers in length. Such faults can maximally sustain M 5–6 earthquakes. Some earthquakes occur on well-known faults that have larger seismic potentials. The length of segments activated can be determined from aftershock distributions.

Oklahoma earthquake activity exhibits both similarities and differences to other induced seismicity. No short-term monthly correlation with injection is apparent and seismicity surged long after the start of injections, 17 years in the case of the Prague sequence. In this it resembles the Wilmington Oilfield, California, where induced seismicity began years after water injection started for enhanced oil recovery (Section 4.1.3). However, it is unlike the "Denver earthquakes" sequence (Section 4.1.1) where seismicity began almost immediately after injections. Induced earthquake sequences do not necessarily start with the largest event, and stress from earlier events may trigger larger ones.

In addition to induction by hydrocarbon-related operations, earthquakes in Oklahoma are also triggered by distant large earthquakes ("remote triggering"). Van der Elst et al. (2013) noted that a M_W 4.1 event near Prague occurred following the 27 February 2010 M_W 8.8 Maule, Chile, earthquake (Fig. 58). Stress changes resulting from distant earthquakes can be calculated and can reveal the failure susceptibilities of faults.

4.1.3. Water injected for enhanced oil recovery

Oil recovery is enhanced by injecting low-salinity water, water-alternating-gas and water viscosifiers, and by thermal and chemical methods to modify either the viscosity of the fluids or the surface properties of the host reservoir. Distinguishing earthquakes induced by these processes from events induced by oil extraction is not straightforward if both are underway simultaneously. Temporal associations are persuasive, e.g., if seismicity surges shortly after water injection commences in producing oilfields that were previously aseismic.

HiQuake contains 38 cases of seismicity proposed to have been induced by enhanced oil recovery. Of these, 24 are from the USA and the rest from Canada, China, Denmark, France, Kuwait, Norway, Romania, Russia and Turkmenistan.

The classic example is that of the Rangely Oilfield, Colorado, where induced earthquakes could be controlled (Section 4.1.8) (Raleigh et al., 1976). Water was injected in wells up to 2 km deep where formation pressure was ~17 MPa. The seismic rate could be increased or decreased by varying the pore pressure around 26 MPa. This case raised hopes that earthquakes might be controlled, including damaging events on the San Andreas fault system. However, it was quickly realized that the fractal nature of earthquakes is such that the stress released by a few moderate earthquakes cannot substitute for a single large earthquake. Thus, hopes that damaging earthquakes might be averted by using engineering means were not realized.

The largest earthquakes postulated to have been induced by enhanced oil recovery are the M 6.2 1983 Coalinga event, the 1985 M_W 6.1 Kettleman North Dome event, and the 1987 M_L 5.9 Montebello Fields (Whittier Narrows) event, all in California. The primary cause for these earthquakes was, however, most likely oil extraction (Section 3.3.2) (McGarr, 1991).

More clear-cut examples come from the Newport-Inglewood fault zone, Los Angeles Basin, California. Of the 3 billion barrels (~ 490,000,000 m^3) of original reserves in the giant Wilmington Oilfield, 2.7 billion (~440,000,000 m^3) have been removed. Early production may have contributed to the damaging 1933 M_L 6.3 Long Beach, California, earthquake, and the events of 1947, 1949, 1951, 1954, 1955 and 1961 (Section 3.3.2) (Kovach, 1974).

Water flooding for enhanced oil recovery and to counteract massive subsidence started in the Wilmington Oilfield in 1954. Earthquakes up

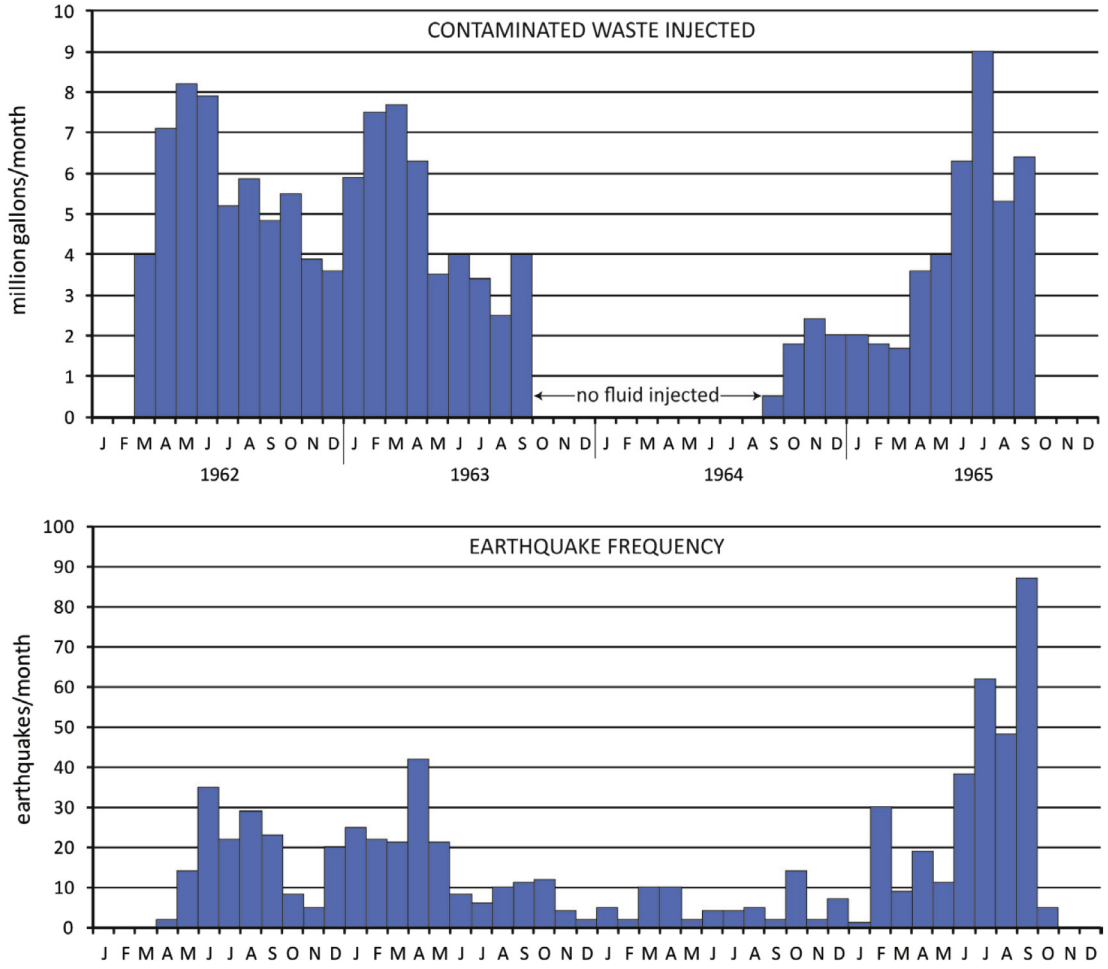

Fig. 49. Volume of waste injected into the Rocky Mountain Arsenal borehole and earthquake frequency. (Redrawn by Hitzman (2013) from Healy et al., 1968).

to M 3.0 that are thought to have correlated with injection volumes occurred in 1971. Injection was continued at approximately the same volumetric rate as production and seismicity did not continue (Nicholson and Wesson, 1992).

A more persuasive case of water-flooding-induced seismicity which caused significant damage and loss of life is that of the Inglewood Field, ~20 km further north along the Newport-Inglewood fault zone. In 1963 an earth dam containing the nearby Baldwin Hills Reservoir failed,

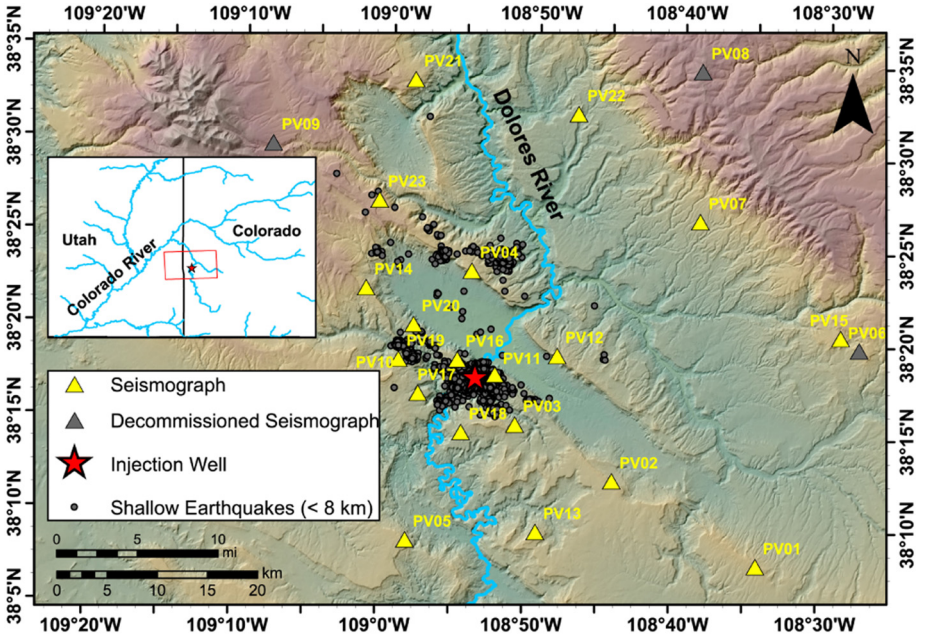

Fig. 50. The region around Paradox Valley, Colorado (the northwest-oriented depression). Yellow triangles: seismic stations; gray circles: earthquakes thought to be induced by brine injections.
(From Yeck et al. (2015).)

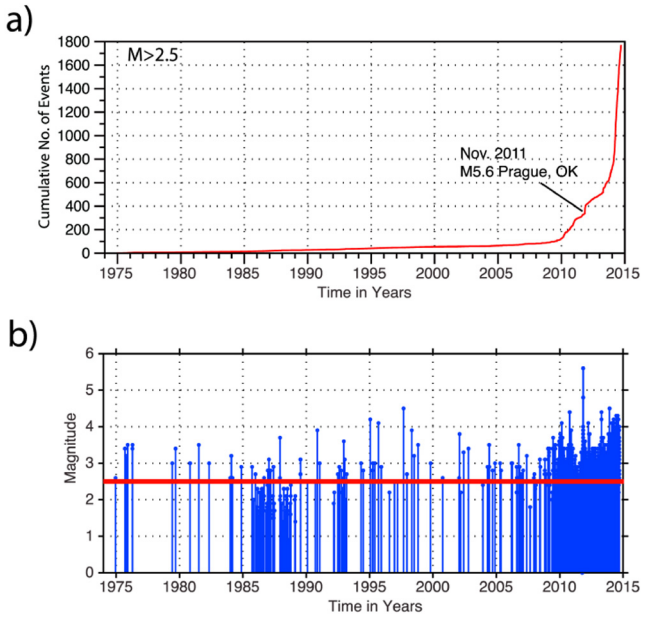

Fig. 51. Earthquakes recorded on the National Earthquake Information Center (NEIC) (http://earthquake.usgs.gov/contactus/golden/neic.php) system for the period 1975 through 2014. a) Cumulative seismicity in Oklahoma with M > 2.5. b) Earthquake magnitudes.
(From McNamara et al. (2015).)

releasing 11 × 10^6 m^3 of water into a residential area. This flood damaged over 1000 homes, killed five people and caused $12 million of damage. Failure of the dam was attributed to cumulative fault displacements that resulted from water flooding of the Inglewood Oilfield for enhanced oil recovery (Castle and Yerkes, 1976; Hamilton and Meehan, 1971).

Discovered in 1924, the Inglewood Oilfield occupies an anticline within a zone of faults and folds. Reserves were initially 430 million barrels but the field is now ~93% depleted. For the first three decades production occurred under only exsolution-gas- (pressure depletion) and peripheral-water drive. Some 83 × 10^6 m^3 of oil, water and sand were extracted. Pressures declined from 3.9 to 0.34 MPa by the 1950s. A well-defined subsidence bowl centered on the oilfield developed. Subsidence was up to 1.75 m during 1911–1963. Horizontal displacements were up to 0.68 m 1934–1961 with radially oriented extension. The Baldwin Hills reservoir lay on the edge of this subsidence bowl.

In 1954 a water-flood program for enhanced oil recovery began. Deformation accelerated immediately. A sharp reduction in subsidence occurred in the eastern part of the field. Horizontal displacements and strain were consistent with the operations and a tectonic origin for the deformation could be rejected to a high degree of certainty.

Shallow seismicity increased in 1962 and the following year the Baldwin Hills dam ruptured. It was deduced that movement on one of the faults allowed water to flow into the soil under the dam, resulting in failure. This case, and that of the Wilmington Oilfield, highlights the risk of major hydrocarbon operations near to dense populations, particularly where prior tectonic activity is known.

4.1.4. Enhanced Geothermal Systems (EGS)

Extraction of geothermal heat from rock with insufficient natural water was pioneered in the 1970s by the "hot dry rock" projects of Fenton Hill, New Mexico, and Cornwall, UK. These did not lead to economic development and were abandoned. The technology was resurrected early in the 21st century as "Enhanced Geothermal Systems" (EGS). An important milestone in this was the report "*The Future of Geothermal Energy*", prepared by the Massachusetts Institute of Technology for the U.S. Department of Energy (Tester et al., 2006).[6]

The fundamental concept of EGS is to pump high-pressure fluid into a well to hydrofracture and thermofracture hot rock, enhancing permeability and creating an underground heat exchanger. Later, cold water is pumped down an injection well, it circulates through the hot rock, and hot water and steam are extracted via production wells drilled into the fractured rock.

The objective of injection is to produce a network of fractures in the otherwise low-permeability target formation. As for shale-gas hydrofracturing, earthquakes are an inevitable consequence of a successful EGS project. Dense seismometer networks are installed prior to hydrofracturing to enable the best possible earthquake locations, magnitudes and source mechanisms. Such state-of-the-art projects are advancing basic seismology.

Notable EGS projects have been conducted at:

- Fenton Hill, New Mexico (e.g., Ferrazzini et al., 1990);
- Cornwall, UK (e.g., Turbitt et al., 1984);
- Soultz-sous-Forêts, France (e.g., Baisch et al., 2010; Calo et al., 2014);
- Basel, Switzerland (e.g., Zang et al., 2014a);
- Newberry volcano, Oregon (Cladouhos et al., 2013);
- the Coso geothermal area, California (Section 4.1.5) (Julian et al., 2010);
- Desert Peak, Nevada (Chabora et al., 2012); and
- Cooper Basin, Australia (e.g., Asanuma et al., 2005).

The Fenton Hill, New Mexico, hot dry rock project was the first of its kind. It was completed in 1977 in rock at ~2.6 km depth 185 °C. Work continued into the 1990s, achieving production of ~10 MW thermal, but was terminated because of lack of funding.

An early modern EGS project commenced at Soultz-sous-Forêts, in the central Upper Rhine Graben, France in 1987 (Fig. 59) (Baisch et al., 2010; Calo et al., 2014). The site lies in highly fractured granite overlain by ~1400 m of sediments. It contains three ~5000 m deep injection wells and several shallower wells. Massive hydraulic stimulations were performed at depths > 4000 m. In 2000, well GPK2 was stimulated with ~23,000 m^3 of water at flow rates of 30–50 l/s and overpressures of up to 13 MPa. Well GPK3 was stimulated in 2003 with ~37,000 m^3 of water at similar flow rates and overpressures. Well GPK4 was stimulated twice with a total of ~22,000 m^3 of fluid. In 2010 the project began to deliver 1.5 MW to the grid.

The injections were monitored using a sparse seismic network of multi-component, down-hole sensors at 1500–3500 m depths. More than 114,000 earthquakes were detected at rates of up to 8000 events/day (Fig. 60). Activity migrated away from the injection wells with time and the largest events occurred after injection stopped. Such behavior causes problems for "traffic light" systems for adjusting injection strategies to avoid large earthquakes on the basis of ongoing seismicity. Earthquake magnitudes eventually reached M_L 2.9 and caused public concern. After the largest event in 2003 the flow rates and injected volumes were reduced. The project demonstrated that better understanding of induced seismicity is needed if it is not to jeopardize commercial implementation of EGS technology.

The most infamous example of nuisance seismicity induced by EGS operations is from Basel, Switzerland. The city of Basel lies where the Upper Rhine Graben intersects the Jura Mountains fold/thrust belt (Fig. 1). Basel has a history of large earthquakes, including the largest historical event in NW Europe, the M ~6.5 earthquake of 1356 which destroyed the city. There may have been additional M ~7 events post-Pleistocene.

A summary of this project is provided by Häring et al. (2008) and a 2014 Special Issue of Geothermics (Zang et al., 2014a). The project was

[6] http://geothermal.inel.gov and http://www1.eere.energy.gov/geothermal/egs_technology.html.

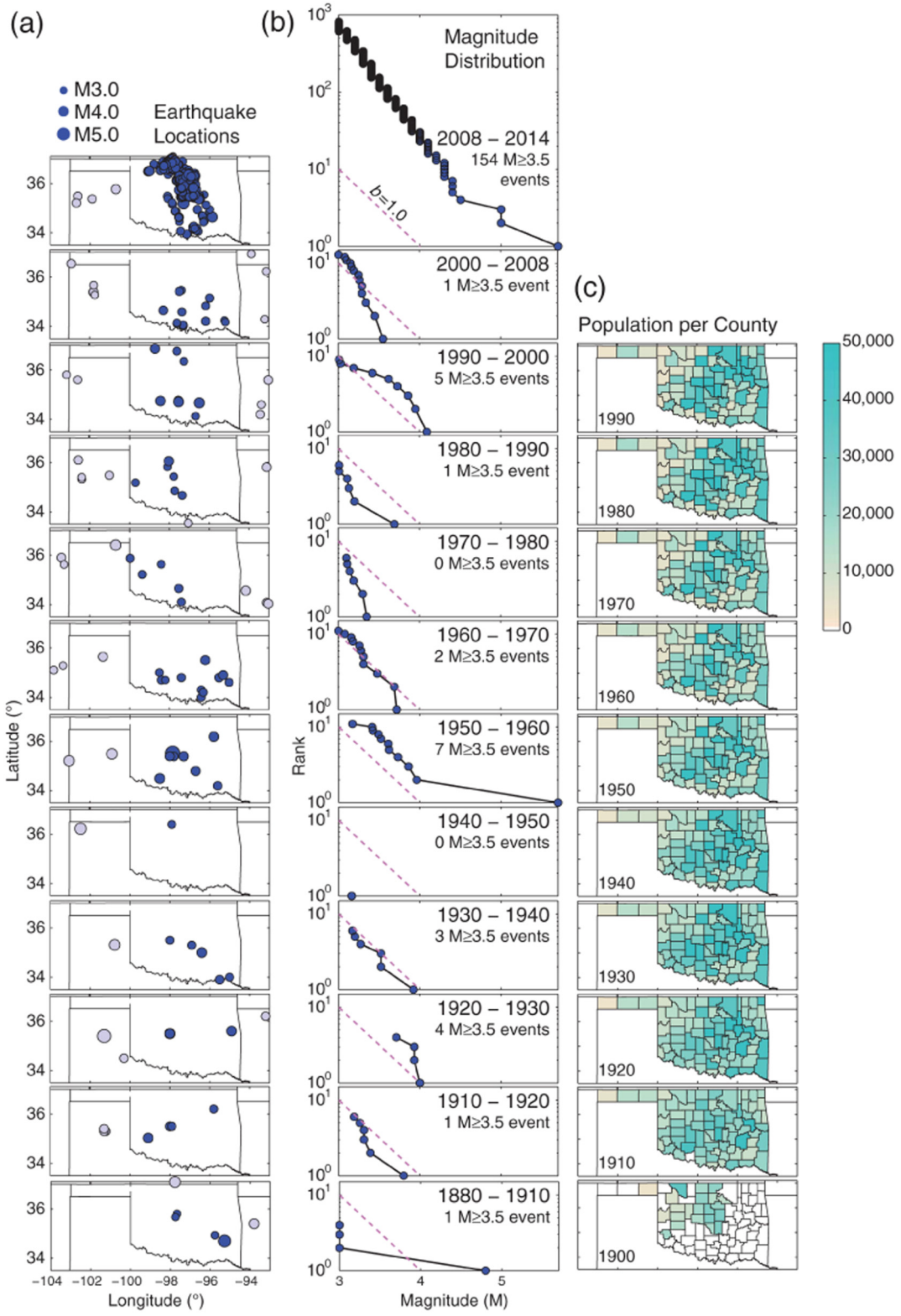

Fig. 52. Oklahoma seismicity. Left panels: Earthquake locations: blue–Oklahoma, gray–neighboring states. Center panels: magnitudes plotted cumulatively 1880–2014. Right panels: human population by county.
(From Hough and Page (2015).)

designed to provide power to Basel. A seismic network was installed in 2006 and the Basel-1 well drilled to 5 km depth. The wellbore intersects 2.4 km of sedimentary rocks and 2.6 km of granitic basement.

The granite in the open hole below 4629 m was hydraulically stimulated by injecting 11,570 m^3 of fluid. It was planned to inject for 21 days. However, seismicity became intense during the first 6 days, with events up to M_L 2.6 occurring at ~4.6–5.0 km depth. These events precipitated cessation of injection in response to a pre-approved procedure. Five hours later an earthquake with M_L 3.4 occurred and a further three M > 3 events followed over the next 56 days (Fig. 61).

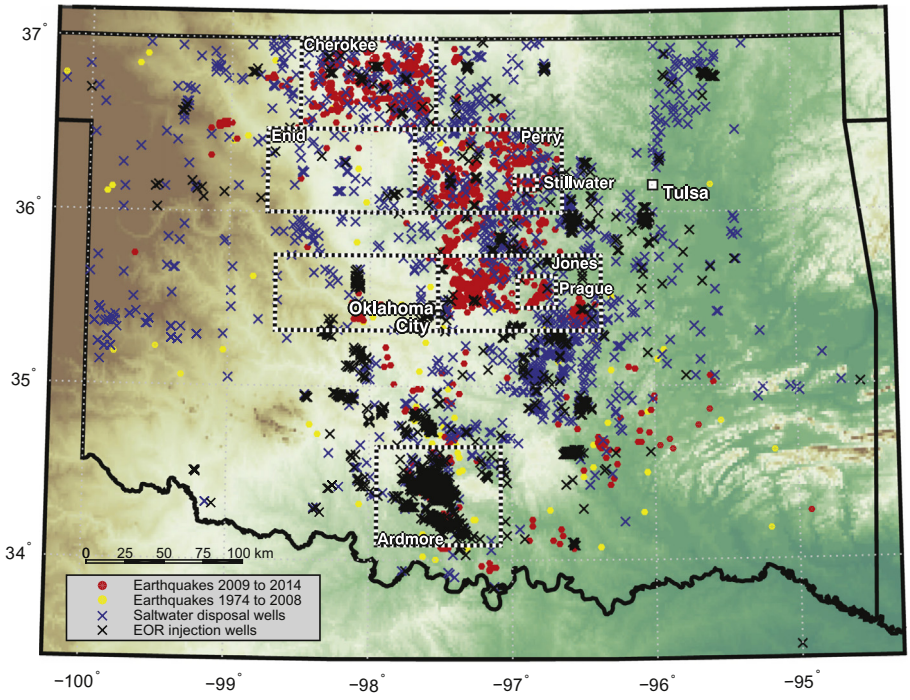

Fig. 53. Earthquakes and injection wells in Oklahoma. Red dots: locations of earthquakes 2009–2014; yellow dots: historical earthquakes 1974–2008; black crosses: enhanced oil recovery wells; blue crosses: salt water disposal wells that injected > 30,000 barrels (~4800 m^3) in any month in the most recent three years of data; boxes: areas of detailed study.
(From Walsh and Zoback (2015).)

There was considerable citizen anxiety and the project is now abandoned.

EGS has been extensively conducted in Cooper Basin, Australia, where the largest earthquake induced to date was M_W 3.7. Cooper Basin is ideal for EGS. It lies in the interior of Australia, remote from population centers. Significant oil and gas resources were explored and exploited since the 1960s and industrial infrastructure was left in place that was used from 2002 when geothermal exploration started. The target heat source is granitic rocks with temperatures up to 240 °C at 3.5 km depth. These are the hottest known granitic rocks in the world at economic drilling depths that are not near active volcanoes.

Six wells were drilled into the granite to 3629–4852 m depths. Four are in the Habanero Field and the other two are 9 and 18 km away in the Jolokia and Savina Fields. EGS fluid injections were conducted 2003–2012 (e.g., Asanuma et al., 2005; Baisch et al., 2009; Baisch et al., 2006; Baisch et al., 2015; Kaieda et al., 2010). These induced up to 20,000 earthquakes well-recorded by dense, modern seismic networks.

Although all the stimulations were conducted in the same granite formation, they induced variable seismic responses (Fig. 62). These are exemplified by two carried out in 2010 and 2012 (Baisch et al., 2015). The 2010 stimulation injected fluid into the Jolokia well at > 4000 m depth. It induced only minor seismic activity, even at extremely high fluid pressures (~120 MPa), and the injection rate achieved was only ~1.0 l/s, one to two orders of magnitude less than typical. Only 73 earthquakes with M_L −1.4 to 1.0 were recorded over an eight-day stimulation period and an additional 139 over the next six months. The largest was M 1.6 which occurred 127 days after injection ceased–another case where the largest event occurred after injection finished. Hypocenters clustered around the injection well a few tens or hundreds of meters away, suggesting that they occurred on fractures poorly oriented for slip in the regional stress field.

The 2012 stimulation in well Habanero 4 injected 34,000 m^3 of water at 4100–4400 m depths with flow rates > 60 l/s, and wellhead pressures of ~50 MPa. This induced > 29,000 earthquakes with M_L

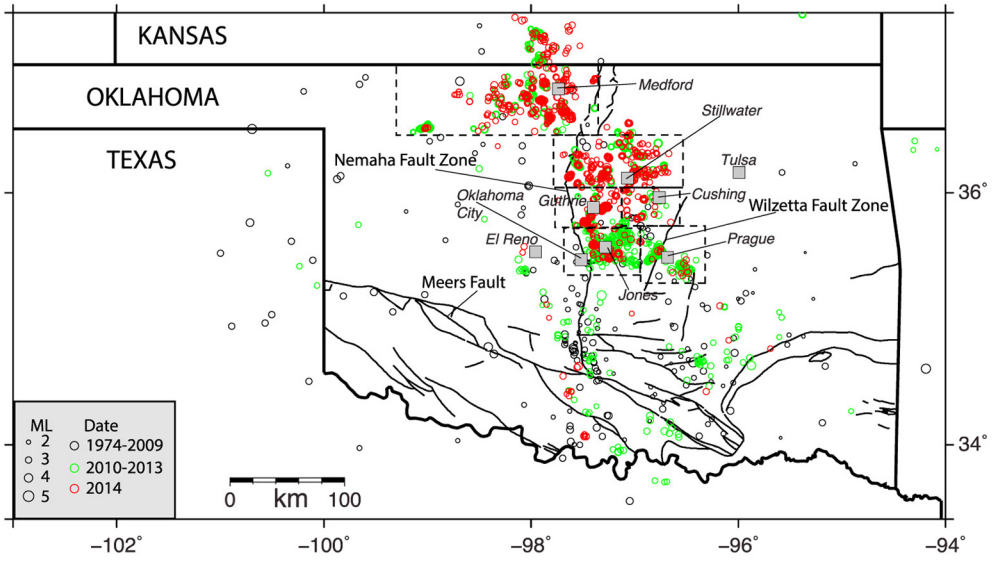

Fig. 54. For Oklahoma, U.S. Geological Survey earthquake epicenters from the National Earthquake Information Center (NEIC) database (http://earthquake.usgs.gov/contactus/golden/neic.php), 1974–2014. Black lines: subsurface and surface faults; dashed black lines: detailed study regions; Meers fault: the only known active fault in Oklahoma prior to the recent increase in seismicity.
(From McNamara et al. (2015).)

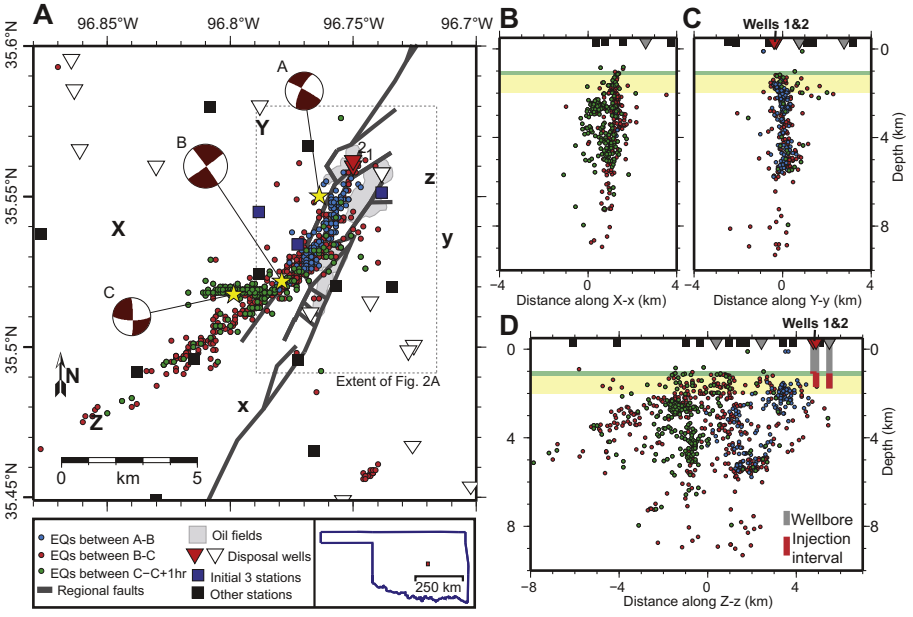

Fig. 55. Seismicity, focal mechanisms, seismic stations, active disposal wells, and oilfields in the neighborhood of the 2011 Prague, Oklahoma, seismic sequence. Stars: major earthquakes in the sequence. B–D: Cross sections showing seismicity projected from up to 4 km out of plane. Vertical lines: wellbores, red where perforated or open; green bands: the Hunton and Simpson Groups; yellow bands: Arbuckle Group which overlies basement. Inset: Oklahoma and location of map area.
(From Keranen et al. (2013).)

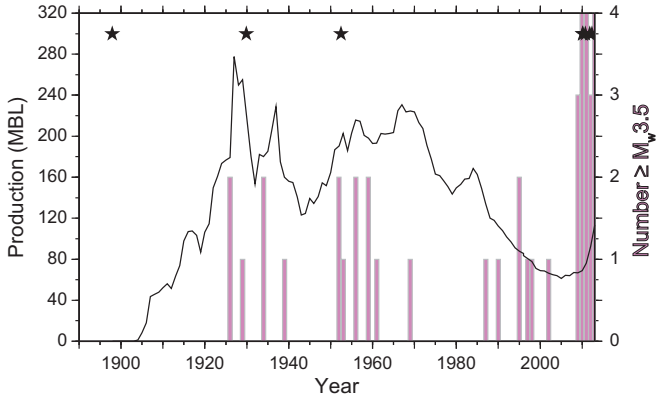

Fig. 56. Oklahoma seismicity rates compared with oil production in millions of barrels (multiply by 0.159 to convert to m^3). Bars: number of earthquakes with M ≥ 3.5 in a given year; black stars: M ≥ 4 events.
(From Hough and Page (2015).)

−1.6 to 3.0 recorded on a local 24-station network. From these data, 21,720 locations and 525 focal mechanisms were derived. This may be the most prolific EGS-induced earthquake dataset ever collected. In contrast to the well-hugging, sub-vertical fracture activated by stimulation of well Jolokia 1, the Habanero 4 stimulation activated a single, sub-horizontal fault zone only a few meters thick, extending > 1.5 km from the well. Failure was consistent with the regional stress field.

These remarkably different seismic responses characterized injections in different wells penetrating the same granite formation. This exemplifies the challenge of predicting the behavior of formations under stimulation, even when excellent geological knowledge is available. Despite the major technological advances achieved in the Cooper Basin project, due to low oil prices and changing government priorities, the project was decommissioned in 2016.

Despite the challenges that currently face development of EGS, much has been learned recently that will underpin the future of the industry. Because it is known beforehand that projects induce seismicity, exemplary seismic monitoring and public outreach practices have been developed. These include installing custom-designed networks of three-component borehole instruments well in advance of operations to obtain a pre-operational baseline for seismic activity. Data are streamed to public websites and outreach includes town-hall meetings, seismometers in public buildings in nearby communities, distributing information to the public by talks, printed materials and the internet, and involving local communities in the commercial activity.

4.1.5. Geothermal reinjection

Water is re-injected into exploited geothermal fields to maintain pressure. Although classified technically as renewable resources geothermal fields are, in reality, not so. If large quantities of hot fluid are removed at high rates for many years, exceeding natural recharge, the resource becomes depleted and progressive reduction in reservoir pressure leads to reduced production. To maintain pressure water is re-injected while avoiding cooling production wells.

The most remarkable case of seismicity attributed to geothermal reinjection is The Geysers field, California (Fig. 46). The Geysers is a rare vapor-dominated reservoir that lies in the strike-slip regime of the San Andreas fault system, California. Exploitation began in the 1860s. Steam was first used to generate electricity in 1922 when 1 kW was produced. Production peaked in 1987 at about 3.5×10^3 kg s^{-1} of steam from which 1800 MW of electricity was generated (Fig. 47).

Power production decreased thereafter because the modest amount of reinjection done could not maintain declining steam pressure. Condensate was the main re-injectate and less was available than the amount of water produced. Reservoir pressure is sub-hydrostatic and thus the water could be reintroduced at atmospheric pressure, i.e. it was poured into boreholes and drained back into the reservoir under gravity.

The US Geological Survey routinely locates > 10,000 earthquakes/year at The Geysers. The annual seismic rate is currently 200–300 M 2 earthquakes and 1–2 M 4 earthquakes. The Geysers earthquake dataset is without doubt the richest set of induced earthquake data available in the world with > 250,000 located events in the catalog of the Northern California Earthquake Data Center.[7]

For many years it was not acknowledged that the industrial activity induced the earthquakes. However, as data accumulated the link could not be denied. It was initially assumed that the earthquakes resulted from the contracting reservoir collapsing in on itself. Surface subsidence rates are up to 5 cm/year (Lofgren, 1978; Mossop and Segall, 1999; Vasco et al., 2013).

It is now clear that seismicity correlates better with reinjection than

[7] http://www.ncedc.org.

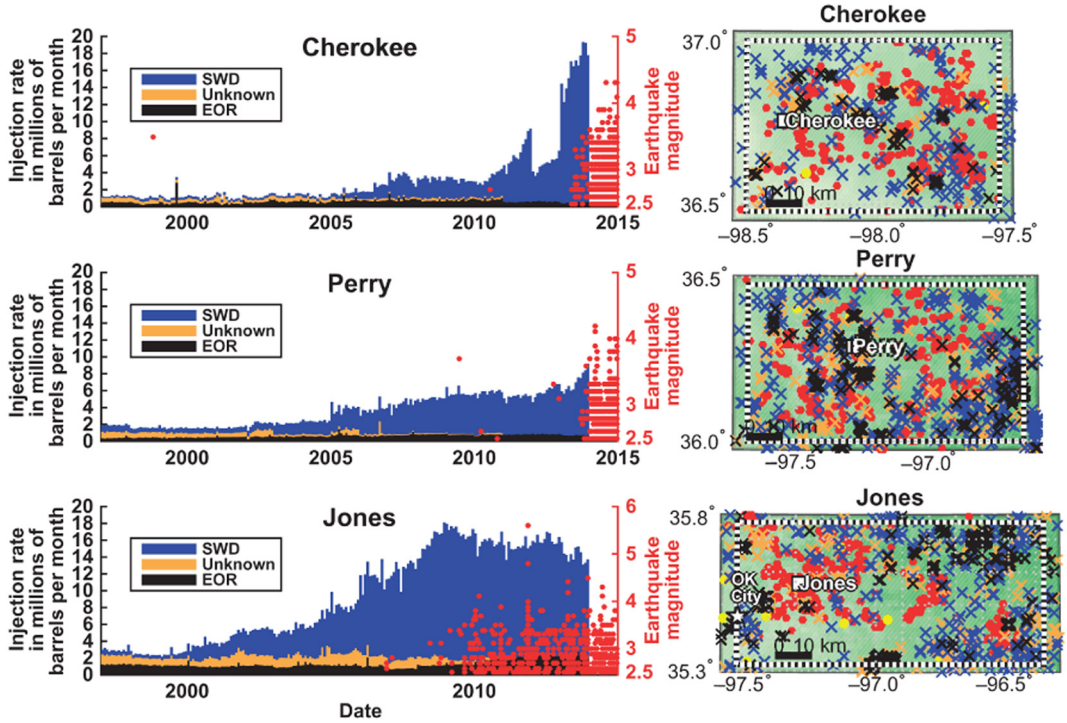

Fig. 57. Injection from enhanced oil recovery, brine disposal, and unknown wells, and earthquakes in the Cherokee, Perry, and Jones study areas (boxes in Fig. 53). Symbols are the same as in Fig. 53. Each study area is 5000 km^2 in size.
(From Walsh and Zoback (2015).)

production (e.g., Majer and Peterson, 2007; Stark, 1990). It has been possible to make this link since 1998 when the first of two major water-acquisition and reinjection projects began. The South East Geysers Effluent Project (SEGEP) began to re-inject water via a 46-km-long pipeline from Lake County that delivers up to 22 × 10^6 l/day of gray water. In 2003 the second project came online, the Santa Rosa Geysers Recharge Project (SGRP), which delivers up to 41 × 10^6 l/day via a 64-km-long pipeline from Santa Rosa (Fig. 47) (Majer and Peterson, 2007). Surges in earthquake rate correlate with the increases in water injection with those projects. Surges of earthquakes also correlate with individual

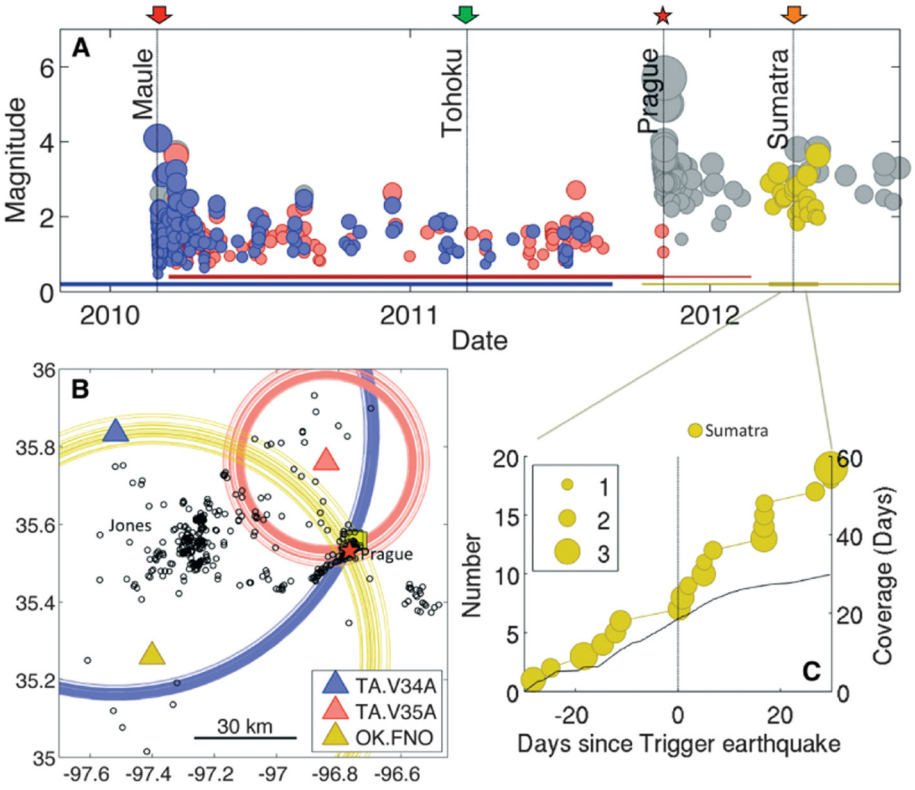

Fig. 58. Earthquakes in the Prague, Oklahoma, area. (A) Detected events, showing triggering by the 2010 Maule, Chile earthquake. Red star: the 6 November 2011 M_W 5.7 Prague earthquake. (B) Distances to detected events. (C) Cumulative number of events in the time period surrounding the 11 April 2012 M_W 8.6 and 8.2 Sumatra earthquakes.
(From van der Elst et al. (2013).)

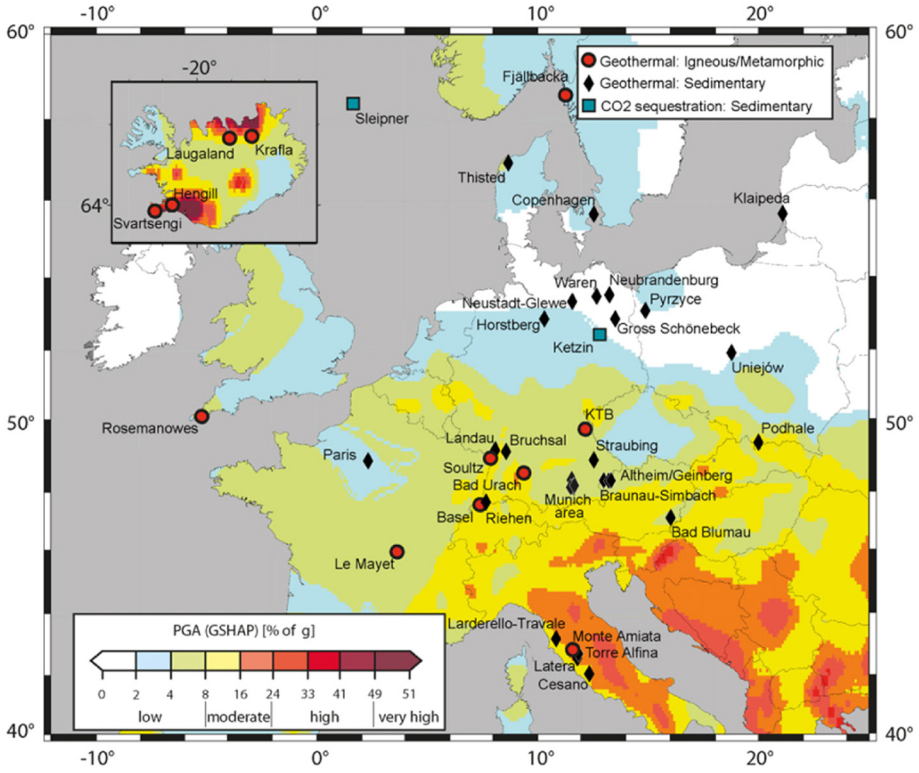

Fig. 59. Location of geothermal and CO_2 injection sites in Europe, superimposed on a seismic hazard map from the Global Seismic Hazard Assessment Program (GSHAP (http://www.seismo.ethz.ch/static/GSHAP)). Color scale denotes GSHAP index of local seismic hazard from natural earthquakes defined as peak ground acceleration in percent of the acceleration due to gravity (g) on stiff soil that has a 10% probability of being exceeded in 50 years (equivalent to a recurrence period of 475 years).
(From Evans et al. (2012).)

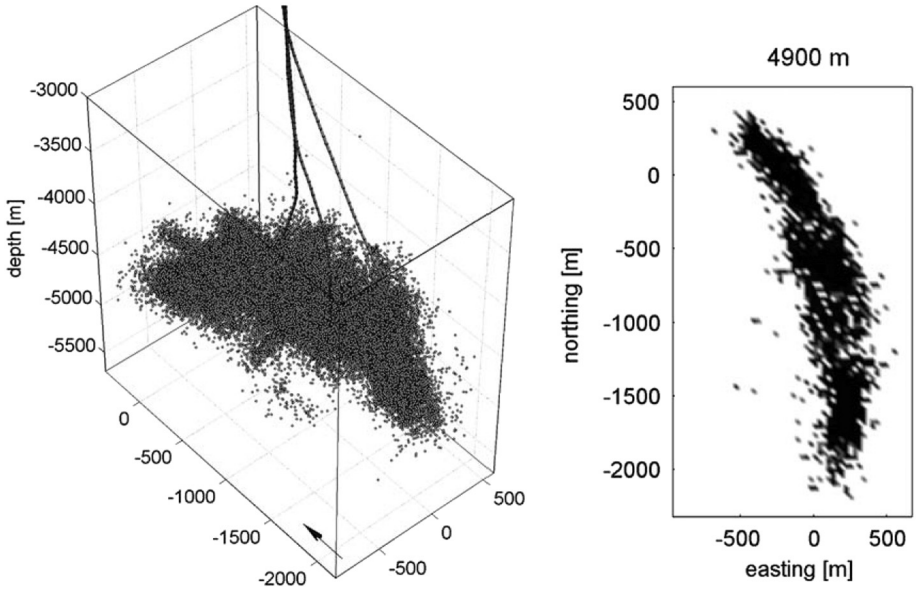

Fig. 60. Top left: Distribution of earthquake hypocenters at the Soultz-sous-Forêts EGS project in perspective view. Solid lines: wells GPK2, GPK3 and GPK4. Top right: Depth slice of the hypocenter density distribution at 4900 m depth. Dark shading: regions of high density.
(From Baisch et al. (2010).)

injections and injection wells (Majer and Peterson, 2007; Stark, 1990), e.g., in the high-temperature northwest Geysers in 2004 (Fig. 63).

Ground shaking from earthquakes with Modified Mercalli intensities of II–VI are felt daily in settlements near The Geysers. The largest earthquake that has occurred is the 2014 M_W 4.5 event. On the basis of historical seismicity, the absence of long faults in the reservoir, and the lack of epicentral alignments, Majer et al. (2007) estimated that the largest earthquake that could occur was M ~5.0. An extensive review of The Geysers seismicity is provided by Majer and Peterson (2007). They conclude that the seismicity results from a diverse set of processes that may work independently or together and either enhance or possibly reduce seismicity. To the processes listed in Section 1.3, thermal contraction from cooling the rock matrix can be added.

A second example of particularly rich geothermal-induced seismicity is from the Coso geothermal field. This field lies in the southwestern corner of the Basin and Range province in eastern California, at a right releasing step-over in the southern Owens Valley fault zone (Monastero et al., 2005). It lies on a US Navy weapons test site, and is thus uninhabited and not generally accessible to the public. Electricity has been generated since the 1980s, producing about 250 MW. Because there is a shortage of local water, only about half the volume produced is replaced by reinjection and the local water table has lowered greatly.

Tectonic seismicity is intense in the region, but even in this context the geothermal field is anomalously seismogenic. Several thousand locatable earthquakes per year occur within the ~5 × 5 km production field, the majority of which must be induced. These earthquakes have

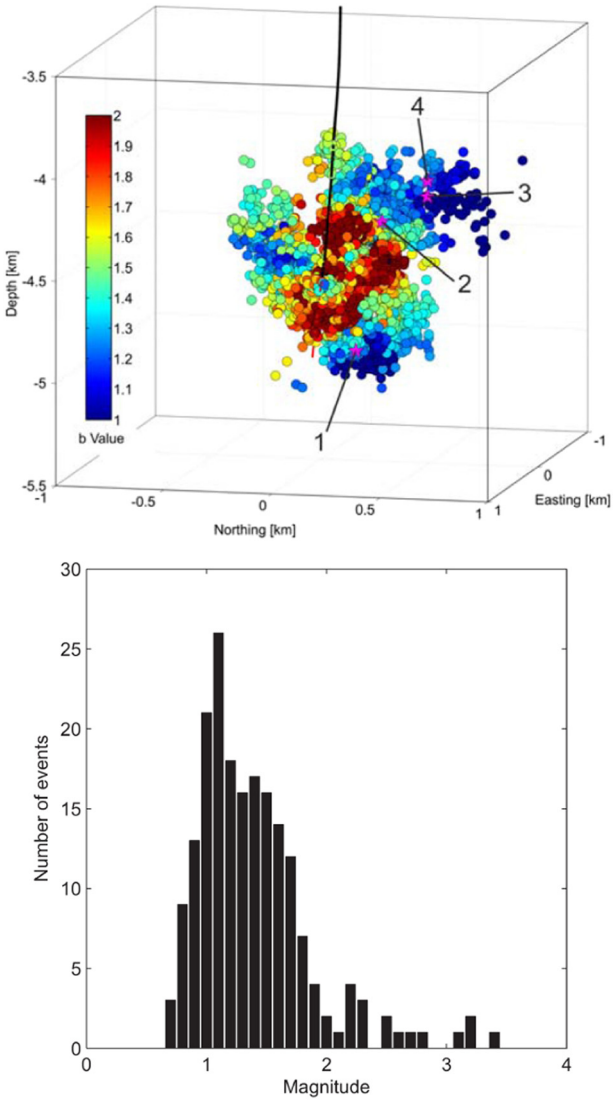

Fig. 61. Top: Earthquakes induced by hydraulic stimulation of the Basel, Switzerland, EGS injection well in 2006 and 2007. Hypocenters are color coded according to *b*-values calculated for the volume in which they occurred. Stars: large earthquakes (from Zang et al., 2014b). Bottom: Magnitude histogram of the induced seismicity recorded by the Swiss Seismological Service 3 December 2006–30 November 2007 (from Deichmann and Ernst, 2009).

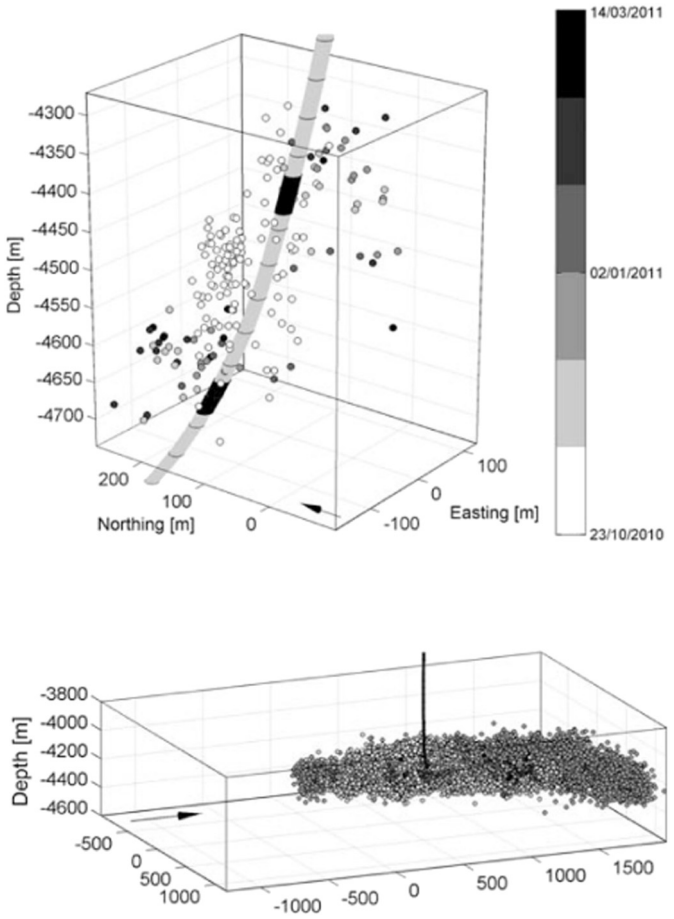

Fig. 62. EGS-induced earthquakes at Cooper Basin, Australia. Top: the Jolokia Field–hypocenters of earthquakes induced by hydraulic stimulation of well 1 in in 2010. Known fracture intersections with the wellbore are shown in black. Bottom: the Habanero field–hypocenters of earthquakes induced by stimulation of well 4 (vertical line) in 2012. (From Baisch et al. (2015).)

been used for detailed research (e.g., Julian et al., 2004; Julian et al., 2007; Kaven et al., 2014; Monastero et al., 2005). Most production and reinjection data are proprietary, so published correlations between operations and seismicity are rare.

One of these rare cases is described by Julian et al. (2007). In 2005 an existing well was used for an EGS experiment. Fluid was injected at rates of up to 20 l/s into well 34-9RD2 in order to increase permeability and enhance production in nearby producing wells. 34-9RD2 was reworked prior to the injection to deepen it and replace the existing slotted liner with an un-slotted one.

Major unexpected circulation-loss zones were encountered resulting in a total loss of up to 20 l/s of drilling mud at 2672 m depth. The planned EGS project thus instantly metamorphosed into an unplanned reinjection operation. A vigorous earthquake swarm began immediately. High-resolution locations, relative locations, and full moment tensors were determined using an exceptionally high-quality dataset acquired on 36 digital, three-component seismic stations of the permanent network operated by the Geothermal Program Office of the US Navy augmented by temporary stations.

The swarm opened, in tensile mode, several hundred meters of a preexisting fault immediately adjacent to the well. The existence of this structure, deduced from the seismic evidence, was confirmed by surface geological mapping and a borehole televiewer log. This was an early demonstration of the potential of earthquake techniques to study the detailed subsurface fracture network in a geothermal reservoir.

In Europe, three geothermal projects have been associated with M > 3 induced earthquakes, all in Italy:

- the Larderello-Travale area (M_{MAX} 3.2);
- the Monte Amiata geothermal field (M_{MAX} 3.5); and
- the Torre Alfina Field (M_{MAX} 3.0).

Of these, the most notable case is Larderello-Travale, Tuscany, which, like The Geysers, is a rare vapor-dominated system. Tuscany is tectonically active with transcurrent-transtensional-strike-slip deformation, high thermal gradients and temperatures up to 400 °C. There are several geothermal fields of economic interest. The shallower Larderello-Travale reservoirs occupy Triassic carbonate and evaporite rocks and the deeper ones fractured metamorphic basement.

Larderello-Travale has generated electricity almost continuously since 1904, and is thought to have a long history of seismicity. In the early 1970s, injection of cold condensate from the power plants started to recharge the upper reservoir and a seismic network was installed (Batini et al., 1985; Batini et al., 1980).

Seismicity is variable in rate and *b*-values. The events are mostly < 8 km deep, with 75% 3.0–5.5 km deep. The largest event reported

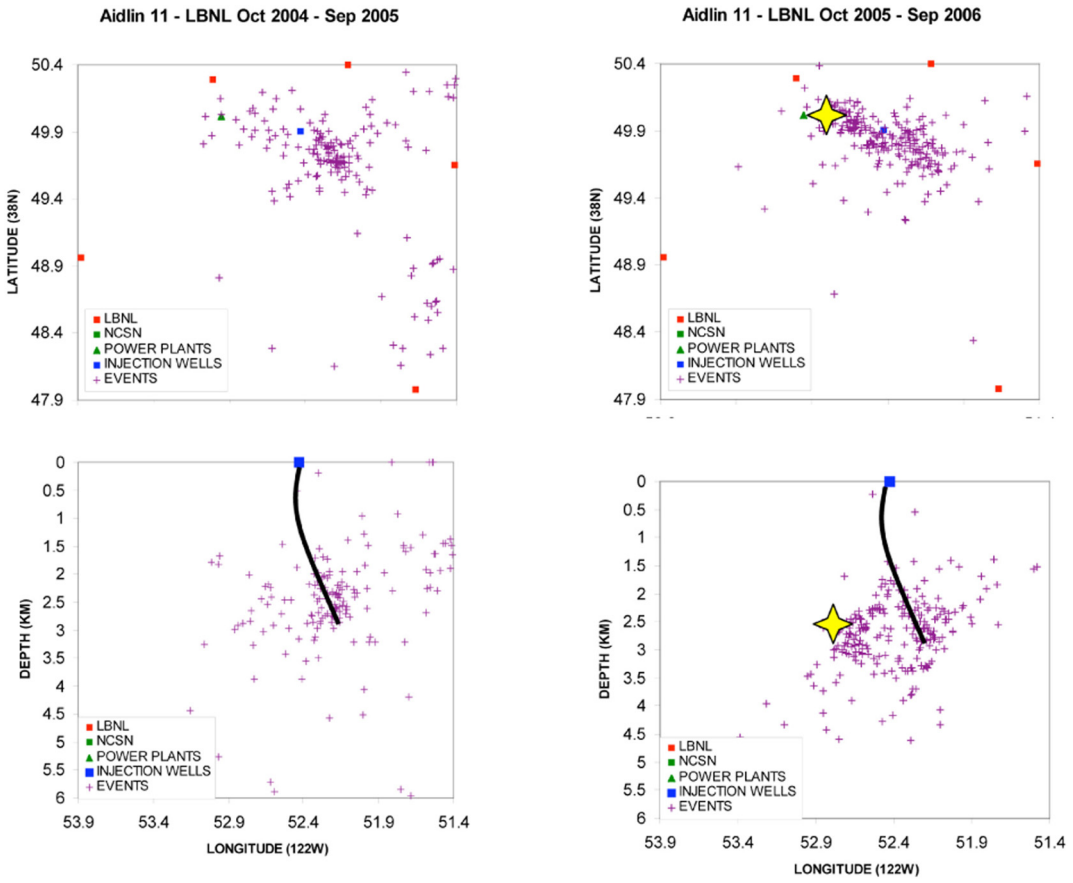

Fig. 63. Earthquakes surmised to be injection-related at the northwest Geysers geothermal area. Maps and east-west cross sections show earthquakes in the Aidlin area. Blue square and black line: injection well; yellow star: a M 4 event that occurred October 2005.
(From Majer and Peterson (2007).)

Fig. 64. States of the USA where shale-gas hydrofracturing is currently ongoing.

was M 3.2 and occurred in 1977. Events have significant non-shear focal mechanism components, indicating tensile failure (Kravania et al., 2000). Because of the long history of seismic activity it has been suggested that many events are natural. However, there is a clear correlation between injected volume and seismic rate (Batini et al., 1985; Evans et al., 2012).

4.1.6. Shale-gas hydrofracturing

Gas-bearing shale formations are hydrofractured ("fracked") to increase permeability and release the contained gas. It is typically done by drilling shallow horizontal wells into the target formation. Fluids are injected containing chemicals and solids designed to propagate fractures and prop them open. It is extensively applied in the USA where it has brought about a major reduction in the cost of natural gas (Fig. 64). As a result of this success there is widespread interest in the technology in other countries. However, in regions where population density is high there may be public concern about potential environmental effects, including ground-water pollution, industrialization and induced earthquakes.

Although over 2.5 million shale-gas hydrofracturing jobs have been completed worldwide, maximum earthquake magnitudes for only 21 cases have been reported. Of these cases, eight are from the USA, 12 from Canada, and one from the UK (Baisch and Vörös, 2011; de Pater and Baisch, 2011). This is only 0.001% of all shale-gas hydrofracturing jobs (Section 7.1). Of those cases, moderately large earthquakes are reported from British Columbia (M 4.4, 4.4 and 3.8 events) and Alberta (M_L 4.4), both in Canada (Kao et al., 2015; Schultz et al., 2015). In the USA the largest shale-gas hydrofracturing-related earthquakes reported have been four M > 3 events in Oklahoma and Ohio (Darold et al., 2014; Skoumal et al., 2015).

These statistics are misleading because the fundamental purpose of hydrofracturing in gas-bearing shale is to crack the rock. Thus, all successful hydrofracturing jobs induce earthquakes but an aim is that they do not cause nuisance. Meeting this objective is helped in the USA and Canada by operating in regions of low population density. Seismic monitoring is often done because the earthquake locations indicate the location and volume of the fracture network created. However, if nuisance seismicity is not induced there is little reason to report it publically. Seismic analyses focus on investigating the spatial distribution and mode of fracturing, the results are not of public interest, and they are likely to remain proprietary.

A remarkable case was associated with injection operations in 2013 near Crooked Lake, Alberta. There, the largest shale-gas hydrofracturing-related earthquakes on record were induced. The target formation was Devonian Duvemay organic-rich shale. Operations involved multi-stage, high-pressure injections of proppant with weight-in-well ~60 MPa and volumes of a few thousand cubic meters. Of ~3000 hydrofracturing operations in Alberta in 2013, only three (0.1%) are reported to have been accompanied by noteworthy seismicity, with 160 events up to M_L 4.4 being observed over a ~2-year period (Schultz et al., 2015).

The quality of information about the sequences is limited because there were no local seismic stations. Data from distant stations were subject to sophisticated processing and suggested close spatial and temporal correlation with the shale-gas hydrofracturing (Fig. 65). Correlation also occurred between injection stages, a "screen-out" (i.e. interruption in slurry flow causing shutdown of injection) and seismicity. Associations between screen-outs and seismicity are reported from elsewhere (Clarke et al., 2014; Skoumal et al., 2015). The seismicity may have hampered operations at Crooked Lake.

The Horn River Basin, British Columbia, is a major shale gas production area. Hydrofracturing commenced in 2006 and gas production peaked in 2010 and 2011 (Farahbod et al., 2015). Prior to the hydrofracturing, seismic rates were low. Only 24 earthquakes with M 1.8–2.9 were located locally in a ~2-year period. When hydrofracturing started the seismic rate increased to > 100 earthquakes/year and correlated with hydrofracturing (Fig. 66). A logarithmic correlation between seismic moment, maximum magnitude and volume injected was observed (Fig. 67).

For the entire Horn River Basin, injected volume was more closely related to seismicity than injection pressure. Increases in volume increased earthquake frequency but not magnitude. Large earthquakes ($> 10^{14}$ N m, i.e., $M_W \sim 3.5$) occurred only when ~150,000 m^3 of fluid were injected per month. Time lags between injections and seismicity ranged from days to months.

The embryonic UK shale-gas industry began with the unfortunate case of the 2011 Preese Hall, Lancashire, earthquake sequence. There, the first UK dedicated multi-stage shale-gas hydrofracturing operation was conducted in a 1000-m section of the Carboniferous gas-bearing Bowland Shale. Following the injection of 2245 m^3 of fluid and 117 t of proppant, a nearby M_L 2.3 earthquake was reported by the British Geological Survey. The earthquake was felt, and was unusual in that location. The nearest monitoring station was 80 km away. Additional

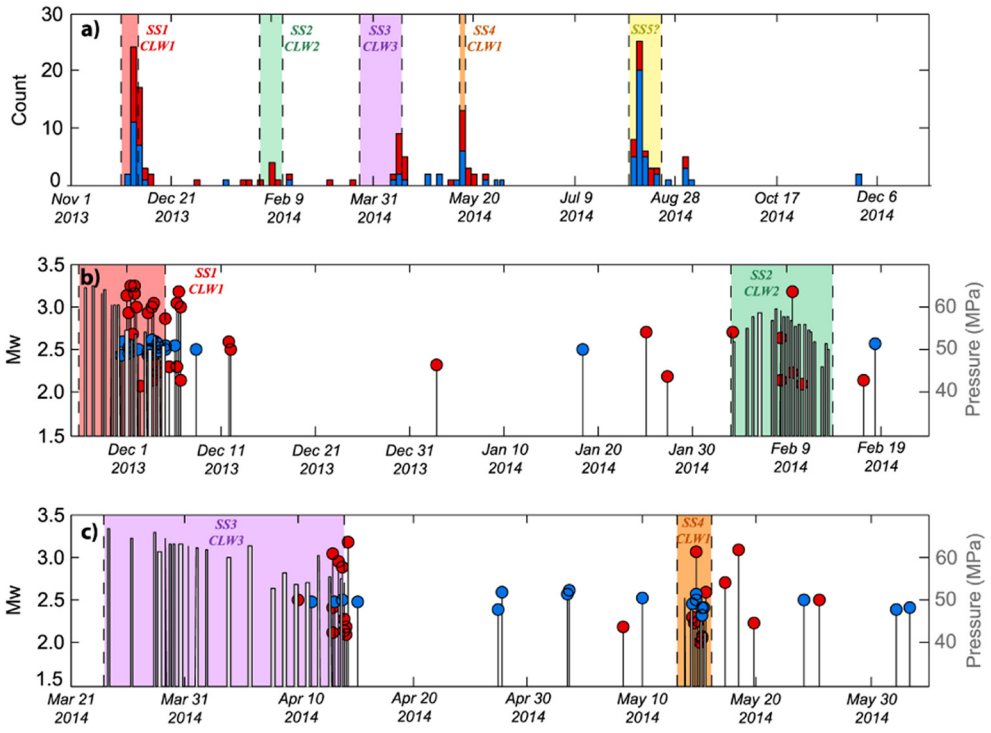

Fig. 65. Comparison of earthquakes and hydraulic fracturing completions at Crooked Lake, Alberta, Canada. (a) Histogram of located seismicity (red bars), with number of earthquakes increased using waveform cross correlation (blue bars). Hydrofracture schedules are bounded by colored boxes and labeled with respective subsequence and borehole. (b) Magnitudes of located (red circles), detected (blue circles) earthquakes and average injection pressure during hydrofracture stages (gray bars). (c) Same as (b) for later borehole completions.
(From Schultz et al. (2015).)

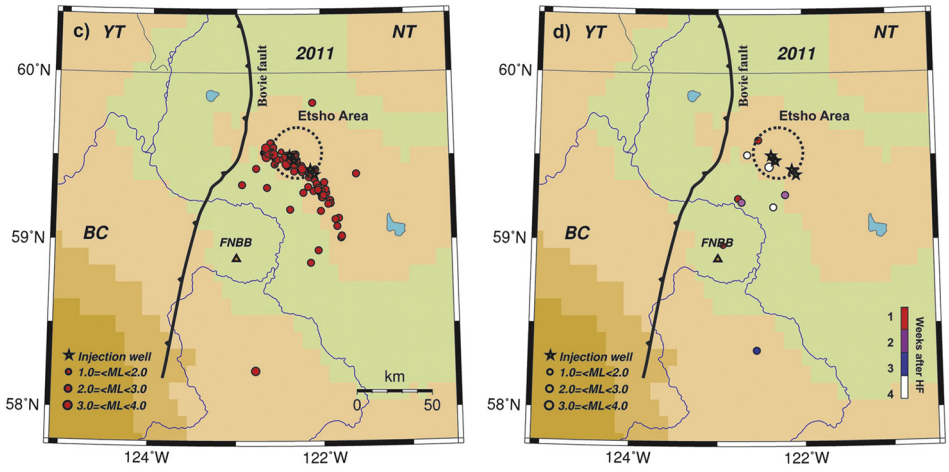

Fig. 66. Map of the Horn River Basin, British Columbia, Canada. Left: seismicity on days when hydrofracturing took place. Right: days when it did not occur.
(From Farahbod et al. (2015).)

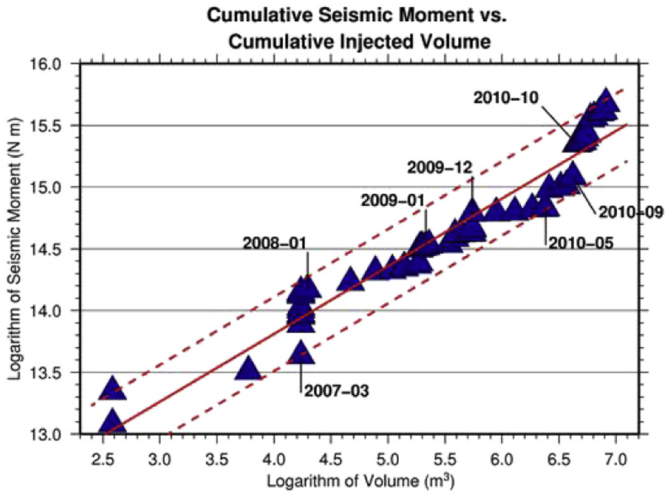

Fig. 67. Logarithm of seismic moment vs. logarithm of volume injected in shale gas hydrofracturing operations in the Etsho area, Horn River Basin, British Columbia, Canada. (From Kao et al. (2015).)

seismic stations were deployed rapidly but no aftershocks recorded. UK shale-gas hydrofracturing thus started with a rare phenomenon–the suspected induction of a nuisance earthquake.

Operations continued, but about six weeks later a second felt event of M_L 1.5 occurred ~1.0 km from the well. Citizen disquiet followed and operations were suspended. A total of 52 earthquakes in the magnitude range M_L −2.0 to 2.3 were detected with similar waveforms to the two largest events. A government enquiry and 18-month suspension of operations ensued while the problem was investigated. The close relationship between hydrofracturing and seismicity left little doubt that the earthquakes had been induced (Fig. 68).

The UK Department of Energy and Climate Change (DECC) commissioned a review and recommendations for mitigation of seismic risk associated with future shale-gas hydrofracturing operations in the UK. Recommendations included monitoring test injections prior to the main injections, monitoring fracture growth during injections, near-real-time seismic monitoring, and halting or changing injection strategy at the occurrence of seismicity with a threshold magnitude of M_L 0.5 (Green et al., 2012).

Detailed studies of the locations and fault mechanisms of the poorly recorded seismicity, combined with seismic reflection data, showed that the earthquakes probably occurred a few hundred meters below the well perforations on a fault that was not previously known (Clarke et al., 2014; Green et al., 2012). The fault does not intersect the borehole but was close enough that hydrofracture fluid may have leaked into it. The structure is an ancient transpressional fault that formed at the end of a Carboniferous basin inversion which had been inactive for 260 Ma. This case illustrates that even long-inactive faults, which are common in most continental crust, are close to failure and may be induced to slip by nearby injections.

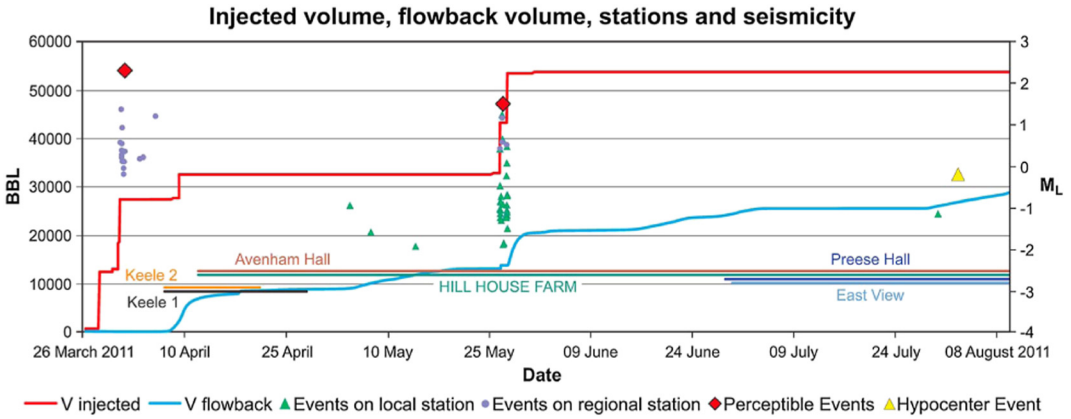

Fig. 68. Injection activity and seismicity associated with shale-gas hydrofracturing at Preese Hall, Lancashire, UK. Red line: injected volume; blue line: flow-back volume from the wellhead in US barrels (0.159 m^3); violet dots: earthquakes detected on seismic stations at distances of > 80 km; green triangles: earthquakes detected on two local stations; yellow triangle: event for which source mechanism and reliable hypocenter were obtained.
(From Clarke et al. (2014).)

Fig. 69. Site of the former Cacoosing Valley, Pennsylvania, quarry. Red oval: approximate boundary of the old quarry. Satellite image from Google Maps.

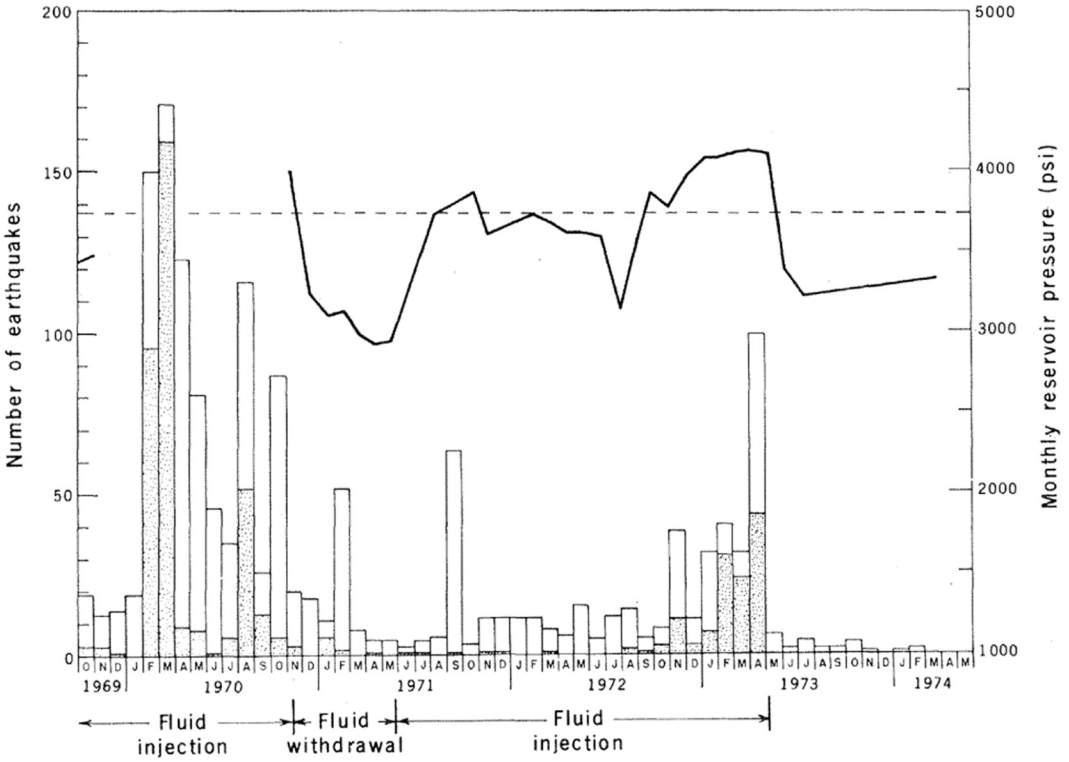

Fig. 70. Frequency of earthquakes at the Rangely Oilfield, Colorado, and reservoir pressures during fluid injection and fluid withdrawal. Stippled bars: earthquakes within 1 km of injection wells; black line: pressure history in injection well Fee 69; dashed line: predicted critical reservoir pressure.
(From Raleigh et al. (1976).)

4.1.7. Allowing mines to flood

Removal of rock from mines lowers confining stress on nearby faults and brings them closer to failure. The simultaneous pumping out of water during mining lowers pore pressure, increasing the strength of faults and counteracting the effect of rock removal. These processes roughly balance until a mine is abandoned and pumping stopped. After this, natural groundwater recharge may encourage seismicity.

A classic case is that of the 1994 Cacoosing Valley, Pennsylvania, earthquake sequence (Fig. 69) (Seeber et al., 1998). Groundwater recharge is implicated in a M_L 4.4 earthquake that occurred beneath an 800-m-wide carbonate quarry from which ~4×10^6 m^3 had been removed. The earthquake caused ~$2 million of damage to nearby homes. The quarry had been excavated to an average depth of 50 m over the 58-year time period 1934–1992. Groundwater pumping done during the mining period stopped after mining ceased and the water table rose by ~10 m in a few months. The rock is permeable karstic carbonate and depletion of groundwater, along with subsequent recharge, likely extended over a wider area than the footprint of the quarry.

Earthquake activity commenced approximately five months after

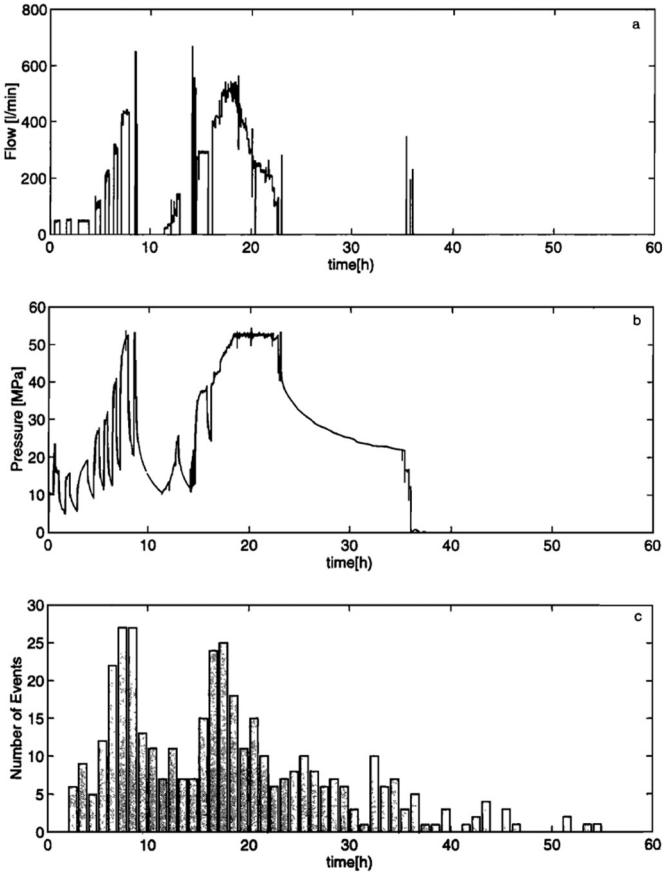

Fig. 71. Flow rates, pressure and number of earthquakes induced by brine injection into the Kontinentales Tiefbohrprogramm der Bundesrepublik Deutschland (KTB–the German Continental Deep Drilling Program) borehole during a 60-hour period. (From Zoback and Harjes (1997).)

pumping ceased. A rapidly deployed temporary seismometer recorded 67 aftershocks. They occurred in the upper 2.5 km in a planar pattern interpreted as the fault plane that slipped. Focal mechanisms suggested the mainshock had a thrust mechanism. The earthquakes occurred in the hanging-wall block such that unloading by rock removal would have encouraged slip. Surprisingly, the seismicity did not activate any of the plentiful, known, large-displacement faults in the region. Instead, stress was released on a set of small, unmapped faults which probably had a more suitable orientation. The mining had reduced confining stress by ~0.13 MPa, while the M_L 4.4 mainshock had a stress drop of 1–4 MPa.

The Cacoosing Valley event may have been similar to one that occurred two decades earlier beneath a large quarry at Wappingers Falls, New York (Pomeroy et al., 1976). A m_b 3.3 earthquake occurred there in 1974. Again, the mainshock and aftershocks nucleated at exceptionally shallow depth with some as shallow as 0.5 km. Slip occurred on a reverse fault immediately below the quarry and had a source mechanism consistent with the regional stress field. Over the preceding ~75 years ~30×10^6 m^3 of rock had been removed by open-casting down to a depth of ~50 m. This changed the stress by ~1.5 MPa at the surface and reduced the normal stress on faults below.

4.1.8. Research projects

In the wake of the Denver, Colorado earthquakes (Section 4.1.1) there was speculation that earthquakes might be controllable. Partly as a result, a series of earthquake-induction experiments have been conducted for research purposes. These have investigated the physical properties of natural fault zones and the processes that accompany earthquake occurrence. *HiQuake* contains 13 cases of earthquakes induced by research projects.

The first such project was conducted in 1969 at the Rangely Oilfield, Colorado (Raleigh et al., 1976). This oilfield occupies Mesozoic and Paleozoic sedimentary rocks at ~1700 m depth and is underlain by crystalline basement at ~3000 m. There is little local faulting, but earthquake activity had occurred with water flooding for enhanced recovery (Section 4.1.3). A seismograph array and prior earthquake record were therefore available. Fluid pressure in wells near the

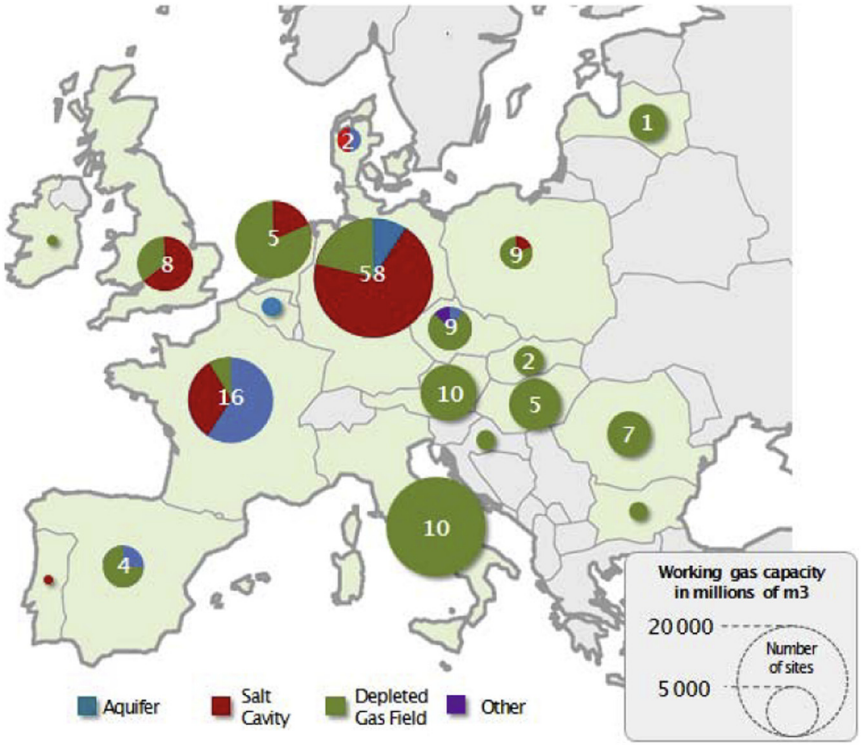

Fig. 72. Working gas capacities of underground storage sites in Europe (http://www.gasinfocus.com/en/; http://www.gie.eu/index.php/maps-data/gse-storage-map).

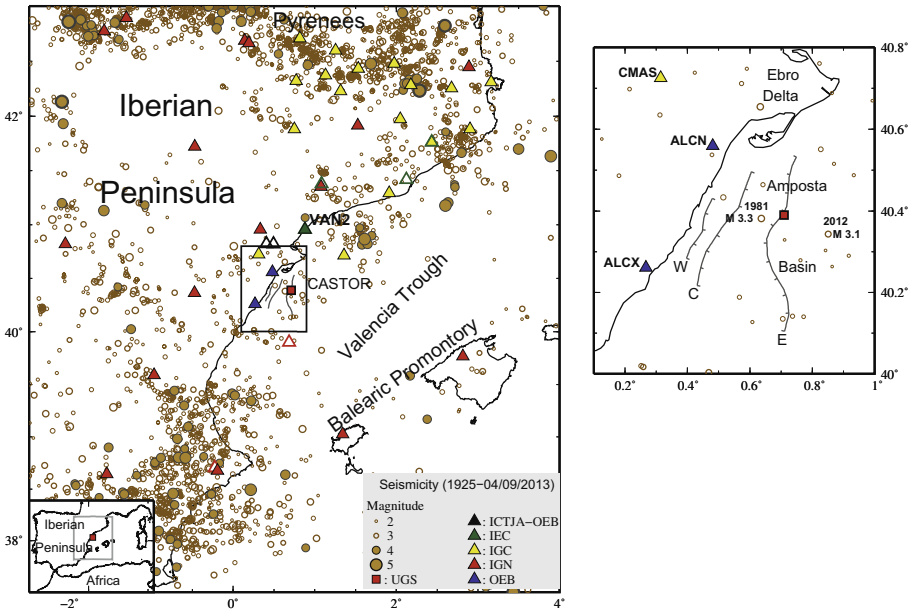

Fig. 73. Seismicity of the eastern Iberian Peninsula, Spain. Triangles: seismic stations; red square: location of the Castor underground gas storage reservoir. W, C and E denote the Western, Central and Eastern Amposta faults. (From Gaite et al. (2016).)

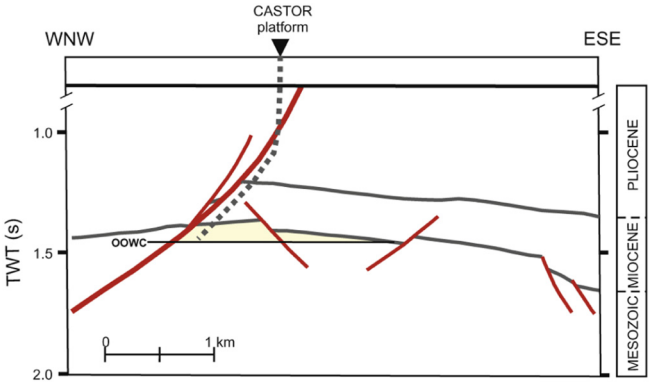

Fig. 74. Schematic diagram of the old Amposta Oilfield, Spain, in WNW-ESE section. TWT: two-way travel time; dashed line: approximate location of the Castor injection well: OOWC: original oil-water contact at 1940 m depth; yellow area: approximate location of the gas reservoir.
(From Gaite et al. (2016).)

earthquakes was experimentally cycled to investigate the effect on the seismicity. There was close correlation between seismicity and high pore pressure and events up to M_L 3.1 were induced (Fig. 70).

In 1970 another experiment was conducted at Matsushiro, Japan. A volume of 2883 m^3 of water at wellhead pressures of 1.4–5.0 MPa was pumped into an 1800-m-deep well to test whether earthquakes were induced by increasing pore pressure in a fault zone. After several days of injection earthquake activity started within a few kilometers of the well (Ohtake, 1974).

After a hiatus in experimenting of 16 years, in 1990, perhaps the best known research experiment to study fluid-induced seismicity was begun–the Kontinentales Tiefbohrprogramm der Bundesrepublik Deutschland (KTB)–the German Continental Deep Drilling Program. Extensive literature documents this project including a 1997 special section of Journal of Geophysical Research (No. 102) (e.g., Baisch and Harjes, 2003; Baisch et al., 2002; Bohnhoff et al., 2004; Erzinger and Stober, 2005; Fielitz and Wegler, 2015; Grasle et al., 2006; Jahr et al., 2005; Jahr et al., 2007; Jahr et al., 2008; Jost et al., 1998; Shapiro et al., 2006; Zoback and Harjes, 1997).

The main borehole was drilled 1990–1994 to a depth of 9.1 km. The first hydraulic stimulation was conducted in 1994 at depths and pressures close to the brittle-ductile transition. About 400 earthquakes up to M_L 1.2 were induced at about 8.8 km depth (Fig. 71). Focal mechanisms were consistent with stress measured in the borehole. Seismicity began within a few hours of pumping and a few tens of meters from the borehole. Modeling suggested that the earthquakes occurred in response to pressure perturbations of < 1 MPa, i.e. $< 1\%$ of the ambient, hydrostatic pore pressure at the nucleation depth.

An important conclusion of this experiment was that differential stress in the crust is limited by the frictional strength of well-oriented, pre-existing faults ("Byerlee's Law") and the crust is in brittle failure equilibrium even at great depth in stable intraplate areas. Hydraulic experiments at the site have continued up to recent years (e.g., Jahr et al., 2008).

A 1997 project in the Philippines injected 36,000 m^3 of water into a well intersecting a creeping portion of the Philippine Fault at the Tongonan geothermal field. The water entered the formation at 1308–2177 m below the surface (Prioul et al., 2000). Several hundred earthquakes occurred but all were away from the fault in the geothermal reservoir. Prioul et al. (2000) concluded that tectonic stress on the fault is relieved aseismically and as a consequence there was no differential shear stress to be released by the water injection.

In the same year, a water-injection experiment was conducted in the Nojima fault zone, Japan, shortly after it ruptured in the 1995 M 6.9 Kobe earthquake (Tadokoro et al., 2000). This experiment gathered information on the physical properties of a fault plane in the immediate post-rupture period. Over periods of a few days, 258 m^3 of water were injected into an 1800-m-deep borehole at a pressure of ~ 4 MPa at the surface, entering the fault zone at 1480–1670 m depth. An increase in M -2 to 1 seismicity occurred a few days after each injection. It was concluded that the fault zone was highly permeable and could slip with pore-fluid pressure increases of $< 10\%$.

Two additional experiments have been conducted in recent years, the first in 2013 as part of the Wenchuan Earthquake Fault Science Drilling (WFSD) project (Ma et al., 2015). This project studied the fault healing process. Over a four-month period 47,520 m^3 of water at 10–15 MPa was injected at rates of up to 1.7 l/s into a 552-m-deep well that intersected a fault zone at 430 m depth. The fault was activated and over 20,000 earthquakes up to M ~ 1 were detected by downhole observations. The hypocentral zone suggested failure in the same sense as the regional stress.

A similar phenomenon was reported by Guglielmi et al. (2015) in an experiment that stimulated an inactive fault in a carbonate formation. The experiment injected 0.95 m^3 of water into a 518-m-deep

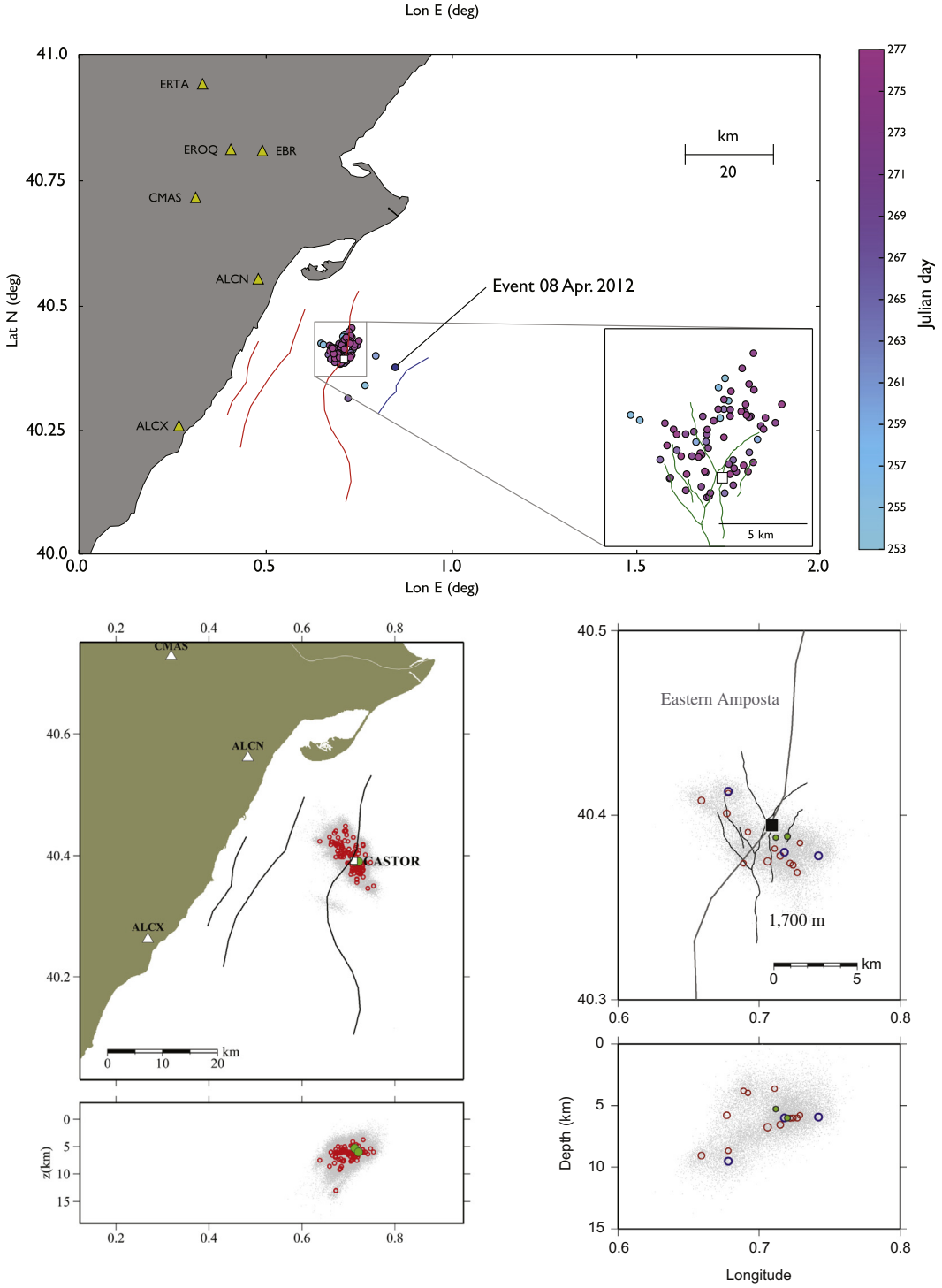

Fig. 75. Top: Faults and epicenters for the largest events in the 2013 earthquake sequence in the old Amposta Field. White square: Castor platform; colored lines: faults near the injection site; red lines: the Amposta faults; blue and green lines: additional faults (from Cesca et al., 2014). Centre left and bottom left: map and cross-section showing 116 earthquakes associated as a multiplet; triangles: seismic stations; white square: injection well; green dots: two events with M 3.0 and 3.2. Centre right and bottom right: map and cross-section of earthquakes with M > 3; black square: injection well (from Gaite et al., 2016).

underground experimental facility in southeastern France where a vertical well intersected a fault at 282 m depth. Aseismic shear slip started at a pressure of ~1.5 MPa, and ~80 earthquakes occurred a few meters from the injection point. These accounted for only a small fraction of the slip on the fault, however. The accumulated moment at the end of the experiment was $M_o = 65 \times 10^9$ N m (equivalent to an earthquake with M_W 1.17). This was far larger than the moment released by the seismicity, which totaled $M_o < 2$ N m. Aseismic slip dominated deformation in the fault zone and the earthquakes occurred in rock mass outside the pressurized zone. Other experiments have been performed in a salt solution mine at Cerville-Buissoncourt in Lorraine, France (Kinscher et al., 2015; Mercerat et al., 2010) and the Wairakei geothermal field, New Zealand (Allis et al., 1985; Davis and Frohlich, 1993).

This multi-decade, multi-national research endeavor has answered some critical questions, not always those originally posed and not

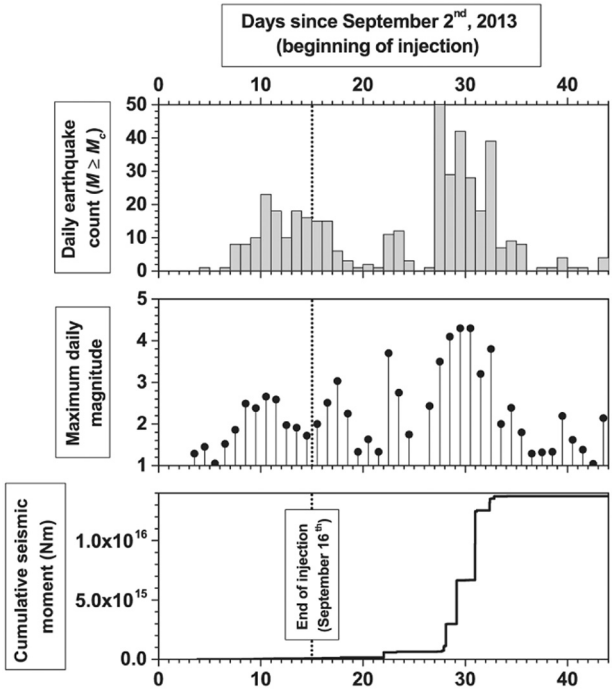

Fig. 76. Temporal evolution of seismicity with M > 2 associated with the Castor project, Spain, for 44 days from the beginning of gas injection, 2 September 2013. Top: daily number of events. Center: maximum daily magnitude. Bottom: cumulative seismic moment.
(From Cesca et al. (2014).)

always with the preferred answer. Relieving in a controlled way the stress naturally released in large earthquakes is scientifically challenging. The continental crust is near to failure, even to great depths and where large faults are not known. Earthquakes can be induced by relatively small stress perturbations, but in some cases stress on a targeted fault is relieved aseismically. In these cases, motion on that fault may induce secondary earthquakes in the surrounding rock mass. Fluid injection may thus induce primarily aseismic slip, and seismicity may be a secondary effect, with imperfect spatial correlation with the injection activities. In many cases of induced seismicity more stress is released than is loaded on faults artificially, since pre-existing tectonic stress is also released. However, the southeastern France experiment illustrates that the reverse sometimes occurs–some of the anthropogenically loaded stress may be released aseismically.

4.2. Gas

4.2.1. Natural gas storage

To stabilize supply and increase energy security nations store natural gas reserves, often underground. In May 2015, 268 underground gas storage facilities existed or were planned in Europe (Fig. 72) and over 400 in the USA.

Depleted hydrocarbon reservoirs, aquifers, and salt cavern formations are obvious repositories because they are usually well understood geologically and engineering infrastructure including wells and pipelines may already be in place. They may also be conveniently close to consumption centers.

HiQuake contains seven cases of induced seismicity reported to have been associated with underground gas storage:

- Gazli, Uzbekistan (Simpson and Leith, 1985);
- the Castor project (in the old Amposta Field), Spain (Cesca et al., 2014; Gaite et al., 2016);
- Bergermeer, Norg and Grijpskerk, Netherlands (Anonymous, 2014);
- Háje, Czech Republic (Benetatos et al., 2013; Zedník et al., 2001);

and

- Hutubi, China (Tang et al., 2015).

At the Bergermeer Gasfield, a few earthquakes up to M 0.7 occurred in 2013 in association with the injection of cushion gas. Up to 15 earthquakes per month up to M 1.5, several of which were felt, were reported for the Háje storage facility. Larger earthquakes occurred in association with gas storage at Hutubi, with over 700 earthquakes up to M 3.6 in the period 2009–2015.

The Gazli Gasfield, Uzbekistan, is primarily renowned for the three damaging M_S ~7 earthquakes that caused death and destruction in the local town of Gazli in 1976 and 1984 (Section 3.3.1). When this field had been largely depleted, it was used for storage. Gas was cycled in and out as required. Plotnikova et al. (1996) report seismicity up to M 5 induced by this process that correlates with the amount of gas stored.

The best-documented case history is that of the 2013 Castor project, Spain. This project aimed to use a depleted oilfield in the Gulf of Valencia, the old Amposta Field, ~20 km from the coast of north-eastern Spain (Fig. 73). It was planned to store 1.3×10^9 m^3 of natural gas there, sufficient to meet 25% of Spain's storage requirements. Earthquakes began shortly after the commencement of gas injection, however, the largest of which was M_W 4.3. Public reaction to the earthquakes was negative, not least because the population was sensitized after the 2011 M_W 5.1 Lorca earthquake only two years before, 250 km to the south along the coast (Section 3.1). We understand that as a result of the earthquakes the project has been discontinued.

The old Amposta oil reservoir occupies fractured and brecciated Lower Cretaceous dolomitic limestone and is one of several in the region (Fig. 74). It produced 56 million barrels (~9×10^6 m^3) of an estimated total in-place volume of 140 million barrels of oil (22×10^6 m^3) 1973–1989. Secondary injection for enhanced recovery was not needed because of strong natural water drive. After 1989 the depleted field lay dormant.

Installation of the necessary infrastructure for conversion of the reservoir into a gas storage facility commenced in 2009 and included a platform and gas pipeline. Injection of an initial ~10^8 m^3 (at 25 °C and 0.1 MPa pressure) of cushion gas (i.e. gas intended as permanent inventory in the reservoir) was conducted in 2013 at 1.75 km below sea level.

Three days after injection began, seismicity with events up to M 2.6 occurred (Figs. 75 and 76). Injection was stopped after 12 days but earthquakes continued to occur. The largest, a M_W 4.3 event, occurred two weeks after injection stopped. In total, over 1000 earthquakes were detected, > 420 with M ≥ 2 (Fig. 76). Seismicity was still ongoing in 2016 (Gaite et al., 2016).

Accurate hypocentral locations were difficult to calculate because the project, being offshore, was monitored by a seismic network with limited coverage. The closest station was 26 km from the Castor platform and, since most of the stations were on land, there was restricted azimuthal coverage (Gaite et al., 2016). As a result, different studies of the hypocentral locations yield different results and even the orientation of the hypocentral distribution as a whole (which might reveal the activated fault structure) and the hypocentral depths (which might show proximity to the injection site) vary significantly between studies. Both NW and NE orientations for the hypocentral zone are reported, along with depths that vary from close to the gas injection depth to several kilometers deeper (Fig. 75) (e.g., Cesca et al., 2014; Gaite et al., 2016).

The epicentral area forms part of the dominantly ENE-WSW Catalan-Valencian normal-faulting extensional region (Perea et al., 2012) and focal mechanism studies of the mainshock show motion compatible with slip in this sense (Cesca et al., 2014). The most significant potentially seismogenic feature near the old Amposta Field is the 51-km-long, NE-SW oriented, Fosa de Amposta fault system (Gaite et al., 2016). If such a major fault zone were to rupture in its entirety a M 5–7 earthquake could occur (Fig. 77). Combined interpretation of the

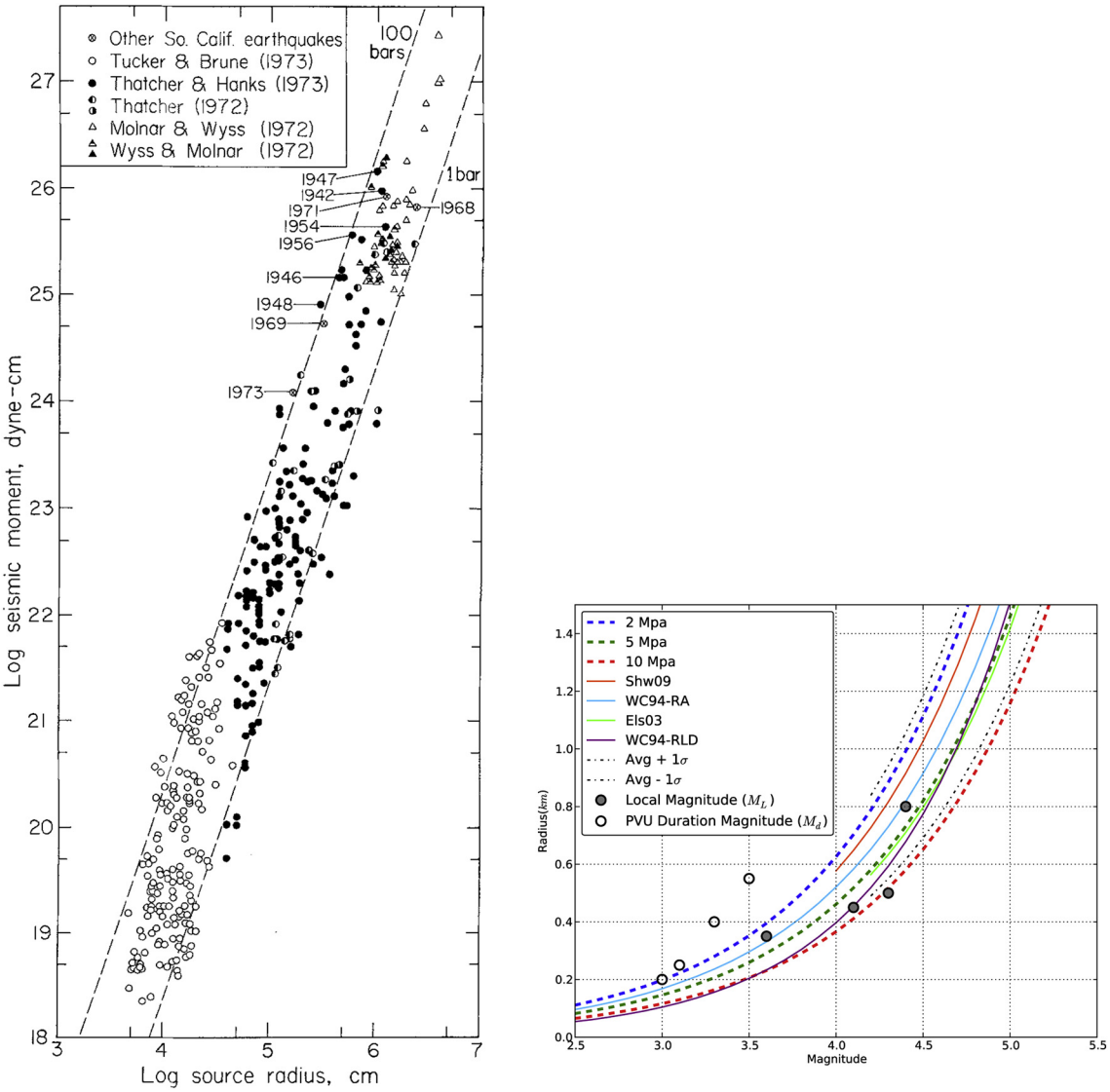

Fig. 77. Left: Set of data for small earthquakes showing the relationship between seismic moment and source radius. Dashed lines are of constant stress drop (Hanks, 1977). Right: Rupture radius vs. duration earthquake magnitude for several models. Black dotted lines: average of these relationships ± 1σ; blue, green and red dashed lines: relationships derived from the moment-magnitude relation of Hanks and Kanamori (1979) for stress drops of 2, 5 and 10 MPa respectively, and estimated fault radius using half the rupture-length-at-depth parameter; gray and white circles: values for individual earthquakes induced at Paradox Valley, Colorado.
(From Yeck et al. (2015).)

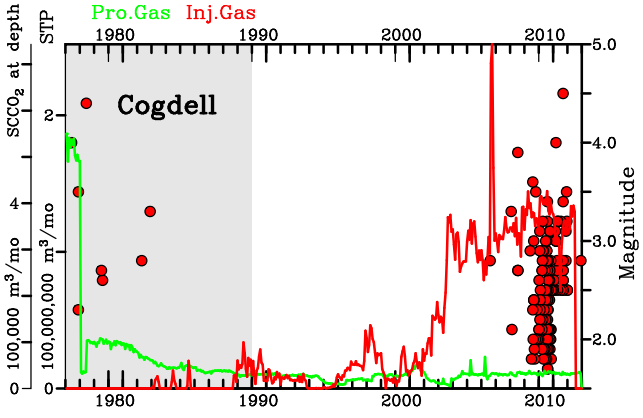

Fig. 78. Operations and seismicity at the Cogdell Oilfield, Texas. Green: monthly volumes of natural gas produced; red: gas injected; red dots: earthquakes detected 1977–2012. There was a clear increase in seismic activity from 2006, five years after the start of CO_2 injection.
(From Gan and Frohlich (2013).)

locations and source mechanisms suggests that this fault was not activated, however.

The seismicity was unusual for the area in both magnitude and seismic rate compared with the preceding two decades (Fig. 73). Although earthquake activity occurs along the coast of Spain to the north and south, the Pyrenees mountain chain in Portugal, and the coast of North Africa, no significant historical seismicity was known on the fault system local to the Castor project prior to the gas injection. For this reason, and because of the close spatial and temporal correlation with gas injection, there is little doubt that the earthquakes were induced.

4.2.2. CO_2 for oil recovery

There are approximately 100 enhanced oil recovery injection sites where CO_2 is used, mostly in Texas. *HiQuake* contains two cases where seismicity is postulated to be induced by this process. These are at the Cogdell Field, Texas (Gan and Frohlich, 2013) and Weyburn Oilfield, Saskatchewan (Maxwell and Fabriol, 2004; Verdon et al., 2013). The latter is a hybrid project and also classified as a Carbon Capture and Storage (CCS) project (Section 4.2.3).

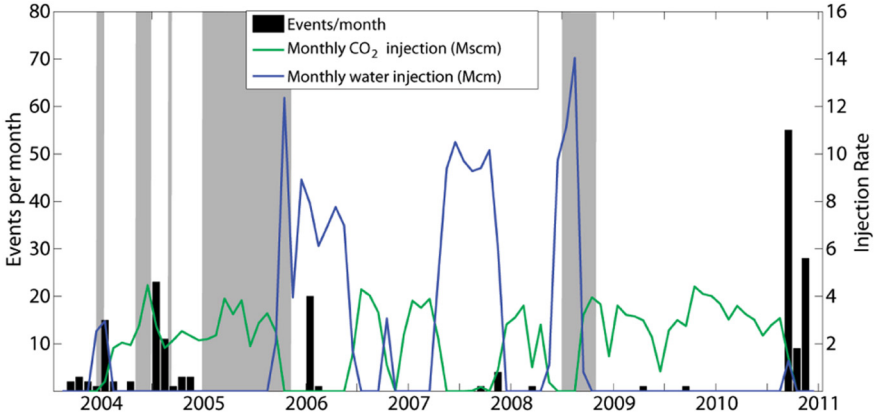

Fig. 79. CO_2, water injection, and associated earthquakes at the Weyburn Oilfield, Saskatchewan, Canada. Shaded periods: monitoring array was inoperative.
(From Verdon et al. (2013).)

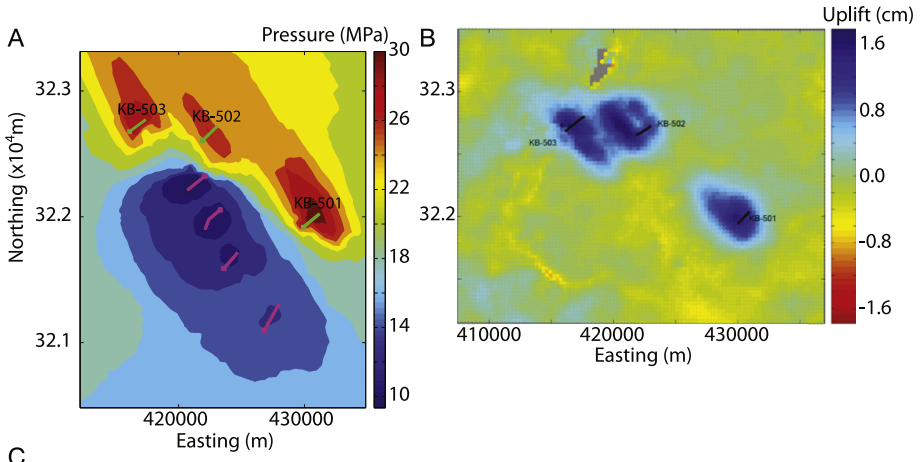

Fig. 80. Modelled pore pressure and geo-mechanical deformation at In Salah, Algeria. A: Map of pore pressure after three years of injection. B: Surface uplift measured by InSAR. C: Modelled pressure at the three injection wells and in the producing part of the reservoir.
(From Verdon et al. (2013).)

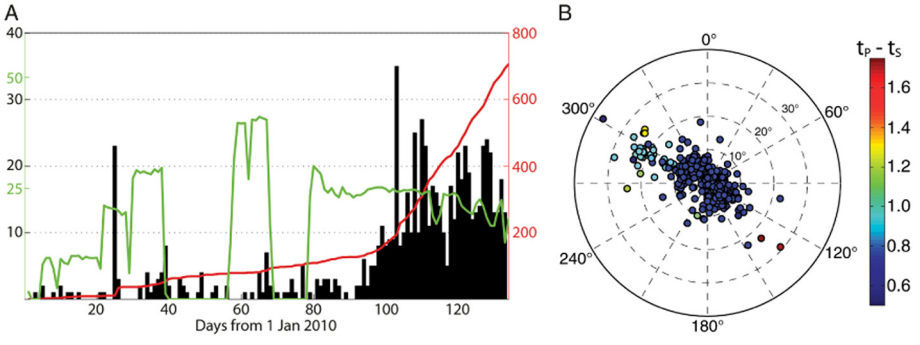

Fig. 81. Microseismicity at In Salah, Algeria. A: Black: daily seismicity rate; red: cumulative number of events January–April 2010; green: CO_2 injection rate in millions of standard cubic feet per day (1 million standard cubic feet of gas per day at 15 °C = 28,250 m^3/day). B. Event arrival angles in polar projection, colored by differential *S*- and *P*-wave arrival times.
(From Verdon et al. (2013).)

Early on in its history, the Cogdell Oilfield generated earthquakes surmised to have been induced by water injection (Gan and Frohlich, 2013). Lately, CO_2 has been injected and is associated with earthquakes up to M_W 4.4 (Fig. 78).

The Cogdell Oilfield is a large subsurface limestone reef mound, not a fault-bounded oil trap, and there are no mapped faults nearby. Production began in 1949 and 1957–1983 oil recovery was enhanced by brine injection. This was associated with earthquakes, including a M_L 5.3 event in 1978. This earthquake was only poorly located as a result of the rudimentary nature of seismic monitoring in Texas at the

Fig. 82. Aerial photograph of the Nevada test site, USA. View of Yucca Flat looking south-southeast. Center of ring road is at 37°N 9.57′, 116°W 4.63′, elevation 4400 m (https://en.wikipedia.org/wiki/Nevada_Test_Site).

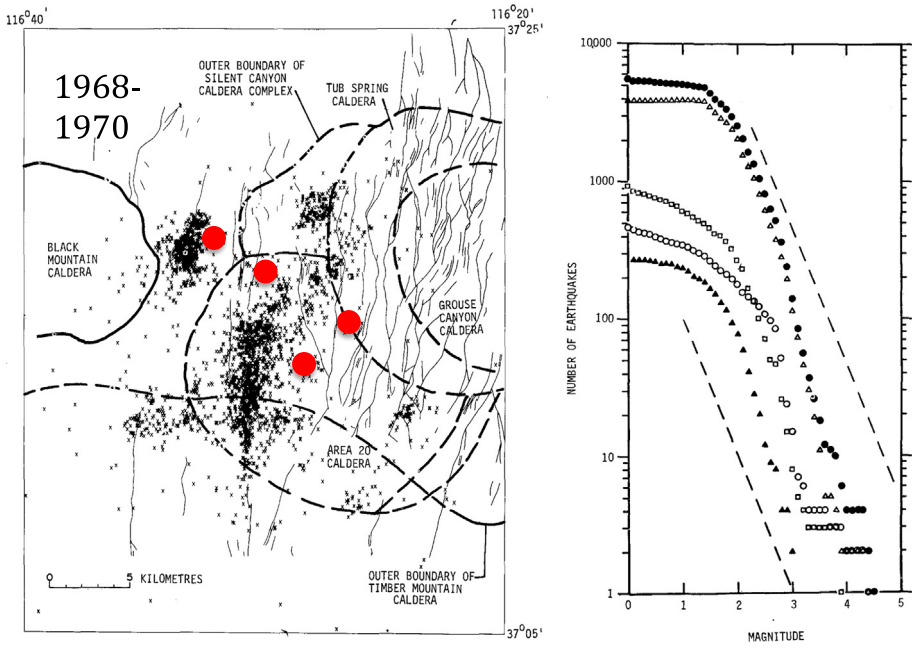

Fig. 83. Left: Epicenters of aftershocks of the Benham (1968), Jorum (1969), Purse (1969), and Handley (1970) nuclear explosions at the Nevada Test Site. Heavy lines: caldera boundaries; light lines: basin-range faults; red dots: locations of nuclear explosions. Right: Frequency-magnitude distribution for aftershocks in Pahute Mesa (from Hamilton et al., 1972). Dots: entire recording period; open triangles: the period Benham to Purse; solid triangles: Purse to Jorum; circles: Jorum to Handley; squares: Handley to the end. Dashed lines have a slope of −1; the data above M 2 define *b*-values of about −1.4 (from McKeown, 1975).

time. Davis and Pennington (1989) suggested that the earthquakes correlated with injection volume and high reservoir pressure gradients.

Gas injection began in 2001 and grew to a constant, high level of ~40 × 10^6 m^3/month from 2004. It was introduced at ~2.1 km depth, 20 MPa pressure and 75 °C, under which conditions CO_2 is supercritical. In 2006, after 23 years of seismic quiescence and following a significant increase in gas injection rate, earthquakes began again. Over the following five years 18 events with M > 3 occurred and in 2011 one of M_W 4.4.

A 21-month period March 2009–December 2010 could be studied in detail because at this time USArray, a rolling program to cover the entire country with temporary seismic stations,[8] swept across Texas. During this period the network recorded 93 locatable events, many within 2 km of wells actively injecting gas. Locations and focal mechanisms showed that the events occurred on previously unknown faults. Although the neighboring Kelly-Snyder and Salt Creek Fields have similar operational histories, seismicity is not induced in them.

4.2.3. Carbon Capture and Storage (CCS)

In the case of Carbon Capture and Storage (CCS), in addition to causing a nuisance, induced earthquakes could rupture the impermeable containment caprock that contains the CO_2 in the storage reservoir, and release it back into the environment. Carbon geostorage is in its infancy, but 20–30 tests are already underway globally, including eight operational commercial-scale plants.[9] Of these, three are seismogenic. An illustrative range of seismic responses is provided by the Sleipner Field, the Weyburn Field (Saskatchewan, Canada) and In Salah

[8] http://www.usarray.org.

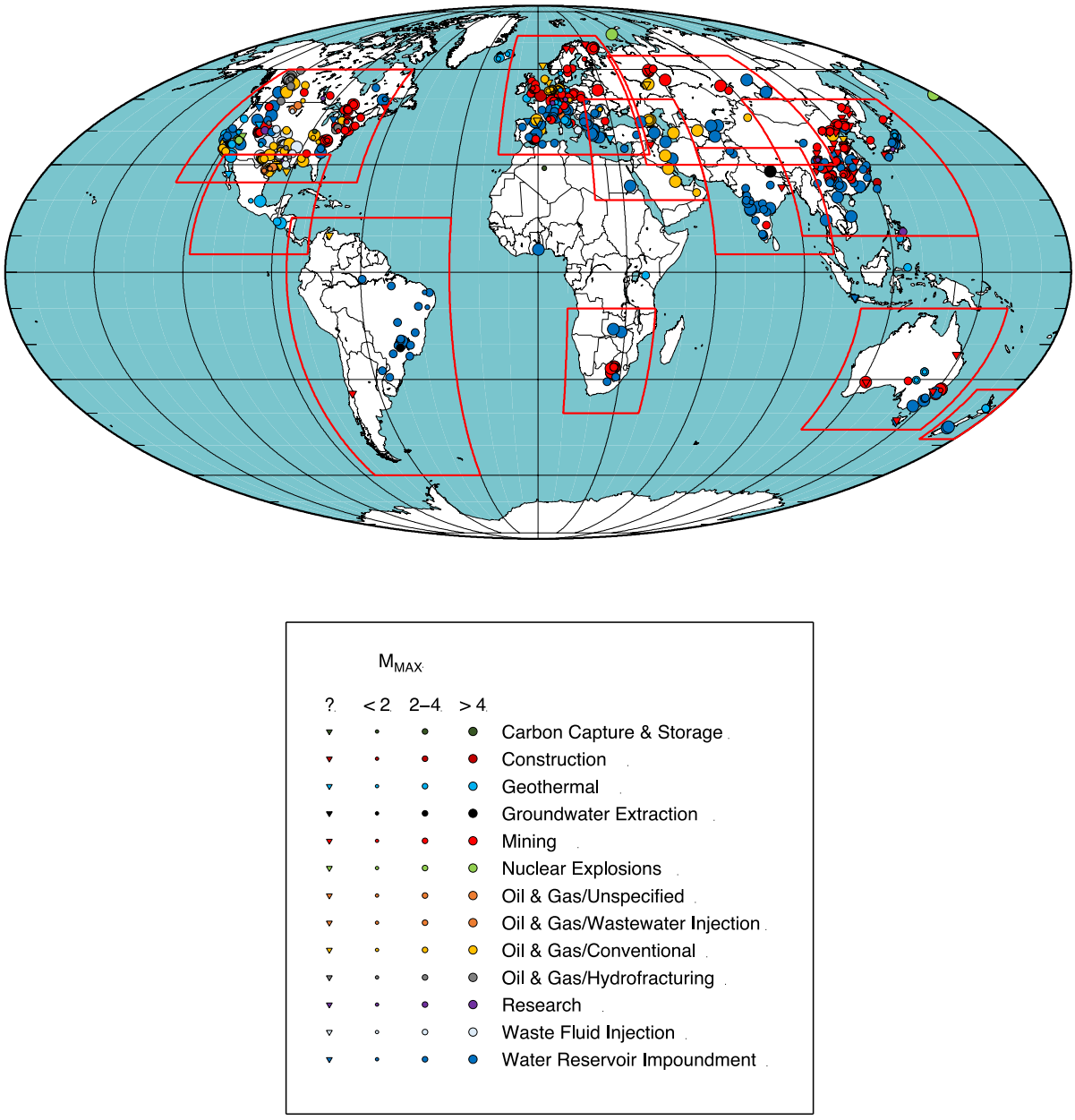

Fig. 84. Cases of human-induced seismicity world-wide, in Mollweide projection, centered on the Greenwich meridian. Colors of symbols indicate different categories of seismogenic activity. Circle sizes indicate the magnitudes of the largest reported induced earthquakes in each category, and inverted triangles indicate cases for which this magnitude was not reported. Red boxes show the locations of the regional maps.

(Algeria) (Verdon et al., 2013).

Since 1996 $\sim 10^6$ t/year of CO_2 has been removed from the natural gas produced from the Sleipner Field (Norwegian North Sea) and re-injected into a shallow saline aquifer (the Utsira Formation). This aquifer is large and comprises well-connected, little-faulted sandstone with high porosity and permeability at ~1 km depth beneath North Sea mean sea level. By 2011 the total volume of CO_2 injected amounted to only ~0.003% of the available pore space. No pore-pressure increase, mechanical deformation or seismicity has been detected for the entire > 20 years of injection. The Sleipner Field is, however, not seismically monitored locally so small earthquakes would go undetected. The nearest earthquakes to the Sleipner Field listed in the British Geological Survey catalog are a M_L 3.5 event at 1 km distance and a M 2.5 earthquake at 6 km distance. The uncertainties in these locations are large.

The Weyburn Oilfield, Saskatchewan, Canada, has been exploited for 45 years and is somewhat seismogenic. CO_2 injections started in 2000 both for enhanced oil production and CO_2 sequestration and now $\sim 3 \times 10^6$ t/year are injected annually. This is accompanied by minor, low-magnitude earthquake activity (Fig. 79). Some earthquakes clustered near injection wells, but no clear temporal correlations are apparent.

In contrast, vigorous earthquake activity accompanied CO_2 sequestration at the producing In Salah Gasfield, Algeria. There, CO_2 was injected into a low-permeability, 13–20% porosity, ~20-m-thick fractured sandstone in a non-producing, water-dominated part of field at 1850–1950 m depth. Hundreds of earthquakes accompanied surface uplift.

CO_2 injection at In Salah 2004–2013 amounted to a total of $\sim 3.85 \times 10^6$ t of CO_2 which was produced from nearby gas wells and

[9] http://www.ccsassociation.org/faqs/ccs-globally/.

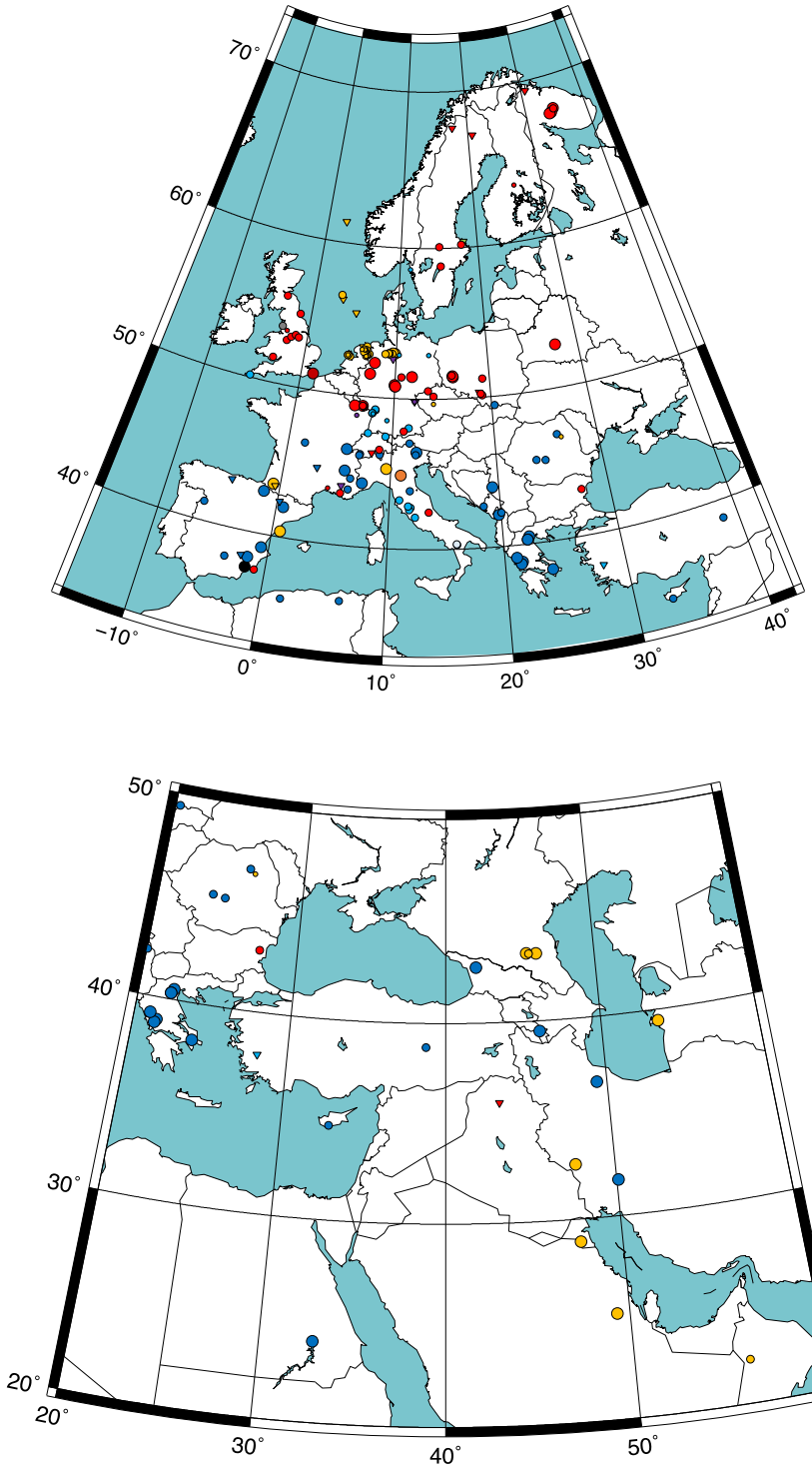

Fig. 85. Same as Fig. 84 except for (top) Europe, and (bottom) Middle East.

re-injected via horizontal boreholes. There was little pressure communication with the producing part of the field. Pore pressures increased from initial conditions of ~18 MPa at the injection points to ~30 MPa while reducing in the production parts of the reservoir (Fig. 80). Deformation monitoring detected surface-blistering type uplift of up to ~1 cm/year locally around the injection wells.

A nearby borehole seismometer detected over 1000 events in 2010. The data were consistent with locations in the receiving formation beneath the injection well though there was no correlation with CO_2 injection (Fig. 81). The project was subsequently terminated because of seal integrity concerns.

Verdon et al. (2013) conclude that at Sleipner, where the target aquifer is large and pressure increases during injection minimal, little deformation, either seismic or aseismic, results. At Weyburn, deformation and seismicity may be partly mitigated by ongoing oil extraction which serves to offset pressure increase resulting from the CO_2 injections. At In Salah, however, the formation into which CO_2 is injected had poor pressure communication with the producing parts of the reservoir and natural gas extraction did not compensate for the injections. Pore pressures increased as a consequence leading to both seismic and aseismic deformation.

Another seismogenic CCS demonstration site is at Decatur, Illinois

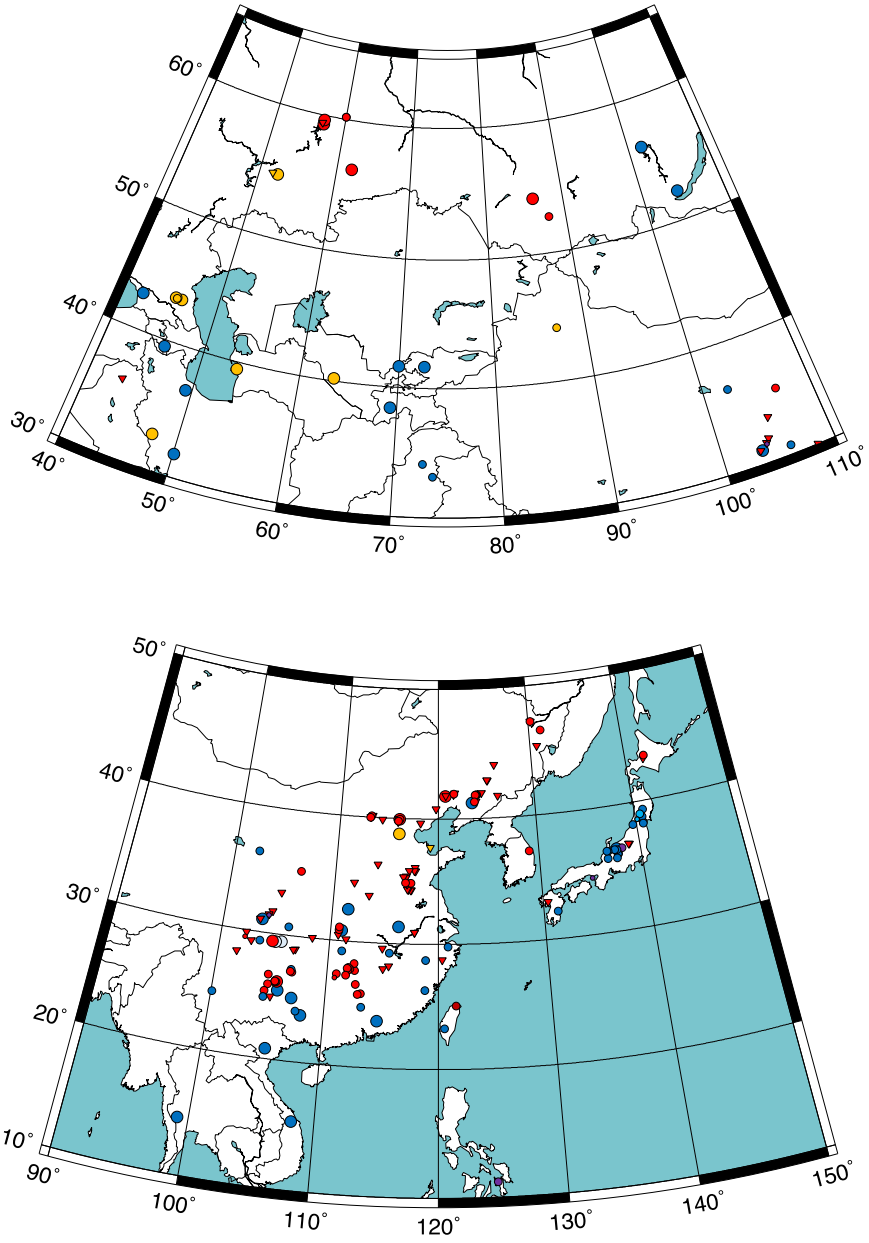

Fig. 86. Same as Fig. 84 except for (top) central Asia, and (bottom) east Asia.

(Kaven et al., 2015). There, ~10^6 t of supercritical CO_2 were injected over a period of three years at a depth of 2.1 km into a regionally extensive, 460-m-thick high porosity/permeability sandstone. The CO_2 used is a by-product of local ethanol production. Approximately 180 earthquakes up to M_W 1.26 occurred over about two years within a few kilometers of the injection well and at the approximate depth of injection. Kaven et al. (2015) concluded that earthquakes nucleated on preexisting faults in the basement well oriented with respect to the regional stress field. Little seismic hazard is posed to the host formation because the earthquakes are remote and small.

All other CCS projects have been shorter in duration and with total volumes no more than 10s or 100s of thousands of tonnes. CCS projects have developed recently in China where eleven projects are reported (Huaman and Jun, 2014). Limited information is available on these projects and none regarding seismicity induced.

4.2.4. Injection into the subsurface: summary

Diverse fluids are injected into the ground for various reasons and related seismogenic behavior is variable. For most projects no earthquakes are reported. For others, small earthquakes occur that are of insufficient general interest to publish details. For a small minority induced seismicity is sufficiently troublesome to hinder operations or result in project abandonment.

Correlations between seismic and operational parameters vary. Earthquakes thought to be induced may be co-located with injections to 10 s or 100 s of meters or they may occur tens of kilometers away. Earthquakes may begin as soon as operations start or be delayed for decades. Small operations may induce large earthquakes and large operations may be aseismic.

Why is Oklahoma highly seismogenic while large-scale injection projects are conducted in many states of the USA without nuisance earthquakes occurring? We are not aware of any current theories as to why this is.

5. Explosions

Since the first test of a nuclear device, the Trinity explosion of July 16, 1945, approximately 2000 such tests have been conducted by eight

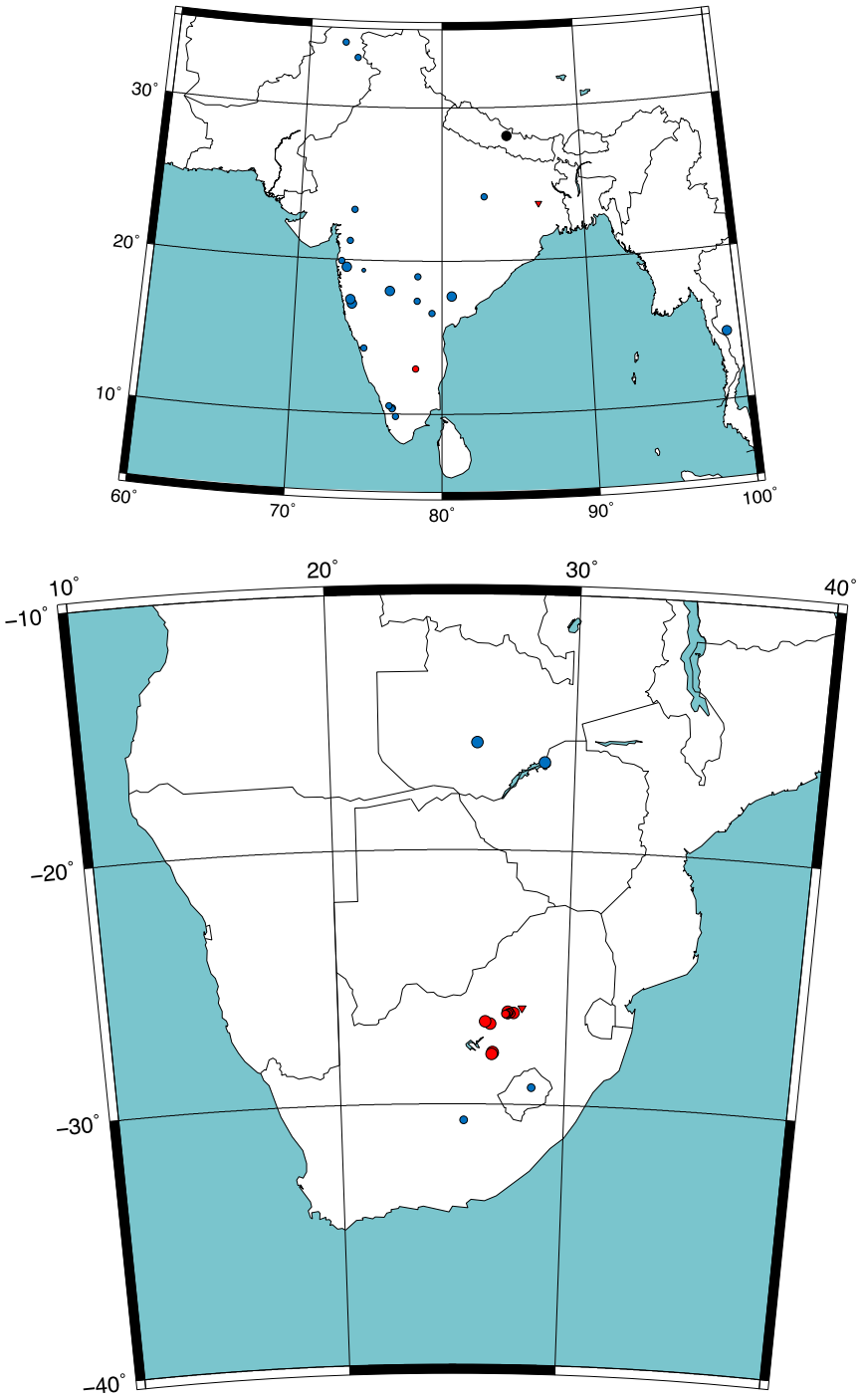

Fig. 87. Same as Fig. 84 except for (top) India and vicinity, and (bottom) southern Africa.

nations, 1352 of them underground. Seismicity was reported to be associated with 22 of these, 21 in the USA and one in Russia (Boucher et al., 1969; Engdahl, 1972; Hamilton et al., 1972; McKeown, 1975; McKeown and Dickey, 1969).

American nuclear tests were conducted at the Nevada Test Site for the 48-year-period 1945–1992 (Fig. 82). Boucher et al. (1969) investigated the possibility of induced seismicity associated with 16 nuclear tests by searching the University of Nevada database of earthquake locations. They reported induced earthquakes after all of the 10 tests where the explosion itself registered $m_b \geq 5.0$. The explosions themselves are not included in the *HiQuake* database. The largest earthquake induced was at least one magnitude unit smaller than the inducting explosion. Earthquakes may have been induced by many, if not all of the tests, but been too small to be clearly recorded.

A test ironically named Faultless (19/1/1968) induced clearly visible surface slip on faults up to 40 km away, even though the test was only one megaton in yield. Ground deformation associated with this, and other nuclear tests, has been captured on film (McKeown and Dickey, 1969).[10]

Detailed studies of the seismicity induced by large nuclear tests were done for the Benham (19/12/1968), Purse (07/05/1969), Jorum (16/09/1969) and Handley (26/03/1970) tests (Fig. 83) (Hamilton et al., 1972; McKeown, 1975). Earthquakes occurred immediately after the tests and clustered on Pahute Mesa where a 4-km-thick sequence of volcanic rocks contains both caldera- and basin-range-type normal

[10] See, for example, https://www.youtube.com/watch?v=6ETHnsKnKiA.

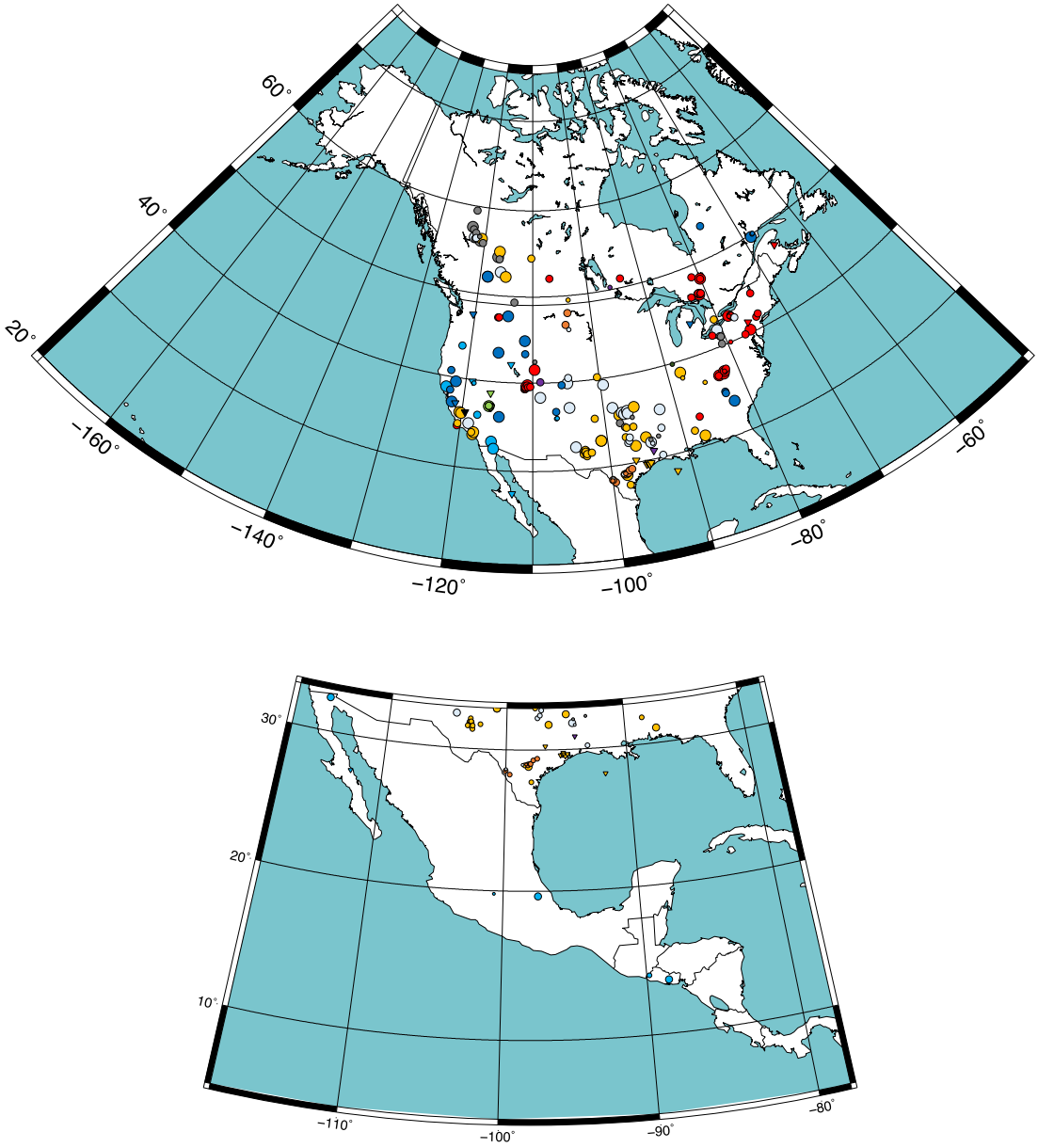

Fig. 88. Same as Fig. 84 except for (top) North America, and (bottom) central America.

faults. Most of the earthquakes induced occurred 10–70 days after the tests, at < 5 km depths and closer than ~15 km to ground zero. The locations of the earthquakes were mostly controlled by local geological structure and lay on faults in the caldera ring-fracture zones (Fig. 83) (McKeown and Dickey, 1969).

Underground nuclear tests in Amchitka, Alaska, resulted in permanent displacement on faults up to 1 m in the vertical and 15 cm in the horizontal for faults up to 8 km long (McKeown and Dickey, 1969). Both the Milrow (1969) and Cannikin (1971) tests generated several hundred small earthquakes with M < 4, thought to be related to deterioration of the explosion cavity. The sequences concluded with large, complex events and simultaneous subsidence of the surface resulting from final collapse of the explosion cavity. In the case of the Cannikin test, small events continued up to 13 km from ground zero for several weeks. The earthquakes are thought to have released ambient tectonic stresses. The more modest post-test seismic response from tests in Amchitka compared with those conducted in Nevada may result from the lower level of tectonic stress (Engdahl, 1972). Tectonic stress is also released simultaneously with the explosions themselves, as shown by blast focal mechanisms involving both shear and explosive components (Fig. 22) (Toksöz and Kehrer, 1972; Wallace et al., 1983). The largest earthquake induced by a nuclear test had a magnitude of m_b 4.9 and was associated with collapse of the cavity of the Cannikin, Amchitka test.

Most large chemical explosions are associated with rocket launching, military research and operations, and accidents in the military, space-program and industrial sectors. Such explosions may be equivalent of several kilotonnes (kt) of TNT. They occur at the surface on land or on ships and are thus poorly coupled to the ground. Tsunamis, but not earthquakes, have been reported in association with some of these.

It has been suggested that deep penetrating bombs may modulate earthquake activity. Balassanian (2005) examined earthquake activity over ~2-year periods spanning bombing incidents at Kosovo, Yugoslavia (1999), Baghdad, Iraq (1991), Tora Bora, Afghanistan (2001) and Kirkuk, Iraq (2003). It was suggested that the incidence of M ≥ 5 earthquakes increased within 1000 km and one year of the bombings at Kosovo and Tora Bora but not after those at Baghdad and Kirkuk.

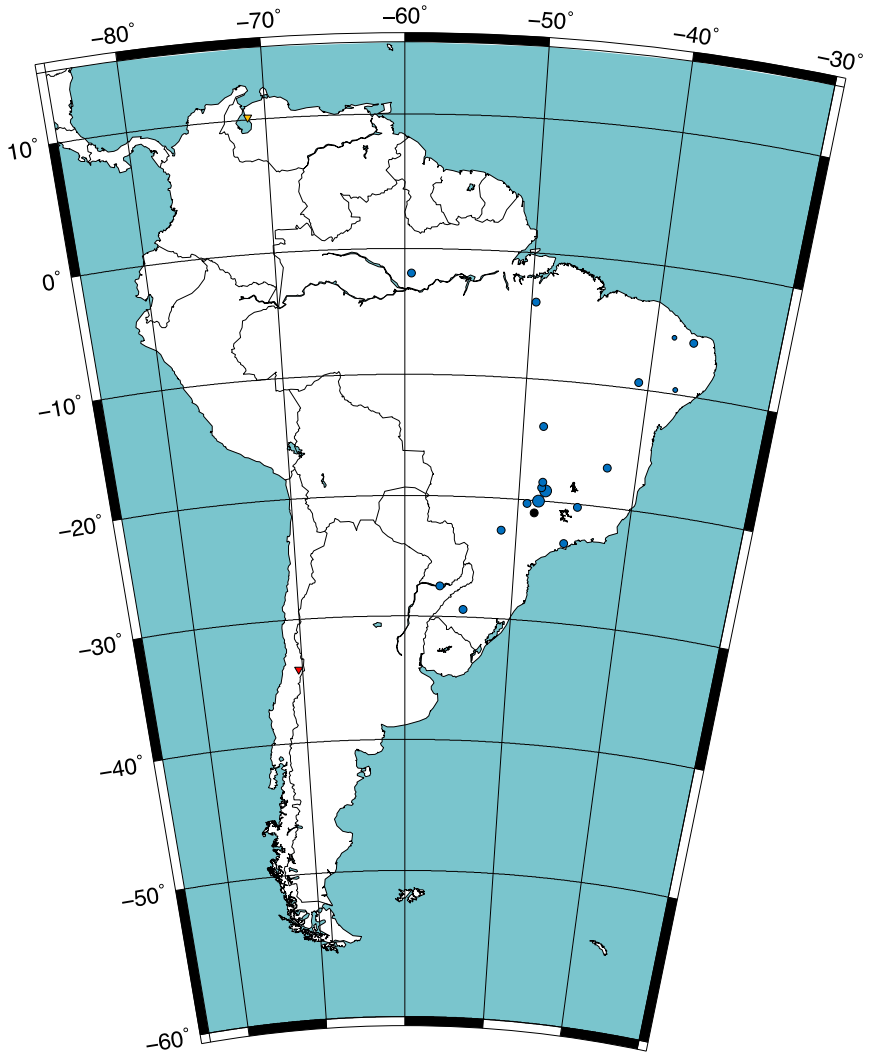

Fig. 89. Same as Fig. 84 except for South America.

Arkhipova et al. (2012) suggested that the 23 October 2011 M 7.8 Van earthquake, eastern Turkey, was encouraged by mass bombing associated with the Libyan conflict, 1300–1500 km away.

Deep penetrating bombs explode at depths of a few meters in the ground, improving the coupling by factors of several tens of percent compared with equivalent surface explosions. Nevertheless, deep penetrating bombs are generally not larger than the equivalent of ~1 kt of TNT, much smaller than the megatonne- or multi-megatonne scale typical of nuclear devices reported to have induced earthquakes. In the case of the nuclear tests, earthquakes have been induced out to a maximum of ~40 km away and activity has decayed away over periods of a few days or weeks (Boucher et al., 1969). Given the relatively small subsurface effects of chemical explosions and the great distances and relatively long time delays of earthquakes postulated to have been induced by them, these suggestions must be considered speculative.

6. Summary

Human-induced earthquakes are reported from every continent except Antarctica (Fig. 84). Figs. 85–90 show regional maps for Europe, the Middle East, central- and east Asia, India and vicinity, southern Africa, North-, central- and South America, Australia and New Zealand. Induced seismicity correlates with industrial activity and not with tectonic plate boundaries.

The magnitudes of the largest earthquakes (M_{MAX}) associated with projects of different types vary widely. The largest have been reported for water reservoirs, conventional oil and gas exploitation, and geothermal operations. Median magnitudes also vary between project types but the most commonly reported are $3 \leq M < 4$ which apply to water reservoirs, construction, conventional oil and gas, hydrofracturing, mining, and research projects. For some types of project the number of cases reported is small. For all project types it is essentially certain that large numbers of smaller induced earthquake sequences have not been reported.

Relationships between seismic and operational parameters have been suggested for a number of projects. For example, seismic moment released and volume injected correlate in shale gas hydrofracturing operations at the Etsho area, Horn River Basin, British Columbia (Fig. 67) (Farahbod et al., 2015). Of interest for future projects is what correlations might exist for all projects of the same kind.

From the point of view of nuisance, the magnitudes of the largest earthquakes induced are the most important. Seismic rate and total number of earthquakes are of secondary importance because the fractal nature of earthquakes means that most are small. Because a large and systematic part of the true dataset is missing (i.e. the unreported cases) correlations with operational parameters cannot convey any information on average M_{MAX}. Of interest is whether *the largest* M_{MAX} for projects of a particular kind correlates with operational parameters.

Fig. 91 shows a plot of M_{MAX} vs. water reservoir volume for 126 cases. The magnitude of *the largest* M_{MAX} (i.e., the apparent M_{MAX} ceiling) increases with reservoir volume. However, there is no correlation between M_{MAX} and reservoir volume for the dataset as a whole. If

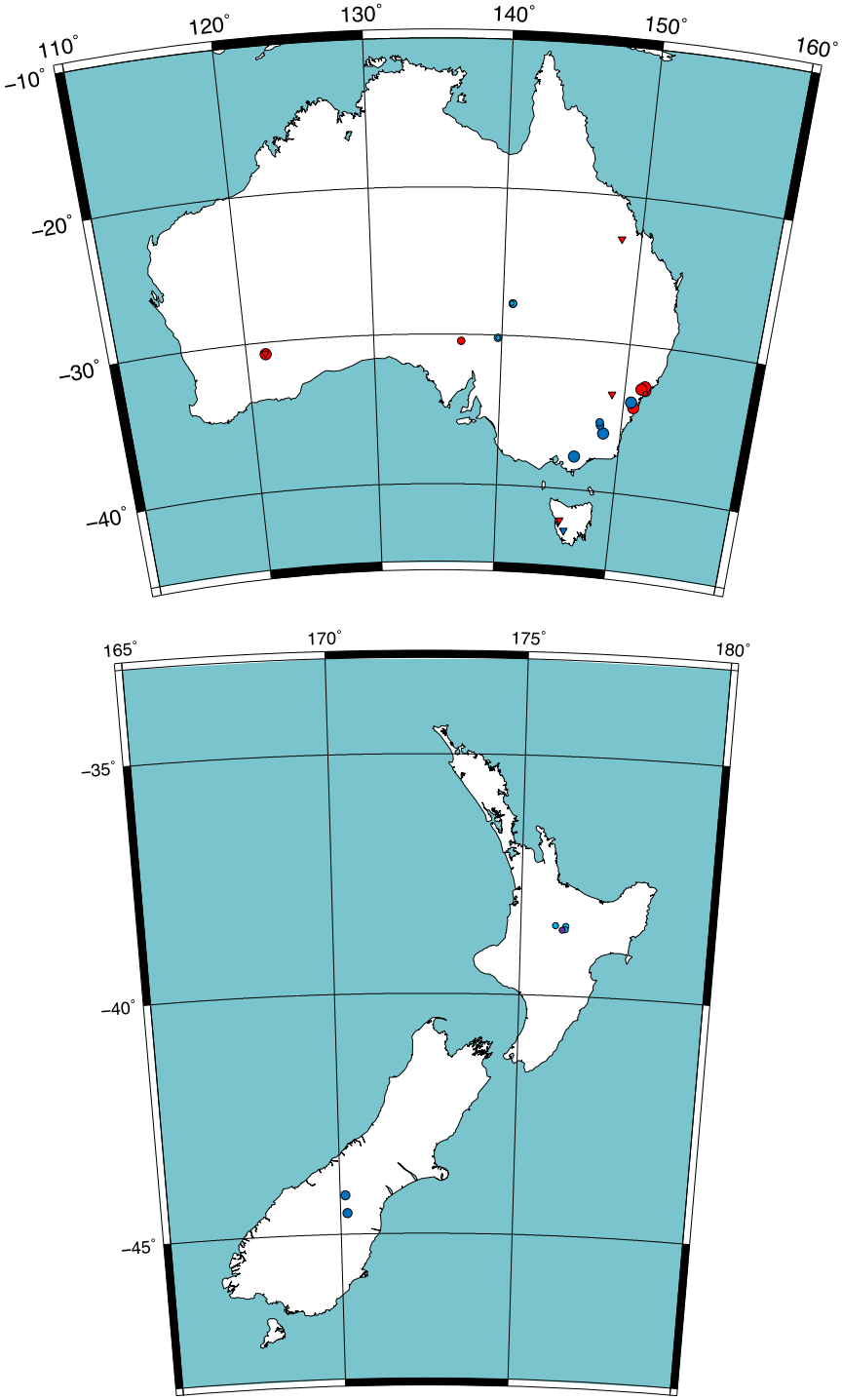

Fig. 90. Same as Fig. 84 except for (top) Australia, and (bottom) New Zealand.

reporting were complete, the region of the plot beneath the observed M_{MAX} upper bound would probably be entirely populated with points. Because the reported data are biased in this way we have not calculated correlation coefficients between all values of M_{MAX} and other parameters.

Relationships observed include:

- *Water reservoir volume* (Fig. 91): Volumes plotted range from 0.004 km^3 to 164 km^3. There is a nearly linear boundary to the upper left of the cloud of points which suggests a relationship between reservoir volume and largest observed M_{MAX}. The 2008 M_W ~8 Wenchuan, China, event, which is disputed because of its seemingly disproportionately large size, also plots on this alignment.
- *Water reservoir mass per unit area* (Fig. 92): The largest M_{MAX} (i.e. the upper bound of M_{MAX}) increases with reservoir water mass per unit area.
- *Volume added or removed in surface operations* (Fig. 93): The largest M_{MAX} increases with this parameter.
- *Volume of material removed from the subsurface* (Fig. 94): We combined conventional oil and gas, geothermal, and mining-produced volumes. The largest reported M_{MAX} increases with volume removed. The relationship for M_{MAX} for injection volumes proposed by McGarr (2014) on the basis of theoretical considerations fits these data well (Fig. 95).

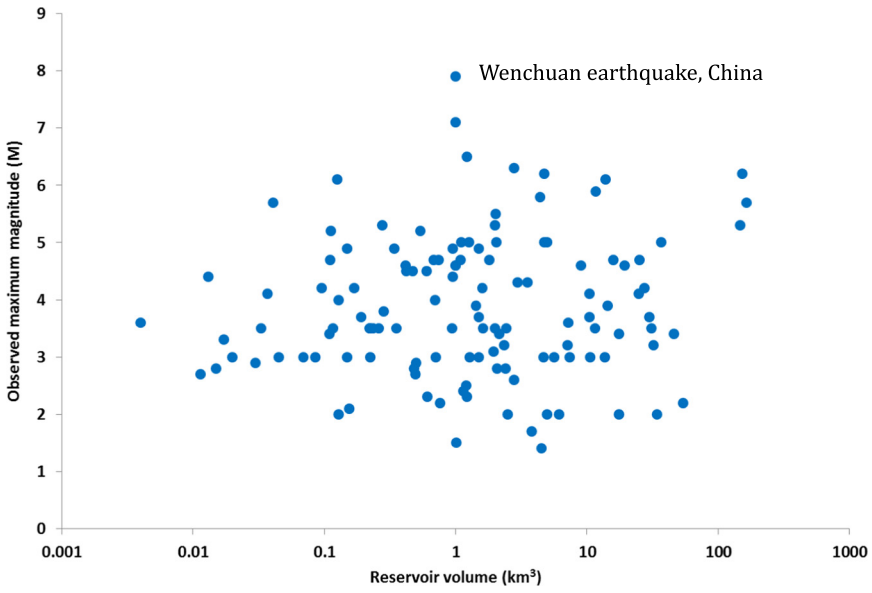

Fig. 91. Plot of M_{MAX} vs. water reservoir volume for the 126 cases for which data are available.

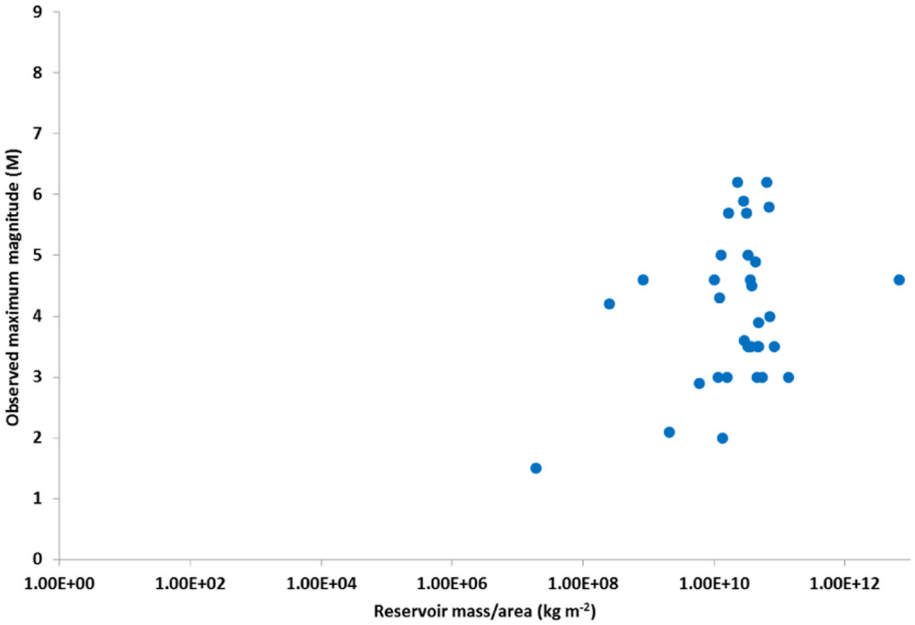

Fig. 92. Plot of M_{MAX} vs. water reservoir mass per unit area for the 33 cases for which data are available.

- *Shale-gas hydrofracturing – injection pressure, rate and volume* (Fig. 96): The largest M_{MAX} increases with all these parameters, in agreement with the relationship proposed by McGarr (2014).
- *Injected volume for all projects* (Fig. 97): Data from 69 cases are available to study this parameter. The largest earthquake plotted is the 2011 M_W 5.7 Prague, Oklahoma, event. This and a small number of additional earthquakes, mostly postulated to be induced by waste fluid injection, slightly exceed the upper-bound magnitude limit proposed by McGarr (2014).
- *Injection pressure* (Fig. 98): Data are available for 79 cases. Pressures range from atmospheric to 89 MPa. There is a tendency for the largest M_{MAX} to reduce with maximum injection pressure.
- *Volume or proxy volume removed from or added to the subsurface* (Fig. 99): We calculated volume or proxy volume (mass converted to volume using an appropriate density) for 218 cases. There is a clear upper bound to M_{MAX}. The relationship proposed by McGarr (2014) for injection volumes fits this wider dataset well with a few exceptions.
- *Mass removed from or added to the subsurface* (Fig. 100): As for volume, there is a clear linear observed upper bound to M_{MAX}.
- *Yield of nuclear devices* (Fig. 101): M_{MAX} for induced earthquakes correlates with explosion size for the seven cases for which data are available. This finding is in agreement with the correlation between the activated-fault length and explosive yield at Pahute Mesa, Nevada Test Site (McKeown and Dickey, 1969).
- *Project scale* (Fig. 102): We updated the plot of McGarr et al. (2002) with 20 additional cases. The data generally confirm the earlier observations. Two cases exceed the empirical upper bound of McGarr et al. (2002)–the 1979 M_L 6.6 Imperial Valley, California, earthquake (linked to the Cerro Prieto geothermal field; Section 3.4) and the 2008 $M_W \sim 8$ Wenchuan, China, earthquake (Section 2.1.1).
- *Project type* (Fig. 103): The largest earthquakes postulated to have been induced, in order of decreasing magnitude, are associated with water reservoirs, groundwater extraction and conventional oil and gas operations. These have all been linked to earthquakes with $M > 7$. Only relatively small earthquakes have been postulated to be associated with CCS, research experiments, construction and hydrofracturing. The number of projects in each category varies.

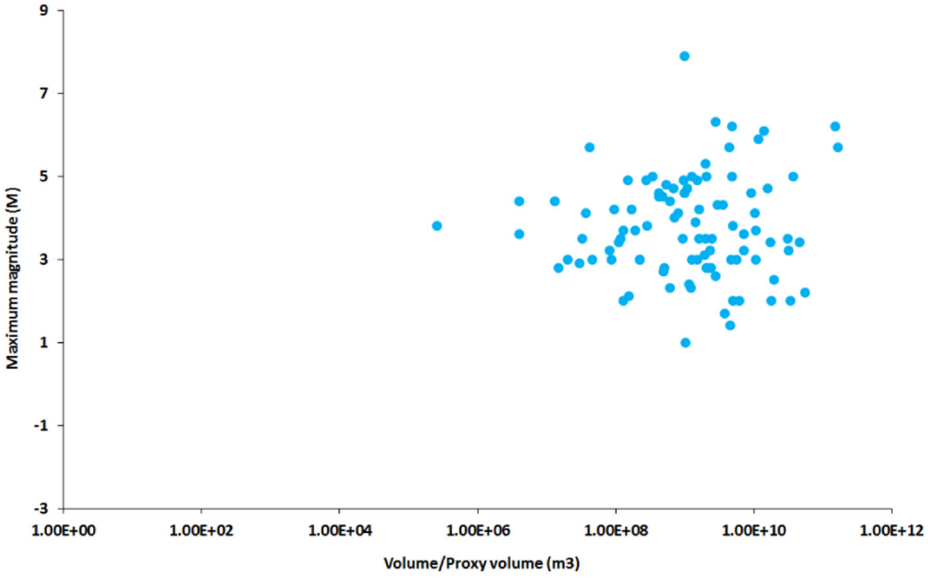

Fig. 93. Plot of M_{MAX} vs. volume added or removed by surface operations.

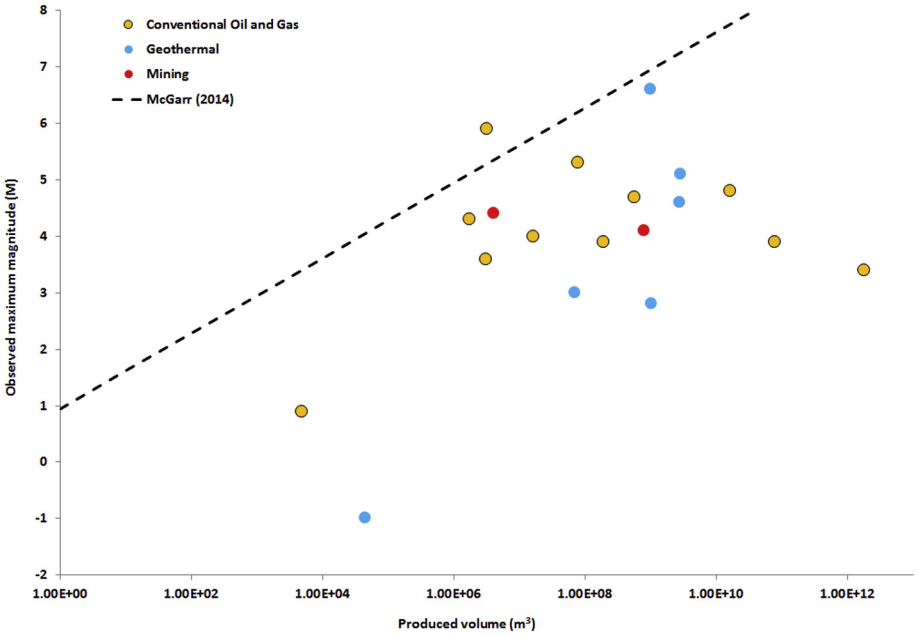

Fig. 94. M_{MAX} vs. produced volume (m^3) for 23 projects that involved extraction of mass from the subsurface. Some of these projects also involved injection, so their association with extraction is not certain. The upper limit to M_{MAX} proposed by McGarr (2014) on the basis of theoretical considerations is also plotted.

- *Distance of epicenter from the inducing project* (Fig. 104): There is a slight tendency for the largest reported M_{MAX} to decrease with distance from the project.

A relationship is not observed for:

- *Dam height* (Fig. 105): Data are available for 159 cases, many from Brazil, China, and the USA.
- *Water reservoir area* (Fig. 106): Areas of seismogenic reservoirs range from 1.6 km^2 to 53,600 km^2. The result that there is no significant tendency for the largest M_{MAX} to increase with reservoir area is perhaps unsurprising because large parts of reservoirs may be shallow.
- *Pressure change in subsurface reservoirs* (Fig. 107): No correlation was found for the 55 cases where data are available.
- *Injection rate for all projects* (Fig. 108): Although some individual projects report correlations there is no clear correlation for projects as a whole.

Fig. 109 shows the distribution of induced earthquakes by tectonic regime. The most numerous cases are from intraplate areas (79% of all cases) with the next largest category (13%) located in convergent plate-boundary zones. Most large industrial projects are conducted on land and most land is in the interior of plates with plate boundaries comprising relatively (though not absolutely) narrow zones. Most spreading plate boundaries are in the oceans and currently beyond reach of industrial development. Because induced earthquakes are mostly in intraplate regions they affect regions not traditionally associated with seismicity nor accustomed to it.

The lack of a relationship between M_{MAX} and operational parameters such as injection rate, coupled with the difficulty of predicting which projects will be seismogenetic and which not, suggests that non-operational parameters are important. The pre-existing stress state is the most obvious such parameter. Several lines of research indicate that most faults in the crust are nearly critically stressed, though they may not be optimally oriented to slip under ambient conditions. The local geology, in particular pre-existing faults and fractures, must be important for understanding the extreme variations in seismogenesis

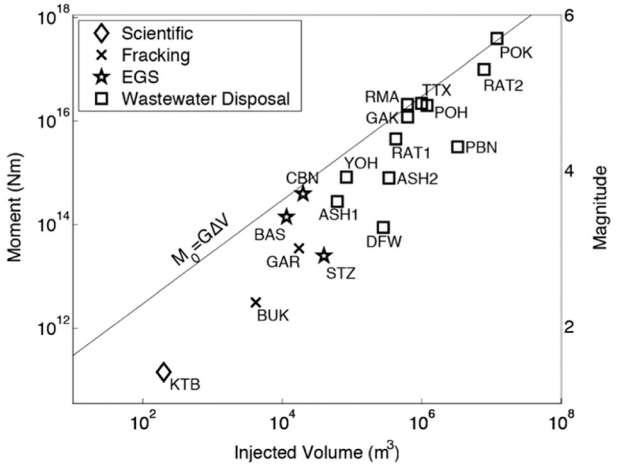

Fig. 95. Maximum seismic moment and magnitude vs. total volume of injected fluid from the start of injection until the time of the largest induced earthquake. The line relates the theoretical upper bound seismic moment to the product of the modulus of rigidity and the total volume of injected fluid, and fits the data well.
(From McGarr (2014).)

between apparently similar projects in different locations. In order for large earthquakes to occur, long faults that are suitably orientated and stressed must pre-exist.

The empirical results of this study have implications for individual projects. For example, at The Geysers geothermal field, California, net production (i.e. total production minus re-injection) since 1960 has been $\sim 1.7 \times 10^9$ m^3. The relationship of McGarr (2014), which links fluid-injection volume to the largest M_{MAX} (Fig. 97) fits well data from all volumetric projects. This relationship predicts that the upper bound to induced earthquakes associated with The Geysers volume change is M 7.0. This geothermal field has a maximum NW-SE long dimension of ~21 km. The largest induced earthquake reported from projects of this scale is ~M 6.6 (Fig. 102). Fig. 110 shows a histogram of numbers of seismogenic geothermal power-producing fields ranked by size (data from Bertani, 2010). The larger the geothermal operation the more likely it is that induced earthquakes are reported.

The largest earthquake that has occurred to date at The Geysers is the 2014 M_W 4.5 event. There is no evidence that a fault long enough to sustain a M 6.6 or 7.0 earthquake exists in the reservoir. However, The Geysers lies between the regional Mercuryville fault to the southwest and the Collayomi fault zone to the northeast, within the active Pacific/North America transform plate boundary zone. There is no evidence that the Mercuryville fault zone is active but the Collayomi fault zone contains at least one active fault (Lofgren, 1981).

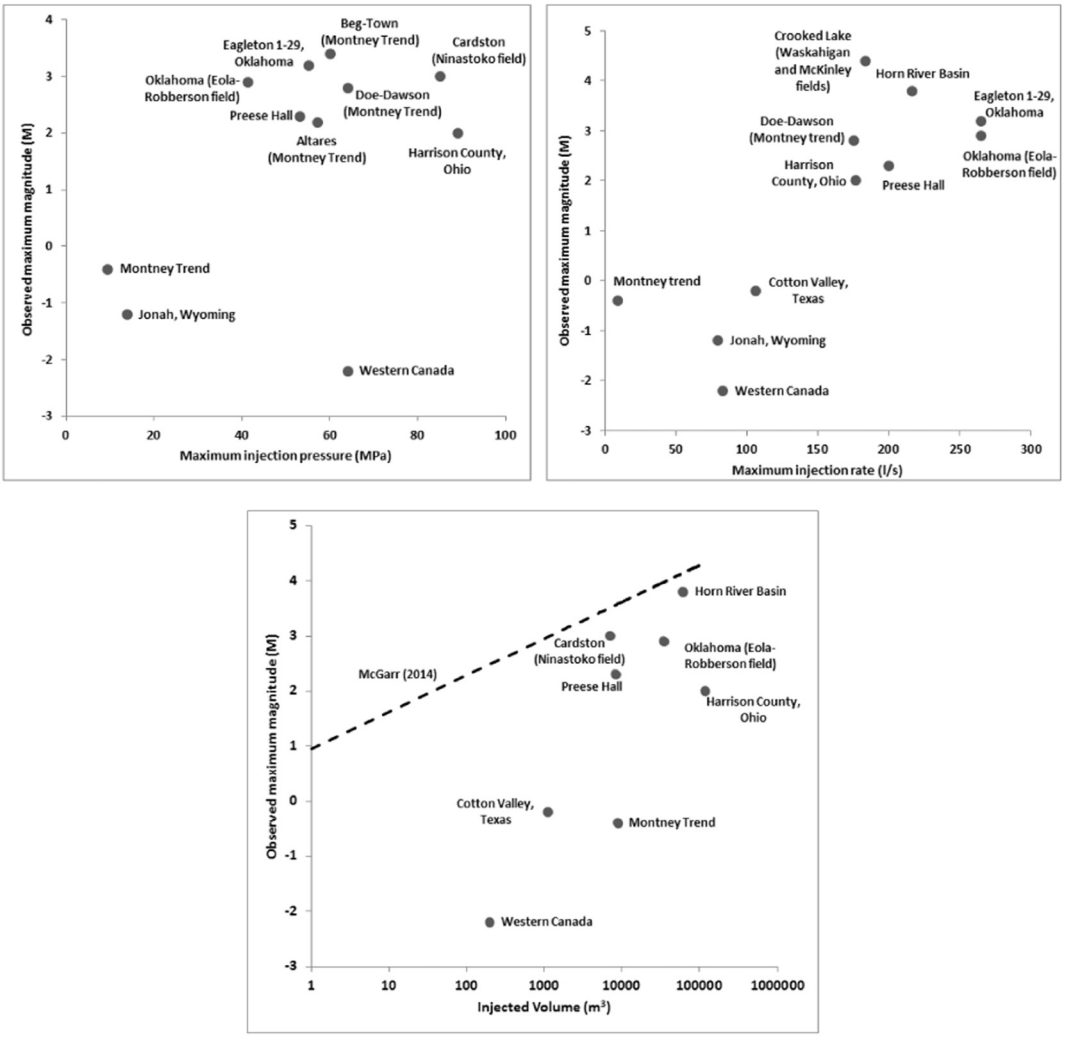

Fig. 96. For all cases of shale-gas hydrofracturing-induced earthquakes in our database where data are available, top left: M_{MAX} vs. maximum injection pressure, top right: M_{MAX} vs. maximum injection rate, and bottom: M_{MAX} vs. injected volume.

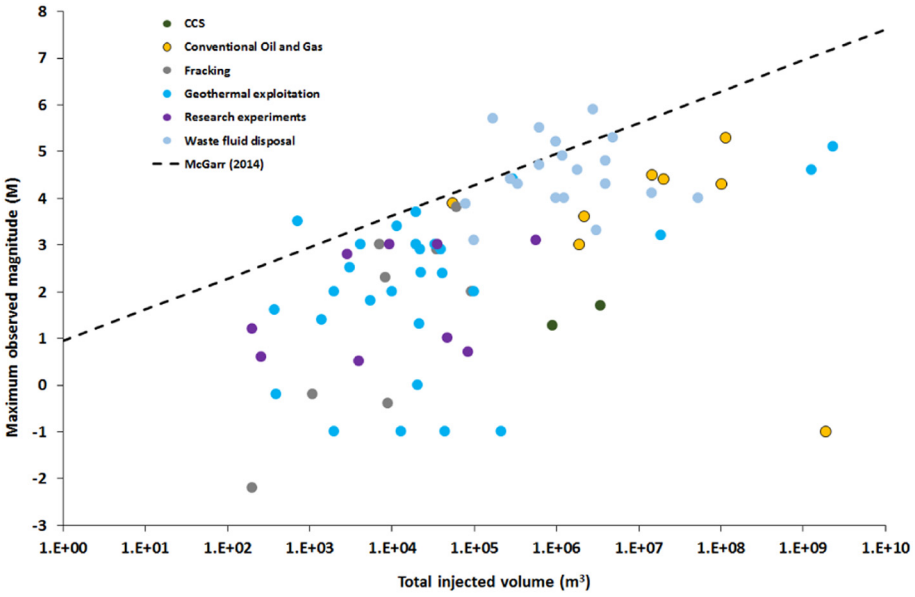

Fig. 97. M_{MAX} vs. total injected volume for the 69 cases of induced seismicity for which data are available. The upper-bound magnitude limit proposed by McGarr (2014) on the basis of theoretical considerations is also plotted.

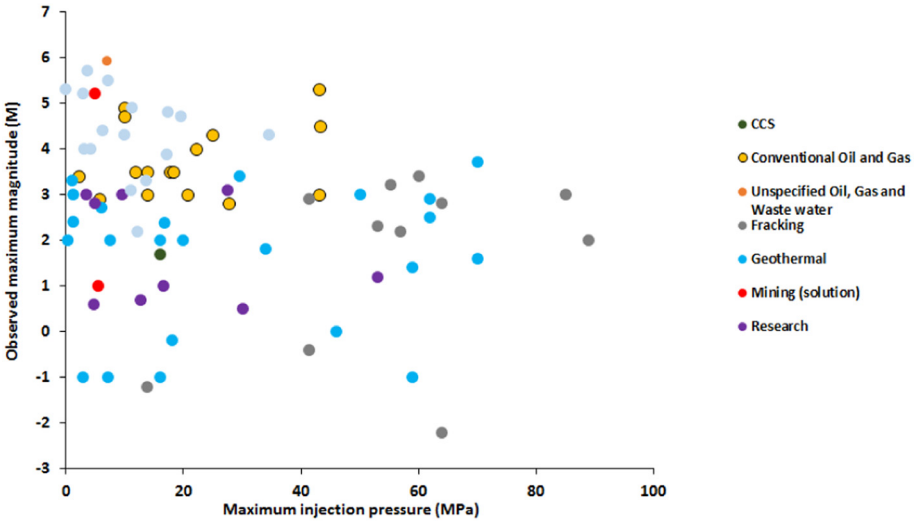

Fig. 98. M_{MAX} vs. maximum wellhead injection pressure for the 79 cases where data are reported.

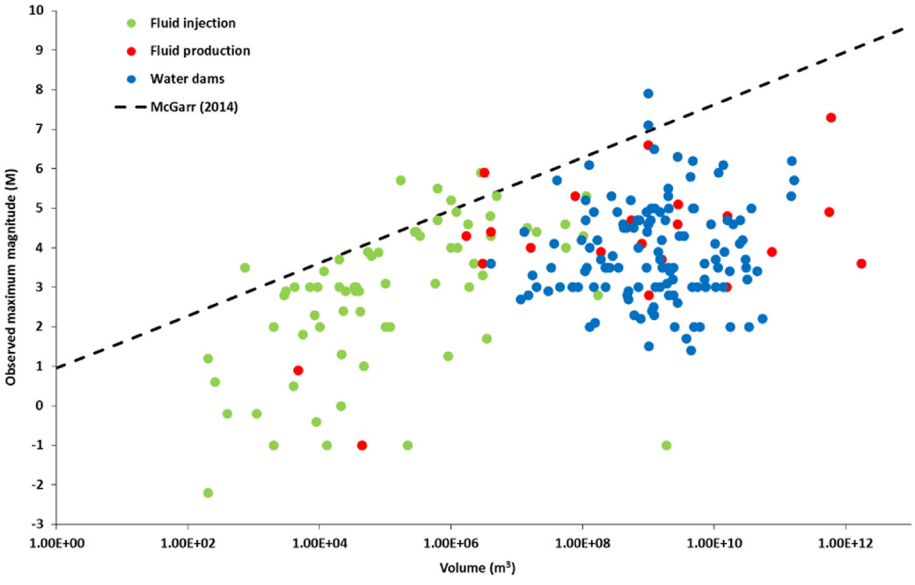

Fig. 99. M_{MAX} vs. volume or proxy volume of material removed or added for the 218 cases for which data are available, along with the relationship proposed by McGarr (2014) on the basis of theoretical considerations. Volumes and proxy volumes were estimated as follows: Water dams–the volume of the impounded reservoir; fluid injection or extraction–fluid volume injected into or extracted from the subsurface; mining–mass of material excavated, converted to volume using an appropriate density; construction–relevant mass converted to volume using an appropriate density for the building materials; CCS–mass of injected CO_2 converted to volume using a density of liquid CO_2 of 1100 kg/m^3.

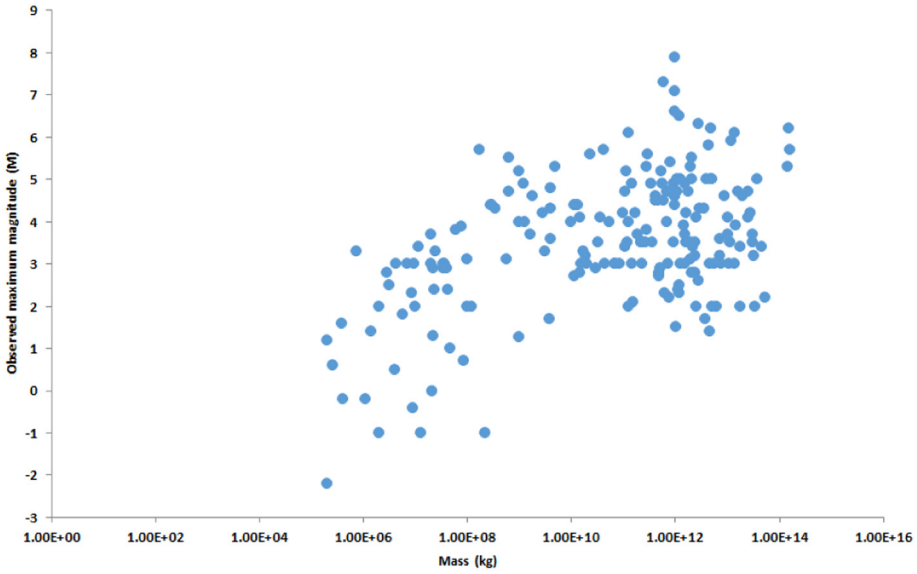

Fig. 100. M_{MAX} vs. mass of material removed or added for the 203 cases where data are available. Water volumes were converted to mass using a density 1000 kg/m^3. Oil and gas are not included in this plot except where quantity was reported in units of mass. Project types plotted include CCS, construction, conventional oil and gas, shale-gas hydrofracturing, geothermal, mining, research experiments, waste fluid injection and water reservoirs.

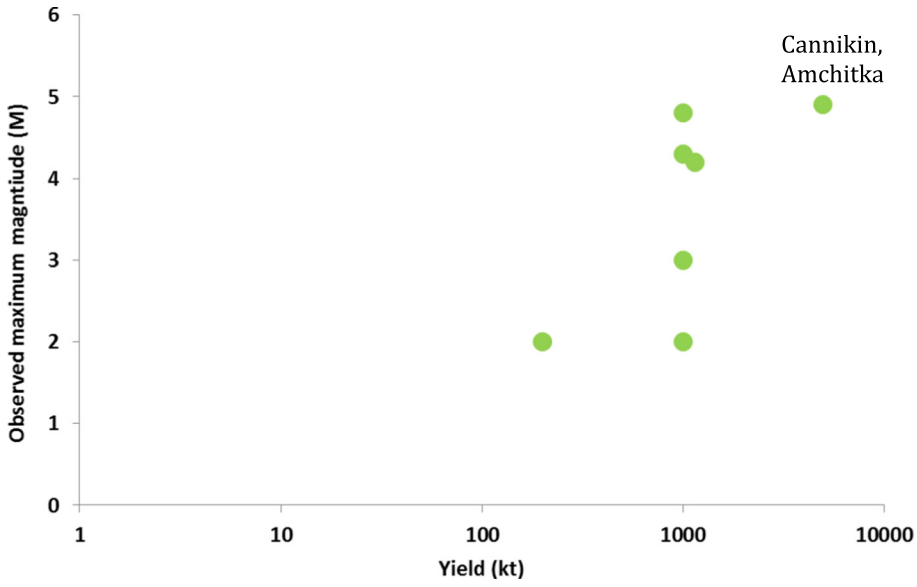

Fig. 101. M_{MAX} vs. yield in kilotonnes for nuclear tests that activated faults for the seven cases reported. Only one of these (Benham) is in common with the dataset of McKeown and Dickey (1969).

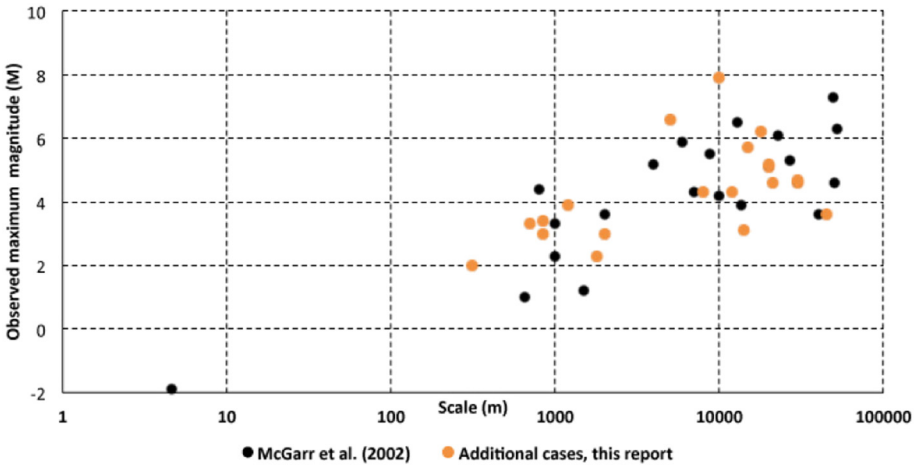

Fig. 102. M_{MAX} vs. project scale in meters. Black dots: cases studied by McGarr et al. (2002); orange dots: 20 additional cases from our database. Project scale was estimated using the longest dimension of the project, e.g., the length of a water reservoir.

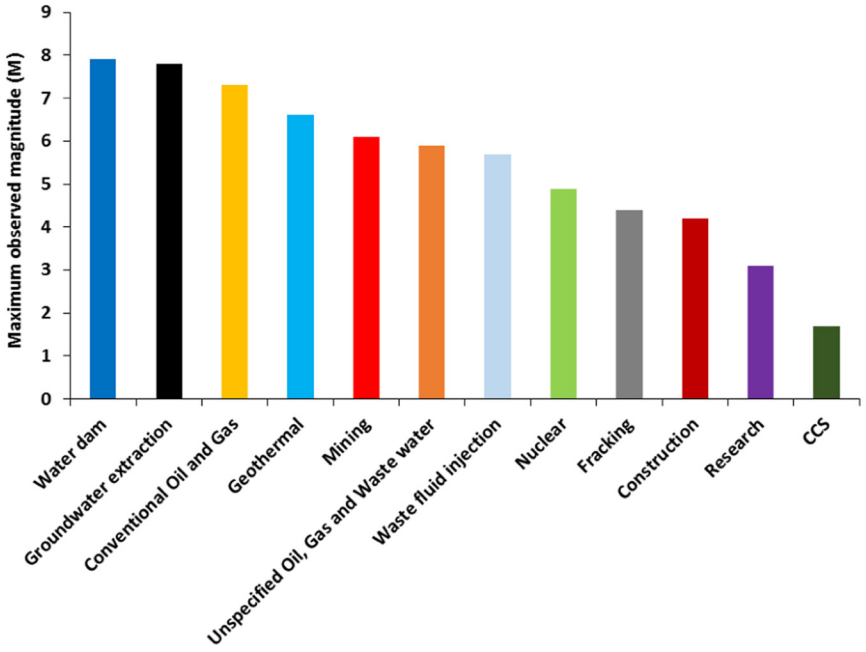

Fig. 103. Histogram of M_{MAX} for different categories of project.

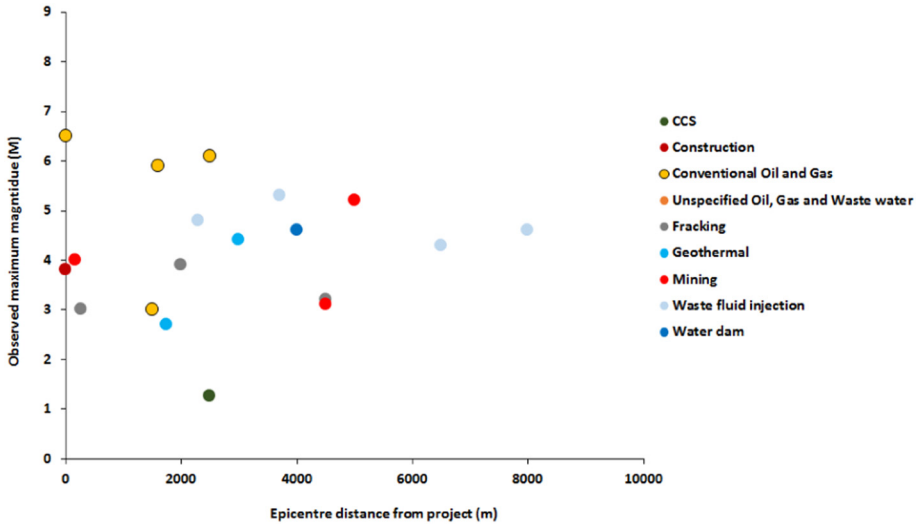

Fig. 104. M_{MAX} vs. distance from project for postulated induced earthquakes up to 10 km away for the 19 cases where data are available.

7. Discussion and conclusions

7.1. How common are induced earthquakes?

The total number of industrial projects in various categories, along with the number reported to be seismogenic are given in Table 3. Without doubt under-reporting is severe. Seismicity at projects remote from settlements is likely to escape notice. Known cases may not be publicized unless they are large and of nuisance or unusual interest. For example, ~2.5 million shale-gas hydrofracture jobs have now been completed world-wide. All successful hydrofracturing projects induce small earthquakes but only 21 cases have been reported (Table 3; Section 4.1.6). The absence of reports of seismicity does not correspond to an absence of seismicity. Statements such as "no seismicity is reported" does not equate to "no induced earthquakes occurred" or "no earthquakes were observed". Some earthquakes may also have been reported by national seismic networks without their induced nature being recognized.

M_{MAX} for the 562 seismogenic projects where this parameter is reported is shown as a plot of cumulative number of cases vs. M_{MAX} in Fig. 111. The linearity of the distribution at the high-magnitude end suggests that reporting is complete for M_{MAX} 5 and above, and that underreporting becomes progressively greater for projects smaller than M_{MAX} 4. Downward extrapolation of the linear, M_{MAX} 5–7 part of the plot suggests that ~30% of M ~4 induced earthquakes have gone unrecognized or unreported, 60% of M ~3 events and ~90% of those with M ~2 (Table 4).

The hydrocarbon fields around Britain provide a regional example of this problem. Comparison of the UK earthquake database of the British Geological Survey with maps of hydrocarbon fields in the North Sea suggests correlations between fields and earthquake locations (Fig. 112). Expanded maps of several fields are shown in Fig. 113. Epicenters cluster near the Beatrice Oilfield (Moray Firth), the Britannia Gasfield, the Southern North Sea Gas Province and the Leman Gasfield.

Most of the recorded earthquakes in the southern North Sea occur in or near fields developed in Permian Rotliegend reservoirs. There, gas is produced using simple pressure depletion from the original hydrostatic pressure. Water is not injected to support production. Many of the poorer-quality wells used to explore and appraise this gas province were prop-fracked to obtain initial gas flow and a few fields (e.g.,

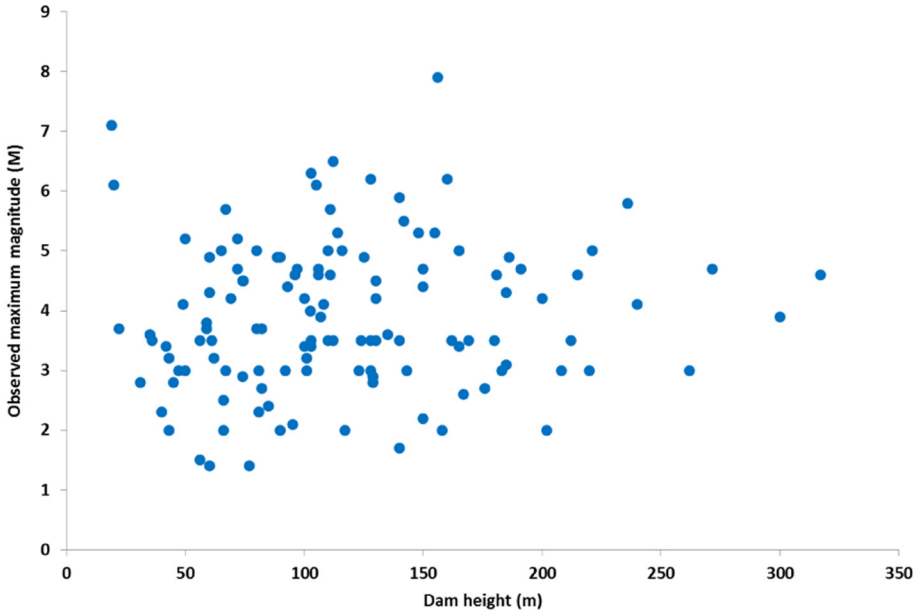

Fig. 105. M_{MAX} vs. dam height for the 159 cases of seismogenic water reservoirs for which data are available.

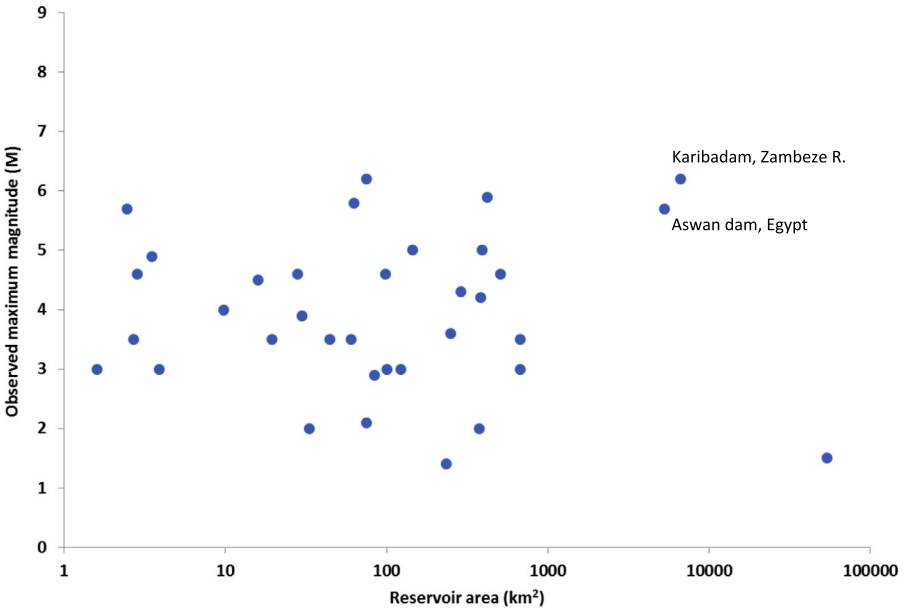

Fig. 106. M_{MAX} vs. water reservoir area for the 35 cases for which data are available.

Clipper South, Gluyas and Swarbrick, in press, 2017; Purvis et al., 2010) used hydrofracturing in development wells. The Viking Graben contains mostly oilfields that were developed by allowing natural pressure decline to deliver the first oil and then injecting water to support continued production. The water used is seawater at typical North Sea temperatures of ~4 °C, while the reservoirs are at 90–140 °C. The central North Sea and Moray Firth contain a heterogeneous mix of oil and gas fields produced by a combination of pressure depletion and water injection. When discovered some fields were naturally at high pressure and close to the fracture gradient.

Many of these activities are potentially seismogenic. Nevertheless, there are no reports of induced seismicity from these fields. Comparison of seismicity with hydrocarbon production information available from DECC for 1975–2008 shows no temporal correlations and, because the North Sea was seismogenic before hydrocarbon production started, it cannot be ruled out that the seismicity is natural. Detailed work on individual events and their possible connection to operations in individual oil and gas fields is required to resolve this ambiguity (Wilson et al., 2015).

7.2. Hydraulics

Groundwater influences earthquake occurrence. Overwhelming, observational data show that pore pressure in fault zones strongly influences seismicity (Section 1.3). The suggestions that large-scale extraction of groundwater influences seismicity imply an unfortunate association between earthquakes and human need to manage water for utilization and flood control.

The five cases we found of earthquakes suggested to be linked to groundwater extraction raise the question of whether other earthquakes that were both shallow and where major water table changes have occurred were induced. An example is the 2011 M 7.1 Christchurch, New Zealand, earthquake (Fig. 114). The city of Christchurch is built on what was once an extensive swamp fed by the rivers Avon and Heathcote and numerous smaller streams. Major engineering works have changed the hydrology there over the last century.

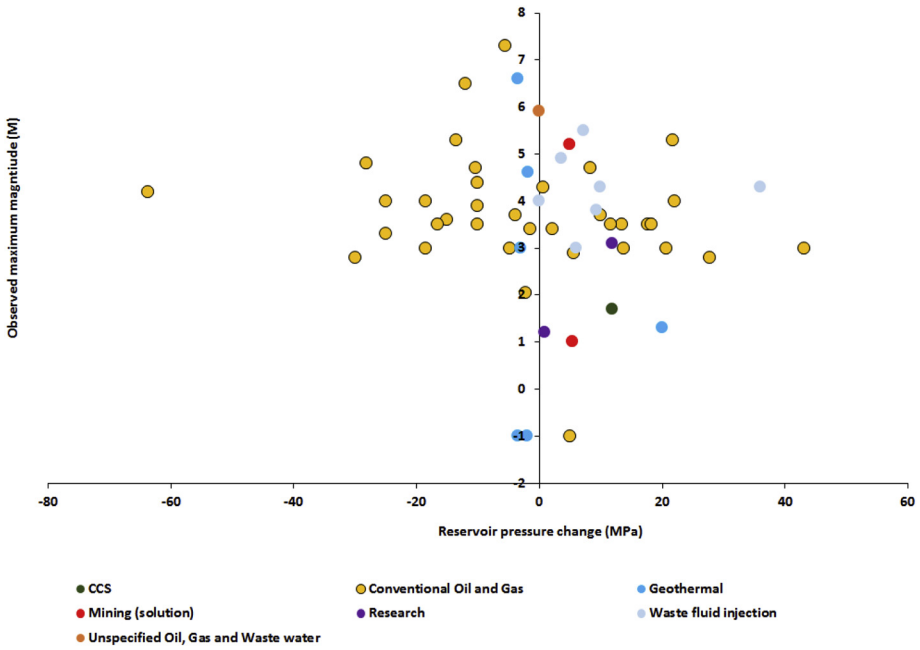

Fig. 107. M_{MAX} vs. change in reservoir fluid pressure resulting from production/injection for the 55 cases where data are available. We include 9 cases of conventional oil and gas where the pressure change results from both injection and production.

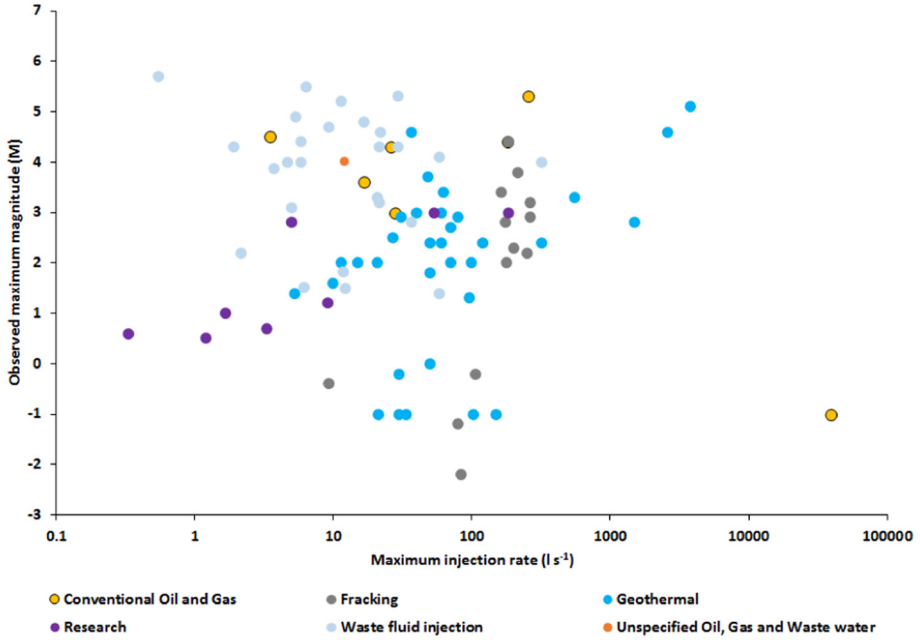

Fig. 108. M_{MAX} vs. maximum injection rate for the 88 cases for which data are reported. Rates of injection varied from 0.33 to ~40,000 l/s. At rates greater than ~1000 l/s, values apply to entire fields rather than individual wells.

The 1811–1812 New Madrid earthquakes occurred in the central Mississippi river valley. This renowned sequence included three M ~7 earthquakes and about seven with M > ~6.5. These earthquakes are remarkable for having been felt at distances of up to 1700 km as a result of efficient transmission of seismic waves through the eastern USA lithosphere. They are also remarkable in occurring in an intraplate area. They are a paradox in any paradigm that expects large earthquakes to occur in plate boundary zones.

The New Madrid earthquakes occurred at and just south of the confluence of the 6000 m^3/s Middle Mississippi and the 8000 m^3/s Ohio rivers which forms the Lower Mississippi River. The possibility that the earthquake activity is linked to local hydraulics has been suggested previously but not seriously entertained. In view of the growing evidence that hydraulic changes can modulate the seismic behavior of faults it may be timely to revisit this possibility with investigation into pre-earthquake hydraulic activity and numerical modeling.

Hydraulic effects may explain why both mass addition and removal can induce earthquakes. This is illustrated by the fact that the commonest earthquake-induction process is mining (i.e. mass removal–38% of cases; Fig. 115) and the second most common is water reservoir impoundment (i.e. mass addition–24%). Hydraulic changes induced by mass redistribution may result in migration of fluid into fault zones, increasing pore pressure. This process may explain the possible induction of earthquakes by erecting the Taipei 101 building (Section 2.1.2). It may also explain earthquake induction by hydrocarbon extraction in the absence of fluid injections, since natural groundwater recharge may occur.

Global earthquake databases show that moderate earthquakes are fairly common near large lakes and reservoirs, e.g., in east Africa, even though induction has not been proposed. Intraplate earthquakes in the UK are not currently understood. At least 21% of UK earthquakes in the

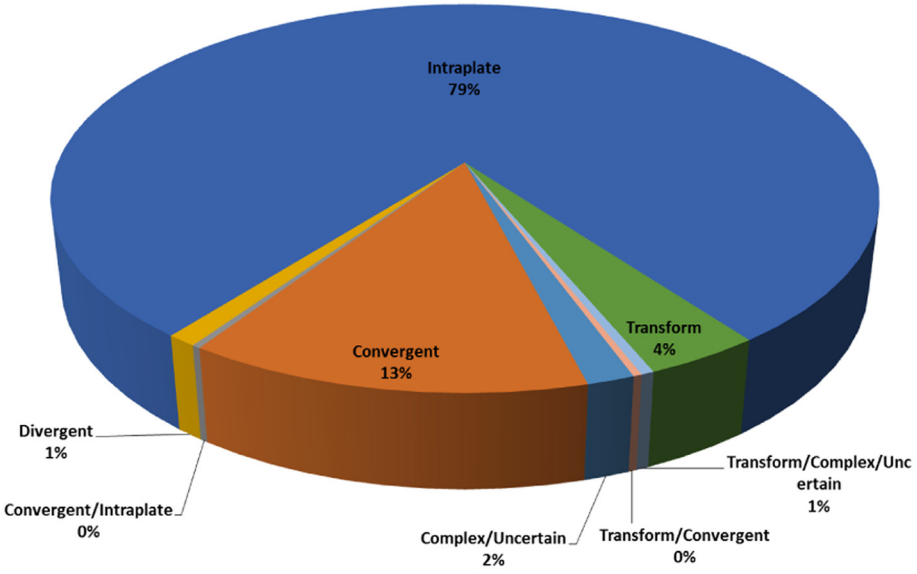

Fig. 109. Tectonic settings of human-induced earthquake activity.

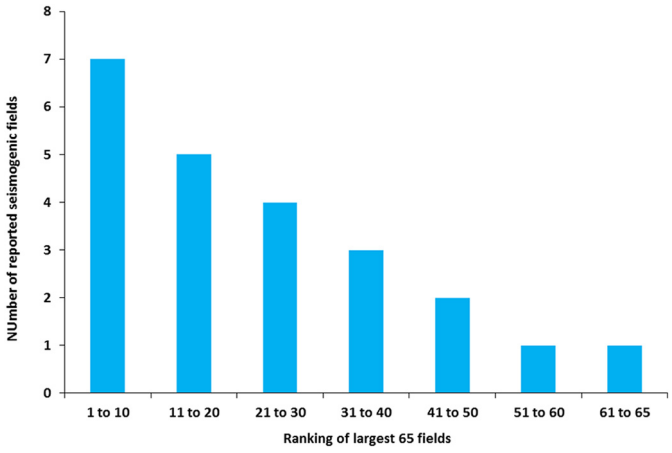

Fig. 110. Number of reports of induced seismicity vs. size of field for the 65 largest global power-producing geothermal fields in groups of 10.

British Geological Survey catalog are thought to be related to mines, but many others are probably natural. The seismic rate in the UK is ~one M_L 3.6 event/year (Wilson et al., 2015). A possible link with hydraulics is under investigation (Graham et al., 2017).

7.3. How much stress loading is required to induce earthquakes?

Earthquakes occur naturally, without any human intervention at all. The minimum amount of added anthropogenic stress needed for an earthquake to start is thus zero.

Many natural processes contribute to stress build-up on faults. These include tectonic deformation, volcanism, natural heat loss, isostatic uplift following deglaciation or oceanic unloading, Earth tides, intraplate deformation resulting from distant plate boundary events, remote large earthquakes, erosion, dissolution, the natural migration of groundwater and weather. To these are added industrial activities. It is an ill-posed question to ask the origin of the final stress increment that "broke the camel's back" and precipitated an earthquake. In the case of large earthquakes this question may be akin to asking whether one particular skier of many was responsible for an avalanche.

Instead of viewing industrial activity as inducing earthquakes, it could instead be viewed as modulating the timescale on which inevitable earthquakes occur. Unfortunately it cannot be known what events would have occurred had the industrial activity not been done because history cannot be re-run with a change of circumstance. Furthermore, had an equivalent earthquake occurred at a different time, it cannot be known if it would have affected people and infrastructure to the same extent. Nevertheless, in the cases of many industrial projects, the association between earthquakes and the project is

Table 3
Induced seismicity statistics for the total numbers of projects of different types, the number that are seismogenic, and related data.

Project type	# projects	# cases in the database	% projects that are seismogenic	Observed maximum magnitude (M_{MAX})	# seismogenic projects reported by Hitzman (2013)	Source for # projects
CCS	75	2	2.67	1.7	–	Huaman and Jun (2014)
Construction	Unknown	2	–	4.2	–	
Conventional oil and gas	67,000 fields	116	0.17	7.3	65	Li (2011)
Fracking	2,500,000 wells	21	0.00	4.4	2	King (2012)
Geothermal	Unknown	56	–	6.6	26	Bertani (2010)
Groundwater extraction	Unknown	5	–	7.8	–	
Mining	13,262 currently active mines	267	2.01	6.1	8 ("other")	http://mrdata.usgs.gov/
Nuclear (Underground)	1352 tests	22	1.63	4.9	–	Pavlovski (1998)
Research	Unknown	13	–	3.1	–	
Waste fluid injection wells (Class II wells)	151,000 wells (USA only)	33	0.02	5.7	11	Hitzman (2013)
Water dam	6862 reservoirs (> 0.1 km^3)	168	2.45	7.9	44	Lehner et al. (2011)
Total		705			156	

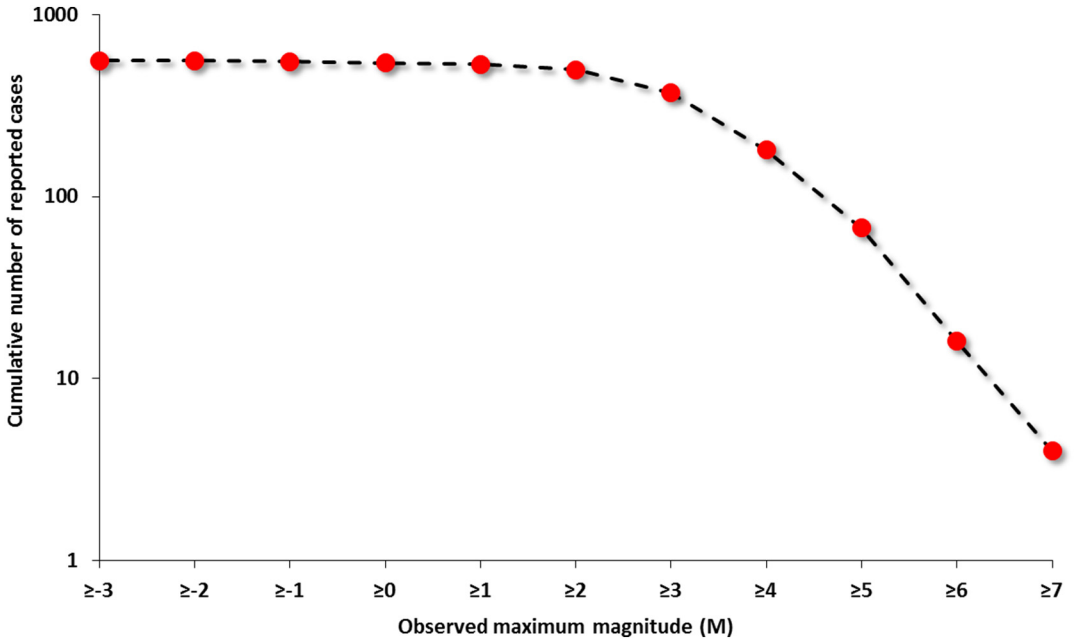

Fig. 111. Cumulative number of reported cases of induced seismicity vs. M_{MAX} for the 562 cases for which data are available.

Table 4
Number of reported M_{MAX} values and number predicted from downward extrapolation of the linear trend of earthquakes with M_{MAX} 5–7 shown in Fig. 111.

M_{MAX}	# reported earthquakes	# predicted earthquakes
7	4	4
6	17	16
5	68	67
4	181	~250
3	371	~1000
2	497	~4000

undeniable. The clear induction of some earthquakes by very small incremental stresses means that objections to induced status on the grounds that the stress perturbation was too small may be weak.

Anthropogenic stress changes proposed to have induced earthquakes range from a fraction of a MPa (e.g., Keranen et al., 2014), the equivalent of about a meter of rock overburden, to several tens of MPa (Table 5) (Fig. 116). For example, both the 2007 M_L 4.2 Folkestone, UK, earthquake and the 2008 $M_W \sim 8$ Wenchuan, China, earthquake have been attributed to anthropogenic stress changes of only a few kPa.

The question "How much stress change is needed to induce earthquakes?" may be unanswerable. However, it may be possible to address the question "What is the smallest stress change observed to induce earthquakes?" This can be attempted using natural stress changes known to correlate with earthquakes, as follows (Table 6).

7.3.1. Earth tides

The spatial non-uniformity of the gravitational fields of the Sun and Moon (and to a much smaller extent, other celestial bodies) produces differential stresses in the solid body of Earth approaching 0.005 MPa. Loading of the solid Earth by ocean tides produces additional stresses that can be about an order of magnitude larger but depend strongly on geographic location. The stress drops of most earthquakes are 1–10 MPa so tides might sometimes have a detectable effect on earthquake occurrence.

Most early studies of earthquakes and tides failed to find any significant correlation. The main cause of this failure was probably oversimplification of the problem. Both stresses and earthquake mechanisms are tensors, but many studies looked, for example, for correlations between seismicity and tidal amplitude ranges, effectively treating both stress and earthquake mechanism as scalars. Another difficulty with such analyses was the difficulty of computing ocean tides from the complicated shapes of ocean basins.

There were, however, two exceptions to this failure. First, deep moonquakes, detected by seismometers placed by Apollo astronauts, correlate strongly with tides (Latham et al., 1973). Second, earthquakes at volcanic and geothermal areas show a tidal effect that is easily detected (e.g., McNutt and Beavan, 1981). Recently, studies that account for earthquake focal mechanisms and compute ocean loading accurately have found that shallow thrust-faulting earthquakes correlate significantly with tidal stresses (Cochran et al., 2004).

7.3.2. Static stress changes resulting from large earthquakes

The 1989 M_W 6.9 Loma Prieta, California, earthquake modulated seismicity from around the epicenter out to distances where the coseismic stress changes were ≥ 0.01 MPa (equivalent to ~0.4 m of overburden) (Reasenberg and Simpson, 1992). The 1992 M_W 7.3 Landers, California, earthquake also modulated nearby seismicity. Aftershocks were abundant up to about two source dimensions from the mainshock (a few tens of km), where the Coulomb stress on optimally orientated faults was increased by > 0.05 MPa. They were sparse where stress was reduced by this amount (Fig. 117). The 1992 M_W 6.5 Big Bear aftershock occurred in a region where stress was increased by 0.3 MPa (King et al., 1994). The effect of static stress changes on neighboring faults has also been expressed in terms of the number of years by which the next large earthquake has been advanced in time (e.g., King et al., 1994; Reasenberg and Simpson, 1992).

7.3.3. Remote triggering

The 1992 M_W 7.3 Landers, California, earthquake is remarkable because it precipitated earthquake activity up to 17 source dimensions distant from the mainshock (1250 km). Most of this activity occurred at volcanic or geothermal areas such as Yellowstone. Static stress changes are vanishingly small at such distances. These remote earthquakes are thought to have been triggered by dynamic stress changes of a few tenths of a MPa in the propagating shear- and surface elastic waves interacting with fluids in hydrothermal and magmatic systems (Hill et al., 1993). This phenomenon of "remote triggering" has subsequently been observed elsewhere. When first unambiguously recognized following the Landers earthquake, it was thought only volcanic and

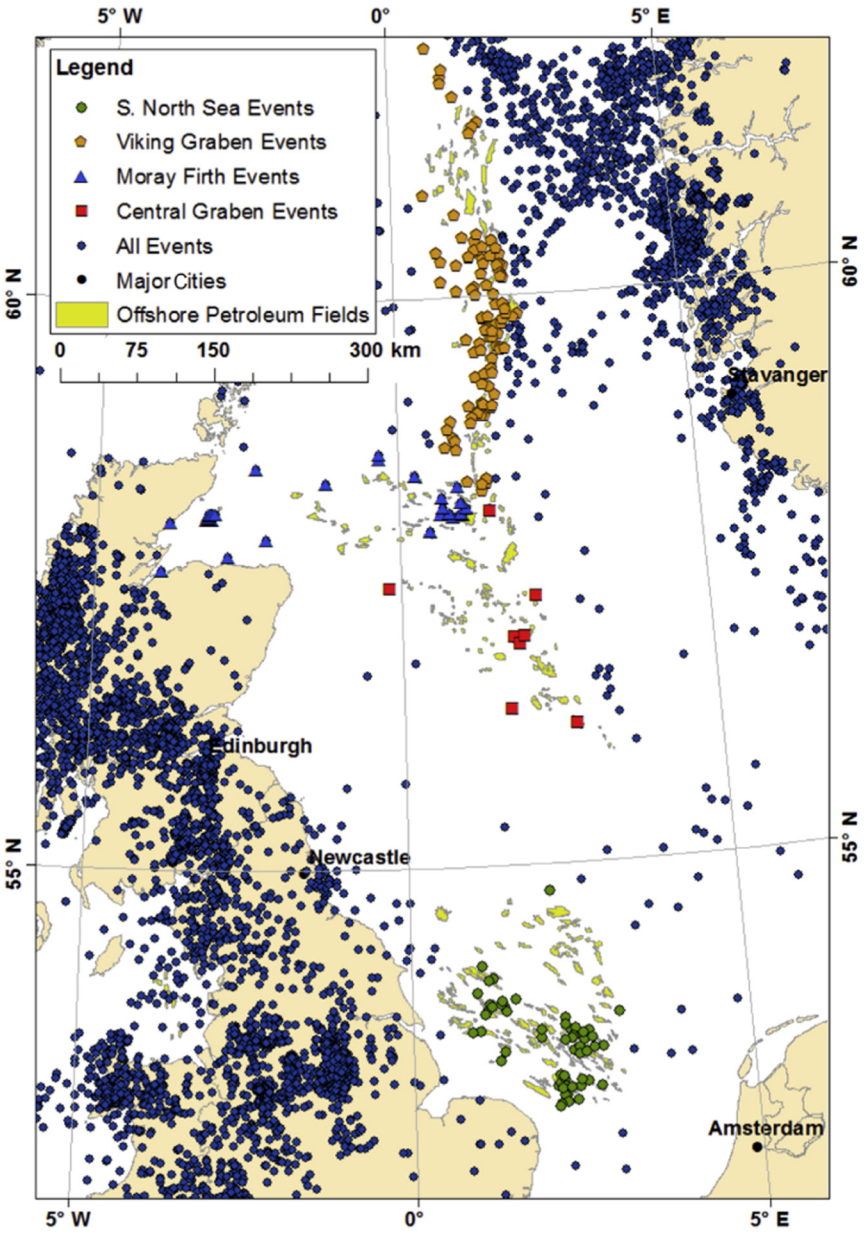

Fig. 112. Epicenters from the UK earthquake catalog of the British Geological Survey. Orange circles: Viking Graben events; blue triangles: Moray Firth events; red squares: Central Graben events; green circles Southern North Sea Gas Province events; yellow shading: offshore hydrocarbon fields.
(From Wilson et al. (2015).)

geothermal areas were affected and the process might reveal the locations of geothermal areas previously unknown. However, remote triggering has now been reported in other environments, e.g., the hydrocarbon region of Oklahoma (Fig. 58) (van der Elst et al., 2013).

7.3.4. Weather

A number of studies have postulated that earthquakes were induced by heavy rainfall (e.g., Husen et al., 2007; Roth et al., 1992). Correlations have also been suggested between "slow earthquakes" (accelerated creep on faults) and atmospheric pressure changes accompanying typhoons in Taiwan (Liu et al., 2009). Such pressure changes alter stress on land areas but not beneath the ocean because seawater flow maintains pressure equilibrium offshore. The effect contributes a stress change of ~0.003 MPa that encourages slip on coast-parallel thrust faults.

7.4. How large are induced earthquakes?

Stress changes postulated induce earthquakes do not correlate with stress drops brought about by the earthquakes or magnitudes. Counter-intuitively, M_{MAX} reported for induced sequences *decreases* with increasing calculated stress perturbation (Fig. 116). The final size of an earthquake is determined by how much of a fault was sufficiently stressed to move once activation began. If slip on a fault reduces to zero before the next event on the same fault starts, a series of discrete events is recognized. If slip does not stop, the event may grow and all the strain release is considered to have occurred in a single event. Great earthquakes that rupture much of the lithosphere typically comprise a cascading chain of M ~7 sub-events, each triggered by the stress changes resulting from the previous ones. Although likely very rare, it cannot be ruled out that industrial activity could contribute to the onset of an initial sub-event. It is also not uncommon for foreshocks to occur immediately preceding the onset of a mainshock several magnitude units higher. An initial M_W 5 earthquake in Oklahoma may have triggered successive earthquakes, including the M_W 5.7 event the following day (Keranen et al., 2013). In the case of the great 2008 M_W ~8 Wenchuan earthquake (Section 2.1.1), once the first sub-event began slip on the fault did not stop until several large fault segments had failed.

This view is consistent with the findings of McGarr (2014). He derived a relationship that related volume injected to the size of injection-

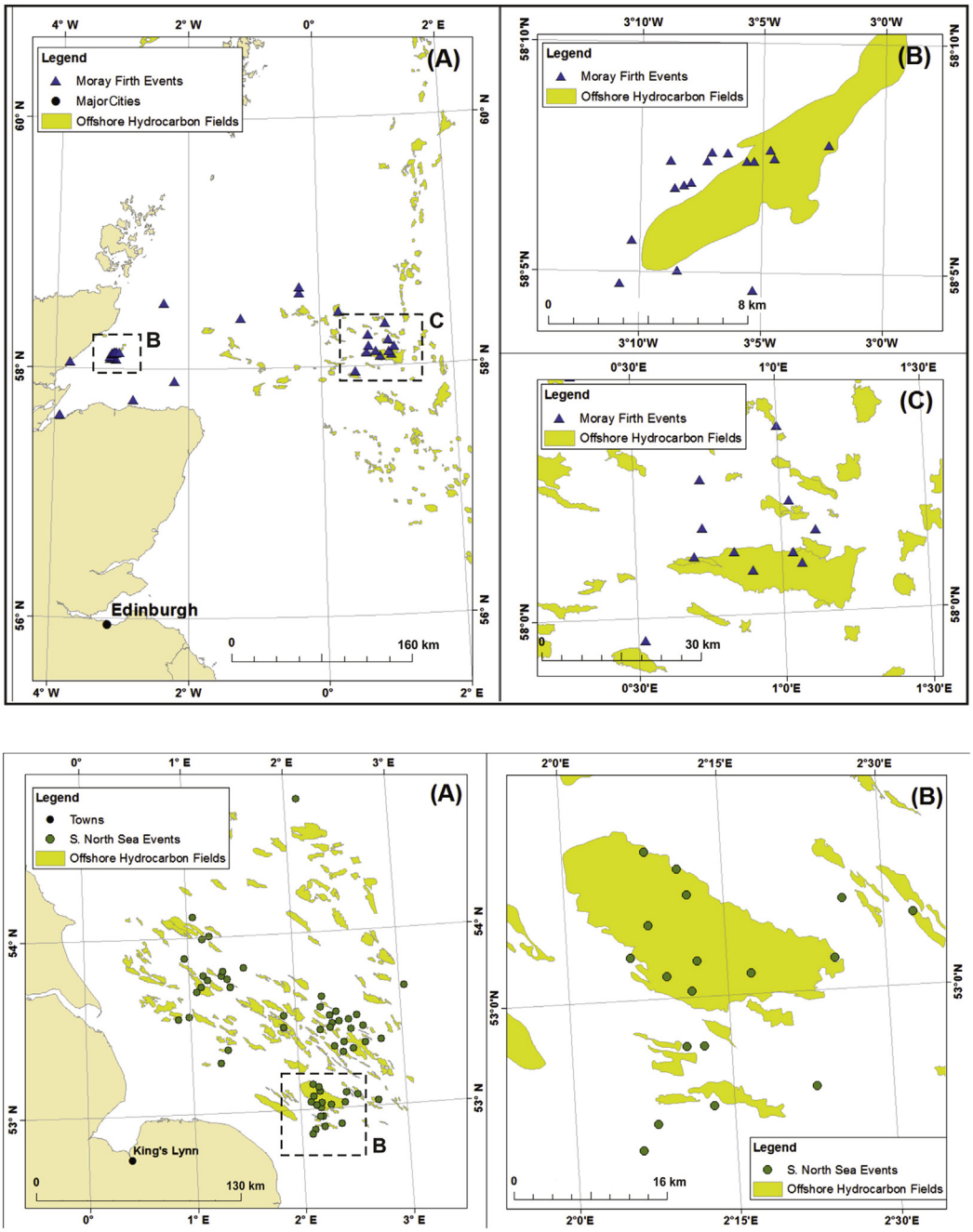

Fig. 113. Expanded view of some parts of Fig. 112. Top row: A–the Moray Firth. Yellow: hydrocarbon fields; blue triangles: earthquakes. B–the Beatrice Oilfield. C–the Britannia Gasfield. Bottom row: A–the Southern North Sea Gas Province. Green dots: earthquakes. Bottom row: B–the Leman Gasfield.
(From Wilson et al. (2015).)

induced earthquakes and showed that it fit well observations of 18 of the largest-magnitude earthquakes (Fig. 95). However, he also pointed out that this upper bound only applies to induced earthquakes whose source regions were confined to the volumes directly affected by the injection, and that if fault slip propagated outside of this volume then larger earthquakes could occur.

7.5. Natural or induced?

The strength of evidence for earthquake induction varies greatly between cases. For some examples the association with an industrial activity is beyond reasonable doubt. For example, over 250,000 earthquakes have been located in a tight cluster in The Geysers geothermal area, California, by the U.S. Geological Survey during the last half century. At the other end of the spectrum, induction has been suggested for cases where only one earthquake occurred and the calculated stress changes were smaller than those induced by Earth tides, e.g., for the 2007 M_L 4.2 Folkestone, UK, earthquake (Klose, 2007b). For those cases, mere coincidence cannot be ruled out (Sections 2.1.3 and 7.3). The suggestion that earthquakes were induced over 1000 km away and over a year later by bombing of cities with non-nuclear weapons is not persuasive strongly supported (Section 5).

The number of postulated induced cases is increasing rapidly and with it the urgency for management strategies. It is desirable, not only to know *a posteriori* whether an earthquake was natural or induced, but also to forecast which projects may be seismogenic in future and how great the hazard is likely to be. In the past, schemes have been proposed to address the question whether earthquakes are natural or induced. For

Fig. 114. Damage done to the cathedral in Canterbury, New Zealand, by the 2010 M 7.1 earthquake (http://www.npr.org/sections/parallels/2015/04/05/397093510/will-new-zealand-rebuild-the-cathedral-my-forefather-erected).

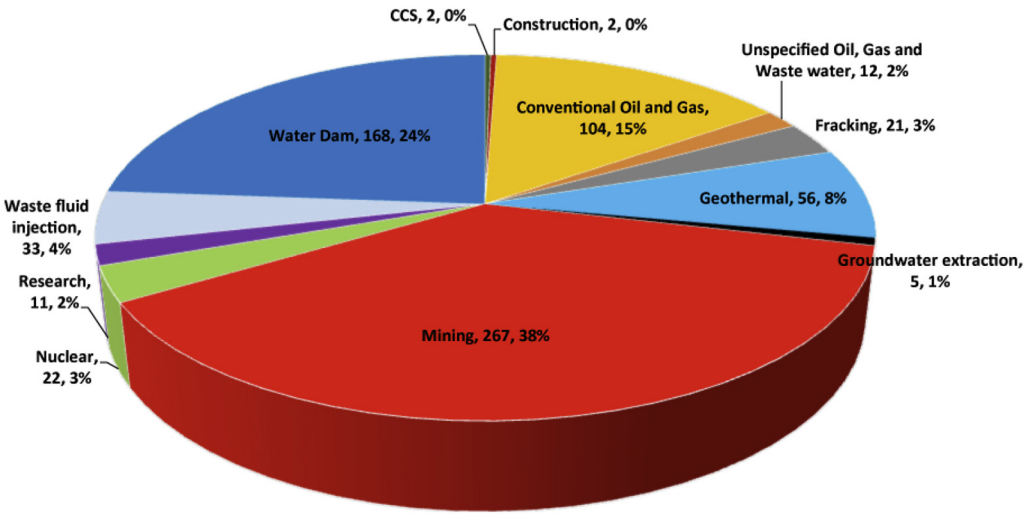

Fig. 115. Percentage of total cases for each project category in the database.

Table 5
Conversions for commonly used units of pressure.

1 bar = 0.1 MPa, equivalent to ~4 m of rock overburden
1 atm = 0.1 MPa
1 kg/cm^2 = 0.1 MPa
1 lb/in.^{2} (psi) = 6.9 × 10^{-3} MPa
1 acre-foot of water/football field[a] = 29 × 10^{-6} MPa
Hydrostatic gradient = 10 MPa/km
Lithostatic gradient = ~25 MPa/km

[a] American football, including end zones.

example, Davis and Frohlich (1993) list seven questions to profile a seismic sequence and judge whether it was induced or not (Table 7). In the light of the large number of case histories now available, some of these parameters can be re-examined:

1. *Whether the region had a previous history of seismicity*. Induced earthquakes have now been postulated to occur in both historically seismic and aseismic areas. Evidence from research in boreholes suggests that faults everywhere are close to failure, regardless of the known history of seismicity.
2. *Close temporal association with the induction activity*. Reported delays in the onset of postulated inducted seismicity vary from essentially zero to several decades.
3. *In the case of injection-related earthquakes, proximity of a few kilometers*. Distances of up to 25 km have now been reported (Fig. 104; Section 4.1.2).
4. *Known geological structures that can channel flow*. Many earthquakes postulated to be induced have been attributed to previously unknown faults.
5. *Substantial stress changes*. Stress changes as small as a few kPa have been postulated to induce earthquakes (Section 2.1.3).

Simple criteria for deciding whether an earthquake is induced or not are elusive. There is extreme diversity in the circumstances of cases. Postulated induction activities may take place over time periods from a few minutes to decades. The volumes of material added or removed vary over many orders of magnitude and the maximum magnitude of events postulated to be induced vary from M < 0 to M ~ 8.

Several unusual characteristics are commonly reported for earthquakes suspected of having been induced. These include:

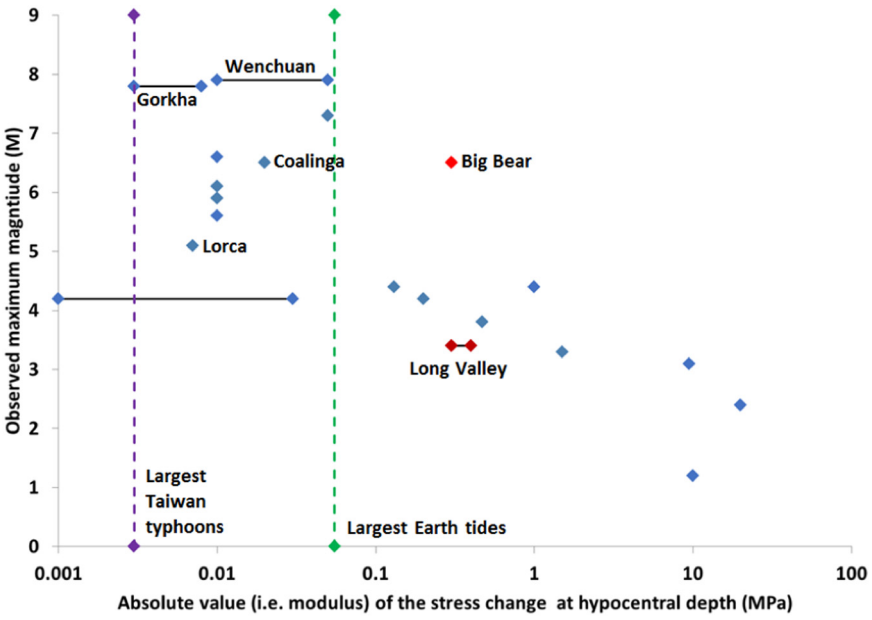

Fig. 116. M_{MAX} vs. absolute value of stress changes calculated by various authors to have occurred at the hypocentral depths of possibly induced earthquakes. Vertical dashed green line: largest Earth tides; vertical dashed purple line: largest Taiwan typhoons. Blue diamonds: earthquakes proposed to have been human-induced, diamonds connected by solid black lines: ranges of stress changes calculated. Some example earthquakes are labeled. Red diamonds: natural earthquakes that followed the 28th June 1992 M_W 7.3 Landers, California, earthquake (data from Hill et al., 1993). The Big Bear earthquake is proposed to have been induced by static stress changes, and the Long Valley earthquakes by the dynamic stresses from the surface waves.

Table 6
Stress changes associated with some natural processes postulated to induce earthquakes.

Effect	Stress change (MPa)
Earth tides	0.05
Seismic static stress changes	0.03
Remote triggering	~0.5
Typhoons	0.003

1. Unusually shallow nucleation depths (e.g., the 2011 M_W 5.1 Lorca, Spain, earthquake, Section 3.1);
2. Occurrence on previously unknown faults ("blind faults"; e.g., in the Cogdell oilfield, Texas, Section 4.2.2);
3. Release of stress in the same sense as the regional on suitably orientated structures (e.g., in Oklahoma, Section 4.1.2);
4. The largest earthquake in a sequence occurring after the induction activity has ceased, suggesting that fluid diffusion is important (e.g., the 1962–1968 Denver earthquakes, Section 4.1.1);
5. Faults in the basement beneath water and hydrocarbon reservoirs being reactivated, sometimes transecting the sedimentary formations above (e.g., the Coalinga, California, earthquake; Section 3.3.2).

These observations raise a number of questions. For example, if induced seismicity commonly occurs on previously unknown faults, could hazard be reduced by extensive subsurface mapping prior to operations? Since the crust is thought to be pervasively faulted and near to failure essentially everywhere, it is not clear this would be the case–perhaps everywhere should be considered potentially seismogenic. Also, if large earthquakes occur after operations have stopped, for how long should seismic hazard mitigation measures be continued after the end of a project?

More reliable, but less universally applicable ways of discriminating include:

1. Simple spatial and temporal associations, e.g., earthquakes beginning to occur as soon as injection starts and close to the injection point;
2. Earthquakes occurring in previously aseismic regions;
3. Visual observation, e.g., gallery collapses in mines or ground rupture when a nuclear test is conducted;
4. Earthquake focal mechanisms, e.g., discriminating between natural, shear-faulting earthquakes and volumetric mining collapses, as was done by McGarr (1992a, 1992b) for well-recorded earthquakes in South African gold mines and Dreger et al. (2008) for a mine collapse in Utah.

Work is currently ongoing to develop additional ways of discriminating induced from natural earthquakes. These include using statistical features of background earthquakes and clustered sub-populations. For example, Zaliapin and Ben-Zion (2016) have suggested several statistical features that may distinguish induced seismicity from natural tectonic activity including a higher rate of background events and more rapid aftershock decay.

7.6. Why are earthquakes induced by some industrial projects and not others?

In addition to needing an explanation for why earthquakes occur at particular projects, any theory for induced earthquakes must also explain why they do not occur at most projects. This endeavor is hampered by under-reporting (Section 7.1; Table 3). A necessary pre-requisite to explaining induced seismicity as a whole or in different categories is to know its true extent.

For industrial activity as a whole, reports of induced earthquakes are extraordinarily rare (Table 3). Induced nuisance earthquakes are even rarer. Only ~2% of mines, water reservoirs, and CCS projects are reported to be seismogenic. All other categories of project for which we found data were < 2% seismogenic.

Individual cases are diverse and site-specific and the lack of similarities is perhaps a stronger feature than common factors. With the exception of large geothermal projects and hydrofracturing (where almost all are probably seismogenic but only 0.001% are reported to be so) it is seemingly unpredictable which projects will report induced earthquakes. Many if not most induced earthquakes, except at hydrofracturing projects, were unexpected. On the other hand, a research experiment that specifically aimed to induce seismicity, by injecting water into an active fault zone, failed to do so (Section 4.1.8) (Prioul et al., 2000).

A majority of induced earthquakes occur in intraplate areas (Fig. 109). This is not surprising in view of the fact that rocks are close to failure everywhere so the potential for inducing earthquakes in intraplate and plate-boundary regions may be similar (Section 1.1). This,

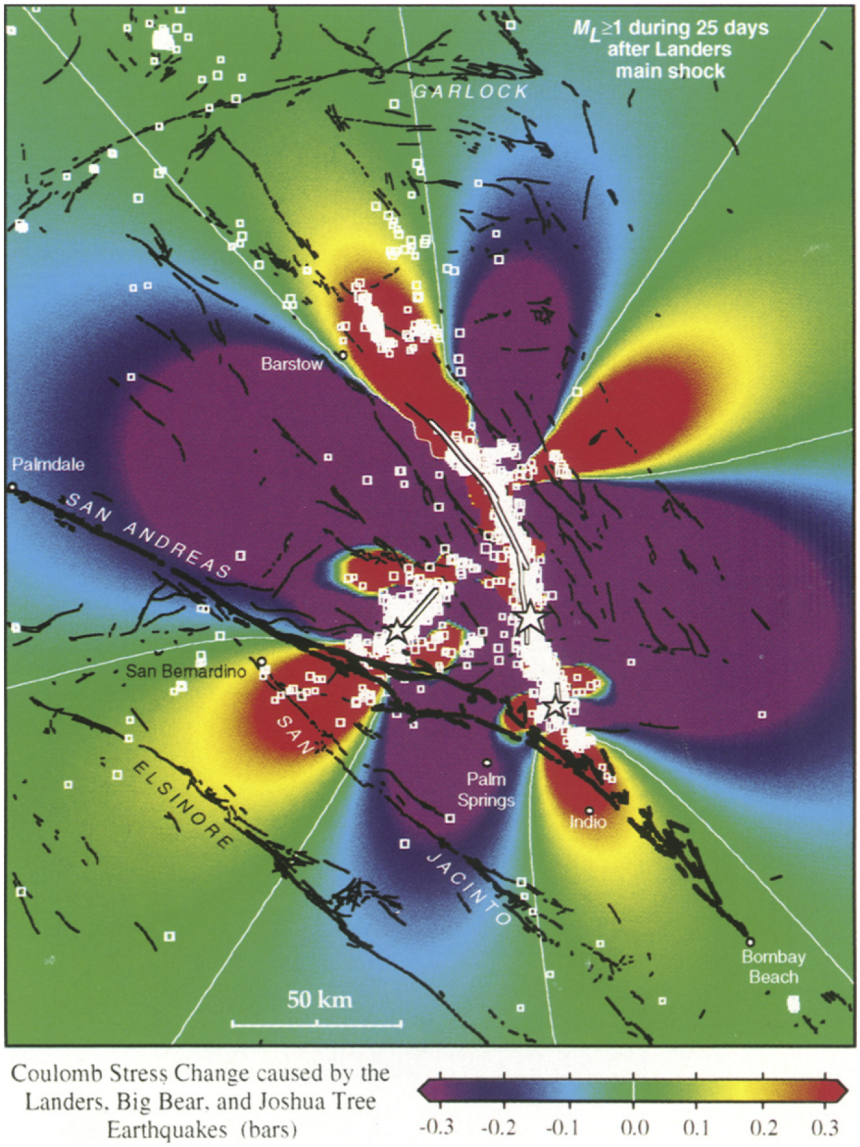

Fig. 117. Coulomb stress changes at a depth of 6.25 km caused by the M_W 7.3 Landers, California, earthquake and large aftershocks. (From King et al. (1994).)

Table 7
Seven questions proposed by Davis and Frohlich (1993) to diagnose earthquakes induced by fluid injection. (From Davis and Frohlich (1993).)

	Question	Earthquakes clearly not induced	Earthquakes clearly induced	I Denver, Colorado	II Painesville, Ohio
	Background seismicity				
1	Are these events the first known earthquakes of this character in the region?	NO	YES	YES	NO
	Temporal correlation				
2	Is there a clear correlation between injection and seismicity	NO	YES	YES	NO
	Spatial correlation				
3a	Are epicenters near wells (within 5 km)?	NO	YES	YES	YES?
3b	Do some earthquakes occur at or near injection depths?	NO	YES	YES	YES?
3c	If not, are there known geologic structures that may channel flow to sites of earthquakes?	NO	YES	NO?	NO?
	Injection practices				
4a	Are changes in fluid pressure at well bottoms sufficient to encourage seismicity?	NO	YES	YES	YES
4b	Are changes in fluid pressure at hypocentral locations sufficient to encourage seismicity?	NO	YES	YES	NO?
	Total “YES” answers	0	7	6	3

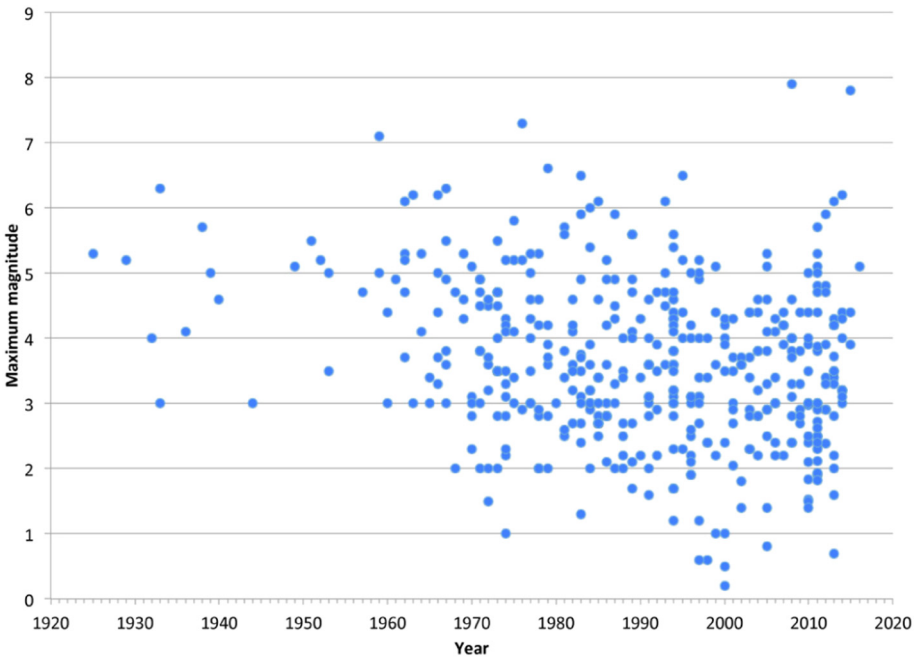

Fig. 118. M_{MAX} vs. year for the 419 cases where data are available.

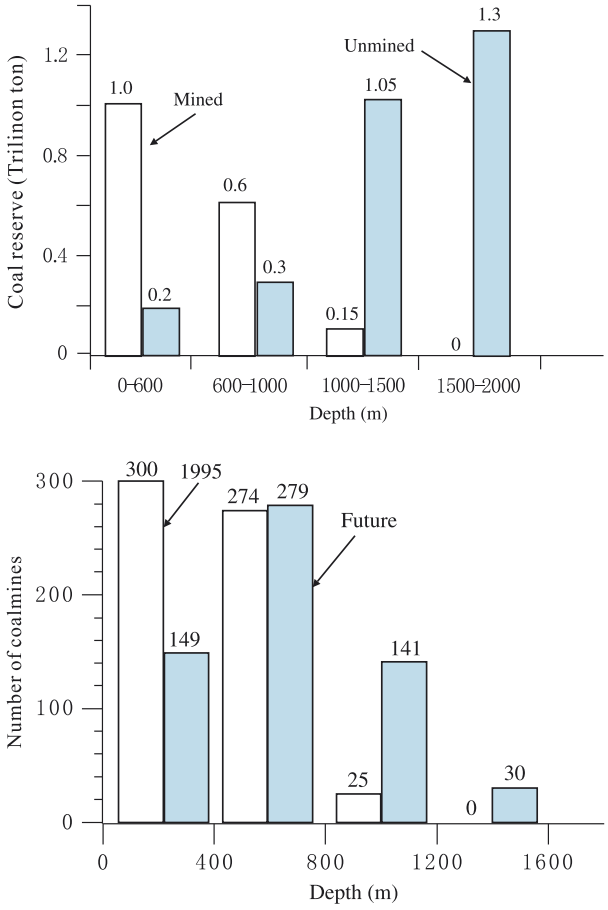

Fig. 119. Top: Depth distribution of Chinese coal reserves (1995 statistics). Bottom: Depth distribution of 599 state-owned Chinese coal mines.
(From Li et al. (2007).)

coupled with many earthquake sequences being unexpected and in areas previously aseismic, means that populations may be unprepared. To add to this, pre-industrial seismic risk assessments may be difficult if there is no history of seismicity or seismic monitoring. Wilson et al. (2015) recently tried to rectify this problem for the UK in advance of possible expansion of the shale-gas industry by estimating a baseline for UK seismicity.

For most non-research purposes the parameter of importance is not whether seismicity is induced but whether nuisance seismicity is induced (Section 1.2). M_{MAX} is thus critical. Section 6 describes an initial examination of *HiQuake* for correlations. The currently observed upper limit to M_{MAX} correlates with water reservoir volume and mass per unit area, volume added or removed at the surface, volume extracted or added to the subsurface, injection pressure (negative correlation), rate and volume, the yield of nuclear tests and scale of project. Most of these are basically measures of project size. Factors such as reservoir pressure change and injection/extraction rate do not correlate with the observed M_{MAX} ceiling.

Suggestions for what operational parameters might be adjusted to mitigate induced seismicity include injecting into formations that are sealed from the basement, and avoiding known faults. There has, however, yet to be a demonstration of an approach that works in general for projects of a particular type. It is also not clear how we would we recognize success since there can be no evidence for the earthquake that did not occur.

7.7. Future trends

7.7.1. Earthquake prediction

There is presently no reliable method to predict earthquakes. Current approaches to reducing hazard comprise long-term forecasting based on the history of past earthquakes including instrumental data, historical information, and paleoseismology using methods such as trenching (e.g., Obermeier, 1996). This approach assumes that patterns of seismicity persist in local areas. It cannot make predictions, even in plate boundary zones (Lindh, 2005), and may work even more poorly in intraplate areas (Section 1.1) (Brooks et al., n.d.; Stein et al., 2015). In regions with little history of seismicity it may not be possible to implement.

Nicol et al. (2011) reviewed this issue from the point of view of CCS. Focus tends to be on reservoir-scale pressure increases and the effect of crustal loading on local faults is not routinely considered. Modeling crustal loading or unloading, along with the likely effects on groundwater, might be fruitful avenues of approach. Another useful approach

could be to study jointly surface deformation and seismicity. The technology to measure surface deformation is well developed. Both satellite and ground-based methods are available but rarely have integrated studies with ground truthing been reported. InSAR and GPS were applied to the depleted Alkmaar Gas Field in the Netherlands (Gee et al., 2016), and Intermittent SBAS satellite data were used to confirm the deformation from earlier GPS work. These results could potentially be integrated with legacy earthquake data.

The two types of data have been jointly interpreted in the case of several projects (e.g., Goertz-Allmann et al., 2014; Keiding et al., 2010). However, systematic relationships have not been explored for induced earthquakes as a whole.

7.7.2. Monitoring recommendations

Good industrial practice first and foremost requires high-quality information. Projects that have the potential to induce earthquakes should be monitored seismically and geodetically. Joint interpretation of these two types of data is more powerful than either in isolation. In addition to the nuisance of seismic deformations (i.e. earthquakes), aseismic deformations can alter the surface and cause nuisance such as infrastructure damage, flooding, and other changes to groundwater circulation.

Geophysical monitoring need not necessarily be elaborate and can be tailored to the circumstances. Unless there is evidence or compelling expectations for earthquakes or surface deformation, minimal instrumentation will suffice. Data should be publically available to all stakeholders.

The current paper contributes a full review of what type of projects have been claimed to induce earthquakes in the past. This is currently the best guide identifying what projects will induce earthquakes in future.

7.7.3. Earthquake management

The largest reported induced earthquake has increased with time from M 6.3 in 1933 to ~M 8 in 2008 (Fig. 118). The number of reported cases has also increased greatly, probably because of the increasing number of large-scale industrial projects. The lower magnitude threshold of reporting is reducing, probably partly because of improved monitoring. These statements, and others made in this paper, should be viewed in the context that they are underpinned by a database of all earthquakes postulated to be induced, with no selection for credibility.

There is a growing need to manage the problem of industrially induced earthquakes and this is well-illustrated by coal mining in China (Section 3.2.1). The expanding Chinese economy is founded on coal as an energy source but at the same time shallow resources are being rapidly depleted (Fig. 119). The future trend is thus to go deeper (Li et al., 2007). In the two decades from 1980 to 2000 the average mining depth increased from 288 m to 500 m. Now, over 75% of the coal has been removed from the top 1000 m and the recent increase in mine seismicity there results largely from increases in mining depth and the size of galleries. Super-deep mines (> 1200 m in depth), such as have induced seismicity in South Africa for decades, are planned in China for the future. Fluid injection for waste disposal, enhanced oil recovery, hydrofracturing and geothermal energy, are also expanding rapidly and have resulted in some of the most significant increases in induced seismicity in recent years (Ellsworth, 2013). Other industries such as building dams and CCS may expand over the coming years.

Management of the problem is moving forward rapidly as additional stakeholders become involved (e.g., Wang et al., 2016). For example, the issue of induced earthquakes is now of concern to the US Army Corps of Engineers because of the threat to critical federal infrastructure, e.g., levees and dams. No societal benefit comes without price–there is no such thing as a free lunch. However, public policy, engineering, preparation, and outreach can enable economically and societally beneficial projects to go ahead under appropriate health-and-safety conditions and in contexts that are understood and acceptable to stakeholders.

Acknowledgments

This work benefitted from discussions with and assistance from Julian Bommer, Kosuke Heki, Tianhui Ma, Steve Spottiswoode, Michelle Grobbelaar, Deborah Weiser, Irene Beardsley and Dan Bloomberg. Ang Li assisted with locating Chinese cases. The authors thank Art McGarr and two anonymous reviewers for helpful reviews, and Giuliano Panza, Editor, for handling the manuscript. The project was funded by the Nederlandse Aardolie Maatschappij BV (NAM), Schepersmaat 2, 9405 TA Assen, The Netherlands. This paper is based on a report submitted to Jan van Elk and Dirk Doornhof (NAM).

Appendix A. Supplementary data

Supplementary data to this article can be found online at http://dx.doi.org/10.1016/j.earscirev.2017.07.008.

References

Ahmad, M.U., Smith, J.A., 1988. Earthquakes, injection wells, and the Perry Nuclear Power Plant, Cleveland, Ohio. Geology 16, 739–742.
Ake, J., Mahrer, K., O'Connell, D., Block, L., 2005. Deep-injection and closely monitored induced seismicity at Paradox Valley, Colorado. Bull. Seismol. Soc. Am. 95, 664–683. http://dx.doi.org/10.1785/0120040072.
Al-Enezi, A., Petrat, L., Abdel-Fattah, R., G. D. M. Technologie, 2008. Induced seismicity and surface deformation within Kuwait's oil fields. In: Proceedings of the Proc. Int. Conf. Geol. Seismol, pp. 177–183.
Allis, R.G., Currie, S.A., Leaver, J.D., Sherburn, S., 1985. Results of injection testing at Wairakei geothermal field, New Zealand. In: Geothermal Resources Council International Symposium on Geothermal Energy: International Volume, pp. 289–294.
Amidzic, D., Murphy, S.K., Van Aswegen, G., 1999. Case study of a large seismic event at a South African gold mine. In: Proceedings of the 9th ISRM Congress.
Amos, C.B., Audet, P., Hammond, W.C., Bürgmann, R., Johanson, I.A., Blewitt, G., 2014. Uplift and seismicity driven by groundwater depletion in central California. Nature 509, 483–486.
Anonymous, 2014. Literature review on injection-related induced seismicity and its relevance to nitrogen injection. In: Earth, Environmental and Life Sciences, Utrecht, Netherlands Report TNO 2014 R11761, pp. 46.
Arkhipova, E.V., Zhigalin, A.D., Morozova, L.I., Nikolaev, A.V., 2012. The Van earthquake on October 23, 2011: natural and technogenic causes. In: Proceedings of the Doklady Earth Sciences Conference, pp. 1176–1179.
Asanuma, H., Soma, N., Kaieda, H., Kumano, Y., Izumi, T., Tezuka, K., Niitsuma, H., Wyborn, D., 2005. Microseismic monitoring of hydraulic stimulation at the Australian HDR project in Cooper Basin. In: Proceedings of the World Geothermal Congress, pp. 24–29.
Avouac, J.-P., 2012. Earthquakes: human-induced shaking. Nat. Geosci. 5, 763–764. http://dx.doi.org/10.1038/ngeo1609.
Awad, M., Mizoue, M., 1995. Earthquake activity in the Aswan region, Egypt. Pure Appl. Geophys. 145, 69–86. http://dx.doi.org/10.1007/bf00879484.
Baisch, S., Harjes, H.P., 2003. A model for fluid-injection-induced seismicity at the KTB, Germany. Geophys. J. Int. 152, 160–170. http://dx.doi.org/10.1046/j.1365-246X.2003.01837.x.
Baisch, S., Vörös, R., 2011. Geomechanical Study of Blackpool Seismicity. pp. 58 Report prepared for Cuadrilla Ltd. by Q-con GmbH.
Baisch, S., Bohnhoff, M., Ceranna, L., Tu, Y., Harjes, H.P., 2002. Probing the crust to 9-km depth: fluid-injection experiments and induced seismicity at the KTB superdeep drilling hole, Germany. Bull. Seismol. Soc. Am. 92, 2369–2380. http://dx.doi.org/10.1785/0120010236.
Baisch, S., Weidler, R., Voros, R., Wyborn, D., de Graaf, L., 2006. Induced seismicity during the stimulation of a geothermal HFR reservoir in the Cooper Basin, Australia. Bull. Seismol. Soc. Am. 96, 2242–2256. http://dx.doi.org/10.1785/0120050255.
Baisch, S., Vörös, R., Weidler, R., Wyborn, D., 2009. Investigation of fault mechanisms during geothermal reservoir stimulation experiments in the Cooper Basin, Australia. Bull. Seismol. Soc. Am. 99, 148–158. http://dx.doi.org/10.1785/0120080055.
Baisch, S., Voeroes, R., Rothert, E., Stang, H., Jung, R., Schellschmidt, R., 2010. A numerical model for fluid injection induced seismicity at Soultz-sous-Forets. Int. J. Rock Mech. Min. Sci. 47, 405–413. http://dx.doi.org/10.1016/j.ijrmms.2009.10.001.
Baisch, S., Rothert, E., Stang, H., Voeroes, R., Koch, C., McMahon, A., 2015. Continued geothermal reservoir stimulation experiments in the Cooper Basin (Australia). Bull. Seismol. Soc. Am. 105, 198–209. http://dx.doi.org/10.1785/0120140208.
Balassanian, S.Y., 2005. Earthquakes induced by deep penetrating bombing? Acta Seismol. Sin. 18, 741–745.
Bardainne, T., Dubos-Sallee, N., Senechal, G., Gaillot, P., Perroud, H., 2008. Analysis of the induced seismicity of the Lacq gas field (southwestern France) and model of deformation. Geophys. J. Int. 172, 1151–1162. http://dx.doi.org/10.1111/j.1365-246X.2007.03705.x.
Batini, F., Bufe, C., Cameli, G.M., Console, R., Fiordelisi, A., 1980. Seismic monitoring in Italian geothermal areas I: seismic activity in the Larderello-Travale region. In: Proceedings of the Second DOE-ENEL Workshop on Cooperative Research in Geothermal Energy, Lawrence Berkeley Laboratory, Berkeley, CA, USA, October

20–22, pp. 20–47.
Batini, F., Console, R., Luongo, G., 1985. Seismological study of Larderello-Travale geothermal area. Geothermics 14, 255–272.
Bella, F., Biagi, P.F., Caputo, M., Cozzi, E., Della Monica, G., Ermini, A., Plastino, W., Sgrigna, V., 1998. Aquifer-induced seismicity in the Central Apennines (Italy). Pure Appl. Geophys. 153, 179–194. http://dx.doi.org/10.1007/s000240050191.
Benetatos, C., Malek, J., Verga, F., 2013. Moment tensor inversion for two micro-earthquakes occurring inside the Haje gas storage facilities, Czech Republic. J. Seismol. 17, 557–577. http://dx.doi.org/10.1007/s10950-012-9337-0.
Bennett, T.J., Marshall, M.E., Barker, B.W., Murphy, J.R., 1994. Characteristics of Rockbursts for Use in Seismic Discrimination. Maxwell Labs Inc., La Jolla, California, pp. 103 (Report SSS-FR-93-14382).
Bertani, R., 2010. Geothermal power generation in the world: 2005–2010 update report. In: Proceedings of the World Geothermal Congress 2010, Bali, Indonesia, 25–29 April 2010.
Block, L.V., Wood, C.K., Yeck, W.L., King, V.M., 2015. Induced seismicity constraints on subsurface geological structure, Paradox Valley, Colorado. Geophys. J. Int. 200, 1170–1193. http://dx.doi.org/10.1093/gji/ggu459.
Boettcher, M.S., Kane, D.L., McGarr, A., Johnston, M.J.S., Reches, Z., 2015. Moment tensors and other source parameters of mining-induced earthquakes in TauTona Mine, South Africa. Bull. Seismol. Soc. Am. 105, 1576–1593. http://dx.doi.org/10.1785/0120140300.
Bohnhoff, M., Baisch, S., Harjes, H.P., 2004. Fault mechanisms of induced seismicity at the superdeep German Continental Deep Drilling Program (KTB) borehole and their relation to fault structure and stress field. J. Geophys. Res. 109. http://dx.doi.org/10.1029/2003jb002528.
Bossu, R., Grasso, J.R., Plotnikova, L.M., Nurtaev, B., Frechet, J., Moisy, M., 1996. Complexity of intracontinental seismic faultings: the Gazli, Uzbekistan, sequence. Bull. Seismol. Soc. Am. 86, 959–971.
Boucher, G., Ryall, A., Jones, A.E., 1969. Earthquakes associated with underground nuclear explosions. J. Geophys. Res. 74, 3808–3820.
Bou-Rabee, F., Nur, A., 2002. The 1993 M 4. 7 Kuwait earthquake: induced by the burning of the oil fields. Kuwait J. Sci. Eng. 29, 155–163.
Bourne, S.J., Oates, S.J., Bommer, J.J., Dost, B., van Elk, J., Doornhof, D., 2015. Monte Carlo method for probabilistic hazard assessment of induced seismicity due to conventional natural gas production. Bull. Seismol. Soc. Am. 105, 1721–1738. http://dx.doi.org/10.1785/0120140302.
Brooks E.M., Stein S., Spencer B.D., Salditch L., Peterson M.D., McNamara D.E., Assessing earthquake hazard map performance for natural and induced seismicity in the central and eastern United States. Seismol. Res. Lett.
Brudy, M., Zoback, M.D., Fuchs, K., Rummel, F., Baumgartner, J., 1997. Estimation of the complete stress tensor to 8 km depth in the KTB scientific drill holes: implications for crustal strength. J. Geophys. Res. 102, 18453–18475.
Calo, M., Dorbath, C., Frogneux, M., 2014. Injection tests at the EGS reservoir of Soultz-sous-Forets. Seismic response of the GPK4 stimulations. Geothermics 52, 50–58. http://dx.doi.org/10.1016/j.geothermics.2013.10.007.
Caloi, P., De Panfilis, M., Di Filippo, D., Marcelli, L., Spadea, M.C., 1956. Terremoti della Val Padana del 15-16 maggio 1951. Ann. Geophys. 9, 63–105.
Carder, D.S., 1945. Seismic investigations in the Boulder Dam area, 1940–1944, and the influence of reservoir loading on local earthquake activity. Bull. Seismol. Soc. Am. 35, 175–192.
Cartlidge, E., 2014. Human activity may have triggered fatal Italian earthquakes, panel says. Science 344, 141.
Castle, R.O., Yerkes, R.F., 1976. Recent surface movements in the Baldwin Hills, Los Angeles County, California. In: U.S. Geological Survey Professional Paper 882. U.S. Geological Survey, Washington, D.C., pp. viii + 125.
Cesca, S., Grigoli, F., Heimann, S., Gonzalez, A., Buforn, E., Maghsoudi, S., Blanch, E., Dahm, T., 2014. The 2013 September–October seismic sequence offshore Spain: a case of seismicity triggered by gas injection? Geophys. J. Int. 198, 941–953. http://dx.doi.org/10.1093/gji/ggu172.
Chabora, E., Zemach, E., Spielman, P., Drakos, P., Hickman, S., Lutz, S., Boyle, K., Falconer, A., Robertson-Tait, A., Davatzes, N.C., Rose, P., Majer, E., Jarpe, S., 2012. Hydraulic stimulation of Well 27-15, Desert Peak geothermal field, Nevada, U.S.A. In: Proceedings of the 37th Standford Geothermal Workshop, Stanford, CA.
Cladouhos, T., Petty, S., Nordin, Y., Moore, M., Grasso, K., Uddenberg, M., Swyer, M., Julian, B., Foulger, G., 2013. Microseismic monitoring of Newberry Volcano EGS Demonstration. In: Proceedings of the Thirty-eighth Workshop on Geothermal Reservoir Engineering, Stanford University, Stanford, California, February 11–13, 2013.
Clarke, H., Eisner, L., Styles, P., Turner, P., 2014. Felt seismicity associated with shale gas hydraulic fracturing: the first documented example in Europe. Geophys. Res. Lett. 41, 8308–8314. http://dx.doi.org/10.1002/2014gl062047.
Cochran, E.S., Vidale, J., Tanaka, S., 2004. Earth tides can trigger shallow thrust fault earthquakes. Science 306, 1164–1166.
Darold, A., Holland, A.A., Chen, C., Youngblood, A., 2014. Preliminary analysis of seismicity near Eagleton 1–29, Carter County, July 2014. In: Oklahoma Geological Survey Open-file Report OF2-2014, pp. 17.
Davies, R., Foulger, G., Bindley, A., Styles, P., 2013. Induced seismicity and hydraulic fracturing for the recovery of hydrocarbons. Mar. Pet. Geol. 45, 171–185. http://dx.doi.org/10.1016/j.marpetgeo.2013.03.016.
Davis, S.D., Frohlich, C., 1993. Did (or will) fluid injection cause earthquakes? - criteria for a rational assessment. Seismol. Res. Lett. 64, 207–224.
Davis, S.D., Pennington, W.D., 1989. Induced seismic deformation in the Cogdell oil field of west Texas. Bull. Seismol. Soc. Am. 79, 1477–1495.
de Pater, C.J., Baisch, S., 2011. Geomechanical study of Bowland Shale seismicity. In: Synthesis Report, pp. 71 Report commissioned by Cuadrilla Resources Ltd., June 2011.
deBruyn, I.A., Bell, F.G., 1997. Mining and induced seismicity in South Africa: a survey. In: Proceedings of the International Symposium on Engineering Geology and the Environment, Athens, Greece, 23–27 June, pp. 2321–2326.
Deichmann, N., Ernst, J., 2009. Earthquake focal mechanisms of the induced seismicity in 2006 and 2007 below Basel (Switzerland). Swiss J. Geosci. 102, 457–466. http://dx.doi.org/10.1007/s00015-009-1336-y.
Dreger, D., Ford, S.R., Walter, W.R., 2008. Source analysis of the Crandall Canyon, Utah mine collapse. Science 321, 217.
Durrheim, R.J., 2010. Mitigating the risk of rockbursts in the deep hard rock mines of South Africa: 100 years of research. In: Brune, J. (Ed.), Extracting the Science: A Century of Mining Research. Society for Mining, Metallurgy, and Exploration, Inc., pp. 156–171.
Durrheim, R.J., Anderson, R.L., Cichowicz, A., Ebrahim-Trolloped, R., Hubert, G., Kijko, A., McGarr, A., Ortlepp, W., van der Merwe, N., 2006. The risks to miners, mines, and the public posed by large seismic events in the gold mining districts of South Africa. In: Proceedings of the Proceedings of the Third International Seminar on Deep and High Stress Mining, 2–4 October 2006, Quebec City, Canada.
Durrheim, R.J., Vogt, D., Manzi, M., 2013. Advances in geophysical technologies for the exploration and safe mining of deep gold ore bodies in the Witwatersrand basin, South Africa. In: Jonsson, E. (Ed.), Mineral Deposit Research for a High-tech World, pp. 118–121.
Eberhart-Phillips, D., Oppenheimer, D.H., 1984. Induced seismicity in The Geysers geothermal area, California. J. Geophys. Res. 89, 1191–1207.
Ellsworth, W.L., 2013. Injection-induced earthquakes. Science 341, 142–149.
Emanov, A.F., Emanov, A.A., Fateev, A.V., Leskova, E.V., Shevkunova, E.V., Podkorytova, V.G., 2014. Mining-induced seismicity at open pit mines in Kuzbass (Bachatsky earthquake on June 18, 2013). J. Min. Sci. 50, 224–228. http://dx.doi.org/10.1134/s1062739114020033.
Engdahl, E.R., 1972. Seismic effects of the MILROW and CANNIKIN nuclear explosions. Bull. Seismol. Soc. Am. 62, 1411–1423.
Erzinger, J., Stober, I., 2005. Introduction to special issue: long-term fluid production in the KTB pilot hole, Germany. Geofluids 5, 1–7. http://dx.doi.org/10.1111/j.1468-8123.2004.00107.x.
Evans, D.M., 1966. The Denver area earthquakes and the Rocky Mountain Arsenal disposal well. Mt. Geol. 3, 23–36.
Evans, K.F., Zappone, A., Kraft, T., Deichmann, N., Moia, F., 2012. A survey of the induced seismic responses to fluid injection in geothermal and CO_2 reservoirs in Europe. Geothermics 41, 30–54. http://dx.doi.org/10.1016/j.geothermics.2011.08.002.
Farahbod, A.M., Kao, H., Walker, D.M., Cassidy, J.F., 2015. Investigation of regional seismicity before and after hydraulic fracturing in the Horn River Basin, northeast British Columbia. Can. J. Earth Sci. 52, 112–122. http://dx.doi.org/10.1139/cjes-2014-0162.
Feignier, B., Young, R.P., 1992. Moment tensor inversion of induced microseismic events: evidence of non-shear failures in the $-4 < M < -2$ moment magnitude range. Geophys. Res. Lett. 19, 1503–1506.
Ferrazzini, V., Chouet, B., Fehler, M., Aki, K., 1990. Quantitative analysis of long-period events recorded during hydrofracture experiments at Fenton Hill, New Mexico. J. Geophys. Res. 95, 21871–21884.
Fielitz, D., Wegler, U., 2015. Intrinsic and scattering attenuation as derived from fluid induced microseismicity at the German Continental Deep Drilling site. Geophys. J. Int. 201, 1346–1361. http://dx.doi.org/10.1093/gji/ggv064.
Foulger, G.R., 1988a. Hengill triple junction, SW Iceland; 1. Tectonic structure and the spatial and temporal distribution of local earthquakes. J. Geophys. Res. 93, 13493–13506.
Foulger, G.R., 1988b. Hengill triple junction, SW Iceland; 2. Anomalous earthquake focal mechanisms and implications for process within the geothermal reservoir and at accretionary plate boundaries. J. Geophys. Res. 93, 13,507–13,523.
Foulger, G.R., Julian, B.R., 2014. Maximizing EGS earthquake location accuracies. In: Proceedings of the Thirty-ninth Workshop on Geothermal Reservoir Engineering, Stanford, California, February 24–26, 2014, SGP-TR-202.
Foulger, G.R., Long, R.E., 1984. Anomalous focal mechanisms; tensile crack formation on an accreting plate boundary. Nature 310, 43–45.
Foulger, G.R., Long, R.E., Einarsson, P., Björnsson, A., 1989. Implosive earthquakes at the active accretionary plate boundary in northern Iceland. Nature 337, 640–642.
Foulger, G.R., Jahn, C.-H., Seeber, G., Einarsson, P., Julian, B.R., Heki, K., 1992. Post-rifting stress relaxation at the divergent plate boundary in Iceland. Nature 358, 488–490.
Gaite, B., Ugalde, A., Villaseñor, A., Blanch, E., 2016. Improving the location of induced earthquakes associated with an underground gas storage in the Gulf of Valencia (Spain). Phys. Earth Planet. Inter. 254, 46–59.
Gan, W., Frohlich, C., 2013. Gas injection may have triggered earthquakes in the Cogdell oil field, Texas. Proc. Natl. Acad. Sci. 110, 18786–18791. http://dx.doi.org/10.1073/pnas.1311316110.
Gee, D., Sowter, A., Novellino, A., Marsh, S., Gluyas, J.G., 2016. Monitoring land motion due to natural gas extraction; validation of the Intermittent SBAS (ISBAS) DInSAR algorithm over gas fields of North Holland, the Netherlands. Mar. Pet. Geol. 77, 1338–1354.
Glowacka, E., Nava, F.A., 1996. Major earthquakes in Mexicali Valley, Mexico, and fluid extraction at Cerro Prieto geothermal field. Bull. Seismol. Soc. Am. 86, 93–105.
Gluyas, J.G., Peters, A., 2010. Late Field-life for Oil Reservoirs – A Hydrogeological Problem, Paper Presented at British Hydrological Society Third International Symposium, Managing Consequences of a Changing Global Environment.
Gluyas, J., Swarbrick, R., 2017. Petroleum Geoscience, 2nd ed. Wiley-Blackwell (in press).

Godano, M., Gaucher, E., Bardainne, T., Regnier, M., Deschamps, A., Valette, M., 2010. Assessment of focal mechanisms of microseismic events computed from two three-component receivers: application to the Arkema-Vauvert field (France). Geophys. Prospect. 58, 772–787. http://dx.doi.org/10.1111/j.1365-2478.2010.00906.x.

Goertz-Allmann, B.P., Kuhn, D., Oye, V., Bohloli, B., Aker, E., 2014. Combining microseismic and geomechanical observations to interpret storage integrity at the In Salah CCS site. Geophys. J. Int. 198, 447–461. http://dx.doi.org/10.1093/gji/ggu010.

González, P.J., Tiampo, K.F., Palano, M., Cannavo, F., Fernandez, J., 2012. The 2011 Lorca earthquake slip distribution controlled by groundwater crustal unloading. Nat. Geosci. 5, 821–825. http://dx.doi.org/10.1038/ngeo1610.

Got, J.-L., Frechet, J., Klein, F.W., 1994. Deep fault plane geometry inferred from multiplet relative relocation beneath the south flank of Kilauea. J. Geophys. Res. 99, 15375–15386.

Graham, S.P., Wilson, M., Foulger, G.R., Julian, B.R., 2017. Earthquake weather. (in preparation).

Grasle, W., Kessels, W., Kumpel, H.J., Li, X., 2006. Hydraulic observations from a 1 year fluid production test in the 4000 m deep KTB pilot borehole. Geofluids 6, 8–23. http://dx.doi.org/10.1111/j.1468-8123.2006.00124.x.

Green, C.A., Styles, P., Baptie, B.J., 2012. Preese Hall shale gas fracturing. In: Review & Recommendations for Induced Seismic Mitigation. UK Deparment of Energy and Climate Change, pp. iv + 26.

Guglielmi, Y., Cappa, F., Avouac, J.-P., Henry, P., Elsworth, D., 2015. Seismicity triggered by fluid injection-induced aseismic slip. Science 348, 1224–1226. http://dx.doi.org/10.1126/science.aab0476.

Gupta, H.K., 2002. A review of recent studies of triggered earthquakes by artificial water reservoirs with special emphasis on earthquakes in Koyna, India. Earth Sci. Rev. 58, 279–310. http://dx.doi.org/10.1016/s0012-8252(02)00063-6.

Hamilton, D.H., Meehan, R.L., 1971. Ground rupture in the Baldwin Hills. Science 172, 333–344.

Hamilton, R.M., Smith, B.E., Fischer, F.G., Papanek, P.J., 1972. Earthquakes caused by underground nuclear explosions on Pahute Mesa, Nevada Test Site. Bull. Seismol. Soc. Am. 62, 1319–1341.

Hanks, T.C., 1977. Earthquake stress drops, ambient tectonic stresses and stresses that drive plate motions. Pure Appl. Geophys. 115, 441–458.

Hanks, T.C., Kanamori, H., 1979. A moment magnitude scale. J. Geophys. Res. 84, 2348–2350.

Häring, M.O., Schanz, U., Ladner, F., Dyer, B.C., 2008. Characterisation of the Basel 1 enhanced geothermal system. Geothermics 37, 469–495.

Harris, D., 2012. The impact of cultural and religious influences during natural disasters (volcano eruptions). http://earthquake-report.com/2012/09/27/the-impact-of-cultural-and-religious-influences-during-natural-disasters-volcano-eruptions/ September 27, 2012.

Hartline, C., 2014. Seismic Monitoring Advisory Committee Review. Calpine Corporation, pp. 44.

Healy, J.H., Rubey, W.W., Griggs, D.T., Raleigh, C.B., 1968. The Denver earthquakes. Science 61, 1301–1310.

Heesakkers, V., Murphy, S.K., van Aswegen, G., Domoney, R., Addams, S., Dewers, T., Zechmeister, M., Reches, Z., 2005. The Rupture Zone of the M = 2.2 Earthquake that Reactivated the Ancient Pretorius Fault in TauTona Mine, South Africa, Fall Meeting of the American Geophysical Union, Abstract S31B-04.

Heki, K., Foulger, G.R., Julian, B.R., Jahn, C.-H., 1993. Plate dynamics near divergent boundaries: geophysical implications of postrifting crustal deformation in NE Iceland. J. Geophys. Res. 98, 14279–14297.

Heki, K., Miyazaki, S., Tsuji, H., 1997. Silent fault slip following an interplate thrust earthquake at the Japan Trench. Nature 386, 595–598.

Herrmann, R.B., 1978. A seismological study of two Attica, New York earthquakes. Bull. Seismol. Soc. Am. 68, 641–651.

Hill, D.P., Reasenberg, P.A., Michael, A., Arabasz, W.J., Beroza, G., Brumbaugh, D., Brune, J.N., Castro, R., Davis, S., dePolo, D., Ellsworth, W.L., Gomberg, J., Harmsen, S., House, L., Jackson, S.M., Johnston, M.J.S., Jones, L., Keller, R., Malone, S., Munguia, L., Nava, S., Pechmann, J.C., Sanford, A., Simpson, R.W., Smith, R.B., Stark, M., Stickney, M., Vidal, A., Walter, S., Wong, V., Zollweg, J., 1993. Seismicity remotely triggered by the magnitude 7.3 Landers, California, earthquake. Science 260, 1617–1623.

Hitzman, M.W. (Ed.), 2013. Induced Seismicity Potential in Energy Technologies. National Academies Press, Washington, D.C. (x + 248 pp).

Hough, S.E., Page, M., 2015. A century of induced earthquakes in Oklahoma? Bull. Seismol. Soc. Am. 105, 2863–2870. http://dx.doi.org/10.1785/0120150109.

Hsieh, P.A., Bredehoeft, J.D., 1981. A reservoir analysis of the Denver earthquakes: a case of induced seismicity. J. Geophys. Res. 86, 903–920.

Huaman, R.N.E., Jun, T.X., 2014. Energy related CO_2 emissions and the progress on CCS projects: a review. Renew. Sust. Energ. Rev. 31, 368–385.

Husen, S., Bachmann, C., Giardini, D., 2007. Locally triggered seismicity in the central Swiss Alps following the large rainfall event of August 2005. Geophys. J. Int. 171, 1126–1134. http://dx.doi.org/10.1111/j.1365-246X.2007.03561.x.

Husen, S., Kissling, E., von Deschwanden, A., 2012. Induced seismicity during the construction of the Gotthard Base Tunnel, Switzerland: hypocenter locations and source dimensions. J. Seismol. 16, 195–213. http://dx.doi.org/10.1007/s10950-011-9261-8.

Jahr, T., Jentzsch, G., Letz, H., Sauter, M., 2005. Fluid injection and surface deformation at the KTB location: modelling of expected tilt effects. Geofluids 5, 20–27. http://dx.doi.org/10.1111/j.1468-8123.2004.00103.x.

Jahr, T., Jentzsch, G., Letz, H., Gebauer, A., 2007. Tilt observation around the KTB-site Germany: monitoring and modelling of fluid induced deformation of the upper crust of the Earth. In: Tregoning, P., Rizos, C. (Eds.), Dynamic Planet: Monitoring and Understanding a Dynamic Planet With Geodetic and Oceanographic Tools, pp. 467–472.

Jahr, T., Jentzsch, G., Gebauer, A., Lau, T., 2008. Deformation, seismicity, and fluids: results of the 2004/2005 water injection experiment at the KTB/Germany. J. Geophys. Res. 113. http://dx.doi.org/10.1029/2008jb005610.

Jaku, E.P., Jager, A.J., Roberts, M.K.C., 2001. A review of rock-related fatality trends in the South African gold mining industry. In: Elsworth, D., Tinucci, J.P., Heasley, K.A. (Eds.), Rock Mechanics in the National Interest, pp. 467–471.

Johnston, A.C., Schweig, E.S., 1996. The enigma of the New Madrid earthquakes of 1811–1812. Annu. Rev. Earth Planet. Sci. 24, 339–384. http://dx.doi.org/10.1146/annurev.earth.24.1.339.

Jost, M.L., Busselberg, T., Jost, O., Harjes, H.P., 1998. Source parameters of injection-induced microearthquakes at 9 km depth at the KTB deep drilling site, Germany. Bull. Seismol. Soc. Am. 88, 815–832.

Julià, J., Nyblade, A.A., Durrheim, R., Linzer, L., Gök, R., Dirks, P., Walter, W., 2009. Source mechanisms of mine-related seismicity, Savuka mine, South Africa. Bull. Seismol. Soc. Am. 99, 2801–2814.

Julian, B.R., Foulger, G.R., Richards-Dinger, K., 2004. The Coso geothermal area: a laboratory for advanced MEQ studies for geothermal monitoring. In: Proceedings of the Geothermal Resources Council Annual Meeting, Palm Springs, August 2004.

Julian, B.R., Foulger, G.R., Monastero, F., 2007. Microearthquake moment tensors from the Coso Geothermal area. In: Proceedings of the Thirty-second Workshop on Geothermal Reservoir Engineering, Stanford University, Stanford, California, January 22–24, pp. SGP-TR-183.

Julian, B.R., Foulger, G.R., Monastero, F.C., Bjornstad, S., 2010. Imaging hydraulic fractures in a geothermal reservoir. Geophys. Res. Lett. 37. http://dx.doi.org/10.1029/2009GL040933.

Kaieda, H., Sasaki, S., Wyborn, D., 2010. Comparison of characteristics of micro-earthquakes observed during hydraulic stimulation operations in Ogachi, Hijiori and Cooper Basin HDR projects. In: Proceedings of the World Geothermal Congress, Bali, Indonesia, April 25–30.

Kao, H., Farahbod, A.M., Cassidy, J.F., Lamontagne, M., Snyder, D., Lavoie, D., 2015. Natural Resources Canada's induced seismicity research. In: Proceedings of the Schatzalp Induced Seismicity Workshop, Davos, Switzerland, 10–13 March.

Kaven, J.O., Hickman, S.H., Davatzes, N.C., 2014. Micro-seismicity and seismic moment release within the Coso Geothermal Field, California. In: Proceedings of the Thirty-ninth Workshop on Geothermal Reservoir Engineering, Stanford University, Stanford, California, February 24–26, 2014, pp. SGP-TR-202.

Kaven, J.O., Hickman, S.H., McGarr, A.F., Ellsworth, W.L., 2015. Surface monitoring of microseismicity at the Decatur, Illinois, CO_2 sequestration demonstration site. Seismol. Res. Lett. 86, 1096–1101.

Keiding, M., Arnadottir, T., Jonsson, S., Decriem, J., Hooper, A., 2010. Plate boundary deformation and man-made subsidence around geothermal fields on the Reykjanes Peninsula, Iceland. J. Volcanol. Geotherm. Res. 194, 139–149. http://dx.doi.org/10.1016/j.jvolgeores.2010.04.011.

Keith, C.M., Simpson, D.W., Soboleva, O.V., 1982. Induced seismicity and style of deformation at Nurek reservoir, Tadjik SSR. J. Geophys. Res. 87, 4609–4624. http://dx.doi.org/10.1029/JB087iB06p04609.

Keranen, K.M., Savage, H.M., Abers, G.A., Cochran, E.S., 2013. Potentially induced earthquakes in Oklahoma, USA: links between wastewater injection and the 2011 Mw 5.7 earthquake sequence. Geology 41, 699–702. http://dx.doi.org/10.1130/g34045.1.

Keranen, K.M., Weingarten, M., Abers, G.A., Bekins, B.A., Ge, S., 2014. Sharp increase in central Oklahoma seismicity since 2008 induced by massive wastewater injection. Science 345, 448–451. http://dx.doi.org/10.1126/science.1255802.

King, G.E., 2012. Hydraulic fracturing 101: what every representative, environmentalist, regulator, reporter, investor, university researcher, neighbor and engineer should know about estimating frac risk and improving frac performance in unconventional gas and oil wells. In: Proceedings of the SPE Hydraulic Fracturing Technology Conference.

King, G.C.P., Stein, R.S., Lin, J., 1994. Static stress changes and the triggering of earthquakes. Bull. Seismol. Soc. Am. 84, 935–953.

King, V.M., Block, L.V., Yeck, W.L., Wood, C.K., Derouin, S.A., 2014. Geological structure of the Paradox Valley Region, Colorado, and relationship to seismicity induced by deep well injection. J. Geophys. Res. 119, 4955–4978. http://dx.doi.org/10.1002/2013jb010651.

Kinscher, J., Bernard, P., Contrucci, I., Mangeney, A., Piguet, J.P., Bigarre, P., 2015. Location of microseismic swarms induced by salt solution mining. Geophys. J. Int. 200, 337–362. http://dx.doi.org/10.1093/gji/ggu396.

Klein, F.W., Einarsson, P., Wyss, M., 1977. The Reykjanes Peninsula, Iceland, earthquake swarm of September 1972 and its tectonic significance. J. Geophys. Res. 82, 865–887.

Klose, C.D., 2007a. Geomechanical modeling of the nucleation process of Australia's 1989 M5.6 Newcastle earthquake. Earth Planet. Sci. Lett. 256, 547–553. http://dx.doi.org/10.1016/j.epsl.2007.02.009.

Klose, C.D., 2007b. Coastal land loss and gain as potential earthquake trigger mechanism in SCRs. In: Proceedings of the Fall Meeting of the American Geophysical Union abstract T51D-0759, San Francisco, 10–14 December.

Klose, C.D., 2012. Evidence for anthropogenic surface loading as trigger mechanism of the 2008 Wenchuan earthquake. Environ. Earth Sci. 66, 1439–1447. http://dx.doi.org/10.1007/s12665-011-1355-7.

Klose, C.D., 2013. Mechanical and statistical evidence of the causality of human-made mass shifts on the Earth's upper crust and the occurrence of earthquakes. J. Seismol. 17, 109–135. http://dx.doi.org/10.1007/s10950-012-9321-8.

Knoll, P., 1990. The fluid-induced tectonic rock burst of March 13, 1989 in Werra potash mining district of the GDR (first results). Gerlands Beitr. Geophys. 99, 239–245.

Kovach, R.L., 1974. Source mechanisms for Wilmington oil field, California, subsidence earthquakes. Bull. Seismol. Soc. Am. 64, 699–711.

Kozlowska, M., Orlecka-Sikora, B., Kwiatek, G., Boettcher, M.S., Dresen, G., 2015. Nanoseismicity and picoseismicity rate changes from static stress triggering caused by a Mw 2.2 earthquake in Mponeng gold mine, South Africa. J. Geophys. Res. 120, 290–307. http://dx.doi.org/10.1002/2014jb011410.
Kravania, S., Batini, F., Fiordelise, A., Panza, G.F., 2000. Full moment tensor retrieval from waveform inversion in the Larderello geothermal area. Pure Appl. Geophys. 157, 1379–1392.
Kundu, B., Legrand, D., Gahalaut, K., Gahalaut, V.K., Mahesh, P., Raju, K.A.K., Catherine, J.K., Ambikapthy, A., Chadha, R.K., 2012. The 2005 volcano-tectonic earthquake swarm in the Andaman Sea: triggered by the 2004 great Sumatra-Andaman earthquake. Tectonics 31. http://dx.doi.org/10.1029/2012tc003138.
Kundu, B., Vissa, N.K., Gahalaut, V.K., 2015. Influence of anthropogenic groundwater unloading in Indo-Gangetic plains on the 25 April 2015 Mw 7.8 Gorkha, Nepal earthquake. Geophys. Res. Lett. 42, 10607–10613.
Kusznir, N.J., Al-Saigh, N.H., Ashwin, D.P., 1982. Induced seismicity generated by longwall coal mining in the North Staffordshire coal-field, U. K. In: Proceedings of the Procedings of the First International Congress on Rockbursts and Seismicity in Mines, Johannesburg, South Africa, pp. 153–160.
Latham, G., Dorman, J., Duennebier, F., Ewing, M., Lammlein, D., Nakamura, Y., 1973. Moonquakes, meteoroids, and the state of the lunar interior. In: Proceedings of the Third Lunar and Planetary Science Conference Abstract, Houston, Texas, January 10–13.
Lehner, B., Liermann, C.R., Revenga, C., Vörösmarty, C., Fekete, B., Crouzet, P., Döll, P., Endejan, M., Frenken, K., Magome, J., 2011. High-resolution mapping of the world's reservoirs and dams for sustainable river-flow management. Front. Ecol. Environ. 9, 494–502.
Lei, X., Yu, G., Ma, S., Wen, X., Wang, Q., 2008. Earthquakes induced by water injection at ~3 km depth within the Rongchang gas field, Chongqing, China. J. Geophys. Res. 113. http://dx.doi.org/10.1029/2008JB005604.
Lei, X., Ma, S., Chen, W., Pang, C., Zeng, J., Jiang, B., 2013. A detailed view of the injection-induced seismicity in a natural gas reservoir in Zigong, southwestern Sichuan Basin, China. J. Geophys. Res. 118, 4296–4311. http://dx.doi.org/10.1002/jgrb.50310.
Leith, W., Simpson, D.W., Alvarez, W., 1981. Structure and permeability - geologic controls on induced seismicity at Nurek reservoir, Tadjikistan, USSR. Geology 9, 440–444. http://dx.doi.org/10.1130/0091-7613(1981)9<440:sapgco>2.0.co;2.
Li, G., 2011. World Atlas of Oil and Gas Basins. Wiley-Blackwell (496 pp).
Li, T., Cai, M.F., Cai, M., 2007. A review of mining-induced seismicity in China. Int. J. Rock Mech. Min. Sci. 44, 1149–1171. http://dx.doi.org/10.1016/j.ijrmms.2007.06.002.
Lin, C.H., 2005. Seismicity increase after the construction of the world's tallest building: an active blind fault beneath the Taipei 101. Geophys. Res. Lett. 32. http://dx.doi.org/10.1029/2005gl024223.
Lindh, A.G., 2005. Success and failure at Parkfield. Seismol. Res. Lett. 76, 3–6.
Lippmann-Pipke, J., Erzinger, J., Zimmer, M., Kujawa, C., Boettcher, M., Van Heerden, E., Bester, A., Moller, H., Stroncik, N.A., Reches, Z., 2011. Geogas transport in fractured hard rock - correlations with mining seismicity at 3.54 km depth, TauTona gold mine, South Africa. Appl. Geochem. 26, 2134–2146. http://dx.doi.org/10.1016/j.apgeochem.2011.07.011.
Liu, M., Stein, S., 2016. Mid-continental earthquakes: spatiotemporal occurrences, causes, and hazards. Earth Sci. Rev. 162, 364–386.
Liu, C., Linde, A.T., Sacks, I.S., 2009. Slow earthquakes triggered by typhoons. Nature 459, 833–836.
Lofgren, B.E., 1978. Monitoring crustal deformation in the Geysers-Clear Lake geothermal area, California. In: Open-File Report 78-597. U.S. Geological Survey, Washington, D.C., pp. iv + 26 (28 maps).
Lofgren, B.E., 1981. Monitoring crustal deformation in the Geyser-Clear Lake region. In: McLaughlin, R.J., Donnelly-Nolan, J.M. (Eds.), Research in the Geysers-Clear Lake Geothermal Area, Northern California. U.S. Geological Survey Professional Paper 1141, Washington, D.C.pp. viii + 259.
Ma, X., Li, Z., Hua, P., Jiang, J., Zhao, F., Han, C., Yuan, P., Lu, S., Peng, L., 2015. Fluid-injection-induced seismicity experiment of the WFSD-3P borehole. Acta Geol. Sin. (English Edition) 89, 1057–1058.
Majer, E.L., McEvilly, T.V., 1981. Detailed microearthquake studies at the Cerro Prieto Geothermal Field. In: Proceedings of the Third Symposium on the Cerro Prieto Geothermal Field, Baja California, Mexico, Lawrence Berkeley Laboratory, Berkeley, California, March 24–26, pp. 347–352.
Majer, E.L., McEvilly, T.V., 1982. Seismological studies at the Cerro Prieto Field: 1978–1982. In: Proceedings of the Fourth Symposium on the Cerro Prieto Geothermal Field, Baja California, Mexico, Lawrence Berkeley Laboratory, Berkeley, California, 10–12 August, pp. 145–151.
Majer, E.L., Peterson, J.E., 2007. The impact of injection on seismicity at The Geysers, California Geothermal Field. Int. J. Rock Mech. Min. Sci. 44, 1079–1090. http://dx.doi.org/10.1016/j.ijrmms.2007.07.023.
Majer, E.L., Baria, R., Stark, M., Oates, S., Bommer, J., Smith, B., Asanuma, H., 2007. Induced seismicity associated with enhanced geothermal systems. Geothermics 36, 185–222. http://dx.doi.org/10.1016/j.geothermics.2007.03.003.
Maxwell, S.C., Fabriol, H., 2004. Passive seismic imaging of CO_2 sequestration at Weyburn. In: Proceedings of the Society of Engineering Geophysicists International Exposition and 74th Annual Meeting, Denver, Colorado, 10–15 October.
McGarr, A., 1991. On a possible connection between three major earthquakes in California and oil production. Bull. Seismol. Soc. Am. 81, 948–970.
McGarr, A., 1992a. Moment tensors of ten Witwatersrand mine tremors. Pure Appl. Geophys. 139, 781–800.
McGarr, A., 1992b. An implosive component in the seismic moment tensor of a mining-induced tremor. Geophys. Res. Lett. 19, 1579–1582.
McGarr, A., 2014. Maximum magnitude earthquakes induced by fluid injection. J. Geophys. Res. 119, 1008–1019. http://dx.doi.org/10.1002/2013jb010597.
McGarr, A., Simpson, D., Seeber, L., 2002. Case histories of induced and triggered seismicity. In: Lee, W.H., Jennings, P., Kisslinger, C., Kanamori, H. (Eds.), International Geophysics Series. International Handbook of Earthquake and Engineering Seismologypp. 647–664.
McKeown, F.A., 1975. Relation of geological structure to seismicity at Pahute Mesa, Nevada Test Site. Bull. Seismol. Soc. Am. 65, 747–764.
McKeown, F.A., Dickey, D.D., 1969. Fault displacements and motion related to nuclear explosions. Bull. Seismol. Soc. Am. 59, 2253–2269.
McNamara, D.E., Benz, H.M., Herrmann, R.B., Bergman, E.A., Earle, P., Holland, A., Baldwin, R., Gassner, A., 2015. Earthquake hypocenters and focal mechanisms in central Oklahoma reveal a complex system of reactivated subsurface strike-slip faulting. Geophys. Res. Lett. 42, 2742–2749. http://dx.doi.org/10.1002/2014gl062730.
McNutt, S.R., Beavan, R.J., 1981. Volcanic earthquakes at Pavlof volcano correlated with the solid earth tide. Nature 194, 615–618.
Mercerat, E.D., Driad-Lebeau, L., Bernard, P., 2010. Induced seismicity monitoring of an underground salt cavern prone to collapse. Pure Appl. Geophys. 167, 5–25. http://dx.doi.org/10.1007/s00024-009-0008-1.
Milev, A.M., Spottiswoode, S.M., 2002. Effect of the rock properties on mining-induced seismicity around the Ventersdorp Contact Reef, Witwatersrand basin, South Africa. Pure Appl. Geophys. 159, 165–177. http://dx.doi.org/10.1007/pl00001249.
Miller, A.D., Foulger, G.R., Julian, B.R., 1998a. Non-double-couple earthquakes II. Observations. Rev. Geophys. 36, 551–568.
Miller, A.D., Julian, B.R., Foulger, G.R., 1998b. Three-dimensional seismic structure and moment tensors of non-double-couple earthquakes at the Hengill-Grensdalur volcanic complex, Iceland. Geophys. J. Int. 133, 309–325.
Mogren, S.M., Mukhopadhyay, M., 2013. Study of Seismogenic Crust in the Eastern Province of Saudi Arabia and Its Relation to the Seismicity of the Ghawar Fields, Paper Presented at American Geophysical Union Fall Meeting, 9–13 December.
Monastero, F.C., Katzenstein, A.M., Miller, J.S., Unruh, J.R., Adams, M.C., Richards-Dinger, K., 2005. The Coso geothermal field: a nascent metamorphic core complex. Bull. Geol. Soc. Am. 117, 1534–1553.
Mossop, A., Segall, P., 1999. Volume strain within The Geysers geothermal field. J. Geophys. Res. 104, 29113–29131. http://dx.doi.org/10.1029/1999jb900284.
Nagel, N.B., 2001. Compaction and subsidence issues within the petroleum industry: from Wilmington to Ekofisk and beyond. Phys. Chem. Earth 26, 3–14.
Newman, A., Stein, S., Weber, J., Engeln, J., Mao, A., Dixon, T., 1999. Slow deformation and low seismic hazard at the New Madrid seismic zone. Science 284, 619–621.
Nicholson, C., Wesson, R.L., 1992. Triggered earthquakes and deep well activities. Pure Appl. Geophys. 139, 561–578.
Nicholson, C., Roeloffs, E., Wesson, R.L., 1988. The northeastern Ohio earthquake of 31 January 1986: was it induced? Bull. Seismol. Soc. Am. 78, 188–217.
Nicol, A., Carne, R., Gerstenberger, M., Christophersen, A., 2011. Induced seismicity and its implications for CO_2 storage risk. In: Gale, J., Hendriks, C., Turkenberg, W. (Eds.), 10th International Conference on Greenhouse Gas Control Technologies, pp. 3699–3706.
Nielsen, S.B., Stephenson, R., Thomsen, E., 2007. Dynamics of Mid-Palaeocene North Atlantic rifting linked with European intra-plate deformations. Nature 450, 1071–1074.
Obermeier, S.F., 1996. Use of liquefaction-induced features for paleoseismic analysis. Eng. Geol. 44, 1–76.
Odonne, F., Ménard, I., Massonat, G., Rolando, J.-P., 1999. Abnormal reverse faulting above a depleting reservoir. Geology 27, 111–114.
Ohtake, M., 1974. Seismic activity induced by water injection at Matsushiro, Japan. J. Phys. Earth 22, 163–176.
Pavlovski, O.A., 1998. Radiological consequences of nuclear testing for the population of the former USSR (input information, models, dose and risk estimates). In: Shapiro, C.S. (Ed.), Atmopspheric Nuclear Tests (Environmental and Human Consequences), Proceedings of the NATO Advanced Research Workshop. Springer, Berlin, pp. 219–260.
Pennington, W.D., Davis, S.D., Carlson, S.M., DuPree, J., Ewing, T.E., 1986. The evolution of seismic barriers and asperities caused by the depressuring of fault planes in oil and gas fields of South Texas. Bull. Seismol. Soc. Am. 76, 939–948.
Perea, H., Masana, E., Santanach, P., 2012. An active zone characterized by slow normal faults, the northwestern margin of the Valencia trough (NE Iberia): a review. J. Iber. Geol. 38, 31–52.
Plotnikova, I.M., Nurtaev, B.S., Grasso, J.R., Matasova, L.M., Bossu, R., 1996. The character and extent of seismic deformation in the focal zone of Gazli earthquakes of 1976 and 1984, M > 7.0. Pure Appl. Geophys. 147, 377–387.
Pomeroy, P.W., Simpson, D.W., Sbar, M.L., 1976. Earthquakes triggered by surface quarrying-the Wappingers Falls, New York sequence of June, 1974. Bull. Seismol. Soc. Am. 66, 685–700.
Pratt, W.E., Johnson, D.W., 1926. Local subsidence of the Goose Creek oil field. J. Geol. 34, 577–590.
Prioul, R., Cornet, F.H., Dorbath, C., Dorbath, L., Ogena, M., Ramos, E., 2000. An induced seismicity experiment across a creeping segment of the Philippine Fault. J. Geophys. Res. 105, 13595–13612. http://dx.doi.org/10.1029/2000jb900052.
Purvis, K., Overshott, K.E., Madgett, J.C., Niven, T., 2010. The Ensign enigma: improving well deliverability in a tight gas reservoir. In: Proceedings of the Petroleum Geology: From Mature Basins to New Frontiers – Proceedings of the 7th Petroleum Geology Conference, London, pp. 325–336.
Raleigh, C.B., Healy, J.H., Bredehoeft, J.D., 1976. An experiment in earthquake control at Rangely, Colorado. Science 191, 1230–1237.
Reasenberg, P.A., Simpson, R.W., 1992. Response of regional seismicity to the static stress

change produced by the Loma Prieta earthquake. Science 255, 1687–1690.
Richardson, E., Jordan, T.H., 2002. Seismicity in deep gold mines of South Africa: implications for tectonic earthquakes. Bull. Seismol. Soc. Am. 92, 1766–1782. http://dx.doi.org/10.1785/0120000226.
Ross, A., Foulger, G.R., Julian, B.R., 1999. Source processes of industrially-induced earthquakes at The Geysers geothermal area, California. Geophysics 64, 1877–1889.
Roth, P., Pavoni, N., Deichmann, N., 1992. Seismotectonics of the eastern Swiss Alps and evidence for precipitation-induced variations of seismic activity. Tectonophysics 207, 183–197. http://dx.doi.org/10.1016/0040-1951(92)90477-n.
Rudajev, V., Sileny, J., 1985. Seismic events with non-shear components: II Rockbursts with implosive source component. Pure Appl. Geophys. 123, 17–25.
Schultz, R., Stern, V., Novakovic, M., Atkinson, G., Gu, Y.J., 2015. Hydraulic fracturing and the Crooked Lake Sequences: insights gleaned from regional seismic networks. Geophys. Res. Lett. 42, 2750–2758. http://dx.doi.org/10.1002/2015gl063455.
Seeber, L., Armbruster, J.G., Kim, W.-Y., Barstow, N., 1998. The 1994 Cacoosing Valley earthquakes near Reading, Pennsylvania: a shallow rupture triggered by quarry unloading. J. Geophys. Res. 103, 24505–24521.
Segall, P., 1985. Stress and subsidence resulting from subsurface fluid withdrawal in the epicentral region of the 1983 Coalinga earthquake. J. Geophys. Res. 90, 6801–6816.
Segall, P., 1989. Earthquakes triggered by fluid extraction. Geology 17, 942–946.
Segall, P., 1992. Induced stresses due to fluid extraction from axisymmetrical reservoirs. Pure Appl. Geophys. 139, 535–560. http://dx.doi.org/10.1007/bf00879950.
Semmane, F., Abacha, I., Yelles-Chaouche, A.K., Haned, A., Beldjoudi, H., Amrani, A., 2012. The earthquake swarm of December 2007 in the Mila region of northeastern Algeria. Nat. Hazards 64, 1855–1871. http://dx.doi.org/10.1007/s11069-012-0338-7.
Shapiro, S.A., Kummerow, J., Dinske, C., Asch, G., Rothert, E., Erzinger, J., Kumpel, H.J., Kind, R., 2006. Fluid induced seismicity guided by a continental fault: injection experiment of 2004/2005 at the German Deep Drilling Site (KTB). Geophys. Res. Lett. 33. http://dx.doi.org/10.1029/2005gl024659.
Simiyu, S.M., Keller, G.R., 2000. Seismic monitoring of the Olkaria Geothermal area, Kenya Rift valley. J. Volcanol. Geotherm. Res. 95, 197–208.
Simpson, D.W., Leith, W., 1985. The 1976 and 1984 Gazli, USSR, earthquakes—were they induced? Bull. Seismol. Soc. Am. 75, 1465–1468.
Simpson, D.W., Negmatullaev, S.K., 1981. Induced seismicity at Nurek reservoir, Tadjikistan, USSR. Bull. Seismol. Soc. Am. 71, 1561–1586.
Simpson, D.W., Soboleva, O.V., 1977. Water level variations and reservoir-induced seismicity at Nurek, USSR. Trans. Am. Geophys. Union 58, 1196.
Skoumal, R.J., Brudzinski, M.R., Currie, B.S., 2015. Earthquakes induced by hydraulic fracturing in Poland township, Ohio. Bull. Seismol. Soc. Am. 105, 189–197.
Stark, M.A., 1990. Imaging injected water in The Geysers reservoir using microearthquake data. Trans. Geotherm. Resour. Counc. 17, 1697–1704.
Stein, S., Liu, M., Calais, E., Li, Q., 2009. Midcontinent earthquakes as a complex system. Seismol. Res. Lett. 80, 551–553.
Stein, S., Liu, M., Camelbeeck, T., Merino, M., Landgraf, A., Hintersberger, E., Kuebler, S., 2015. Challenges in assessing seismic hazard in intraplate Europe. In: Landgraf, A., Kuebler, S., Hintersberger, E., Stein, S. (Eds.), Seismicity, Fault Rupture and Earthquake Hazards in Slowly Deforming Regions. Geological Society, London, Special Publications, London.
Styles, P., Gasparini, P., Huenges, E., Scandone, P., Lasocki, S., Terlizzese, F., 2014. Report on the Hydrocarbon Exploration and Seismicity in Emilia Region. International Commission on Hydrocarbon Exploration and Seismicity in the Emilia Region, pp. 213.
Suckale, J., 2009. Induced seismicity in hydrocarbon fields. Adv. Geophys. 51, 55–106.
Suckale, J., 2010. Moderate-to-large seismicity induced by hydrocarbon production. Lead. Edge 29, 310–319. http://dx.doi.org/10.1190/1.3353728.
Tadokoro, K., Ando, M., Nishigami, K., 2000. Induced earthquakes accompanying the water injection experiment at the Nojima fault zone, Japan: seismicity and its migration. J. Geophys. Res. 105, 6089–6104. http://dx.doi.org/10.1029/1999jb900416.
Talwani, P., 1995. Speculation on the causes of continuing seismicity near Koyna reservoir, India. Pure Appl. Geophys. 145, 167–174. http://dx.doi.org/10.1007/bf00879492.
Tang, C., Wang, J.W., Zhang, J., 2010. Preliminary engineering application of microseismic monitoring technique to rockburst prediction in tunneling of Jinping II project. J. Rock Mech. Geotech. Eng. 3, 193–208.
Tang, L., Zhang, M., Sun, L., Wen, L., 2015. Injection-induced seismicity in a natural gas reservoir in Hutubi, southern Junggar Basin, northwest China. In: Transactions of the American Geophysical Union, Abstract S13B-2847.
Terashima, T., 1981. Survey on induced seismicity at Mishraq area in Iraq. J. Phys. Earth 29, 371–375.
Tester, J.W., et al., 2006. The Future of Geothermal Energy. Massachusetts Institute of Technology, Cambridge, Massachusetts, pp. 372.
Toksöz, M.N., Kehrer, H.K., 1972. Tectonic strain release by underground nuclear explosions and its effect on seismic discrimination. Geophys. J. R. Astron. Soc. 31, 141–161.
Turbitt, T., Walker, A.B., Browitt, C.W.A., Morgan, S.N., 1984. Monitoring the background and induced seismicity for the hot dry rock programme in Cornwall. In: Proceedings of the Third International Seminar on the Results of EC Geothermal Energy Research, Munich, pp. 712–716 (November 1983).
van der Elst, N.J., Savage, H.M., Keranen, K.M., Abers, G.A., 2013. Enhanced remote earthquake triggering at fluid-injection sites in the midwestern United States. Science 341, 164–167.
van Eck, T., Goutbeek, F., Haak, H., Dost, B., 2006. Seismic hazard due to small-magnitude, shallow-source, induced earthquakes in The Netherlands. Eng. Geol. 87, 105–121.
Van Wees, J.D., Buijze, L., Van Thienen-Visser, K., Nepveu, M., Wassing, B.B.T., Orlic, B., Fokker, P.A., 2014. Geomechanics response and induced seismicity during gas field depletion in the Netherlands. Geothermics 52, 206–219. http://dx.doi.org/10.1016/j.geothermics.2014.05.004.
Vasco, D.W., Rutqvist, J., Ferretti, A., Rucci, A., Bellotti, F., Dobson, P., Oldenburg, C., Garcia, J., Walters, M., Hartline, C., 2013. Monitoring deformation at The Geysers Geothermal Field, California using C-band and X-band interferometric synthetic aperture radar. Geophys. Res. Lett. 40, 2567–2572. http://dx.doi.org/10.1002/grl.50314.
Verdon, J.P., Kendall, J.-M., Stork, A.L., Chadwick, R.A., White, D.J., Bissell, R.C., 2013. Comparison of geomechanical deformation induced by megatonne-scale CO_2 storage at Sleipner, Weyburn, and In Salah. Proc. Natl. Acad. Sci. 110, E2762–E2771.
Villegas-Lanza, J.C., Nocquet, J.-M., Rolandone, F., Vallée, M., Tavera, H., Bondoux, F., Tran, T., Martin, X., Chlieh, M., 2016. A mixed seismic–aseismic stress release episode in the Andean subduction zone. Nat. Geosci. 9, 150–154. http://dx.doi.org/10.1038/ngeo2620.
Waldhauser, F., Ellsworth, W.L., 2000. A double-difference earthquake location algorithm: method and application to the northern Hayward Fault, California. Bull. Seismol. Soc. Am. 90, 1353–1368.
Wallace, T., Helmberger, D.V., Engen, G.R., 1983. Evidence of tectonic release from underground nuclear explosions in long-period P waves. Bull. Seismol. Soc. Am. 73, 593–613.
Walsh, F.R., Zoback, M.D., 2015. Oklahoma's recent earthquakes and saltwater disposal. Sci. Adv. 1, e1500195. http://dx.doi.org/10.1126/sciadv.1500195.
Wang, P., Small, M.J., Harbert, W., Pozzi, M., 2016. A bayesian approach for assessing seismic transitions associated with wastewater injections. Bull. Seismol. Soc. Am. 106, 832–845.
Wilson, M.P., Davies, R.J., Foulger, G.R., Julian, B.R., Styles, P., Gluyas, J.G., Almond, S., 2015. Anthropogenic earthquakes in the UK: a national baseline prior to shale exploitation. Mar. Pet. Geol. 68, 1–17. http://dx.doi.org/10.1016/j.marpetgeo.2015.08.023.
Wilson, M.P., Foulger, G.R., Gluyas, J.G., Davies, R.J., Julian, B.R., 2017. HiQuake: the Human-Induced Earthquake Database. Bull. Seismol. Soc. Am (submitted).
Wong, I.G., McGarr, A., 1990. Implosional failure in mining-induced seismicity: a critical review. In: Fairhurst, C. (Ed.), Rockbursts and Seismicity in Mines. Bakema, Rotterdam, pp. 45–51.
Wong, I.G., Humphrey, J.R., Adams, J.A., Silva, W.J., 1989. Observations of mine seismicity in the eastern Wasatch Plateau, Utah, U. S. A.: a possible case of implosional failure. Pure Appl. Geophys. 129, 369–405.
Wright, C., Kgaswane, E.M., Kwadiba, M.T.O., Simon, R.E., Nguuri, T.K., McRae-Samuel, R., 2003. South African seismicity, April 1997 to April 1999, and regional variations in the crust and uppermost mantle of the Kaapvaal craton. Lithos 71, 369–392. http://dx.doi.org/10.1016/s0024-4937(03)00122-1.
Yabe, Y., Nakatani, M., Naoi, M., Philipp, J., Janssen, C., Watanabe, T., Katsura, T., Kawakata, H., Georg, D., Ogasawara, H., 2015. Nucleation process of an M2 earthquake in a deep gold mine in South Africa inferred from on-fault foreshock activity. J. Geophys. Res. 120, 5574–5594. http://dx.doi.org/10.1002/2014jb011680.
Yakovlev, D.V., Lazarevich, T.I., Tsirel, S.V., 2013. Natural and induced seismic activity in Kuzbass. J. Min. Sci. 49, 862–872.
Yeck, W.L., Block, L.V., Wood, C.K., King, V.M., 2015. Maximum magnitude estimations of induced earthquakes at Paradox Valley, Colorado, from cumulative injection volume and geometry of seismicity clusters. Geophys. J. Int. 200, 322–336. http://dx.doi.org/10.1093/gji/ggu394.
Zaliapin, I., Ben-Zion, Y., 2016. Discriminating characteristics of tectonic and human-induced seismicity. Bull. Seismol. Soc. Am. 106, 846–859.
Zang, A., Majer, E., Bruhn, D., 2014a. Analysis of induced seismicity in geothermal operations. Geothermics 52, 1–5. http://dx.doi.org/10.1016/j.geothermics.2014.07.006.
Zang, A., Oye, V., Jousset, P., Deichmann, N., Gritto, R., McGarr, A., Majer, E., Bruhn, D., 2014b. Analysis of induced seismicity in geothermal reservoirs - an overview. Geothermics 52, 6–21. http://dx.doi.org/10.1016/j.geothermics.2014.06.005.
Zedník, J., Pospíšil, J., Růžek, B., Horálek, J., Boušková, A., Jedlička, P., Skácelová, Z., Nehybka, V., Holub, K., Rušajová, J., 2001. Earthquakes in the Czech Republic and surrounding regions in 1995–1999. Stud. Geophys. Geod. 45, 267–282.
Zhang, Y., Feng, W., Xu, L., Zhou, C., Chen, Y., 2008. Spatio-temporal rupture process of the 2008 great Wenchuan earthquake. Sci. China Ser. D Earth Sci. 52, 145–154. http://dx.doi.org/10.1007/s11430-008-0148-7.
Ziegler, M., Reiter, K., Heidbach, O., Zang, A., Kwiatek, G., Stromeyer, D., Dahm, T., Dresen, G., Hofmann, G., 2015. Mining-induced stress transfer and its relation to a 1.9 seismic event in an ultra-deep South African gold mine. Pure Appl. Geophys. 172, 2557–2570. http://dx.doi.org/10.1007/s00024-015-1033-x.
Zoback, M.D., Harjes, H.P., 1997. Injection-induced earthquakes and crustal stress at 9 km depth at the KTB deep drilling site, Germany. J. Geophys. Res. 102, 18477–18491. http://dx.doi.org/10.1029/96jb02814.
Zoback, M.D., Healy, J.H., 1984. Friction, faulting, and insitu stress. Ann. Geophys. 2, 689–698.